MODELING THE EFFECT OF TEMPERATURE AND CHEMICALS AT DIFFERENT LEVELS OF BIOLOGICAL ORGANIZATION

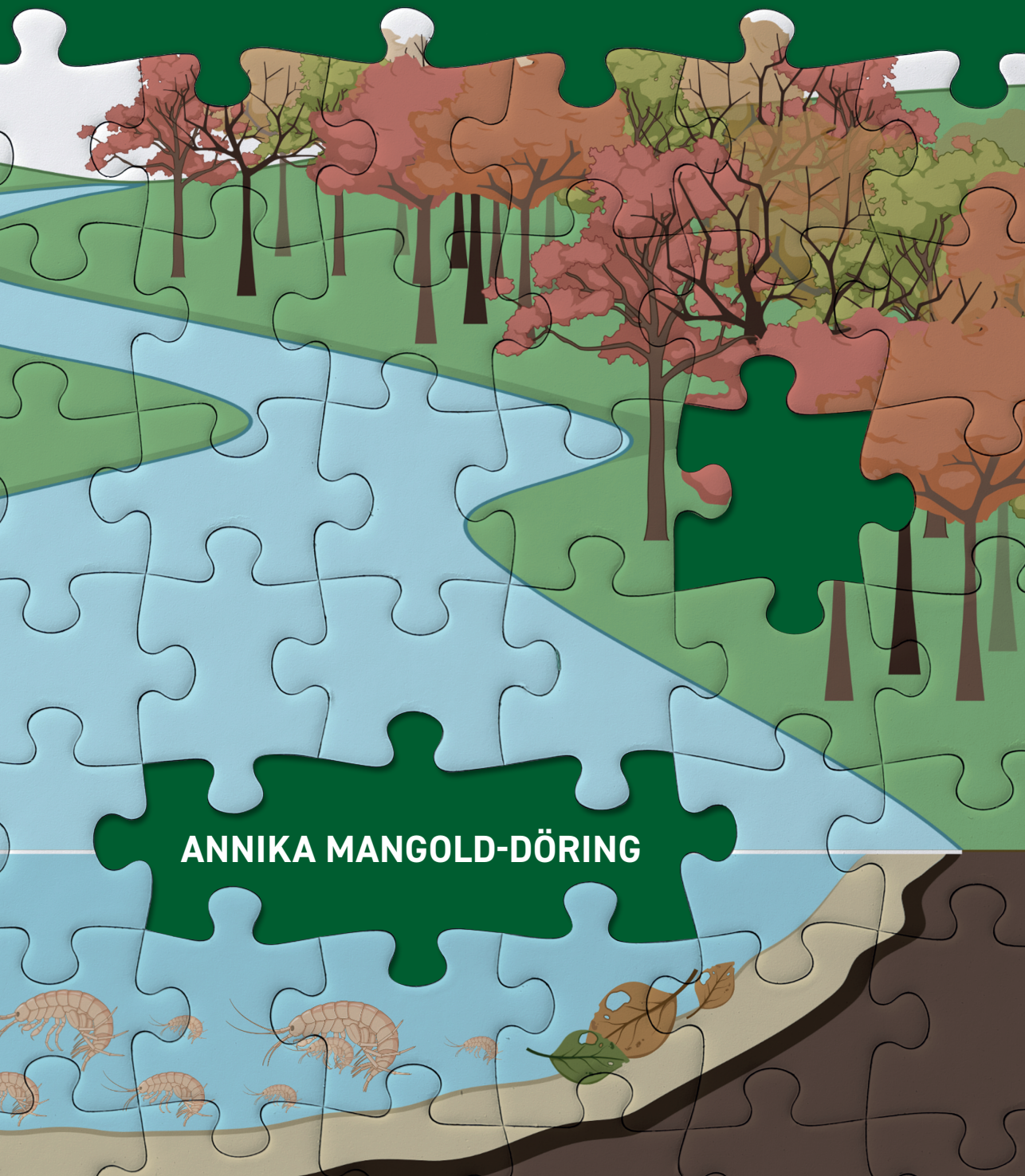

ANNIKA MANGOLD-DÖRING

Propositions

1. The biggest value of effect models lies in the opportunity to ask questions rather than provide answers.
(this thesis)

2. Modeling the effects of chemicals across levels of biological organization remains the aim, even though it will never be reached.
(this thesis)

3. Experts are often not the best communicators for topics within their expertise.

4. Poor reporting of raw data reflects a lack of transparency and hampers progress in science.

5. In science communication, simpler is always better.

6. Transparency is the most effective basis for long-lasting trust.

7. The positive influence of good communicators is undervalued by society.

Propositions belonging to the thesis, entitled

Modeling the effect of temperature and chemicals at different levels of biological organization

Annika Mangold-Döring

Wageningen, 13 November 2023

Modeling the effect of temperature and chemicals at different levels of biological organization

Annika Mangold-Döring

Thesis committee

Promotor

Prof. Dr Paul J. van den Brink
Personal chair, Aquatic Ecology and Water Quality Management
Wageningen University & Research

Co-Promotors

Dr Egbert H. van Nes
Researcher, Aquatic Ecology and Water Quality Management
Wageningen University & Research

Prof. Dr Andreas Focks
Professor, System Science Group
Osnabrück University, Germany

Other members

Prof. Dr. Carolien Kroeze, Wageningen University & Research
Prof. Dr. Sandrine Charles, Université Claude Bernard Lyon 1, France
Dr. Nika Galic, Syngenta Crop Protection AG, Basel, Switzerland
Dr. Josef Koch, Gaiac, Aachen, Germany

This research was conducted under the auspices of the Graduate School for Socio-Economics and Natural Sciences of the Environment (SENSE)

Modeling the effect of temperature and chemicals at different levels of biological organization

Annika Mangold-Döring

Thesis

submitted in fulfilment of the requirements for the degree of doctor
at Wageningen University
by the authority of the Rector Magnificus,
Prof. Dr A.P.J. Mol,
in the presence of the
Thesis Committee appointed by the Academic Board
to be defended in public
on Monday 13 November 2023
at 1.30 p.m. in the Omnia Auditorium.

Annika Mangold-Döring
Modeling the effect of temperature and chemicals at different levels of biological organization,
203 pages.

PhD thesis, Wageningen University, Wageningen, the Netherlands (2023)
With references, with summary in English
ISBN: 978-94-6447-870-9
DOI: https://doi.org/10.18174/637731

Summary

In this thesis, I investigate the effects of temperature and chemicals at different levels of biological organization through modeling. Due to global change, both of these two factors will increase in their relevance as environmental stressors in the future. Thus with this thesis, I aim to support future environmental risk assessment though the development and improvement of mechanistic effect models. For this, I focused on toxicokinetic-toxicodynamic models at the individual level, from where I connect also to the sub-individual level, and the population level.

Starting this thesis with **Chapter 1**, I provide a general introduction to ecotoxicology, environmental risk assessment of chemicals and effect modeling in laymen's language. I present my research objectives and give an overview of my thesis chapters.

The first scientific chapter (**Chapter 2**) examines the effect of temperature on toxicokinetics and the chronic toxicity of imidacloprid and flupyradifurone towards *Gammarus pulex.* To investigate how temperature changes the toxicokinetics of these insecticides, we conducted laboratory experiments at different temperatures and applied a toxicokinetic model. A chronic exposure was used to understand how temperature affects the effects of the two insecticides on lethal and sublethal endpoints which are relevant for their environmental risk assessment. We found that both compounds' uptake and elimination rate constants increased with increasing temperature, though in different magnitudes. Furthermore, the biotransformation of imidacloprid into its toxic metabolite imidacloprid-olefin was accelerated, partially explaining the observed increase in toxicity with increasing temperature in the chronic experiment. For flupyradifurone the enhancing influence of temperature on toxicity was less severe. Elevated temperatures intensified adverse effects of both insecticides not only on death and immobilization, but also on food consumption and dry weight. With these findings we provide evidence that temperature needs to be considered when assessing the risks of insecticides in the context of increasing temperature scenarios of future climates.

Building on these results, we dive deeper into the investigation of temperatures effect on the processes of the toxicokinetics and toxicodynamics of these insecticides in **Chapter 3**. Here, the aim was to determine how we can account for temperature in mechanistic effect models. By applying the full version of the General Unified Threshold model for Survival (GUTS), we identified the effects of temperature on toxicokinetic and toxicodynamic processes separately, by applying the Arrhenius equation to correct the models rate parameters. For this we used the data of **Chapter 2** to parameterize the temperature corrected GUTS-T model. We found that toxicokinetic and toxicodynamic parameter scale differently with temperature and that there are differences between imidacloprid and flupyradifurone that urge for further research to unravel the underlying mechanisms.

To enable the assessment of temperature as a single stressor to organisms, we developed a new temperature damage model in **Chapter 4**. Inspired by the ecotoxicological damage model in the GUTS framework, the temperature damage model assumes that damage accumulation and repair depend on temperature, and mortality is driven by the damage level exceeding a threshold. Model calibration using experimental data of *G. pulex* exposed to different constant temperatures showed a good agreement with the measured survival. Further, model simulations, including constant temperatures, daily temperature fluctuations, and heatwaves, demonstrated the model's ability to predict temperature effects for various environmental scenarios. Applying the damage concept of the GUTS model this new model facilitates a future combination with GUTS models for chemicals to assess the combined effect of chemicals and temperature and their interactions at the individual level.

Moving on to **Chapter 5**, we switch to the sub-individual level and investigate the toxicokinetics of the insecticide thiacloprid, again on *G. pulex*. Combining molecular in vitro and in vivo assays for receptor binding with toxicokinetic exposure experiments, we developed, calibrated and validated a two-compartment model to describe the toxicokinetics of this compound. This study delivers evidence to an irreversible binding of thiacloprid to the nicotinic acetylcholine receptor (nAChR), providing insights in the underlying mechanisms of toxicity at sub-individual level. Irreversible binding to the nAChR may also be the underlying mechanism for other insecticides targeting this receptor, thus existing TKTD models should be updated accordingly.

In **Chapter 6** we then move on to the population level. Here, we investigate the relevance of temperature corrections of toxicity parameters for the dynamics of populations in order to investigate the relevance of including temperature adjustment for environmental risk assessment of chemicals. By applying an individual based population model based on the dynamic energy budget model and a GUTS implementation for accounting for toxicity, we simulate different environmental scenarios and their effect on the population dynamics of *G. pulex*. Our findings indicate that higher temperature fluctuations lead to broader observed population size ranges in simulations. However, exposure scenarios counterbalance this impact by decreasing maximum population sizes. At lower temperature extremes, these combined effects result in an overall reduction of the mean population size. These outcomes emphasize the importance of incorporating temperature-sensitive parameterization into population models to conduct reliable risk assessments under anticipated climate conditions marked by heightened variability.

Concluding in **Chapter 7**, I provide a general discussion of the results of these research chapters in the overall context of the thesis aim and objectives, considering the scientific literature. For the future of cross-level extrapolations, I suggest the linking of the sub-organismal level (**Chapter 5**) with individual-level approaches like GUTS and population

level models like GUTS based IBMs (**Chapter 6**). Additionally, I promote the combination of experimental and modeling approaches (as in **Chapter 2** and **5**) to build a new, stronger basis for environmental risk assessment. Finally, I suggest addressing complexity in environmental risk assessment based on a common understanding of modeling tools and a shared protection goal. Ultimately, I encourage a shift toward effective communication based on valuable insights from engagement in citizen science communication to advance the fields of ecotoxicology and environmental risk assessment.

Contents

Chapter 1

Introduction

Disclaimer

Dear reader,

Thank you for taking the time to read my thesis or even just parts of it. This research is close to my heart, and I am delighted you find it interesting too. I want to give you a heads-up before you start reading, as the writing style of this introductory chapter is quite different from the scientific chapters after that. Chapters 2-6 are written for scientific journals, where we don't have much space to write a long explanation and thus have to use a certain scientific language for brevity. Unfortunately, by using this language, only a smaller (expert) audience will be able to follow those articles. But let me be honest, sometimes, even experts need multiple reads to actually understand what has been written for them. So, for a change, with this introductory chapter, I want to explain my research in a way everyone can understand and connect to without having to learn the scientific language used in the rest of my thesis. For the readers amongst you that prefer the scientific writing style, I would like to point out that there is an introduction part in all the separate chapters. In this general introduction however, I did my best to find relatable examples or metaphors and to avoid jargon. Funny enough, *jargon* is a word I did not even know before I worked on my PhD, which describes the use of words that only an expert audience will understand. From my perspective, using the word jargon is jargon to explain jargon. I find that funny. But I am getting off track here. All I want to say is that I hope you, with or without any scientific background, will enjoy reading this introduction and getting an impression of what research I have spent the last four years on.

Okay, one more thing before we start: As it is important to provide the original sources of information, in scientific writing as much as in any writing where scientific topics are discussed, I will provide those references in the same format as done in scientific publications. This means that sometimes at the end of a sentence, you may see something like this: (Einstein, 1905). This marks a citation of a scientific publication from the author Einstein, in the year 1905. The title of this publication, and where to find it, is then listed under the references list at the end of the thesis. Now, without further ado, let's get to it!

1.1 When it rains, it pours! - How one stressor seldomly stays alone

Figure 1.1: Stress scale. These emojis represent different stress levels from low (green, on the left) to high (red on the right).

Have you been stressed lately? What kind of stress did you have; the kind where you don't have enough time to fit everything you need to do into one day? Or maybe it was the kind where you felt physically exhausted because you worked out a lot, you felt sick, or it was a very hot summer day. Sometimes, you may even experience a combination of these conditions that stress you. Imagine feeling very stressed because you are trying to fit the tasks of the whole week into only one day, which happens to be a very hot summer day. Consequently, your mind and body are both stressed in their own way due to different factors. In this example, your mind is experiencing stress through the time pressure to finish the tasks, making you feel anxious, and your body is stressed because the temperature is very uncomfortable, and you are sweating a lot. Regardless of the origin of the stress you are experiencing, stressful situations always cost you energy to get through them, right? Fortunately, we humans can recharge our energy through holidays or other activities that relax our bodies and minds to stay healthy. But what about animals, insects, and plants? What I just discussed about our human stress is also true for these organisms. Although the mental stress of humans is not the same kind of stress that other organisms experience, they can be stressed by multiple factors as well. So, how do they cope with their stress? I mean, have you ever seen a bee doing yoga or an apple tree getting a relaxing root massage?

Figure 1.2: Bee comic. In this comic, Agate and Magrit discuss their holiday plans. Agate (left) refers to insect hotels recently gaining popularity in people's gardens. Margrit (right), however, thinks that the bed and breakfast hotels promoted through the company AirBnB are advertised for bees. Made from memory of a comic seen somewhere on the internet.

Most organisms are facing conditions in the environment that do stress them on a daily basis. And exactly like us humans, they need to spend a lot of energy to deal with their stress which otherwise impacts their health and, in some instances, even kills them.

In my research, I looked into the stress factors of aquatic organisms, like the little freshwater shrimp *Gammarus pulex* (Figure 1.3). Two of the main factors threatening these aquatic organisms are **insecticides** and **temperature**. Though there are other factors that threaten aquatic organisms (i.e., habitat loss or overfishing), in my thesis, I focused on insecticides and temperature because they are particularly concerning in the near future. This is due to the expectations of experts that extreme weather events with very high temperatures will increase due to global climate change (IPCC, 2012; Woolway et al., 2021). At the same time, it is not expected that insecticide use will be reduced (Bernhardt et al., 2017; United Nations Environment Programme, 2019). Therefore, it is likely that we will see more aquatic organisms struggle with the combined stressors temperature and insecticide in the future. Thus, we should be prepared to take action in protecting these organisms and preserve the services and benefits they provide to us (i.e., their contribution to a good water quality).

Figure 1.3: *Gammarus pulex*. In this figure, Gilbert introduces himself. Gilbert had his debut at my presentation at the annual scientific conference of the Society of Environmental Toxicology and Chemistry in Copenhagen 2022. Ever since he helps me to explain my research on his species, *Gammarus pulex*.

Infobox - stress factor insecticides

Insecticides are chemicals specifically designed to kill insects or other "pest" organisms. In agriculture, farmers use insecticides against insects that would otherwise destroy their crops (Figure **1.4**). While insecticides are supposed to kill those *target species* (e.g., sucking insects like planthoppers or the whitefly *Bemisia argentifolii)*, it is not guaranteed that they do not kill, harm, or stress other *non-target species* that live in those habitats (e.g., pollinators like bees), or other habitats close by (e.g., freshwater fish like trout and small shrimps like *Gammarus pulex*) as well. Usually, the way insecticides work is, that they interfere with a specific receptor of the target species (Simon-Delso et al., 2015a). In this case, the insecticide is not expected to be dangerous to other, unrelated species, simply because they do not have these receptors (i.e., a pesticide used to suppress weeds are unlikely to be dangerous for insects and vice versa). However, amongst related species, i.e., arthropods, a lot of species have common receptors. The non-target arthropod species will thus also be sensitive to the insecticide (Maltby et al., 2005). Consequently, they may be affected negatively, even if this was not the original intention of the insecticide use. Thus, we have to control the application of those insecticides to minimize any adverse side effects on the environment and protect the sensitive, non-target species.

Figure 1.4: Insecticide application on an agricultural field.

Infobox - stress factor temperature

When it gets very hot outside, there are only limited options to escape this uncomfortable condition. We can search for places in the shadow and cool off in the lake for a swim. But there is no direct way for us to control the outside temperature. In addition, through human-driven climate change, temperatures are becoming more extreme (hotter and colder) (IPCC, 2012; Woolway et al., 2021). This makes it more stressful for species living on earth because they have to adapt to these extremes at an unusual tempo (Jones and Mann, 2004). Every organism has its preferred temperature range, in which it can survive. This range has an optimum point at which the organism is most productive and healthy, and it has boundaries at both ends, outside of which the organism cannot survive. The closer the temperature is to these boundaries, the more stress the organism experiences. And as you can imagine, an already stressed organism might not be able to handle additional stress as well as a non-stressed one. Thus, a temperature-stressed insect may be affected by insecticides even more because it lacks the energy to fight it. Unfortunately, we cannot regulate the outside temperature as effectively as the use of insecticides. Therefore, we need to understand when temperature is an additional stress for our water organisms, as this will determine how strict we have to be with controlling the use of insecticides.

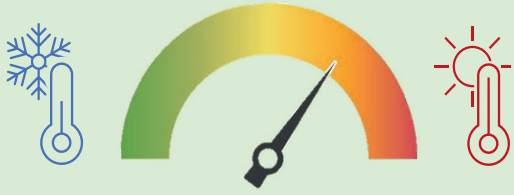

Figure 1.5: Temperature scale from low (left) to high (right) temperatures.

1.2 What can we do about those environmental stressors?

When I meet new people and they ask me what I work in, I usually answer: *I study ecotoxicology, which is basically about chemicals in the environment*. For this introduction I would like to extend this, with a bit more general information. So, here we go: *Ecotoxicology* is an environmental science that wants to identify and understand the impacts of chemical substances (i.e., insecticides, but also natural chemicals like sodium and phosphorus) on nature (Fent, 2013). In doing so, all levels of biological organization, from the lowest level (i.e., molecules and cells) to the highest (i.e., populations, communities and whole ecosystems), are considered. We humans apply insecticides to our crops in order to secure our food production while at the same time, we know it might be dangerous for some species we don't want to harm but are exposed to the insecticides too. Thus, we need to identify the potential **hazards** and **risks** those substances pose to the environment. Both aspects, need to be evaluated for insecticides before they are sold on the European market. This process is called **environmental risk assessment** (**ERA**) of chemicals. The aim of environmental risk assessment is basically in the name itself – to assess the risk of chemicals to the environment. But what is a risk for the environment, and what does it mean to assess it? Furthermore, when do we accept a risk, and when do we not? All these questions are addressed in ERA and ecotoxicological studies provide the necessary scientific evidence.

Even though chemicals are the main concern for ecotoxicologists, other stress factors like temperature may influence the same processes in organisms as chemicals do. As a consequence, understanding not just the single stressors but the complex interactions between stressors like chemicals and temperature is a growing focus of our research in ecotoxicology (Arenas-Sánchez et al., 2019; Hooper et al., 2013; Noyes et al., 2009a; Noyes and Lema, 2015; Polazzo et al., 2022).

To estimate the risk of insecticide applications, we need to understand two things: first, how much insecticide actually reaches the different environmental compartments (e.g., soil, air, water), which is called the fate of the chemical and determines the **exposure** concentration for each environmental compartment. Secondly, we need to know what the insecticide does with the organisms when it reaches them or their food. In other words: what is the **effect** of the insecticide on the organisms? Getting the information on the exposure can be tricky. We might know how much insecticide is sold or how much a farmer uses on their fields. But how much of this really reaches the rivers and streams depends on many factors (e.g., rainfall, weather conditions, soil type, slope of field and the chemical characteristics of the insecticide). The exposure side is, however, not the focus of this thesis. Instead, I focused on the effect side.

Infobox - the difference between hazard and risk

In the field of ecotoxicology, it is important to distinguish between the words *hazard* and *risk*, as they are related and often used interchangeably, when people are unaware of their distinct concepts. While the term **hazard** describes the potential of a substance to cause harm, the term **risk** considers how likely it is that this harm actually occurs in a specific context. As an example: a hammer poses a high hazard to humans, but the risk is low when it is used by an experienced carpenter. Contrastingly, the risk is high, if we find the hammer in the hands of a child.

We know that insecticides are hazardous substances because they were designed to kill. Therefore, we need to evaluate how likely they cause unacceptable environmental harm. This *hazard identification* is done by testing the chemical in controlled laboratory or field experiments, in which researchers investigate the potential hazards of the chemical in question. In these experiments, it is documented what happens when test organisms are brought in contact with the chemical. For instance, by evaluating the concentration at which the organisms die, they are affected in their movement or reaction time, or they stop to reproduce. All these effects on the organisms would be considered hazardous for the species' survival, and it is very important to identify all possible hazards caused by the chemical. While the experiments are done by researchers at universities, research institutes, consultancy firms or industry, the environmental risk assessment is usually conducted by the insecticide industry and submitted to and evaluated by national regulatory agencies, like the Dutch Board for the Authorization of Plant Protection Products and Biocides (Ctgb) for the Netherlands and the European Food Safety Authority (EFSA) Europe-wide. In Europe, an insecticide first has to be registered by EFSA before it can be considered for registration by the individual EU member states.

In the *risk characterization* stage of the environmental risk assessment of a chemical, we try to get a good idea about the chemical's actual risk to the environment (Figure 1.6). We do so based on our knowledge of its hazardous properties and the quantity in which it will enter the environment via the different exposure routes. If we have a highly hazardous substance but only used in the laboratory, and thus the likelihood of it entering the environment is very low, the overall risk for the environment is low. The same is true if we have a substance that exhibits a very low hazard but used in high quantities in the environment. The likelihood that non-target species are exposed might be very high, however, due to the low hazard, the overall risk for the environment is still low.

Figure 1.6: Measuring risk. Abstract representation of a risk assessor (on the right) measuring the risk with a scale.

Infobox – exposure and effect

With the word **exposure**, we describe the degree of contact of the organisms or the environment with the chemical. Ideally, we want to know how the contact happens (i.e., how the chemical comes from the place of its use to the site of contact) and, especially, to what extent (i.e., how much of it will be found at the site of contact). Thus, in an exposure assessment, we calculate how much of the chemical ends up in the environment, considering all possible ways it can take (Figure 1.7).

Figure 1.7: Chemical exposure routes. A chemical may be distributed along different paths (black dotted lines) to different environmental destinations (yellow pins) in different amounts (represented through pin size).

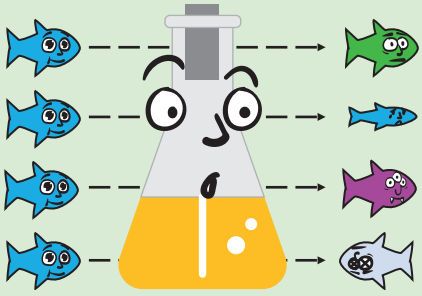

Figure 1.8: Chemical effects. The fish on the left are all the same. When they get exposed by the chemical however (following the black dotted arrows) they may show effects, here represented by the different shapes and colors of the fish, after the chemical exposure.

When we talk about the **effects** of a chemical, we refer to the influences the chemical has on the organism depending on the concentration of the chemical. How does the organism react to the chemical when they get in contact? Most importantly, does it survive? If so, does it change its behavior, and in what way? Important characteristics to look at in *effect assessments* are survival, growth, reproduction, and body abnormalities (Figure 1.8).

The effect of chemicals is traditionally assessed through toxicity tests. Those are controlled laboratory experiments in which certain organisms are exposed to the chemical of interest. Then the effects of the chemical on the organisms are observed and recorded as results, i.e., if they are affected in their survival, movement, growth, or reproduction. This method has a downside: living organisms are used as laboratory test animals and are disposed afterwards. To reduce the use of live organisms for such investigations, ecotoxicologists have been developing computer models to study these effects without the need for further organism testing (Ashauer and Escher, 2010; Grimm and Martin, 2013). These models are called **effect models**, and I developed and applied them in my thesis. When I started my thesis, these effect models were developed for assessing insecticide stress but did not include the effect temperature can have on organisms, let alone their interaction. Therefore, in my thesis, I improved the effect models to consider multiple stress scenarios, i.e., both the insecticide and the temperature stress. But first, let's talk a bit more about what a computer model is and how they work. Be prepared, here comes another metaphor!

1.3 How we use crash test dummies in ecotoxicology

When a new car is built, some safety aspects for the passengers are tested in deliberate crash tests. Crash test dummies are used to understand the impacts on passengers if the car should crash. These dummies are placed in the car seats looking like average passengers. They not only look like humans, but they also have special mechanical sensors imitating different human organs to record the forces they experience during the crash. These records can then be used to estimate how badly an actual passenger would have been injured in a real crash. Then we know if this new car model meets the minimal safety criteria or if it needs more safety features.

These crash tests are obligatory for every new car entering the market. Thus, the risk is assessed before any hazardous situation can occur. This is called *prospective risk assessment*, in contrast to *retrospective risk assessment*, where the risk is studied afterward. It is easy to understand why we use these dummies instead of crashing the cars with real people and asking them how they are doing after the crash. We want to know the hazards of a collision for a passenger without actually putting the passenger at risk. This "crash-test" principle is also applied in an environmental risk assessment of chemicals. Instead of exposing the environment to the chemical and see what happens, we test this prospectively using experiments and models.

So, do we also have crash test dummies in ecotoxicology? Certainly! However, not exactly in the same sense. Standard test species, acting as representatives or substitutes, are used in ecotoxicological experiments. There is, for example, standard species as substitute for fish and vertebrates (e.g., zebrafish *Danio rerio*), for invertebrates (e.g., the water flea *Daphnia magna*), and for phytoplankton and plants (e.g., *Lemna* sp.). The idea behind these substitute species is similar to the crash test dummies. Zebrafish are assumed to be functioning similarly enough to represent all vertebrate species, i.e., they have similar organs and metabolism. Then they are exposed to the chemical, i.e., representing the crash test in our metaphor, and it is assessed if and what harm has been done dependent on the exposure concentration, which compares to assessing the sensors of the crash test dummies.

You might be thinking: *but these Zebrafish are real animals, not just lifeless puppets with a few mechanical sensors.* True! Unfortunately, it is far more complicated to build mechanical sensors for the various effects that chemicals can have on an organism compared to the sensors recording the physical forces during a car crash. Therefore, we still need to use real animals in ecotoxicological experiments to ensure the safety of the products we employ in the environment. However, these experiments are conducted under consideration of the **3R** principle (Russell and Burch, 1959). Thus, whenever possible, these experiments are ***r****eplaced* by other methods (I'll get back to those in a bit), and if that is not achievable, they

are ***r**educed* to a minimum. Those experiments that are unavoidable for environmental risk assessment are ***r**efined* in a way that the most benefit (i.e., knowledge in the form of data) is gained with the minimum suffering for the animal. As far as alternative methods go, there is a variety of so-called *new approach methodologies* that range from biological methods like cell assays to more technical methods like **computer simulations**. In my research, I mainly worked with computer models and simulations; hence I will explain those in more detail.

A *computer simulation,* in the broad sense, is the imitation of a real-life process that is created by a *computer model*. Next to imitating something from the real world, a simulation can also predict what could happen under certain circumstances. An example of a computer model whose predictions we use in our everyday life is the weather forecast. The weather forecast is based on digital weather models that take the input from weather stations, measuring parameters like air pressure and humidity used to predict the weather of the following hours, days, and weeks. Similarly, we can use the biological information about a species and the data from the ecotoxicological experiments to inform a digital model of an organism exposed to chemicals. These models are called **effect models**. In those models, we basically built a digital dummy allowing us to run crash test simulations for different chemical exposure conditions.

With effect models, it is possible to reduce or refine experiments with real organisms as we can simulate different exposure conditions with our digital dummies and do not need to test them in separate experiments. In environmental risk assessment, this is a particularly useful approach as the simulation conditions can be chosen specifically for the situation that needs to be assessed, i.e., for the time-variable exposure condition in a ditch next to an agricultural field. By this, we make the best use of the data obtained from the mandatory experiments while adhering to the 3R principle.

1.4 Ecotoxicology's next top models

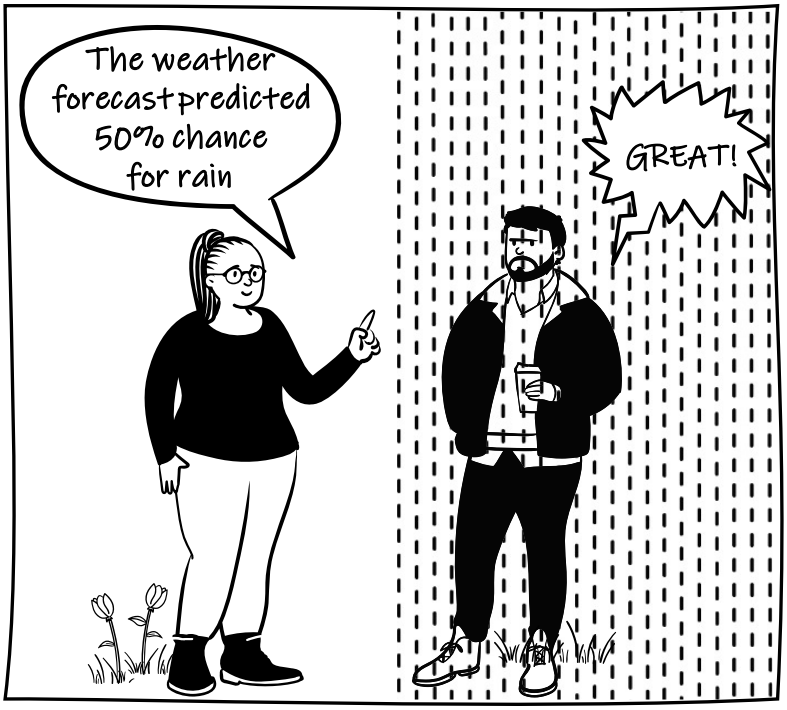

Figure 1.9: In this scene, Monica (standing on the left, in the dry) explains to Jeff (standing in the rain, on the right), that the weather forecast for this day predicted 50 % of rain. Modified by Wallbaum comics (www.illustratoon.de).

I guess we are all painfully aware that weather forecast predictions are not always accurate (Figure 1.9). Unfortunately, this is also true for effect models. In fact, the first thing one learns about modeling in science is that, quote: "***all models are wrong...***". This is because models, in general, are only as good as the assumptions they are based on. Thus, if we have the wrong assumption about the processes we try to model, the simulations will not match the real-world data, and we will get the wrong predictions. But does this mean we shouldn't use effect models in ERA after all? By no means! Because the quote I started earlier has a second part to it: ***"... but some are useful"***. This quote by George E. P. Box sums up the essence of effect modeling in ecotoxicology. It means that we should be aware of and transparent about the model's shortcomings, that the model can never be the same as the real organism, they will always lack some detail that we are unaware of, and therefore they will always be wrong. But at the same time, they are incredibly useful as they allow us to gain detailed insight into the results we observe in experiments and enable us to extrapolate these findings beyond the circumstances used in these experiment (e.g., concentration profile, temperature and duration). By comparing the results of our digital dummy with the real organism, we gain insights into the underlying processes needed to construct the

computer model. Furthermore, we can use the computer model to ask and answer different research questions about the effect of chemicals on organisms without necessarily testing those in additional experiments. By running simulations, we basically conduct digital experiments, helping us to test our scientific hypothesis without sacrificing organisms. At the same time, we safe time and money, as simulations on a computer are much cheaper and quicker than laboratory experiments.

The effect models I used in my PhD research are the so-called *toxicokinetic-toxicodynamic* effect models. These two words are definitely jargon but can be explained relatively simply: **toxicokinetic** processes describe what the organism does with the chemical, i.e., how the chemical is taken up and excreted by the organism. For water organisms, the chemical is usually taken up from the water via the organism's surface, which can be the skin or the gills, or via the food. Once the chemical is inside the organism, it may get distributed to different organs, where it either gets broken down (i.e., the organism may break down the chemical, similar to digesting food) or transported to the exit, where it gets excreted from the body. All these transport processes are summed up under the term toxicokinetics. The term **toxicodynamics,** on the other hand, describes what the chemical does with the organism. The effects of the chemical on the organism's survival, reproduction, growth, or behavior are all grouped under this term. Toxicokinetic-toxicodynamic models have been used in ecotoxicological research for decades and were also deemed ready for environmental risk assessment by the European Food Safety Authority (EFSA (PPR), 2018). But are those models equipped to simulate the effects of chemicals under the different temperature conditions we face currently and in the future?

1.5 Thesis aim and overview

When I first discovered effect models during my master's studies, I was especially intrigued by their potential to refine, reduce, and even replace animal experiments. I thought this was the way to go; if we can use technology to spare organisms' lives, I just had to know more about this. Over time, my passion for this topic grew even more. Next to the ethical aspects, I simply enjoy the combination of biology, mathematics, and the part of informatics needed for coding the computer models. Thus, I decided to take on this PhD project to explore their potential of effect models in the context of global climate change and support their use in environmental risk assessment (Figure 1.10).

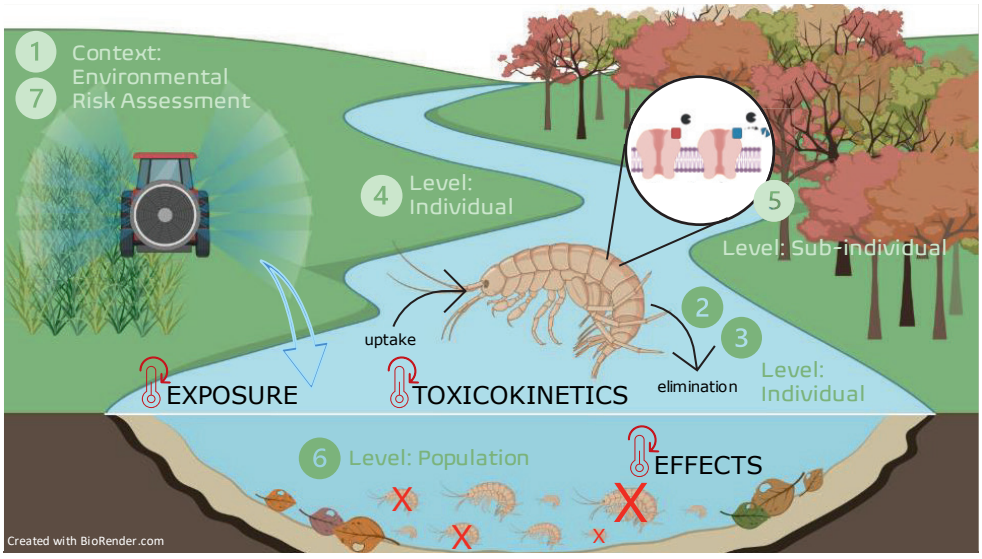

Figure 1.10: Overview of thesis chapters. The different thesis chapters (i.e., round numbers from 1 to 7) along with a short description are shown in their common context. Displayed is a typical environmental scene where insecticides are applied on a crop field next to a stream, which is a typical habitat of the non-target species *Gammarus pulex*. The applied insecticide can reach the stream, where it comes in contact with the organisms (i.e., exposure). The interaction of the organism with the insecticide (i.e., toxicokinetics) can be modeled at individual level by toxicokinetic-toxicodynamic effect models, as done in Chapter 2 and 3 of this thesis. Also, the influence of temperature as a single stressor was assessed at individual level with a new temperature damage model (Chapter 4). The interaction of the insecticide with the receptors inside of the organisms were investigated in Chapter 5 and represent the sub-individual level. For the effect of the insecticide and temperature on the population level, individual-based models were used in Chapter 6. An introduction (Chapter 1) and general discussion (Chapter 7) provide the overall context for these research chapters. Created with BioRender.com

Temperature, as I mentioned in the beginning, can be a stressor to organisms on its own and may also influence their ability to cope with other stressors, like chemicals. Experimental studies showed that the toxicity of chemicals mostly increased with increasing temperature conditions (Heugens et al., 2001; Holmstrup et al., 2010; Noyes et al., 2009a). Interestingly, for some chemicals, the reverse has been found (Harwood et al., 2009). So, no clear relationship between temperature and chemical effect has been established for environmental risk assessment. What is more, while we found these relationships between toxicity of chemicals and temperature in experiments, they were however, not reflected in the state-of-the-art TK-TD models at the time I started my PhD research. Thus, if we want to use effect models to inform environmental risk assessment, we need investigate whether our current assumptions for those models are representative enough, or if they need updating.

Therefore, I had three main objectives for my thesis:

1) investigate the effect of temperature on toxicokinetic and toxicodynamic processes of chemicals in organisms
2) develop an individual-level model that is able to describe the effect of temperature as a stressor
3) implement the effects of temperature on the toxicity of an insecticide into effect models of different levels of biological organization.

With these goals in mind, I collaborated with my co-authors on writing five scientific chapters covering different aspects of this endeavor. In **Chapter 2**, we tested how individuals of *Gammarus pulex* react when facing two stressors, the insecticides imidacloprid or flupyradifurone, and different temperatures. We observed the survival of these organisms over 28 days to see if temperature affects how harmful the insecticides are to them (toxicodynamics). We also measured how the insecticides behaves within the organisms at different temperatures. For this, we measured how much of the insecticide is taken up by the organism and how fast, but also how quickly it is broken down or excreted again (toxicokinetics).

Our findings in **Chapter 2** showed that temperature does indeed influence how toxic the insecticides are to the organisms. This meant that the existing effect models used to predict their toxicity needed to be updated. For this, we looked at the model parameters if an existing model**,** to see how they change at different temperatures (**Chapter 3**). This led to the development of a new model that can accurately predict the toxicity of chemicals, taking into account different temperature conditions.

While **Chapter 3** focused on improving the current state-of-the-art modeling approach, in **Chapter 4,** we developed a new model that specifically looks at the impact of temperature on its own, apart from the chemical effects. This model serves as a starting point for considering both temperature and chemicals as stressors in future studies, to enable a more realistic environmental risk assessment.

After focusing on the individual level in these previous chapters, we zoom in to the sub-individual level in **Chapter 5**. In this chapter, I collaborated with colleagues outside of my university group to investigate how a different insecticide, thiacloprid, interacts with the target receptors in *Gammarus pulex*. We found that a portion of this insecticide binds irreversibly to the target receptor in the organism, meaning it stays inside the organism and does not get excreted.

In **Chapter 6**, we zoomed out again, this time to the population level, again for the species *Gammarus pulex*. Population models are powerful tools that help us understand how populations respond to various exposure conditions. Temperature is usually implemented in the biological part of those models but not yet in the toxicity part. Thus, we investigated how the consideration of temperature in the effect model part, influences the overall prediction of the population responses to imidacloprid exposure.

Finally, in **Chapter 7**, I discuss the results of these research chapters and share my thoughts on how these effect models can be used in environmental risk assessment of chemicals.

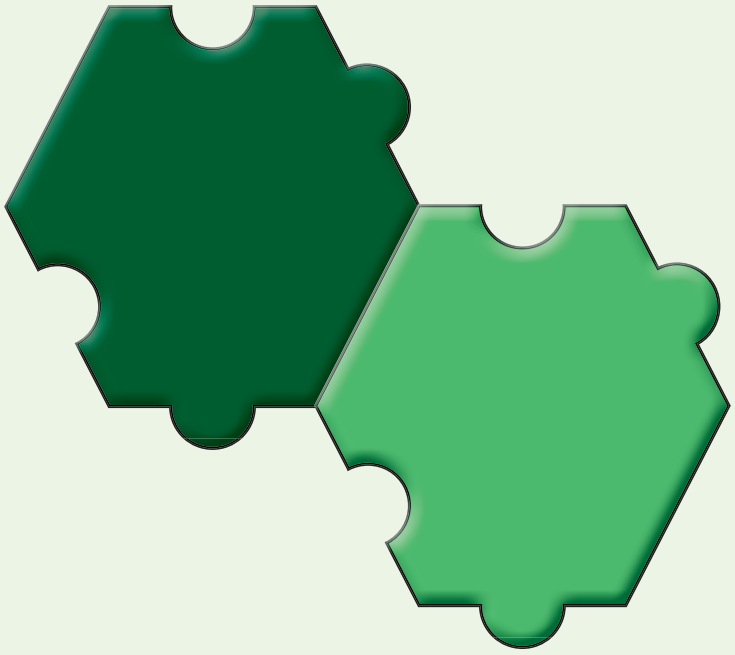

Chapter 2

The effect of temperature on toxicokinetics and the chronic toxicity of insecticides towards *Gammarus pulex*

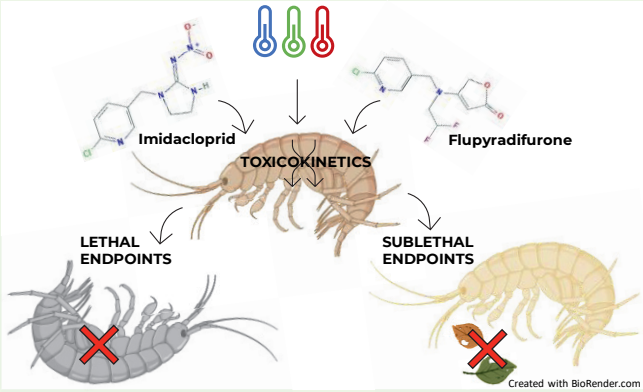

Figure 2.1: Graphical abstract of Chapter 2. *Gammarus pulex* was exposed to imidacloprid and flupyradifurone at different temperature conditions. Lethal and sublethal endpoints were assessed. Created with BioRender.com

This chapter is based on:
Anna Huang, Annika Mangold-Döring, Huitong Guan, Marie-Clair Boerwinkel, Dick Belgers, Andreas Focks, Paul J. van den Brink, 2022. The effect of temperature on toxicokinetics and the chronic toxicity of insecticides towards *Gammarus pulex*.

Science of The Total Environment, Volume 856, Part 2, p.158886.
https://doi.org/10.1016/j.scitotenv.2022.158886

Abstract

A comprehensive understanding of chemical toxicity and temperature interaction is essential to improve ecological risk assessment under climate change. However, there is only limited knowledge about the effect of temperature on the toxicity of chemicals. To fill this knowledge gap and to improve our mechanistic understanding of the influence of temperature, the current study explored toxicokinetics and the chronic toxicity effects of two insecticides, imidacloprid (IMI) and flupyradifurone (FPF), on *Gammarus pulex* at different temperatures (7 – 24 °C). In the toxicokinetics tests, organisms were exposed to IMI or FPF for 2 days and then transferred to clean water for 3 days of elimination at 7, 18, or 24 °C. In the chronic tests, organisms were exposed to the individual insecticides for 28 days at 7, 11, or 15 °C. Our research found that temperature impacted the toxicokinetics and the chronic toxicity of both IMI and FPF, while the extent of such impact differed for each insecticide. For IMI, the uptake rate and biotransformation rate increased with temperature, and mortality and food consumption inhibition were enhanced by temperature. While for FPF, the elimination rate increased with temperature at a higher rate than the increasing uptake rate, resulting in a smaller pronounced effect of temperature on mortality compared to IMI. In addition, the adverse effects of the insecticides on sublethal endpoints (food consumption and dry weight) were exacerbated by elevated temperatures. Our results highlight the importance of including temperature in the ecological risk assessment of insecticides in light of global climate change.

2.1. Introduction

There is growing awareness that climate change and other anthropogenic activities, such as removal of riparian vegetation, may cause surface water warming and affect the toxicity of many chemicals to aquatic organisms (Noyes and Lema, 2015; Polazzo et al., 2022). Thus, the influence of temperature needs to be incorporated into the ecological risk assessment (ERA) of chemicals (Noyes and Lema, 2015; Van den Brink et al., 2018) . In protocolized toxicity studies, researchers are required to use a set temperature in both acute and chronic tests (e.g., between 18 and 22 °C for Daphnia (OECD, 2012a, 2004), which can underestimate or overestimate the effects of chemicals for realistic temperature scenarios. Therefore, studying a range of temperatures, including low and high temperatures, is critical to understanding the interactive effect of temperature on chemicals (Hooper et al., 2013; Moe et al., 2013).

The key to understanding chemical toxicity is comprehending its toxicokinetics inside the organism. Toxicokinetic (TK) processes are the chemical uptake into the organism, its biotransformation inside the organism, and finally, the elimination of the chemical out of the organism. The temperature can influence these kinetic processes by speeding up the underlying physiological mechanisms. The frequently proposed mechanism for the uptake rate is an increase in the organism's metabolic activity with rising temperatures, leading to an increase in oxygen demand (Pörtner, 2010). Additionally, the oxygen concentration in water decreases at higher temperatures. To counter the oxygen deficiency, the organism may increase its ventilation rate (Camp and Buchwalter, 2016) simultaneously increasing the uptake of contaminants present in the water (Buchwalter et al., 2003). The temperature influence on the elimination rate can be the same mechanism as the uptake (i.e., when the compound is eliminated via diffusion across the gills), or it can be driven by the temperature influence on biotransformation. The biotransformation of neonicotinoids in invertebrates is mediated by microsomal cytochrome P450 monooxygenases (CYP450s) (Casida, 2011; Honda et al., 2006). Like all enzymes, these enzymes have a temperature at which their catalytic performance is optimal (Topt). Thus, if temperature increases from below their Topt towards it, we can expect increased biotransformation rates. However, only limited knowledge exists on the influence of temperature on TK processes of imidacloprid (IMI) (Camp and Buchwalter, 2016), while this has not been studied to our knowledge for flupyradifurone (FPF), which is one of the alternative to IMI (Huang et al., 2022a).

In addition, current ecotoxicity studies are mainly conducted over a short period (4 to 7 days) and focus on lethal effects (Schuijt et al., 2021). For example, it was previously shown that the acute lethal effects of IMI on several aquatic arthropods were higher at higher temperatures (Camp and Buchwalter, 2016). However, the life-history traits of organisms, such as feeding rate, growth, and reproduction, may be influenced by temperature as well

and also govern the population dynamics (Macaulay et al., 2020; Tran et al., 2020; Vellinger et al., 2012). Hence, the impact of temperature on the long-term effects of chemicals on lethal and non-lethal endpoints needs further investigation.

The present study uses IMI and FPF because of their high water solubility (log Kow value 0.57 for IMI and 1.2 for FPF) and environmental persistence. The dissipation of IMI in water merely depends on photolysis with a half-life ranging from 1 day to 150 days (Morrissey et al., 2015a; Sumon et al., 2018). For FPF, the half-life in an outdoor microcosms study was 63.9 days (Glaberman and White, 2014; Sanford and Prosser, 2020). IMI is one of the most used insecticides worldwide (Macaulay et al., 2020). The environmental concentration of IMI in surface water ranges from ng · L-1 to µg · L-1 levels (Morrissey et al., 2015a; Sánchez-Bayo et al., 2016). Many studies showed the toxicity of IMI towards aquatic systems (Morrissey et al., 2015a). Based on an acute species sensitivity distribution (SSD), the hazardous concentration 5th percentiles (HC05) of IMI was reported as 0.36 µg · L-1 in a recent study (Huang et al., 2022a). Besides, IMI is well known for its delayed or cumulative adverse effect caused by generating a bioactive metabolite, imidacloprid olefin (IMI-ole) (Huang et al., 2021). The new butenolide pesticide FPF is considered a safer alternative to IMI (Giorio et al., 2021). To the best of our knowledge, there is only little monitoring data of FPF with the highest detected concentration of 0.16 µg · L-1 in a watershed of Canada (Metcalfe et al., 2019). Lately, several studies have found that FPF showed acute toxic effects on aquatic species (Bartlett et al., 2018; Huang et al., 2022a; Maloney et al., 2020). The HC05 of FPF was 15 µg · L-1 based on the acute SSD (Huang et al., 2022a). Current knowledge of the biotransformation FPF suggests that it has no or less toxic metabolites (Jeschke et al., 2015a).

Gammarus pulex belongs to the family of amphipod crustaceans that spends its entire life cycle in water and is one of the most common and essential invertebrate species in streams of Northern Europe (Cold and Forbes, 2004). As a detritivore, it plays a vital role in the degradation of leaf litter in aquatic systems (Dangles et al., 2004). A previous study has found that IMI could inhibit the feeding rate of *G. pulex* (Agatz et al., 2014). Moreover, *G. pulex* is a frequently used aquatic species in toxicity studies since it is sensitive to temperature and chemicals (Agatz and Brown, 2014; Sutcliffe et al., 1981; Vellinger et al., 2012).

The objective of this study was to explore the influence of temperature on the effect of the two insecticides on *G. pulex*. As temperature influences on the TK may change the actual internal exposure to the chemical and, therefore, indirectly affect the apparent chemical's toxicity to the organism, we conducted both a systematic evaluation of the temperature influences on TK and toxicity. The choice of temperature ranges was based on the thermal windows of *G. pulex* (Maazouzi et al., 2011; Moenickes et al., 2011) and the yearly field

temperature of the site where we collected the organisms (ranging from 7 to 24 °C, depending on exposure time). We hypothesized that increasing temperature would enhance the effect of insecticides on both lethal and sublethal endpoints (immobility, food consumption, growth, fresh weight, dry weight, and water content).

2.2. Materials and methods

2.2.1 Chemicals and test organisms

Imidacloprid (IMI; CAS: 138261-41-3), its bioactive metabolite imidacloprid-olefin (IMI-ole; CAS: 115086-54-9), flupyradifurone (FPF; CAS: 951659-40-8) and its metabolite 6-chloronicotinic acid (6-CNA; CAS: 5326-23-8) were obtained from Sigma Aldrich. Stock solutions of IMI and FPF were dissolved into MiliQ water. Imidacloprid-d4 (IMI-d4; CAS: 1015855-75-0) was used as an internal standard during the analytical measurements of any organism samples. Stock solutions of IMI-d4 (200 µg · mL-1) were dissolved into 2 % acetone (v:v) to ensure that the compound was fully dissolved.

Gammarus pulex was collected from an uncontaminated brook, the Heelsumse brook (coordinates 51.973400, 5.748697) in July (for TK experiments) and December (for chronic experiments of IMI and FPF) of 2020. This brook is groundwater-fed and cool in summer. That brook's yearly water temperature range is from 4 °C to 17 °C based on personal observation. The experimental temperatures 7, 11, 15, 18, and 24 °C are within the thermal tolerance of the organism, as *G. pulex* has a temperature optimum of 10-20 °C and an upper thermal limit of 27-33 °C and an lower limit in previous experiments as 0 to 5 °C (Maazouzi et al., 2011; Moenickes et al., 2011; Sutcliffe et al., 1981).

2.2.2 Toxicokinetic (TK) experiments

Juvenile organisms with an average length of 6.87 mm (sd: 0.96 mm) were brought to the laboratory, counted, and separated into three groups. After 12 h acclimatization to the laboratory conditions at catchment temperature (14 °C) and a 12:12 h light:dark cycle, the individual water bath compartments were adjusted to 7, 18, and 24 °C at a rate of 0.5 °C per hour. The organisms were kept at these experimental temperatures for another minimum of 24 h. During the whole acclimatization procedure, the organisms were fed with Populus leaves ad libitum.

During the experiment, a replicate system consisted of ten individuals in a 1.5 L glass jar filled with 1 L groundwater retrieved from the Sinderhoeve experimental station (the Netherlands; www.sinderhoeve.org). We placed a piece of metal mesh in each jar as a substrate for the organisms to increase the surface area on which they can sit on or attach

to, aiming to prevent cannibalistic behavior. During the uptake phase, the organisms were exposed to either 17.62 (sd: 0.49) µg · L-1 IMI or 18.24 (sd: 1.00) µg · L-1 FPF. The exposure concentrations were 0.1 times the 50 % effective concentration after 2 days of exposure (48h, EC50) of *G .pulex* for IMI and FPF, respectively (Huang et al., 2022a, 2021).

Internal concentrations were measured after 6, 24, and 48 h in the uptake phase and after 72, 96, and 120 h in the elimination phase. After 48 h, all remaining organisms were transferred to new jars with uncontaminated groundwater for the elimination phase. At each time point, three exposed replicates were sampled destructively. Organisms' survival was monitored throughout the whole experiment. At each time point, the respective jars were removed from the water bath, the organisms were washed with demineralized water, quickly dried on a paper towel, weighed to get the fresh weight, and frozen at -20 °C before further analysis of the internal concentration of the chemicals in the organisms.

2.2.3 Toxicokinetic (TK) modeling

Considering the generation of metabolites, different TK model types were used for IMI and FPF. As no metabolites were measured in the organism samples exposed to FPF, a simple one-compartment first-order TK model was calibrated on the measured internal concentrations for each temperature (Supplementary data Text S1, Table S1, eq. 1). For the exposures to IMI, no metabolite was detected at 7 °C, so this data set was also calibrated to a simple one-compartment model. During the elimination phase in the experiments conducted at 18 and 24°C, IMI-ole was detected. Thus, these results were calibrated to a one-compartment TK model with metabolite, considering the biotransformation of IMI into IMI-olefin (Supplementary data Text S1, Table S1, eq. 2-3).

All model calibrations were performed in the software Matlab (2020b), starting from scripts available within the Bring Your Own Model (BYOM) modeling platform (www.debtox.info/byom.html, Version 5.2). Matlab scripts that were used can be downloaded from GitHub (https://github.com/NikaGoldring/Toxicokinetic-models-for-pesticides-in-Gammarus-pulex). The model parameters (Supplementary data Text S1, Table S1) were estimated based on the Nelder-Mead simplex optimization algorithm provided in the BYOM platform and their confidence intervals were generated applying the likelihood region method.

2.2.4 Chronic experiments

Chronic experiments of 28 days were performed with *G. pulex*. After field collection, healthy juvenile individuals (without parasite seen as an orange dot on the back) with similar lengths

(around 5 mm) were randomly selected and put into three buckets with a mixture of field water and pre-aerated groundwater from the Sinderhoeve experimental station (the Netherlands; www.sinderhoeve.org). *G. pulex* was acclimatized in three water bath sections at field temperature (11 °C) for two days. Afterward, the temperature in each section was gradually increased or decreased to the experimental temperatures at a rate of 0.5 °C per hour. The intended temperatures were 7 ± 1 °C, 11 ± 1 °C and 15 ± 1 °C. After each section reached its experimental temperatures, *G. pulex* was acclimatized for at least two days. During the acclimation period, organisms were fed leached Populus leaves ad libitum. A light:dark regime of 12:12 hours was used. Previous chronic pilot study (at 7, 18 and 24 °C) found that the control mortality at 18°C and 24°C was above 20% after 28 days experiment (data not shown), thus we selected 7, 11 and 15 °C in the formal chronic experiment.

Experiments were performed with three replicates per treatment level and five replicates for controls. In addition, 5 concentration levels plus control were used. The experimental setups are in line with OECD requirements (OECD, 2004). At the start of the experiment, each replicate consisted of 11 individuals added to 1 L groundwater, after which a volume was dosed to reach a concentration of 0, 0.3, 1, 3, 10 or 30 µg · L-1 for both IMI and FPF. The selection of the concentration was based on previous chronic IMI and FPF test results at 18°C (Huang et al., 2022a; Roessink et al., 2013). Gentle aeration was provided in the test systems. Immobility and mortality were monitored every 2 to 3 days during the experiment based on a method described in Roessink et al. (2013) (Roessink et al., 2013). Individuals were scored as immobile when no movement of any kind, except for the heart, was observed for a period of 20 s and were scored as dead when no response of any kind was observed during 3 to 5 s of gentle stimulation using a Pasteur's capillary pipette. Dead organisms were removed from the test vessels. Water samples were taken every week to measure the exposure concentrations of the analytes (section 2.6), and the stability of chemicals were verified. In addition, we renewed the system every two weeks, all remaining animals were genteelly transferred to new medium.

The food consumption of *G. pulex* was measured every two weeks in this study. The pre-treated (i.e., leached in stream water then progressively acclimatized to the test water before use) Populus leaves were cut into circles with the same surface area (3.2 cm radius) using a cork borer and dried at 60 °C for at least 48 h (McGrath et al., 2007). Two pieces of dry leaf discs were provided for every replicate. The dry weight of the leaves of each replicate was recorded before adding them into the system. The dry leaves were added to each replicate 3 days before the organisms and the chemical to allow the leaves to soak in the water. The leaves in the test jars were changed every two weeks together with the refreshment of the system. The weight of the remaining leaves was recorded after drying at 60°C in the oven for at least 48 h. Two jars with only stainless-steel mesh and conditioned

Populus leaves, and no *G. pulex*, were installed to estimate the microbial degradation of the leaves. The food consumption of each replicate was calculated as the difference between the initial leaf's weight and the remaining leaf's weight after the loss was corrected for microbial degradation (Eq. 2.1 and Eq. 2.2).

Dry mass (DM, mg) of leaves consumed by *G. pulex* per jar (L_e) after two weeks was calculated as:

$$L_e = L_i - L_f - Lc \quad \text{(Eq. 2.1)}$$

Where $L_i$and L_f are the initial and final dry mass (mg) of leaves, Lc is the average dry mass loss of the control group accounting for microbiological degradation.

To obtain the food consumption per organism, we divided the total amount of food consumed per jar by the numeric mean of the remaining organisms at each observation time (Eq. 2.2). The food consumption per organism (F_{total}) after two weeks was calculated as:

$$F_{total} = \frac{L_e}{\frac{\sum(n_1+n_2+n_3+n_4+n_5+n_6)}{6}} \quad \text{(Eq. 2.2)}$$

Where n is the number of remaining organisms at each observation time (1-6), observed on days 1, 4, 7, 9, 11, and 14 in the first two weeks and on days 16, 18, 21, 23, 25, and 28 for the last two weeks.

To obtain the food consumption F per individual per day, we divided F_{total} by the two weeks period (Eq. 2.3).

$$F = \frac{F_{total}}{14} \quad \text{(Eq.2.3)}$$

The internal concentration, fresh weight, dry weight, and water content of the remaining organisms were measured at the end of the experiment (28 day). For fresh weight, individuals from the same jar were dabbed dry and weighed on a microbalance (0.1 mg). Then the samples were frozen for 12 h at -20 °C and freeze-dried for ≥24 h, after which dry weight was measured. The water content of the organisms from the same jar was calculated by the difference between the fresh and dry weights. The internal concentration measurement is described in section 2.6.

The physicochemical water parameters, dissolved oxygen, pH, electrical conductivity, and temperature were measured only in the control and the highest treatment weekly. The results are provided in the raw data of water quality parameters in Mendeley data (Huang et al., 2022c).

2.2.5 Size measurement of *Gammarus pulex*

The initial size of *Gammarus pulex* was measured in both TK and chronic experiment. The body length of *G. pulex* was measured from the anterior margin of the caput to the posterior end of the pleon (not including telson), along with the curved shape of the pereon (Figure S5). Each organism was observed under the microscope with a reference object for scale. The program ImageJ (1.53, National Institute of Health, USA) was used for image analysis and length measurements (Figure S5). In the chronic experiment, after 28 days experiment, the sizes of the remaining organisms were measured too, and the results were presented in Figure S6. The initial size of *G. pulex* in TK experiment was 6.9 ± 0.9 mm, and in chronic experiment, the initial size in the FPF experiment was 5.7 ± 0.7 mm, while it was 4.2 ± 0.7 mm in the IMI experiment (Huang et al., 2022c).

Note that the timing of collection may affect the results, but we exclude this influence with two reasons. The first one is in both TK and chronic experiment, we selected similar sized organisms to ensure their consistence (age is not applicable as we worked with organisms from field catchment); secondly, TK experiment were conducted in May, and chronic experiment were conducted in December, both animals can be considered a "summer generation" which have not experienced the cold winter in Netherland (which is during Jan-April).

2.2.6 Chemical analyses

Groundwater and surface water have been analyzed by LC/MS-MS to confirm the absence of all the tested analytes. The light in the experiment did not contain ultraviolet light to prevent the photodegradation of FPF and IMI which was confirmed by the analytical measurement with LC/MS-MS. The chemical stability of both IMI and FPF in the 2 days TK and the 28 day chronic experiments was verified by the water samples measurement performed at every timepoint in TK tests or every week in chronic tests (Huang et al., 2022c).

All water and organism samples were analyzed by reversed-phase liquid chromatography-tandem mass spectrometry (LC-MS/MS) based on the measurement of IMI as described by (Huang et al., 2021). The analyses were performed on an Agilent 1260 Infinity liquid chromatography coupled with a 6460 Triple quad mass spectrometer (Agilent Technologies, USA). Separations were carried out on an Agilent Eclipse Plus C18 column (4.6 × 150 mm, 5 µm) at 40 °C. The injection volume of the samples was set at 10 µL. The mobile phase used was MeOH + 0.1 % Formic acid (C) and Milli-Q water+ 0.1 % Formic acid (D) with the following multistep gradient: 0-1.5 min: 90/10 (C/D, v:v); 1.5-2.5 min: 90/10 (C/D, v:v) to 50/50 (C/D, v:v); 8 min: 50/50 (C/D, v:v); 8-8.1 min: 50/50 (C/D, v:v) to 0/100 (C/D,

v:v); 9 min: 0/100 (C/D, v:v); 9-9.1 min: 0/100 (C/D, v:v) to 90/10 (C/D, v:v); 9.1-12 min: 90/10 (C/D, v:v) at a flow rate of 0.7 mL · min^{-1}. The mass spectrometer was operated using an Agilent jet stream electrospray ionization source in positive mode. Nitrogen was used both as nebulizer and collision gas, the capillary voltage was 5000 V, and the temperature of the ion source was set at 300 °C. The compounds were detected in the multiple reaction monitoring using two transitions per compound. The MS/MS transitions of all compounds are provided in Supplementary data in Text S2, Table S4.

Injected samples were quantified by peak area using the calibration curve constructed from the calibration standards included in the same sample sequence. Agilent Masshunter software (version 8.0) was used for instrument control and data acquisition. The extraction recovery of FPF and IMI in the organisms, evaluated at two concentrations by spiking them into the clean organisms, were acceptable based on recovery and repeatability. The limit of quantification (LOQ) of IMI in water samples was 0.01 µg · L^{-1}, 0.45 µg · kg^{-1} in organism samples; and the LOQ of FPF in water samples was 0.06 µg · L^{-1}, 4.6 µg · kg^{-1} in organism samples. The results of all water samples and internal concentration samples were above LOQ. For further information on analysis methods and recovery results, see Supplementary data Text S2, Table S4-S7.

2.2.7 Data analysis

Data analysis for mortality and immobility. The mortality and immobility observed during the IMI or FPF experiment period were analyzed using generalized linear mixed models (GLMMs) with a binomial error structure (dead vs. alive and immobile vs. alive and mobile) and logistic regression function. Temperature and concentration were fixed factors, the exposure time was the covariate variable, and the jar number was the random factor. In addition, three types of interactions, temperature:concentration, temperature:time, and concentration:time, were included. The interaction of temperature:concentration:time was not significant in any case; thus, it was not included in the GLMM. $\chi 2$ and p-values of each factor or interaction in generalized regressions were calculated with the 'car' package (Fox and Weisberg, 2018) in open-source software R version 4.0.5 (Ritz et al., 2015).

In addition, the statistical analysis of NOEC at each temperature was based on the OECD guideline (OECD, 2006). The dose-response relationship for lethal (mortality) and sublethal endpoint (immobility) of IMI and FPF at each temperature was fitted using the log-logistic regression, using GenStat (15th edition, Laws Agricultural Trust; VSN International) (Roessink et al., 2013).

Data analysis for other sublethal endpoints. Sublethal endpoints, such as food consumption and dry weight, were compared among concentration levels and temperatures.

The assumption of normally distributed data was evaluated using the Shapiro-Wilk test, while the assumption of equal variance was assessed using a Spearman rank correlation between the residuals and the dependent variable. Data were expressed as mean ± standard deviation. A two-factor analysis of variance (ANOVA) was used to analyze the main effects of temperature and concentration and to detect an interaction between these two variables. The Tukey procedure was used to compare individual means, and a p-value of <0.05 was considered statistically significant. Post-hoc pairwise comparisons of significant interactions were made using Tukey contrasts with the TukeyHSD function in the package of "agricolae" in R (version 4.0.5).

2.3. Results and discussions

2.3.1. Toxicokinetics of IMI and FPF at different temperatures

All raw data of this study can be obtained from our Mendeley Data (Huang et al., 2022c). The measured internal concentrations of IMI and FPF in *G. pulex* showed a steep increase within the uptake phase (i.e., up to day 2) and decreased during the elimination phase (Figure 2.2). The internal concentration of IMI on day 2 was lowest in the 7 °C treatment (with an average concentration across replicates of 62 µg · kg-1, compared to 89 µg · kg-1 at 18 °C) and highest in the 24 °C treatment (with 100 µg · kg-1), suggesting an increased uptake with increasing temperature. The opposite trend was observed for FPF, however, with a smaller effect size, as average concentrations were of the same order of magnitude across temperatures, with 46 µg · kg-1 at 7 °C, 42 µg · kg-1 at 18 °C, and 40 µg · kg-1 at 24 °C. Additionally, the replicated measurements for the internal concentration of FPF at 7 °C showed a larger variation compared to the values measured at the other temperatures (Figure 2.2, B1, black triangles). The final internal concentration on day 5 (end of the elimination phase) did not differ much among temperatures for IMI (57 µg · kg-1 at 7 °C, 64 µg · kg-1 at 18 °C, and 59 µg · kg-1 at 24 °C). In contrast, it was lowest in the 24 °C treatment for FPF (with 15 µg · kg-1, compared to 30 µg · kg-1 at 7 and 18 °C). From this, we observe that both compounds' elimination increased with increasing temperature.

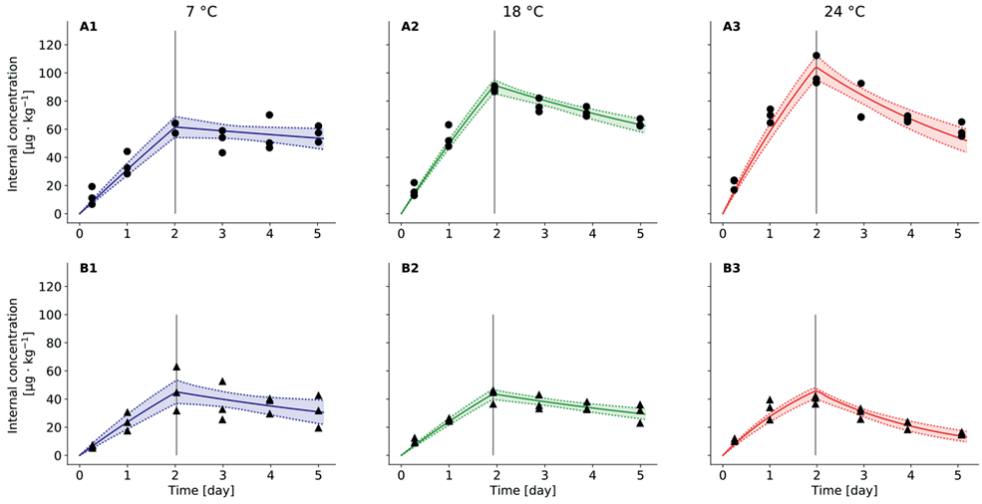

Figure 2.2: Internal concentrations and toxicokinetic models of imidacloprid (IMI) and flupyradifurone (FPF) at different temperatures in *Gammarus pulex*. Black dots for IMI (A1-A3) and triangles for FPF (B1-B3) are measured internal concentrations in µg · kg^{-1} at 7, 18, and 24 °C, respectively. Solid lines are the TK model fits with lower and upper confidence intervals (dotted lines). The grey vertical line represents the transition timepoint from the uptake to the elimination phase for each temperature and chemical.

The model calibration for each dataset separately (Figure 2.2) resulted in three parameter sets, one for each temperature (Supplementary data Text S1, Table S2-3). These parameters reflect the same pattern previously described by increasing uptake and elimination rate constants with increasing temperature for IMI and FPF. However, the temperature influence was different between parameters (i.e., for IMI, a 2 fold-difference for k_u and a 3.6 fold-difference for k_e) and between the two insecticides (with only a 1.3 fold-difference for k_u and a 3.1 fold-difference of k_e for FPF).

For IMI, increased uptake with increasing temperature was previously reported within a range of aquatic invertebrates (Camp and Buchwalter, 2016). However, no elimination kinetics was evaluated in their study, leaving limited grounds for concluding statements about temperature's effect on the bioconcentration of IMI. In our study, the calibrated parameters could be used to calculate the kinetic bioconcentration factor (BCF_{kin}) for each temperature. For both insecticides, the BCF_{kin} decreased with increasing temperature. However, the BCF_{kin} for FPF at the lowest and the medium temperature was practically the same with 11.2 L·kg^{-1} at 7 °C and 11.0 L·kg^{-1} at 18 °C, while there was a linear decrease observed for IMI (Supplementary data Text S1, Figure S1).

Another difference between the two insecticides concerns the presence of biotransformation products. No metabolite was detected in the organisms exposed to FPF at any temperature, whereas the metabolite IMI-olefin was detected during the elimination period of the

exposures to IMI at 18 and 24 °C (Figure 2.3). The metabolite formation rate k_m increased from 0.023 L · kg^{-1} · d^{-1} at 18 °C to 0.051 L · kg^{-1} · d^{-1} at 24 °C. The metabolite elimination rate also increased with increasing temperature from 0.69 L · kg^{-1} · d^{-1} at 18 °C to 0.87 L · kg^{-1} · d^{-1} at 24 °C.

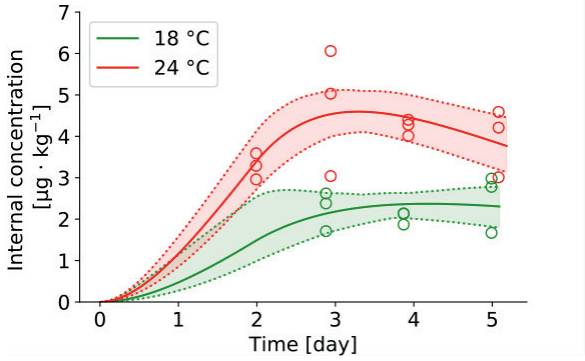

Figure 2.3: Internal concentration and toxicokinetic model of imidacloprid-olefin (IMI-ole) at different temperatures in *Gammarus pulex*. Empty green and red circles are measured internal concentrations of IMI-ole in µg · kg^{-1} at 18, and 24 °C, respectively. Solid lines are the TK model fits with lower and upper confidence intervals (dotted lines).

Interestingly, no metabolites were found in the organisms after the 28-day exposure of the chronic toxicity study at any concentration or temperature. For this, we see two possible explanations i) the metabolites are further degraded and thus not measured after 28 days, or ii) the metabolites are not produced at the temperatures used in the chronic experiments (i.e., 15 °C). With regards to the first consideration, to our knowledge, no studies have measured the internal concentrations of long-term exposure to IMI in aquatic species. A previous study found that IMI was biotransformed into IMI-ole in G. pulex (Huang et al., 2021). However, this study performed an acute (short time, i.e., 6 days) exposure. IMI-ole can be further biotransformed to 6-CNA in *G. pulex* (Huang et al., 2022d). In addition, IMI can be biotransformed to some intermediates which were not checked for in our LC-MS/MS analysis (Fusetto et al., 2017; Suchail et al., 2001). In line with the second consideration, the temperature may influence biotransformation. While IMI-ole was detected in the TK experiments conducted at 18 and 24 °C, the highest temperature in our chronic study was 15 °C. We speculate that 15°C might inhibit or delay the biotransformation process of IMI. Nevertheless, we did not measure the internal concentration over time during the chronic exposure experiment. Thus, we are limited in interpreting the internal concentration measured at the end of the 28 days experiment.

2.3.2. Lethal effects of IMI and FPF at different temperatures

The chronic results after 28 days. In all chronic experiments, the water concentration of FPF and IMI was stable during 28 days experiment and within 20 % deviation with nominal concentration. Thus, the nominal concentration was used in reporting the result below.

The control mortality at each temperature was less than 20 % (Table 2.1) For the mortality caused by IMI, temperature, concentration, time, the interaction between temperature and concentration, and the interaction between concentration and time explain a significant part of the variation in the data (Table 2.1). The NOEC values for mortality and immobility were the same at each temperature; the values were 10 μg · L-1, 0.3 μg · L-1 and <0.3 μg · L-1, for 7 °C, 11 °C and 15 °C, respectively (Table 2.2). The LC10 and LC50 values were also presented in Table 2.2, which decreased with temperature. Regarding FPF, no significant influence of temperature on the lethal effects was detected by the GLMM model (Table 2.1). However, the LC10 and LC50 values decreased with temperature (Table 2.2). Similar to IMI, for FPF, the NOEC values for mortality and immobility were the same at each temperature; the values were 10 μg · L-1, 3 μg · L-1 and 1 μg · L-1, for 7 °C, 11 °C, and 15 °Ct, respectively (Table 2.2). Compared to previous studies which conducted chronic tests of IMI (Roessink et al., 2013) and FPF at 18 °C (Huang et al., 2022a), the LC50 values at 18 °C were similar to our results at 15 °C in this study, taking into account the relatively large confidence intervals. To be specific, the LC50 of IMI was 33.8 (20.9 – 54.6) μg/L, and the EC50 of IMI was 15.4 (9.80 – 24.1) μg/L at 18 °C (Roessink et al., 2013); the LC50 of FPF was 10.6 (2.4 – 18.8), the EC50 of FPF was 10.6 (4.5 – 16.6) μg/L at 18 °C (Huang et al., 2022a).

Table 2.1: Generalized linear mixed models (GLMMs) of imidacloprid (IMI) and flupyradifurone (FPF) for mortality and immobility. Effects : tem = temperature, conc = concentration.

Chemical	IMI						FPF					
Effect	mortality			immobility			mortality			immobility		
	χ2	Df	P	χ2	Df	P	χ2	Df	P	χ2	Df	P
tem	10.72	2	4.70E-03	18.90	2	7.86E-05	3.36	2	0.19	3.51	2	0.17
conc	23.47	5	2.74E-04	38.58	5	2.88E-07	15.92	5	7.09E-03	21.30	5	7.10E-04
day	15.32	1	9.09E-05	9.82	1	1.72E-03	25.37	1	4.74E-07	27.81	1	1.34E-07
tem : conc	29.28	10	1.12E-03	33.50	10	2.25E-04	16.96	10	0.08	18.46	10	0.048
tem : day	0.86	2	0.65	15.78	2	3.75E-04	1.79	2	0.41	1.04	2	0.60
conc : day	16.36	5	5.88E-03	8.32	5	0.14	11.86	5	0.04	8.84	5	0.12

Table 2.2: Toxicity endpoints for imidacloprid (IMI) and flupyradifurone (FPF) at each temperature after 28 days of exposure. Lethal concentrations (LC_{10} and LC_{50}), effect concentrations(EC_{10} and EC_{50}) with their 95% confidence interval, and the NOEC values obtained for the endpoints mortality, immobility. Temp = temperature in °C and toxicity endpoints in $\mu g \cdot L^{-1}$.

chemical	Temp	LC_{10}	LC_{50}	EC_{10}	EC_{50}	mortality	immobility
	7	9.8 (*)	163.2 (*)	7.8 (1.8 – 34.4)	93.2 (13.3 – 650.1)	10	10
IMI	11	1.5 (0.5 – 4.5)	24.3 (12.0 – 49.5)	1.5 (0.5 -4.3)	20.1 (11.0 – 36.8)	0.3	0.3
	15	0.1 (0.02 – 3.0)	30.1 (5.2 – 174.2)	0.03 (0.0-3.2)	34.5 (4.0 – 294.9)	<0.3	<0.3
	7	10.3 (4.6 – 22.9)	33.7 (21.8 – 52.1)	10.2 (4.7 – 21.9)	31.4 (21.3 – 46.3)	10	10
FPF	11	5.5 (2.6 – 11.7)	18.7 (13.4 – 26.2)	5.4 (2.6 – 10.9)	16.9 (12.2 – 23.3)	3	3
	15	5.1 (2.2 – 12.1)	16.3 (11.2 – 23.8)	5.9 (2.8 – 12.3)	15.9 (11.8 – 22.5)	1	1

Besides, based on the values of NOEC, LC_{10}, and LC_{50} values at each temperature, the observed enhancement of the lethal effects through temperature increase was higher for IMI than for FPF. This finding is consistent with our internal concentration results after 28 days, as we found higher internal concentrations of IMI at higher temperatures (Supplementary data Text S3, Figure S3). An additional factor for the higher toxicity of IMI could lay in its increased biotransformation into the toxic metabolite IMI-ole. Although no IMI-ole was detected at the end of the chronic experiment, we cannot exclude its presence during the course of the experiment.

Our findings are in line with several studies which conducted acute tests. Previous studies have revealed that increased temperature increases the lethal effects of IMI on several aquatic species. For example, higher temperature decreased the time to immobility for *Isonychia* bicolor (Camp and Buchwalter, 2016), and elevated toxicity of imidacloprid was found under the influence of increasing temperature for *Coloburiscus humeralis (Coloburiscidae)* and *Deleatidium spp* (Macaulay et al., 2020). Insecticides are not the only group of chemicals impacted by temperature. Temperature has been identified as an ion transport modifier, leading to increased influx of mayor ions (e.g., 22NA, 35SO4 and 45Ca) with increased temperatures (Orr and Buchwalter, 2020). Additionally, the toxic effects of organic chemicals (Freitas et al., 2019), metals (Bednarska et al., 2017; Haque et al., 2020; Sokolova and Lannig, 2008), and nano plastics (Sulukan et al., 2022) were enhanced by temperature.

Furthermore, a previous study (Sumon et al., 2018) found that a much lower 96h, EC50 value (0.0055 µg · L-1) for an insect species, Cloeon sp. at 27.5 °C compared to Roessink et al. (2013) who tested *Cloeon dipterum* at 18 °C and found a 96h, EC50 of 1.02 µg · L-1 (Roessink et al., 2013). Furthermore, the study also indicates that (sub-)tropical aquatic ecosystems can be much more sensitive to imidacloprid compared to temperate ones due to the higher temperature (Sumon et al., 2018). Thus, together with many other studies, the temperature-enhanced toxicity observed in the present study emphasizes the need to consider this abiotic factor in ecological risk assessment (Heye et al., 2019).

The temporal patterns of chronic toxicity. In addition, we also found differences in the temporal toxicity patterns between IMI and FPF. In general, the effects of IMI increased after 14 days of exposure, while the effects of FPF remained almost unchanged (Figure 2.4). Specifically, for IMI, we found that the difference between temperatures becomes more significant over time (Figure 2.4). For example, at all three temperatures, the effect of 1 µg · L^{-1} IMI was below 20 % on day 23 and reached nearly 30 % on day 28 at 15 °C, while the other temperatures remained below 20 % (Figure 2.4, A3). In the 30 µg · L^{-1} IMI treatment (Figure 2.4, A6), the mortality on day 14 at 7 °C, 11 °C, and 15 °C was 9 %,

18 %, and 24 %, respectively. However, these values increased to 21 %, 42 %, and 60 % on day 28, respectively.

To the best of our knowledge, only a few studies investigated the influence of temperature on toxicity in a chronic toxicity test (Macaulay et al., 2021). Macaulay et al. (2021) presented clear time-cumulative toxicity of IMI, which first affected mayfly's mobility after 12 days but eventually caused a strong effect (i.e., impairment) at the end of 36 days of exposure, and the heatwave increased the toxicity of IMI.

Our TK results on biotransformation can explain the observed difference in the temporal toxicity pattern between IMI and FPF. For IMI, the biotransformation rate was higher at higher temperatures, resulting in the formation of the toxic metabolite, IMI-ole. Thus, two compounds, the toxic parent compound IMI and its metabolite IMI-ole, which is less toxic but has a slower elimination rate (Huang et al., 2021), affected the organisms. This combined exposure resulted in an accumulating effect over time, also accelerating with increasing temperature. Since, for FPF, no toxic metabolites were detected, there was no such effect (Huang et al., 2022a). Our results indicated that it is essential to consider biotransformation in temperature assessment for toxicity testing, as also indicated in a recent study (Cerveny et al., 2021). In their study, they discovered that the water temperature affects the biotransformation and accumulation of a psychoactive pharmaceutical, temazepam, and its metabolite in aquatic organisms. They further found that the influence of temperature on accumulation and biotransformation was different in different species (Cerveny et al., 2021).

In conclusion, we observed that temperature enhanced the lethal effects of IMI and FPF, where the enhancement extent was greater for IMI than for FPF, and the influence of temperature on IMI became more significant with time due to its biotransformation.

2.3.3. Sublethal effects of IMI and FPF at different temperatures

The food consumption inhibition. Higher temperatures increased food consumption while IMI and FPF decreased it (Figure 2.5 and Figure 2.6). Furthermore, higher temperatures exacerbated the food consumption inhibition of IMI and FPF (Figure 2.5 and Figure 2.6). For IMI, in the first two weeks, at 15 °C, the food consumption at 1 μg · L-1 was significantly lower than in the control group, while it was 3 μg · L-1 at 11 °C, and there was no significant difference among concentrations at 7°C (Figure 2.5, A1). However, in the late two weeks, only 30 μg · L-1 IMI significantly inhibited food consumption compared to the control at 15 °C (Figure 2.5, A2). For FPF, the food inhibition extent was less than for IMI. Only 30 μg · L-1 significantly inhibited food consumption compared to the control at 15 °C, and only in the first two weeks (Figure 2.6, A1 and A2).

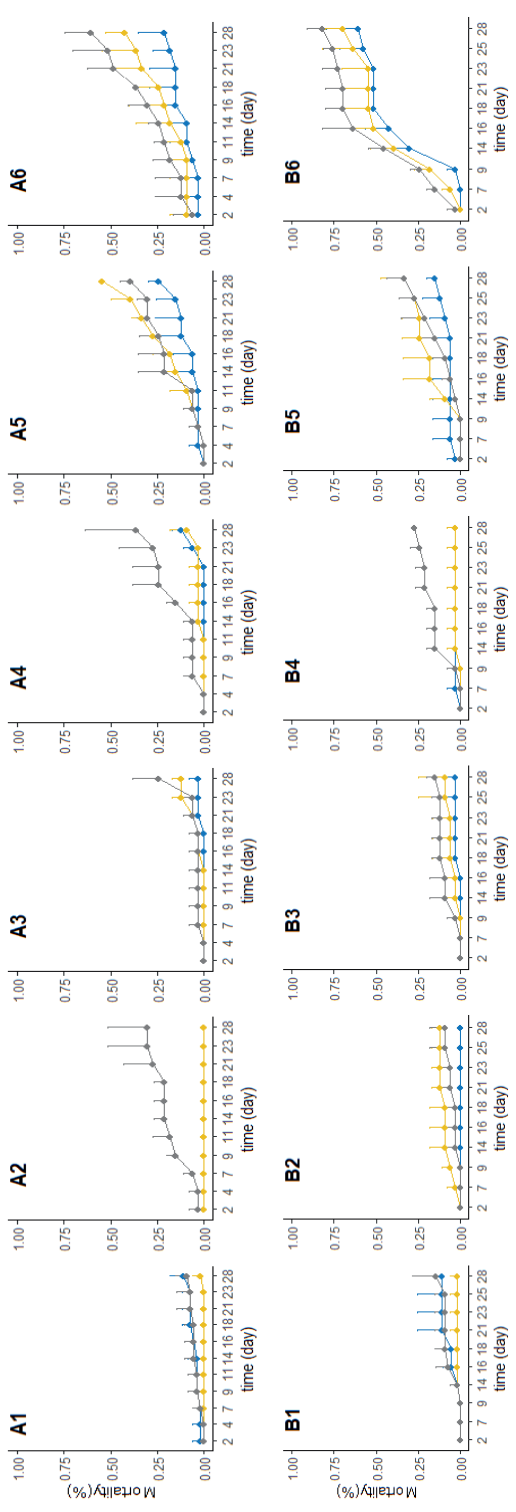

Figure 2.4: The mortality under imidacloprid (IMI, A) and flupyradifurone (FPF, B) exposure over time at 7, 11, and 15 °C. Tiles 1 to 6 represent the control group (0 µg · L^{-1}) and the treatments (0.3, 1, 3, 10, 30 µg · L^{-1}), respectively. Plotted are means + s.d. with n= 5 for control groups and n =3 for treatment groups. tem = temperature in °C

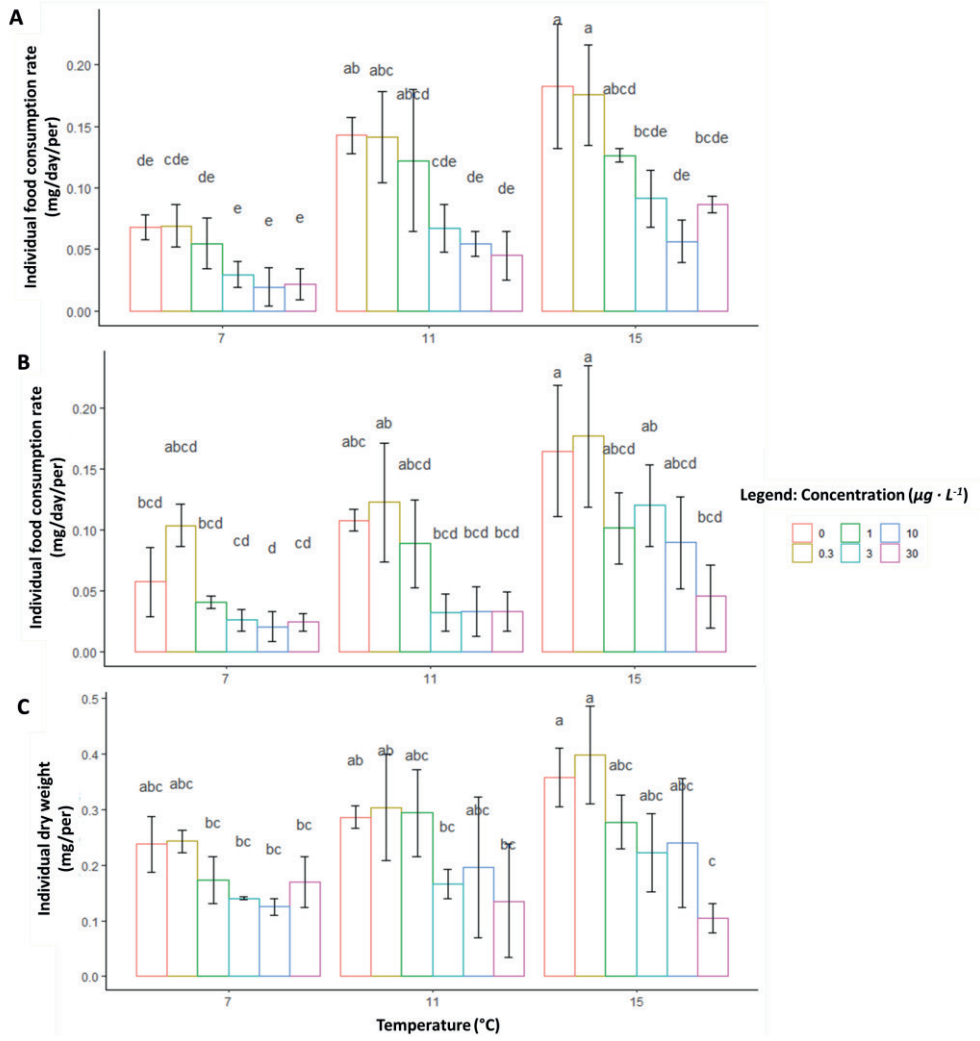

Figure 2.5: Food consumption rates per individual in the first two weeks (A) and the last two weeks (B), and the dry weight of *Gammarus pulex* in the IMI experiment (n = 5 for control, n=3 for treatment groups). Different letters indicate significant differences between clones and treatments, using TukeyHSD ($P < 0.05$). conc = concentrations in μg · L^{-1}, temperature in °C.

Feeding activity is a sensitive sublethal indicator at the individual level, impairing higher levels such as population, community, or ecosystem (Rinderhagen et al. 2000). The detritivorous activity of *G. pulex* is vital to aquatic systems (Dangles et al., 2004). The effects of temperature (Nilsson, 1974) and pesticides have been explored separately in previous studies. Inhibition of food consumption by IMI and FPF has been found (Agatz et al., 2014; Huang et al., 2022a; Nyman et al., 2013a). It was observed that the feeding rate of *G. pulex* was significantly reduced after continuous exposure to 30 μg · L-1 IMI for 4 days

and 15 µg · L-1 IMI for 14 days at 13 °C (Agatz et al., 2014; Nyman et al., 2013a). FPF inhibited the food consumption of *G. pulex* at concentrations higher than 0.3 µg · L-1 after 28 days of exposure at 18 °C (Huang et al., 2022a). Overall, our study showed the effect of temperature and IMI and FPF on food consumption and indicated that the interactive effect is higher for IMI than for FPF.

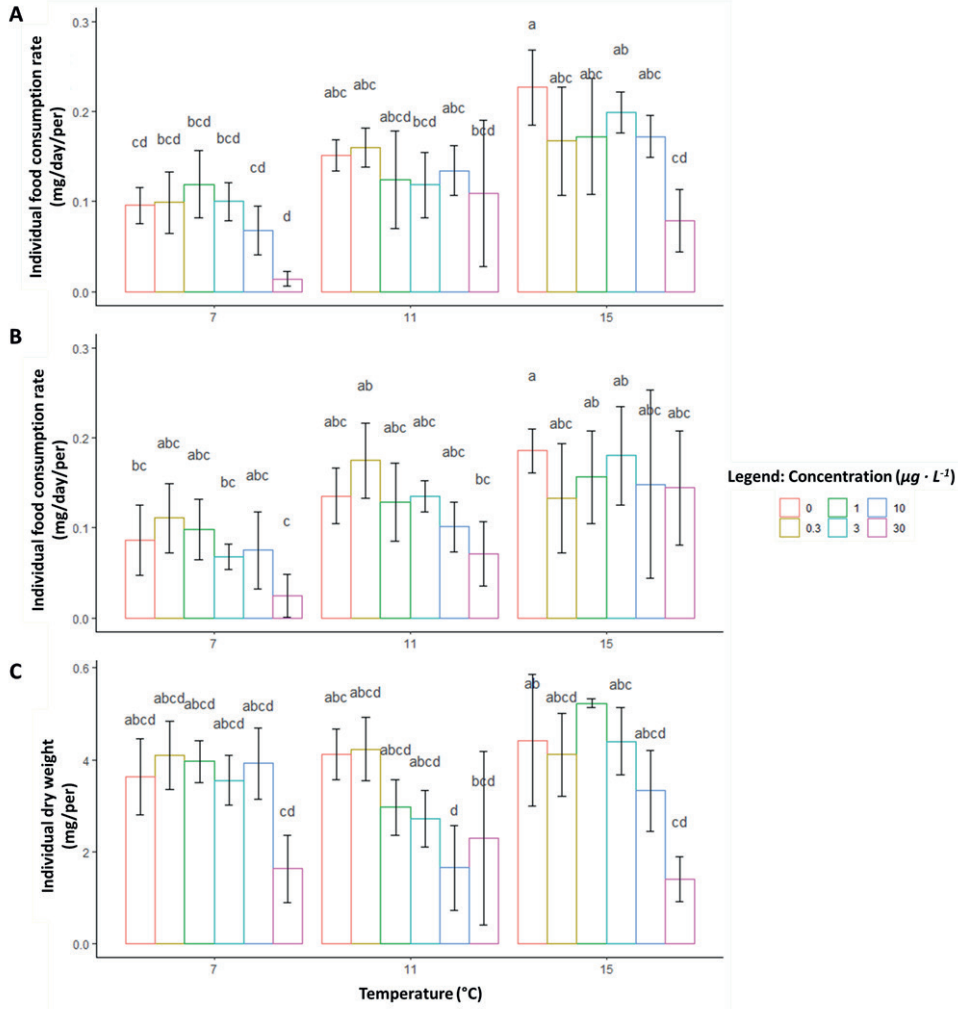

Figure 2.6: Food consumption rates per individual in the first two weeks (A) and the last two weeks (B), and the dry weight of *Gammarus pulex* in the FPF experiment (n = 5 for control, n=3 for treatment groups). Different letters indicate significant differences between clones and treatments, using TukeyHSD ($P < 0.05$). conc = concentrations in µg · L^{-1}, temperature in °C.

To the best of our knowledge, only a few studies have explored the interactive effects of temperature and chemicals on food consumption. In a recent study by Theys et al. (2020), the food consumption of another freshwater isopod, *Asellus aquaticus,* was measured under

exposure to the pesticide chlorpyrifos, combined with increased mean temperature and in the presence or absence of daily temperature fluctuations (DTF) (Theys et al., 2020). They found that organisms' food consumption decreased when exposed to chlorpyrifos and DTF simultaneously.

The influence of temperatures and chemicals on body weight of *G. pulex.* The dry weight results of *G. pulex* were consistent with the food consumption result (3.3.1; Figure 2.5 and Figure 2.6). Higher temperature enhanced food consumption and increased the dry weight of organisms, whereas IMI and FPF exposure inhibited food consumption and decreased weight. The food consumption inhibition by FPF exposure in the last two weeks was not significant, which is consistent with the fresh weight results (Supplementary data Text S3, Figure S4 A and B). The water content increased with chemical treatment and temperature (Supplementary data Text S3, Figure S4 C and D). These results could be related to the physical characteristic of *G. pulex* as a previous study found that the water content of *G. pulex* was higher under higher temperature conditions (Maazouzi et al., 2011). They explained that the chitin exoskeleton fixes the body volume of crustaceans, and the lost tissue mass, used as a metabolic fuel, must be replaced with water to maintain the same body volume (Maazouzi et al., 2011). In line with their findings, we also did not find size differences between treatments at each temperature (Supplementary data Text S4).

2.4. Conclusion

We assessed the effect of temperature on the toxicokinetics and the chronic toxicity of IMI and FPF towards *G. pulex*. For both IMI and FPF, the uptake and elimination rate constants increased with temperature but in different magnitudes. In addition, temperature increased the biotransformation rate of IMI and thus accelerated the generation of the toxic metabolite IMI-ole. Furthermore, we found that higher temperatures increased the toxicity of IMI and FPF over time, where the increase was higher for IMI than for FPF. In addition, the adverse effects of insecticides on sublethal endpoints (i.e., food consumption and dry weight) were exacerbated by elevated temperatures. Overall, our results provided more evidence and understanding of the interaction between increasing temperatures and chemicals' lethal and sublethal effects. Our study indicated the importance of integrating temperature into future toxicity and risk assessments in light of global climate change.

Supporting Information Available

Supplementary data to this article can be found online at:
https://doi.org/10.1016/j.scitotenv.2022.158886

The raw data is provided in the Mendeley repository
https://data.mendeley.com/datasets/6dbgkhzxvx

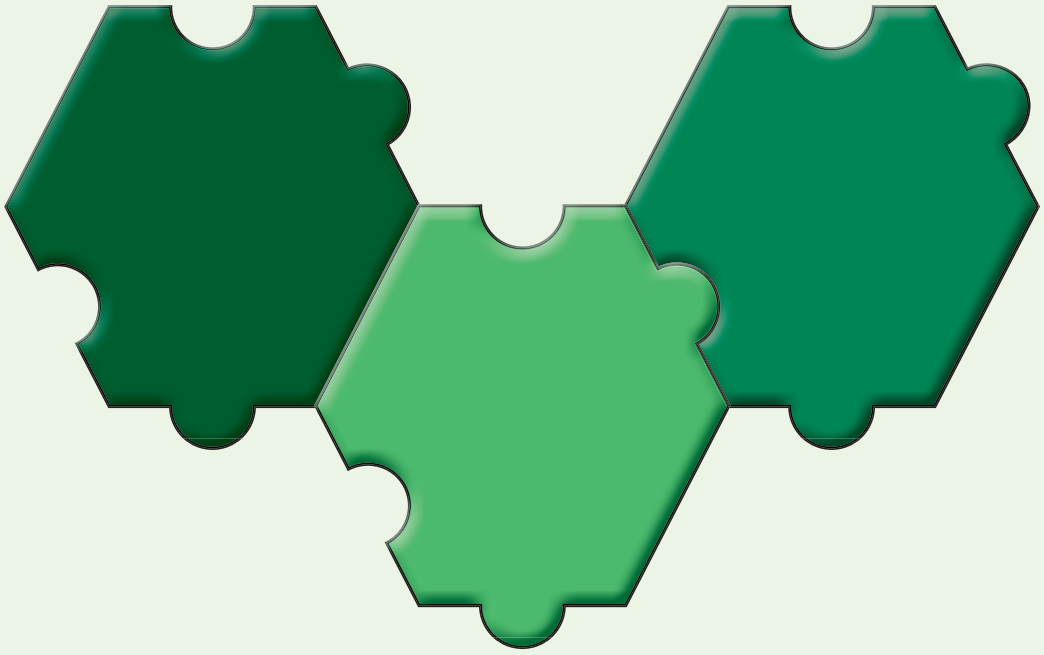

Chapter 3

Explicit consideration of temperature improves predictions of toxicokinetic-toxicodynamic models for flupyradifurone and imidacloprid in *Gammarus pulex*

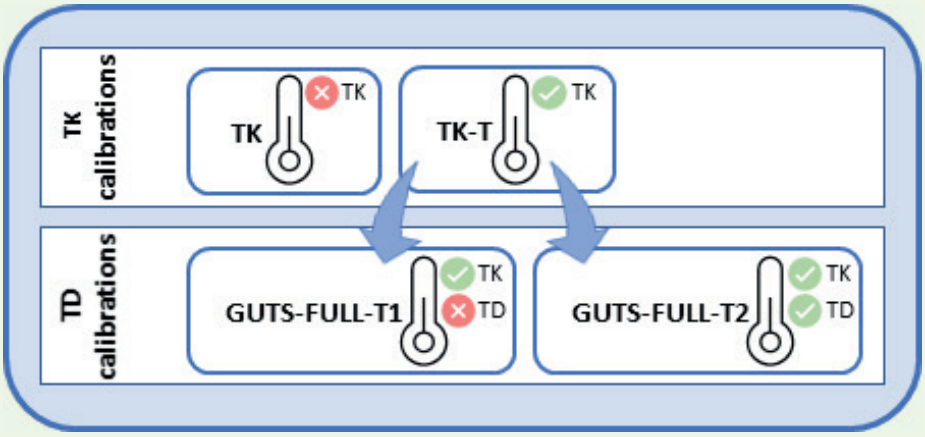

Figure 3.1: Graphical abstract of Chapter 3. Overview of the used toxicokinetic (TK) and toxicodynamic (TD) calibration approaches. A red cross or green check mark indicates whether temperature influences were explicitly modeled for the respective process.

This chapter is based on:
Annika Mangold-Döring, Anna Huang, Egbert H. van Nes, Andreas Focks, Paul J. van den Brink, 2022. Explicit Consideration of Temperature Improves Predictions of Toxicokinetic–Toxicodynamic Models for Flupyradifurone and Imidacloprid in *Gammarus pulex*.

Environ. Sci. Technol. 2022, 56,15920−15929.
https://doi.org/10.1021/acs.est.2c04085

Abstract

In the face of global climate change, where temperature fluctuations and the frequency of extreme weather events are increasing, it is needed to evaluate the impact of temperature on the ecological risk assessment of chemicals. Current state-of-the-art mechanistic effect models, such as toxicokinetic-toxicodynamic (TK-TD) models, often do not explicitly consider temperature as a modulating factor. This study implemented the effect of temperature in a widely used modeling framework, the General Unified Threshold model for Survival (GUTS). We tested the model using data from toxicokinetic and toxicity experiments with *Gammarus pulex* exposed to the insecticides imidacloprid and flupyradifurone. The experiments revealed increased TK rates with increasing temperature and increased toxicity under chronic exposures. Using the widely used Arrhenius equation, we could include the temperature influence into the modeling. By further testing of different model approaches, differences in the temperature scaling of TK and TD model parameters could be identified, urging further investigations of the underlying mechanisms. Finally, our results show that predictions of TK-TD models improve if we include the toxicity modulating effect of temperature explicitly.

3.1 Introduction

As an environmental factor whose variability is intensifying in the course of global climate change, temperature is expected to play an increasing role in the environmental fate and toxic effects of contaminants (Bednarska et al., 2013; Hooper et al., 2013; Noyes et al., 2009b; Polazzo et al., 2022). However, temperature variability is not included in standard toxicity tests of contaminants, which are usually conducted at one constant temperature (e.g., OECD Test No. 211) (OECD, 2012a). Fortunately, an increasing number of studies include the role of temperature on the effect of contaminant toxicity. The majority of such studies using aquatic organisms showed increased toxicity with increasing temperature (reviewed in Heugens et al., 2001, Holmstrup et al., 2010, and Noyes et al., 2009b). Nevertheless, also decreased toxicity with increasing temperatures has been observed, for instance, for DDT (dichlorodiphenyltrichloroethane) and pyrethroid insecticides (Harwood et al., 2009). These contradictory results underline the demand to explicitly consider the impact of temperature in studies for environmental risk assessments (ERA), aiming to reduce uncertainty.

Mechanistic or process-based models, such as toxicokinetic-toxicodynamic (TK-TD) models, are a powerful tool to investigate contaminant's effects and allow screening of many exposure scenarios. In combination with experiments, previous TK-TD model applications have been proven useful to test hypotheses on temperature-modified toxicity and its underlying mechanisms. For instance, Heugens et al., 2003 showed in a model study combined with experiments that the temperature effect on cadmium toxicity of *Daphnia magna* could not be ascribed to accumulation kinetics alone; the altered susceptibility of the daphnids also played a vital role. Nonetheless, how temperature modulates both TK and TD processes is rarely studied. However, there have been proposals (see methods section) on how to account for temperature (Jager and Ashauer, 2018a) in current state-of-the-art effect modeling approaches, e.g., in the widely used General Unified Threshold model of Survival (GUTS) (Tjalling Jager et al., 2011).

GUTS is a TK-TD model framework deemed ready for use in ERA by the European Food Safety Authority (EFSA PPR, 2018). Recently, Gergs et al., 2019 included the effect of temperature in a simplified GUTS model to illustrate temperature's influence on the sensitivity of many species. For their study, they used the reduced GUTS version (GUTS-RED), which does not allow to separately investigate the temperature influence on TK and TD model parameters. To our knowledge, a systematic evaluation of the temperature scaling for both TK and TD parameters has not been done for the GUTS-FULL model.

This research aims to understand the influence of temperature on TK-TD processes through GUTS modeling, applied to toxicity data of the freshwater arthropod *Gammarus pulex* exposed to the insecticides imidacloprid (IMI) and flupyradifurone (FPF). For this, we used

the results of previously published toxicity experiments (Huang et al., 2022a). To account for temperature effects on the TK processes, we applied the widely used Arrhenius equation (Arrhenius, 1889) to correct TK rates for different exposure temperatures (Figure 3.2, TK-calibrations). Further, we investigate if only correcting the TK parameter in a GUTS application is sufficient to account for changes in toxicity at different temperatures or if TD model parameters need to be corrected additionally (Figure 3.2, TD-calibrations).

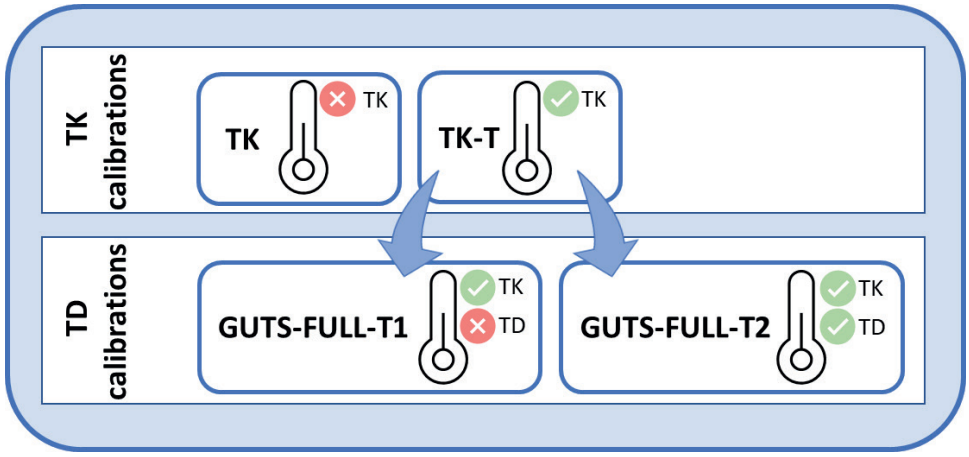

Figure 3.2: Overview of the used toxicokinetic (TK) and toxicodynamic (TD) calibration approaches.

TK calibrations (Data: measured internal concentrations over time)

TK: Datasets from different temperatures are used as replicates, no consideration of temperature.
Assumption: TK is not influenced by temperature

TK-T: Datasets from different temperatures are used simultaneously, explicit consideration of temperature by applying the Arrhenius equation.
Assumption: TK is influenced by temperature and can be captured by the Arrhenius equation

TD calibrations (Data: measured survival over time)

GUTS-FULL-T1: Datasets from different temperatures are used simultaneously, TK-T parameters are used and corrected for temperature by the Arrhenius equation
Assumption: While TK is influenced by temperature, TD is not influenced by temperature

GUTS-FULL-T2: Datasets from different temperatures are used simultaneously, TK-T parameters are used and corrected for temperature by the Arrhenius equation along with TD parameters
Assumption: Both, TK and TD are influenced by temperature

3.2 Materials and methods

Toxicokinetics (TK) and toxicodynamics (TD) in the GUTS framework. GUTS simulates the probability of death of individuals over time, based on TD processes in connection to a simulated internal concentration of an insecticide resulting from its TK (Jager and Ashauer, 2018a). We applied the full version of the model (GUTS-FULL), which is

calibrated on both survival data and internal concentrations. These data were obtained from TK and toxicity experiments previously published (Huang et al., 2022b).

Starting from scripts available within the Bring Your Own Model (BYOM) modeling platform (www.debtox.info/byom.html, Version 6.2), we extended the TK model and GUTS model with a temperature correction. The values for the model parameters (Supporting Information 01, Table S1) were optimized based on the parameter space explorer (Jager, 2021a). With samples of the parameter space explorer, the confidence intervals of model curves were produced. All calculations were performed in Matlab 2021b. Matlab scripts can be downloaded from GitHub (https://github.com/NikaGoldring/Temperature-explicit-TK-TD).

The TK rates are derived from first-order one-compartment models. With this, we represent the organism as one well-mixed compartment. Insecticides are taken up to and are eliminated from this compartment following first-order kinetics. Only limited knowledge of the biotransformation products of the insecticides was obtained. For FPF, no biotransformation products were measured at any temperature, thus, the TK of FPF was described by a simple first-order bioconcentration model (Supporting Information 01, Table S1, eq. S2a). For IMI the metabolite IMI-olefin was only detected in the experiments conducted at 18 and 24 °C after 72 h and 48 h, respectively. Considering the biotransformation of IMI into imidacloprid-olefin (IMI-ole), these results were calibrated to a TK model with first-order metabolism (Supporting Information 01, Table S1, eq. S2b, and S2c).

During the TK model calibrations, we also calculated the kinetic bioconcentration factor (BCF_{kin}) (Arnot and Gobas, 2006) for FPF (eq. 3.1) and IMI (eq. 3.2) based on the calibrated TK rates. For the CIs of the BCF_{kin} values, a sample from the parameter space explorer was used (Jager, 2021a).

$$BCF_{kin} = \frac{k_u}{k_e} \qquad \text{eq. (3.1)}$$

$$BCF_{kin} = \frac{k_u}{k_e + k_m} \qquad \text{eq. (3.2)}$$

The TD processes are based on internal damage D_i (Supporting Information 01, Table S1, eq. S3), which can accumulate in the organism and from which organisms can recover. Model assumptions concerning the mechanism that links this damage to the death of the organism can be either the stochastic death (SD, Supporting Information 01, Table S1, eq. S4 and S5) or individual tolerance (IT, Supporting Information 01, Table S1, eq. S6-S9) approach (Jager and Ashauer, 2018a).

We performed different calibration approaches testing different assumptions on temperature's influence on the model parameters (Figure 3.2). To account for the influence of (experimental) temperature on model parameters, we used the Arrhenius equation (Arrhenius, 1889; Jager and Ashauer, 2018a; S.A.L.M. Kooijman, 2010) (Supporting Information 01, Table S1, eq. S1). The Arrhenius temperature T_A was estimated as an additional parameter along with standard GUTS model parameters. We added two such parameters, T_A-tk and T_A-td, to allow the investigation of temperature influence on the TK and TD parts separately. The resulting models were calibrated to data from the previously published TK experiments (conducted at 7, 18, and 24 °C) and toxicity experiments (conducted at 7, 11, and 15 °C) with *G. pulex* exposed to IMI and FPF (Huang et al., 2022b). Briefly, both experiments were conducted with field caught *G. pulex* from the Heelsumse brook (coordinates 51.973400, 5.748697). During the 5-day period of the TK experiments, the organisms were not fed, and their body size was 6.87 mm, sd: 0.96 mm. Slightly smaller organisms (i.e., 5.23 mm, sd: 1.09 mm) were used during the 28-day chronic exposure, during which organisms were fed with *Populus* leaves.

TK calibrations. Measured internal concentrations of FPF, IMI, and IMI-ole in *G. pulex* were used to calibrate a first-order one-compartment TK model. To evaluate if and how temperature influences the uptake, biotransformation, and elimination of the insecticides, different model calibrations (Figure 3.2, TK calibrations) were done (per insecticide):

(i) for all temperature datasets simultaneously without temperature correction (TK),

(ii) for all temperature datasets simultaneously with temperature correction (TK-T), explicitly considering temperature.

For the TK-T model, we extended the TK models with the Arrhenius equation to correct the rates k_x (i.e., uptake rate k_u, elimination rate k_e, formation rate k_m, and elimination rate of the metabolite k_{em}) for the respective experimental temperatures T, by using eq. (3.3):

$$k_x(T) = k_{x,T_{ref}} \cdot e^{\left(\frac{T_A}{T_{ref}} - \frac{T_A}{T}\right)} \qquad \text{eq. (3.3)}$$

whit the Arrhenius temperature T_A, and the reference temperature T_{ref} (here, 20 °C = 293.15 K). The respective TK-T model for FPF was:

$$\frac{dC_i(t)}{dt} = k_u \cdot C_w(t) - k_e(T) \cdot C_i(t) \qquad \text{eq. (3.4)}$$

with C_w as the exposure concentration (i.e., concentration in the water) and C_i as the internal concentration. Note: k_u was not corrected for temperature (see results section).

And the TK-T model for IMI was:

$$\frac{dC_i(t)}{dt} = \left(k_u(T) \cdot C_w(t) - k_e(T) \cdot C_i(t)\right) - k_m(T) \cdot C_i(t) \quad \text{eq. (3.5)}$$

$$\frac{dC_m(t)}{dt} = k_m(T) \cdot C_i(t) - k_{em}(T) \cdot C_m(t) \quad \text{eq. (3.6)}$$

with C_m as the concentration of the metabolite IMI-ole.

TD calibrations. The survival data of *G. pulex* in all three tested temperatures were used to calibrate the two options of the GUTS model (i.e., GUTS-FULL-SD and GUTS-FULL-IT). Internal concentrations have not been measured in the chronic survival experiments over time. Thus, the previously calibrated TK-T model parameters were fixed in the GUTS-FULL model calibrations (Figure 3.2, TD calibrations).

Model calibration was done in two versions that follow different assumptions: The first version assumes that it is sufficient to correct only the TK parameters (i.e., as in TK-T) to capture the survival probability at different temperatures. In this version, hereafter referred to as GUTS-FULL-T1, TD parameters were calibrated without temperature correction. In the second version, hereafter referred to as GUTS-FULL-T2, besides the TK parameters, also the TD parameters with time in their dimension were corrected with the Arrhenius equation to evaluate the temperature effect (Figure 3.2, TD calibrations). For these GUTS-FULL-T2 models, eq. S3,S4 and S9 were adapted as follows:

$$\frac{dD_i(t)}{dt} = k_r(T) \cdot \left(C_i(t) - D_i(t)\right) \quad \text{eq. (3.7)}$$

$$h_z = b_i(T) \cdot \max(0,\, D_i(t) - m_i) + h_b(T) \quad \text{eq. (3.8)}$$

$$S_{IT}(t) = \left(1 - F\left(D_{i,max}\right)\right) \cdot e^{-h_b(T) \cdot t} \quad \text{eq. (3.9)}$$

Please refer to Supporting Information 01, Table S1 for the parameter explanations.

Model evaluation and toxicity predictions. Finally, we compared the model fits using Akaike's information criterion (AIC). Model fits of the same dataset were assumed to be substantially different if the difference in their AIC values was > 10, (according to Burnham and Anderson, 2002) while the model fit with the smallest AIC value was deemed the best one. Additionally, a visual examination was conducted for the interpretation of the results. With the best-fitting parameter set, we then predicted LC_{10} and LC_{50} values for both insecticides at different temperatures (i.e., 7, 11, 15, 18, 20, 24 °C) with their 95% confidence intervals.

Theoretical considerations for temperature scaling of TKTD parameters. An effect of temperature on the TK-TD model parameter has been assumed previously (Jager and Ashauer, 2018a), although not evaluated quantitatively (but see Heugens et al., 2003). As a starting point, Jager and Ashauer, 2018a discuss the general assumption applied in the Dynamic Energy Budget theory, where all physiological rates scale with temperature in the same way (S.A.L.M. Kooijman, 2010), while pointing out the open question for transferring this approach to the GUTS framework. Here, we provide a brief reflection of the theoretical consideration for temperature scaling of TK-TD parameters, while a detailed rationale for each parameter corrected (or not corrected) for temperature is provided in Supporting Information 01.

With increasing temperature, chemical reactions accelerate, with their rates often following the Arrhenius equation (Arrhenius, 1889). Within this concept, temperature influences the time axis by increasing or decreasing the reaction rate, i.e., speeding up or slowing down the process, respectively. Thus, starting with the most straightforward approach, we can assume that all rates (i.e., parameters that include the dimension of time) scale with temperature. This includes all TK rates, the damage repair rate (k_r), the background hazard rate (h_b), and the killing rate (b_i) of the SD mechanism. Due to the simplifications (or assumptions) made to construct the model, particularly for the central damage concept, it is not trivial to translate the potential mechanisms behind this damage to the real-life scenario. This depends on the compound and the organism.

The mechanism of toxic action for neonicotinoids and other nicotinic acetylcholine receptor (nAChR) agonists, like FPF, has been described in considerable detail (Casida, 2018; Casida and Durkin, 2013; LaLone et al., 2017; Maloney, 2020; Tomizawa and Casida, 2004). Despite this detailed description (see Supporting Information 01) of the adverse outcome pathway (AOP) of IMI, which we also deem to be applicable for FPF, quantifying these processes explicitly is beyond the scope of this research. Nonetheless, the generic damage concept of GUTS indirectly integrates those processes through fitting the measured survival. However, we would like to emphasize that the considerations for the temperature scaling of the TK-TD parameter as further elaborated in the Supporting Information 01, though based on the mechanistic understanding of the AOP for neonicotinoids, are theoretical and not quantitatively confirmed. As such, these considerations should be treated with care when applied to other compounds, organisms and exposure scenarios.

3.3 Results

3.3.1 Toxicokinetic modeling

Disregarding temperature in TK modeling (TK). When using the datasets to calibrate the TK model without considering the experimental temperatures (i.e., treating the datasets as replicates), the model failed to capture the measured internal concentrations for the low and high temperatures (Figure 3.3, blue lines). The TK approach overestimated the internal concentrations of IMI at 7 °C and slightly underestimated them at 24 °C. Reasonably, the model fitted the medium temperature (18 °C) well for IMI, as the measured internal concentrations were in between those from the low and the high temperatures. Similarly, for the FPF datasets, we observed a good fit at 18 °C. Due to the high variation of measured concentrations, the model was within the measured values at 7 °C, whereas it overestimated the internal concentration during the elimination phase at 24 °C.

Temperature explicit TK modeling (TK-T). For the TK-T model, temperature was explicitly considered in the calibration through an additional parameter, the Arrhenius temperature T_A. Comparing the TK-T with the TK model where temperature is not considered, the TK-T results were a better fit, with an AIC difference of 37.9 for IMI and 5.4 for FPF (Supporting Information 02, Table S3).

For the IMI data, the profile likelihoods for the individual parameters were well-defined (Supporting Information 01, Figure S3, plots on the diagonal). Thus, all model parameter and their CIs were identified (Table 3.1). However, the likelihood-based joint-confidence regions showed high correlation of model parameters, specifically k_e and k_{em}, visible in their narrow-shaped bounds (Supporting Information 01, Figure S3).

During the TK-T model calibration for the FPF data, it was noticed that the parameter boundaries for the T_A were not significantly different from zero when correcting both rates (k_u and k_e) with the Arrhenius equation (Supporting Information 01, Figure S4). As k_u for FPF did not differ substantially across temperatures, the TK-T approach could not fit the parameter T_A. Thus, when finally calibrating the TK-T model for the FPF dataset, we did not correct k_u for temperature, but only k_e, which resulted in well-defined confidence regions for T_A (Supporting Information 01, Figure S5). Furthermore, the model with only k_e corrected for temperature resulted in a significantly better fit, i.e., it had an AIC value of 417 compared to 425 for the model with both rates corrected for temperature. An alternative method to address the different temperature sensitivity of the rates would be to introduce separate T_A values for uptake and elimination (i.e., T_A-k_u and T_A-k_e). Though this approach would likely result in a good fit capturing the temperature changes of both rates individually, it would also increase the risk of model overfitting or non-identifiability. We decided to favor the model version with fewer parameters.

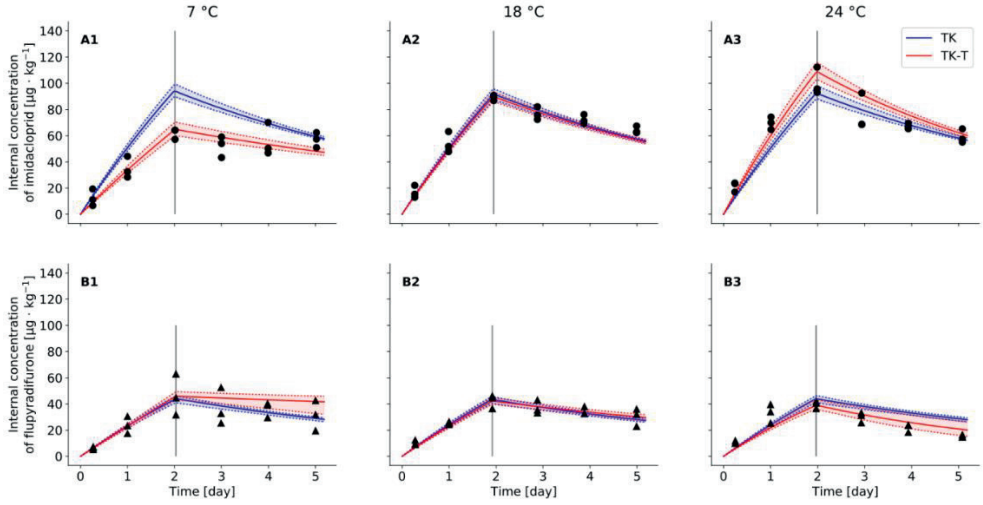

Figure 3.3: Internal concentration of insecticides in *Gammarus pulex* at different temperatures. Black symbols are measured internal concentrations at 7, 18, and 24°C, respectively. Blue solid lines are the TK model fits (without temperature correction), and red solid lines are TK-T model fits (with temperature correction) with lower and upper confidence intervals (dotted lines). The vertical grey line marks the transition timepoint from uptake to elimination phase for each temperature and insecticide. Upper panel A1-A3: imidacloprid; lower panel B1-B3: flupyradifurone.

3.3.2 Effect modeling

Explicit consideration of temperature in effect models. On visual examination, the model calibrations for GUTS-FULL-T1 (i.e., only TK parameters corrected for temperature) and GUTS-FULL-T2 (i.e., also TD parameters corrected for temperature) resulted in reasonable fits to the survival data of *G. pulex* exposed to IMI or FPF (Figure 3.4). For IMI, the survival probability estimated by both models at 11 °C overestimated the measured survival in the 10 µg · L^{-1} treatment, which is related to the experimental data showing no difference between 10 and 30 µg · L^{-1} treatments. Furthermore, the measured survival at 15 °C in the 0.3 and 3 µg · L^{-1} treatments showed a similar pattern as the 10 µg · L^{-1}, which was not well captured by both model fits. Again, the observed survival over time shows no systematic influence of the concentration except for the highest treatment level, so the TK-TD modeling could not fit the observed variations in the lower treatments, which might be predominantly related to variation in background mortality. Slightly better model performance was achieved for the survival data of *G. pulex* exposed to FPF. Here, the survival in the 10 µg · L^{-1} treatment at 7 °C was underestimated and overestimated in the 3 µg · L^{-1} treatment at 15 °C by both models. When focusing on the two highest concentrations tested, the different model applications overlap at the intermediate temperature (11 °C) for both chemicals (Figure 3.4 center panels). While the GUTS-FULL-T1 (blue curves) approach underestimated the survival in lower temperatures and

overestimated it in higher temperatures, GUTS-FULL-T2 (red curves) fitted the survival data obtained at 7 and 15 °C better for both chemicals (Figure 3.4).

The AIC differences between the model approaches also support GUTS-FULL-T2 as the better-performing model. With an AIC difference of 21 for the IMI models and 27 for the FPF models, GUTS-FULL-T2-SD overall performed significantly better than GUTS-FULL-T1-SD (Table 3.1). The same conclusion was obtained for the IT models with an AIC difference of 22 for IMI and 23 for FPF (Supporting Information 02, Table S3). Overall, the AIC value evaluation revealed GUTS-FULL-T2-IT to be the best performing model for IMI and GUTS-FULL-T2-SD for FPF (Table 3.1).

Considering the likelihood-based joint-confidence regions for the model parameter (Supporting Information 01, Figure S8-S15), potential identifiability problems are apparent for both approaches, i.e., GUTS-FULL-T1 and GUTS-FULL-T2. For IMI, the method revealed identifiability problems for the damage repair rate (k_r) parameter in all models and the median threshold for survival (m_i) in SD models (marked with an asterisk Table 3.1).

The exposure of *G. pulex* to FPF caused an effect on the survival, mainly in the two highest concentrations tested (Figure 3.4, B). Here, the model parameter's profile likelihoods presented overall well-defined parabolic shapes (Supporting Information 01, Figure S10, S11, S14, and S15) and identified internal threshold values as significantly different from zero. For both the GUTS-FULL-T1 and the GUTS-FULL-T2 approach k_r ran into the set boundaries of the parameter space explorer for SD models (Table 3.1 and Supporting Information 02, Table S2) and was here as well correlated strongly to the internal threshold values m_i, which ran into the lower boundary in the GUTS-FULL-T2-IT model.

Temperature influences the toxicity of insecticides. With the calibrated parameters of the best-fitting models (Table 3.1), we predicted a 28-day LC50 of 7.89 (95 %-CI: 4.32 - 14.9) µg · L-1 for IMI and 16.7 (95 %-CI: 12.9 – 20.7) µg · L^{-1} for FPF at the reference temperature (20 °C). The LC_{50} predictions at 7, 11, 15, 18, 20, and 24 °C showed a different pattern for both insecticides (Figure 3.5). While LC_{50} and LC_{10} values for IMI decreased with increasing temperature, and remained the same ratio, the LC_{50} values for FPF slightly decreased from 7 to 18 °C and increased again from 20 to 24 °C (Supporting Information 02, Table S4). The LC_{10} for FPF decreased from 7 to 11 °C and then increased with rising temperatures from 15 °C to 24 °C.

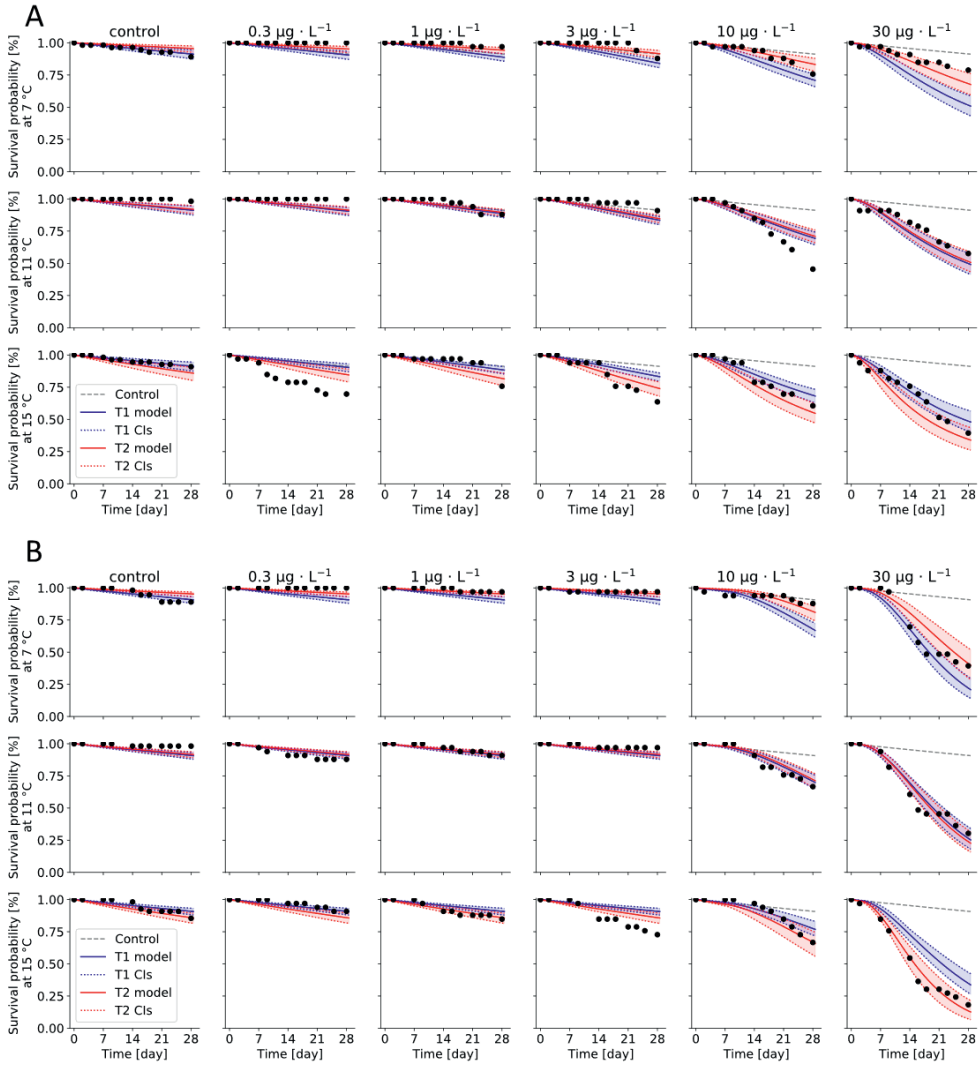

Figure 3.4: Concentration-response curves for the survival of *Gammarus pulex* exposed to imidacloprid (A) and flupyradifurone (B) at different temperatures. Black dots represent the measured survival (replicates pooled) at the different exposure levels in µg · L^{-1} (column headings) and the different temperatures in degrees Celsius (y-axis label). The blue line shows the GUTS-FULL-T1 model (i.e., only toxicokinetic parameters corrected for temperature) prediction for survival, and the dotted blue lines show the boundaries of its 95 % confidence interval (blue area). The red line shows the GUTS-FULL-T2 model (i.e., also toxicodynamic parameters corrected for temperature) prediction for survival, and the dotted red lines show the boundaries of its 95 % confidence interval (red area). The gray dotted line shows the control mortality as modeled under GUTS-FULL-T1 for each temperature. For IMI the IT models are shown and for FPF, the SD models.

Table 3.1: Model parameter for *Gammarus pulex*. For flupyradifurone models, k_u was fitted without temperature correction; thus, the TK-T table eads $k_u(T)$ for imidacloprid and k_u for flupyradifurone. The parameters were estimated for a reference temperature (T_{ref}) set to 20 °C. Parameter symbols are explained in Supporting Information 01, Table S1. CI = confidence interval, AIC = Akaike's information criterion, SD = stochastic death, IT = individual tolerance.

		Imidacloprid				Flupyradifurone			
Parameter	unit	value	95 % CI			value	95 % CI		
Toxicokinetic model parameter TK-T									
$k_u(T)$ or k_u	$L \cdot kg^{-1} \cdot day^{-1}$	3.250	(3.077 - 3.446)			1.313	(1.229 - 1.416)		
$k_e(T)$	d^{-1}	0.140	(0.089 - 0.155)			0.135	(0.118 - 0.158)		
$k_m(T)$	$L \cdot kg^{-1} \cdot day^{-1}$	0.022	(0.014 - 0.068)			-			
$k_{em}(T)$	d^{-1}	0.488	(0.219 - 1.542)			-			
T_A-tk	K	3044	(2316 - 3724)			9243	(1943 - 15870)		
Toxicodynamic model parameter GUTS-FULL-T1		SD		IT		SD		IT	
		value	95 % CI	value	95 % CI	value	95 % CI	value	95 % CI
k_r	d^{-1}	0.069	(0.002 - 10*)	0.001*	(0.001* - 0.017)	1.714	(0.327 - 10*)	0.082	(0.006 - 0.202)
m_i	$\mu g \cdot kg^{-1}$	0.001*	(0.001* - 9)	12	(8 - 182)	69.0	(39 - 101)	284.3	(38 - 412)
h_b	d^{-}	0.004	(0.003 - 0.005)	0.003	(0.002 - 0.005)	3.41^{-03}	(2.51^{-03} - 0.004)	0.003	(0.002 - 0.004)
b_i	$kg \cdot \mu g^{-1} \cdot d^{-1}$	1.28^{-04}	(5.51^{-05} - 0.007)	-		1.40^{-04}	(1.02^{-04} – 1.87^{-04})	-	
Fs	[-]	-		42	(18 - 107)	-		8	(5 - 15)
AIC		1218.40		1219.26		1129.12		1124.72	

GUTS-FULL-T2		SD		IT		SD		IT	
$k_r(T)$	d^{-1}	0.252	(0.001* - 10*)	0.001*	(0.001* - 0.052)	8.372	(1.079 - 10*)	0.145	(3.61^{-05} - 0.590)
m_i	$\mu g \cdot kg^{-1}$	1.00^{-6}*	(1.00^{-6}* - 9.807)	3.4	(2 - 148)	81.9	(50 - 108)	184.2	(0.1* - 333)
$h_b(T)$	d^{-}	0.009	(0.006 - 0.016)	0.011	(0.006 - 0.019)	0.011	(0.007 - 0.017)	0.009	(0.005 - 0.016)
$b_i(T)$	$kg \cdot \mu g^{-1} \cdot d^{-1}$	2.41^{-04}	(1.31^{-04} - 0.031)	-		5.56^{-04}	(3.16^{-04} - 9.46^{-04})	-	
Fs	[-]	-		41	(19 - 101)	-		8	(5 - 15)
T_A-td	K	8510	(4690 - 13170)	12150	(7189 - 17610)	11730	(7342 - 15910)	11310	(6919 - 16140)
AIC	[-]	1196.91		1196.82~		1101.41~		1101.82	

* Boundary of the parameter space explorer

~ Lowest AIC

3.4 Discussion

3.4.1 Toxicokinetic modeling

Explicitly considering temperature improved the TK modeling of IMI and FPF in *G. pulex*. Our results showed an evident temperature influence on the TK of both insecticides. This temperature influence was well captured by the TK-T model calibration (Figure 3.3), supporting the use of the Arrhenius equation to correct for temperature effects on toxicokinetic processes. Furthermore, the previously calibrated TK parameter in Huang and Mangold-Döring et al. can be used for comparison (Huang et al., 2022b). It is important to emphasize that the TK model calibrations on the same datasets in this previous study (Huang et al., 2022b) were done separately for each experimental temperature, i.e., implicitly accounting for temperature. In contrast, the TK-T calibration in the present study accounted for temperature explicitly via the Arrhenius equation using all three temperature datasets simultaneously. Comparing the two different model fits, there is almost no difference (Supporting Information 01, Figure S1). Thus, by explicitly accounting for temperature in the TK-T model, it is possible to describe the toxicokinetic processes of IMI and FPF in *G. pulex* by one parameter set per chemical (Table 1), in contrast to three separate factors parameter sets in the conventional approach previously used (Huang et al., 2022b).

However, the observed temperature influence in the previous study was different between the uptake and the elimination rates (i.e., for IMI, a 2.1 fold-difference of k_u and a 4.9 fold-difference of k_e) and between the two insecticides (with only a 1.3 fold-difference for k_u and a 3.1 fold-difference of k_e for FPF). Thus, with the data currently available for the uptake kinetics of FPF, we found no significant scaling with temperature (also see the reasoning in the results section) and therefore treated this rate to be constant in the TK-T approach. Even though the fit to the data supports removing the temperature correction for k_u in the FPF model, this is no proof that the uptake processes of FPF are not affected by temperature. Assuming diffusion to be the main uptake route, a temperature influence on the uptake is to be expected, although not represented in our data. However, for the elimination kinetics, the 3.1 fold-difference was well captured through the correction with the Arrhenius equation (Figure 3.3).

Furthermore, the scaling of the TK processes with temperature appeared to be different between the two chemicals. While the confidence interval of the T_A-tk overlapped, the best fitting value for IMI, with 3 044 K, was only a third of the value for FPF with 9 243 K (Table 3.1). The larger confidence interval (95%-CI: 1 943 – 15 870 K) for FPF compared to IMI (95%-CI: 2 316 – 3 724) is likely related to the limited information in the data for FPF, i.e., T_A-tk was fitted to the elimination kinetics only.

Increased uptake of insecticides with increasing temperature was reported in previous studies for aquatic invertebrates (Buchwalter et al., 2003; Camp and Buchwalter, 2016; Harwood et al., 2009; Lohner and Warwick Fisher, 1990; Lydy et al., 1999). The predominantly proposed mechanism for this result is the increase in the organism's metabolic activity with rising temperatures. A higher metabolic activity demands an increase in oxygen supply, which the organism may achieve by increasing its ventilation rate, simultaneously increasing the uptake of contaminants present in the water (Buchwalter et al., 2003; Camp and Buchwalter, 2016).

Elimination processes mediated by enzyme activity (e.g., biotransformation) will likely also show an increase with increasing temperature, at least up to the enzyme's temperature optima. As reported in Huang and Mangold-Döring et al. (Huang et al., 2022b), the biotransformation of IMI to IMI-ole increased 2.2 fold from 18 to 24 °C, also visible in the TK-T model fits of this study (Supporting Information 01, Figure S2). Unfortunately, the temperature influence on elimination rates appeared to be understudied for aquatic organisms. However, the few available studies show an increase with increasing temperature, for cadmium (Odin et al., 1997), pyrethroid insecticides (Harwood et al., 2009), and persistent organic pollutants (Brown et al., 2021), in accordance with the present study of IMI and FPF.

3.4.2 Effect modeling

Correcting TK and TD parameters for temperature results in a better fit of GUTS. A parameter identifiability problem (Janzén et al., 2016) arises when the observed datasets do not hold enough information (e.g., too little difference in effects between concentration levels tested) to properly determine one or more model parameter and their confidence intervals. A lack of information can result in a model parameter not being differentiated from zero; therefore, the lower confidence limit cannot be adequately determined. Thus, the observed identifiability problems for the model parameters in estimating their likelihood-based joint-confidence regions are probably related to the low effect sizes observed during the 28-day exposure, i.e., significant effects only in 10 and 30 µg · L^{-1} treatments (Figure 3.4). Another reason for identifiability problems to occur is when there is “slow kinetics”, as discussed in the GUTS e-book by Jager and Ashauer (Jager and Ashauer, 2018a). In this case, the compound’s dynamics are slow compared to the exposure duration, resulting in the parameters boundaries of k_e and m_i going towards zero and b_i going towards infinity (for the SD model), and those parameters correlating with each other.

From comparing the distinctive calibration approaches of the GUTS-FULL models, we conclude that GUTS-FULL-T2 (i.e., TK and TD parameters corrected for temperature) explains the variation in the data under different temperatures best for both insecticides.

Therefore, only accounting for the temperature influence on TK parameters (i.e., GUTS-FULL-T1) is, although possible, less appropriate to model insecticides' toxicity at different temperatures. Thus, our study suggests that TD processes are also affected by temperature. It should be noted that the difference between both applications mainly arises from the two highest concentration levels. In support of this result, additional toxicity experiments with more distinctive effect levels are needed. Nevertheless, our results support the explicit consideration of temperature in GUTS-FULL applications with the help of the Arrhenius expression, as presented in our GUTS-FULL-T2 approach.

Differences in temperature scaling of TK and TD model parameters. The GUTS-FULL-T2 approach fits only one Arrhenius temperature (T_A-td) to correct all TD parameters simultaneously. This approach was conducted in line with the argumentation for a single (species-specific) T_A that scales all metabolic rates, as maintaining homeostasis would otherwise be troublesome for the organism (Jusup et al., 2017; S.A.L.M. Kooijman, 2010). We applied the same argumentation to the TK parameters, which were scaled with one T_A-tk. Hence, in this approach, it cannot be determined if single parameters might also change with temperature differently. We refrained from evaluating this question in the current study, as the observed effects in the available datasets were predominantly in the two highest concentrations, limiting the information needed to identify single parameters' temperature sensitivity successfully. However, Heugens et al., 2003 observed that parameters were not affected by temperature in the same way. Thus, it remains to be determined which TD parameter is most sensitive to temperature and if a single T_A-td applied to all parameters is sufficient. For TK rates of organic contaminants, Raths et al., 2022 showed that the uptake and elimination rates scale with a similar T_A when evaluated separately with the Arrhenius equation, supporting the approach used in this study.

The Arrhenius temperatures for TK and TD were considerably different for IMI but more similar for FPF, due to the large confidence interval (Table 3.1). With 3 044 K (2 316 – 3 724 K) for IMI and 9 243 K (1 943 – 15 870 K) for FPF, T_A-tk were smaller than T_A-td values for IMI 12 150 K (7 189 – 17 610 K), and FPF 11 730 K (7 342 – 15 910 K). This result indicates that the temperature scaling described by the Arrhenius equation is considerably different for processes of TK and TD, especially for IMI. Furthermore, it would be interesting to investigate if the temperature scaling of TK processes for insecticides is similar across aquatic organisms. Using the uptake rates of IMI in *Isonychia bicolor* reported by Camp and Buchwalter, 2016, we could obtain a T_A-tk of 4 700 K. Though this value is close to the T_A-tk value in the present study, it remains unclear if this parameter can be applied to correcting the TK rates of IMI across species or chemicals. Looking for the same comparison on the TD side, there are no literature values available. As the TD processes in the GUTS approach are generally related to an abstract internal damage state, they cannot be associated with a specific effect mechanism. However, it is possible to determine a T_A

based on physiological processes, e.g., growing and aging, with the Add-my-Pet (AmP) tool (https://add-my-pet.github.io/AmPtool/docs/index.html) following the Dynamic Energy Budget Theory (S.A.L.M. Kooijman, 2010). With the entries for *G. pulex* in the AmP collection, a T_A of 10 556 K is obtained (Zimmer et al.,("Add-my-Pet," 2021) parameter estimated based on code version 20210703). Interestingly, the T_A-td values in the present study are within the range of the T_A derived from the AmP collection. This could indicate that the TD processes reflected in GUTS are affected by temperature in the same way as the physiological processes, i.e., growth, reproduction, and aging.

Insecticide-specific increase or decrease of toxicity with temperature. The predicted LC_x values based on the best fitting GUTS-FULL-T2 models differed at the various temperatures for both insecticides (Figure 3.5). For FPF, LC_{50} values first decreased from 7 to 18 °C as observed for IMI but then increased again in higher temperatures. As for IMI, the uptake and the elimination rates in TK-T increase with rising temperatures, and the LC_{50} and LC_{10} values show a constant decrease. However, the uptake rate for FPF in the TK-T approach was kept constant for discussed reasons, which explains the increase in LC_x values for FPF. With a constant uptake rate (k_u) but the elimination rate (k_e) scaling with temperature, there is a point where the elimination of FPF is faster than its uptake, resulting in a lower toxicity (i.e., a higher LC_x).

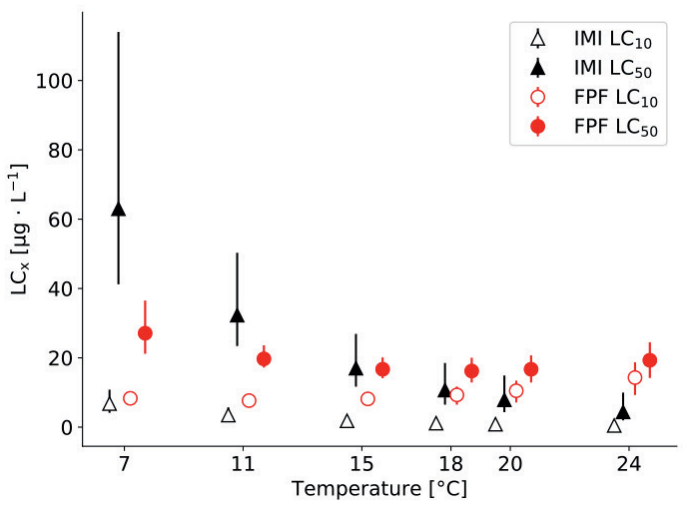

Figure 3.5: Simulated lethal concentrations (LCx) for insecticides at different temperatures after 28 days. Solid shapes for LC50 of imidacloprid (IMI, black triangles) and flupyradifurone (FPF, red circle) and empty shapes for the LC10, respectively. Error bars represent the 95 % confidence intervals based on the parameter sets between the dotted horizontal lines of the profile likelihoods of Figure S13 for IMI and Figure S11 for FPF.

For comparison, we can consult the results of the previous analysis of the measured survival data (Huang et al., 2022b). The LC_{10} and LC_{50} values obtained from the concentration-response-curve analysis based on a log-logistic regression decreased with increasing

temperature for both compounds, suggesting increased toxicity of both compounds with increasing temperature in the range of 7 to 11 °C, in line with the analysis in this study. The differences in the obtained values are associated with the different analysis approaches. The regression analysis fits the model curve only to the survival data of each temperature dataset separately, while the GUTS-FULL approach presented in this study considers survival and internal concentration measures based on the mechanistic assumptions underlying the GUTS framework using all data. Nevertheless, in both results, the influence of temperature on the toxicity differs for the two compounds (i.e., effects do not scale with temperature the same).

These findings highlight the importance of further investigation of the chemical-dependent influence of temperature on the toxicity mechanism of insecticides, even when they have the same molecular target, i.e., for IMI and FPF, the binding to the organism's nAChRs (Casida, 2018; Casida and Durkin, 2013). A good starting point to investigate the temperature-dependent toxicity of insecticides with the same molecular target could be their binding affinities. E.g., for pyrethroid insecticides (i.e., sodium channel modulators) (Sparks and Nauen, 2015), it has been observed that the binding to their target site is higher in lower temperatures (Motomura and Narahashi, 2000), increasing their toxicity (Harwood et al., 2009). However, as the evaluation of temperature influence on binding affinities of neonicotinoids to nAChR has not been investigated, further studies are required.

Advantages, Usefulness, and Limits of the temperature explicit TK and GUTS models. By explicitly considering the influence of temperature on TK-TD processes, the internal concentrations of an insecticide and its effect on organism survival can be predicted for various temperature settings. However, it is important to note that the Arrhenius expression only applies within the species' thermal window. For temperatures beyond the lower and upper critical temperatures, the exponential relationship inherent to the Arrhenius equation may lose its applicability, i.e., organisms may reduce metabolic activity; thus, physiological rates are likely to decrease. Therefore, when predictions outside the thermal tolerance range of an organism are necessary, other temperature models (Mallet et al., 1999; Sharpe and DeMichele, 1977) should be tested, as outlined in the supporting information of Goussen et al., 2020. Nevertheless, the temperature explicit mechanistic effect models as presented in this study hold the potential to investigate further the underlying mechanisms of temperature effects on the toxicity of chemicals in other environmental scenarios, i.e., daily temperature fluctuations (Verheyen and Stoks, 2019a).

The temperature explicit models evaluated in this study provide a parameter set at a reference temperature (here 20 °C), enabling a temperature-neutral comparison for various insecticides' uptake and elimination properties and their toxicity. Furthermore, we showed that data obtained for the same species at different temperatures could be combined to

parameterize the temperature explicit models, which will improve cross-study evaluations. The results of our experimental and modeling studies on the influence of temperature on the adverse effects of insecticides in aquatic organisms show the relevance of temperature for the observed effects. This study demonstrates that applying mechanistic effect models to experimental data gains insights beyond the standard toxicity information. While GUTS modeling provides the advantage of understanding toxicity in time, this study expands the understanding to the additional dimension of temperature influences on toxicity, i.e., which processes governing toxicity are affected by temperature. In our analyses, these insights are restricted by the model's mechanistic details and assumptions. The damage concept of GUTS remains a simple black box, where critical molecular processes are not explicitly considered without further knowledge of the contaminant's mode of toxic action. By extending the GUTS framework with these chemical and organism-specific processes, a more detailed analysis of those underlying processes is possible. Thus, attempts to connect generalized mechanistic concepts as the adverse outcome pathways with effect models such as GUTS (Murphy et al., 2018) can be used to open the box and fully understand the mechanisms behind contaminants' effects on organisms and how temperature modulates it.

Supporting Information Available

The Supporting Information is available free of charge at:
https://pubs.acs.org/doi/10.1021/acs.est.2c04085

1) Supporting Information 01: Text document holding the rationale for temperature correction of the TK–TD parameter, model equations, and additional figures from the analysis (PDF)
2) Supporting Information 02: Spreadsheet with all TK–TD model parameters, AIC comparison, and LCx predictions (XLSX)

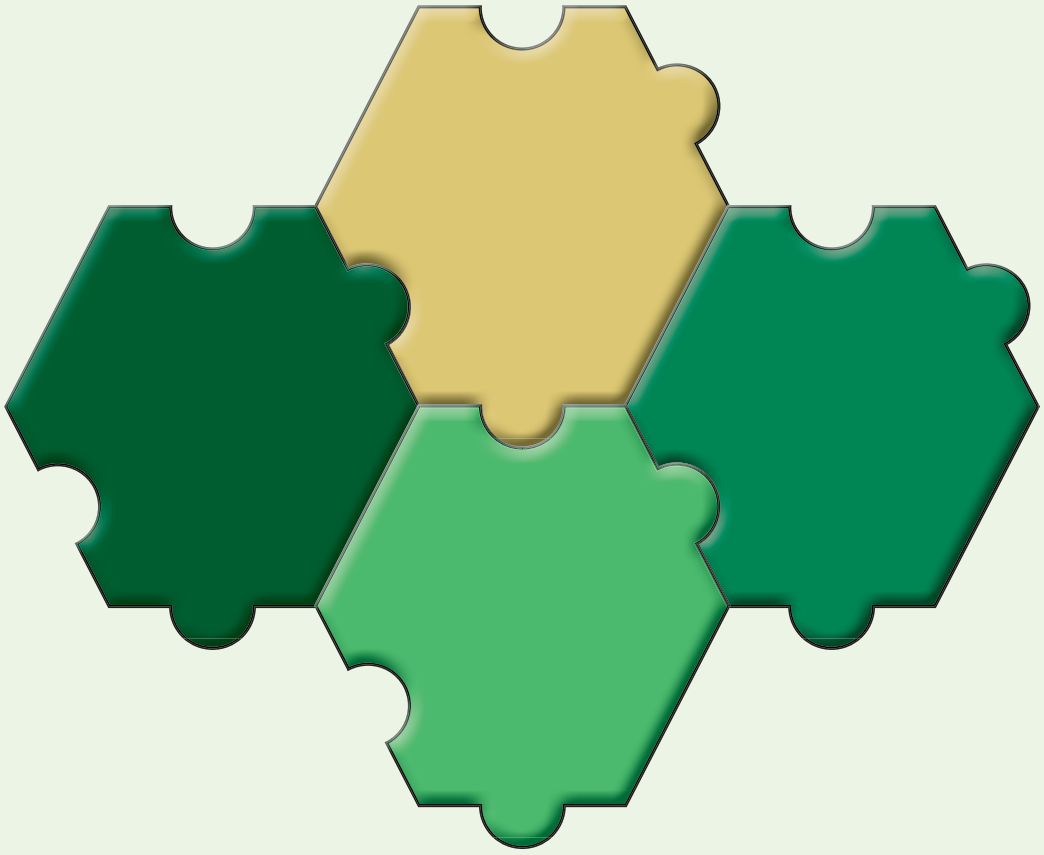

Chapter 4

A toxicokinetic-toxicodynamic model to assess effects of temperatures

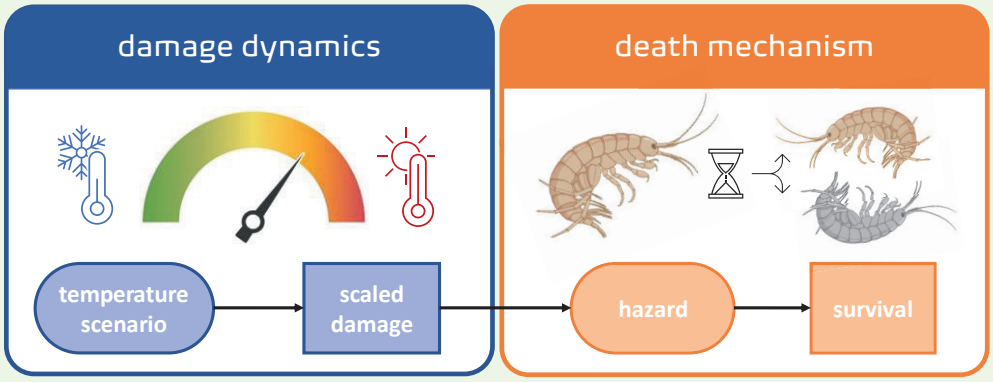

Figure 4.1: Graphical abstract of Chapter 4. Conceptual representation of temperature damage model grouped in damage dynamics in blue (left box) and death mechanism in orange (right box).

This chapter is based on the manuscript:
Annika Mangold-Döring, Jan Baas, Paul J. van den Brink, Andreas Focks, Egbert H. van Nes
A toxicokinetic-toxicodynamic model to assess effects of temperatures

Under Review

Abstract

Temperature is a crucial environmental factor affecting ectothermic organisms' distribution and performance. This study introduces a new temperature damage model to interpret temperature effects. Inspired by the ecotoxicological damage model in the General Unified Threshold model for Survival (GUTS) framework, the temperature damage model assumes that damage accumulation and repair depend on temperature, and mortality is driven by the damage level exceeding a threshold. Model calibration using experimental data of *Gammarus pulex* exposed to different constant temperatures showed a good agreement with the measured survival. Further, model simulations, including constant temperatures, daily temperature fluctuations, and heatwaves, demonstrated the model's ability to predict temperature effects for various environmental scenarios. With this, the present study contributes to the mechanistic understanding of temperature as a single stressor while facilitating the incorporation of temperature as an additional stressor alongside chemicals in mechanistic effect models.

4.1 Introduction

As a factor shaping the environmental niche for organisms, temperature influences the distribution of species around the globe (Sunday et al., 2012). For ectotherms, i.e., organisms whose regulation of body temperature depends on external drivers, the relationship of their distribution with temperature is often defined via the organisms' thermal tolerances and performance, constrained by, i.e., lower and upper temperature limits (Kassahn et al., 2009; Pörtner et al., 2006; Stoks et al., 2017). All internal processes depend on temperature, and it is often found that respiration and other processes are exponentially increasing with temperature (S. A. L. M. Kooijman, 2010; Pörtner, 2010; Schulte et al., 2011). At the limits of species' thermal tolerances, temperature becomes a stress factor that can lead to mortality (Foucreau et al., 2014; Kassahn et al., 2009). Next to the thermal limits, species' sensitivity to other environmental factors determines their performance and survival in the environment (Litchman and Thomas, 2023). From an ecotoxicological perspective, it is particularly interesting to investigate how temperature changes projected due to climate change will influence species' sensitivity to pesticides or other chemicals in the environment. Indeed, there have recently been a variety of studies looking at those interactions, which found evidence for an increase in toxicity by increasing temperature conditions (Camp and Buchwalter, 2016; de Souza et al., 2023; Henry et al., 2017; Huang et al., 2023; Verheyen and Stoks, 2023). This highlights the need to address future climate scenarios in environmental risk assessment (ERA) for chemicals (Polazzo et al., 2022).

A promising way to incorporate temperature scenarios in ERA is the implementation of the influence of temperature in mechanistic or process-based models like toxicokinetic-toxicodynamic (TK-TD) models. TK-TD models enable extrapolation to realistic environmental circumstances (i.e., time-variable exposure patterns) and give mechanistic insight into the TK (i.e., uptake and elimination of the chemical) and TD processes (i.e., through the damage concept). However, temperature may affect the inherent sensitivity of an organism to chemical exposure (i.e., influence the effect threshold represented in the TD processes), or the kinetics of the chemical (i.e., TK processed). Thus, it is essential to include temperature in TK-TD approaches to interpret observed effects correctly. There are two different ways to include temperature's influence on chemical effects. Firstly, temperature can be interpreted as a modulating factor influencing the TK-TD processes of the chemical (Gergs et al., 2019; Mangold-Döring et al., 2022a). Secondly, temperature can be approached as a stressor by itself, in addition to the chemical stress. Even though, in reality, it might be a combination of both, looking at these two different approaches will help to understand the mechanisms of the combined stressors, chemicals, and temperature.

Although the influence of temperature on organisms has been investigated frequently (Bennett et al., 2018; Cereja, 2020), it seems to be challenging to derive general models to

quantitatively describe those thermal responses (Arroyo et al., 2022). In biology, the most used model to account for temperature influences is the empirical Arrhenius equation (Arrhenius, 1889), although its limitations have been discussed (Goussen et al., 2020; Meynet et al., 2020; Mundim et al., 2020). Most importantly, the Arrhenius equation fits only the exponentially increasing parts of the temperature response relationship, while in reality, an optimum effect is more likely (Stoks et al., 2017). For example, the non-monotonous effect of temperature can be observed in daphnids, where the reproduction is highest between 15 and 20 °C and decreases significantly below and above these temperatures (Goss and Bunting, 1983).

Experimentally, the temperature tolerance of aquatic species is commonly assessed in static or dynamic assays, determining the temperature performance curves (Schulte et al., 2011; Sinclair et al., 2016; Verheyen and Stoks, 2023). In pursuit of a unified model to estimate thermal tolerance limits for ectotherms across different experimental conditions, Jorgensen and colleagues presented a thermal injury model (Jørgensen et al., 2021). Their model is based on a static knockdown time t_{Ls} and the temperature-related injury accumulation rate R. Given that the injury is the product of exposure duration and the injury accumulation rate (which increases exponentially with temperature), the model can be applied to static and dynamic temperature exposures. This approach is closely related to the ecotoxicological damage model in the GUTS framework. In the GUTS framework, damage is an abstract concept used to represent aspects of toxicodynamics. This approach relies on the existence of a threshold for effect, i.e., as long as the internal damage level is below a threshold, there are no effects of the chemical on mortality (Jager and Ashauer, 2018a).

In this study, we translate the damage model, as used for chemical effects in GUTS, to a damage model for the effects of temperature and, as such, create a TK-TD model for the interpretation of temperature effects. The parallels between the GUTS concept and the injury model by Jørgensen and colleagues (Jørgensen et al., 2021) and the mathematical derivation of the temperature damage model are presented in the Supporting Information (S01 and Table S1). After model calibration based on experimental data for the freshwater amphipod *Gammarus pulex*, model simulations were conducted for constant temperatures, daily temperature fluctuations, and heatwaves, deepening our understanding of temperature as a stressor presenting itself in various environmental scenarios. With this, we lay the foundation to incorporate temperature as an additional stressor alongside chemicals in mechanistic effect models.

4.2 Methods

4.2.1 Temperature damage model concept and assumptions

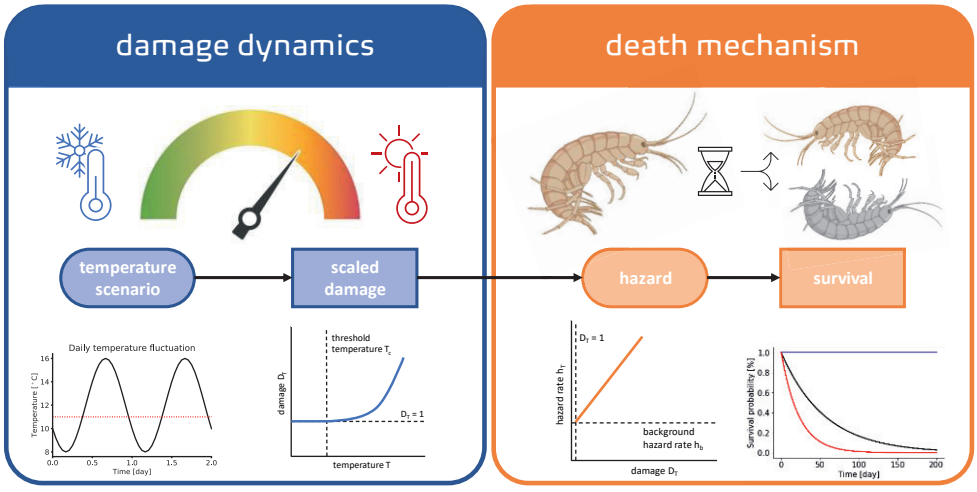

Figure 4.2: Conceptual representation of temperature damage model. Model elements grouped in damage dynamics in blue (left box) and death mechanism in orange (right box) are accompanied by visual representations in the top panel and an example data representation in the lower panel. The model state variables (i.e., scaled damage and survival probability) are in squares, while the ellipses represent the temperature scenario (as a forcing variable) and the hazard rate (as integration from damage levels). Created with BioRender.com

The temperature damage model (Figure 4.2) comes with a set of assumptions, which for consistency, were phrased closely related to the assumptions made in the GUTS approach used to model the TK-TD of chemicals (Jager and Ashauer, 2018a). The assumptions related to the damage dynamics comprise that the accrual flux of damage depends on the surrounding temperature, i.e., experimental water temperature when it exceeds a critical temperature, and the repair flux is proportional to the damage level. Furthermore, the surrounding temperature is not influenced by damage accrual in the organism, and damage is treated as one homogeneous (well-mixed) compartment. It is important to note that the damage described here is not a measurable endpoint but rather a latent variable. Thus, we assume that the accrual or cumulation and the repair of such damage exist, but they cannot be measured directly.

Regarding the death mechanism, we assume that the damage level drives the temperature effect. Each individual organism has a threshold for the damage level. The value for this threshold is assumed to be the same for individuals of a species and can be chosen based on a priori knowledge and the optimal rearing temperature. When the damage level is below the threshold, there is no effect of the temperature on mortality. When damage exceeds the threshold value, the hazard rate due to the temperature stress becomes proportional to the value of the damage above the threshold.

Further, the background mortality is independent of the mortality caused by the temperature. To achieve this independence, the temperature conditions for the control group defining the background mortality must be set up at a temperature where the species is at optimal condition. The background hazard rate can be constant for short temperature exposure tests. Finally, we assume that the organism does not change over time; in other words, the model parameters remain constant.

4.2.2 Mathematical treatment

A detailed description of the derivation of the new temperature damage model equations (derived from the injury model as presented in Jørgensen et al., 2021 and the GUTS damage model shown in Jager and Ashauer, 2018) is offered in the supporting information (S01). The temperature damage model assumes that the damage due to temperature (D_T) increases when the temperature exceeds a critical temperature (T_c). Above T_c the damage accumulates exponentially dependent on temperature, with a temperature coefficient of α. Below T_c, any existing damage will be repaired. Note that we hereby assess only heating stress explicitly, not cold extremes. As we cannot measure the damage directly, we defined it as a dimensionless variable and defined arbitrarily that there is no damage if D_T equals one (eq.4.2). Damage accumulation and repair is modeled as a first-order process (eq.4.1) with a dominant rate of k_T. The hazard rate (h_T) is proportional to the dimensionless damage with a coefficient of b_T (eq.4.2). Finally, the survival function ($S_T(t)$) defines the probability that the individuals survive till a certain time. This function is both dependent on the hazard rate due to temperature and other causes of death, such as background mortality (h_b) (eq.4.3). All temperature model parameters, their unit, and the calibrated values are listed in Table 4.3.

$$\frac{dD_T(t)}{dt} = k_T \cdot \left(\max\left(e^{\alpha(T(t)-T_{c*})}, 1\right) - D_T(\mathrm{t})\right) \qquad \text{eq. 4.1}$$

$$h_T(\mathrm{t}) = b_T \cdot (D_T(\mathrm{t}) - 1) \qquad \text{eq. 4.2}$$

$$\frac{dS_T(t)}{dt} = -(h_T(t) + h_b(t)) \cdot S_T(t) \qquad \text{eq. 4.3}$$

Table 4.3: Temperature damage model variable and parameter symbols and explanations. The respective model equation is provided for model variables, and for the parameters, their best-fit value, along with their 95% confidence interval, is provided.

Symbols	Explanation	Unit	Value	95 % CI
Variables				
D_T	Damage due to temperature	[-]	Eq. 4.1	
h_T	hazard for individual in temperature damage model	d^{-1}	Eq. 4.2	
S_T	Survival probability for individual in temperature damage model	[-]	Eq. 4.3	
T	Absolute temperature (here: water temperature)	K	Forcing variable (model input)	
Parameters (AIC = 282, R^2 = 0.9521 , NRMSE = 0.0287)				
k_T	dominant rate for temperature related damage accrual and/or temperature related damage repair	d^{-1}	5.76	0.322-100*
α	Scaling parameter for the temperature effect	K^{-1}	0.033	2.97^{-05}-0.287
T_c	Critical temperature where damage accumulation starts	K	284.15	set value
h_b	background hazard rate	d^{-1}	0.004	2.88^{-04}-0.018
b_T	killing rate temperature	d^{-1}	0.127	0.001-100*

*Boundary of the parameter space explorer

4.2.3 Model calibration and simulations

The model equations were implemented in the Bring Your Own Model (BYOM) modeling platform (www.debtox.info/byom. html, version 6.2) using MATLAB 2021b to perform all calculations. The model scripts are accessible at GitHub (https://github.com/NikaGoldring/Temperature-GUTS).

Experimental data of the control group from Henry and colleagues were used for model calibration (Henry et al., 2017). Briefly, they exposed 10 *Gammarus pulex* individuals to each of the four different constant temperatures (10, 15, 20, 25 °C) over eight days in three replicates, checking for mortality twice per day. They observed decreasing survival with increasing temperature. Using these measured survival data over time, the model parameters and their confidence ranges were estimated using the parameter space explorer (Jager, 2021a). Based on samples of the parameter space explorer, confidence ranges of model curves were created.

As discussed by Jørgensen et al., the real T_c of most species is unknown and will also likely depend on biological factors such as acclimation, age, sex, diet, etc. (Jørgensen et al., 2021). Thus, following the recommendation of Jørgensen et al. to choose a value by considering the rearing temperature (which was 15 °C in the experiment of Henry et al., 2017) and the evidence from their experiments where 10 °C did not show significant effects

on survival, we chose a value of 11 °C as the set value for T_c. Further, calibrating T_C based on the available data was not possible. Using a fixed threshold parameter contrasts with the GUTS model approach, where the threshold parameter is estimated from the available effect data. We also calibrated the model with a T_c set to 14 °C as a sensitivity assessment of this parameter, resulting in a similar model fit (Supporting Information, S02).

During the model simulations for different temperature scenarios, the background mortality h_b was set to zero for practical reasons. This implies that all hazard is caused by effects of temperature. Model simulations investigated the predicted temperature effects under different temperature scenarios. Three categories were analyzed to cover scenario types applicable to the laboratory conditions 1) constant temperatures, and to more realistic environmental conditions 2) daily temperature fluctuations, and 3) heatwave. Furthermore, a detailed analysis of different heatwave (HW) scenarios was conducted to investigate the relationship between HW duration and intensity. For this, simulations with varying combinations of these factors were performed, and survival probability was used as an evaluation variable for comparison between temperature scenarios. The ranges for tested HW duration (i.e., 7 - 100 days) and intensities (i.e., 3 – 6 °C) were chosen considering the assessment made by Woolway and colleagues predicting average lake HW intensities based on the RCP scenario 8.5 (representative concentration pathway, i.e., business as usual) (Woolway et al., 2021). For the heatwave scenario simulations, the daily temperature fluctuations of 4 °C around the average of 12 °C were increased by the intensity, and each heatwave started at day 10.

4.3 Results

4.3.1 Calibration

The experimental data of *G. pulex* exposed to different constant temperatures were fitted well by the temperature damage model during the model calibration. Across all temperature scenarios, the measured survival probabilities decreased with increasing temperature. The measured data matched well with the calibrated model (R^2 = 0.9521, NRMSE = 0.0287) and lay within the 95% confidence intervals (Figure 4.3). However, the confidence limits of some parameters were very large (Table 4.3). The parameter space plot for the calibration shows well-defined boundaries for the background mortality (h_b) and alpha (α) but reveals possible identifiability problems for the dominant rate (k_T) and the killing rate (b_T), both missing a well-defined upper limit (Supporting Information, Figure S1).

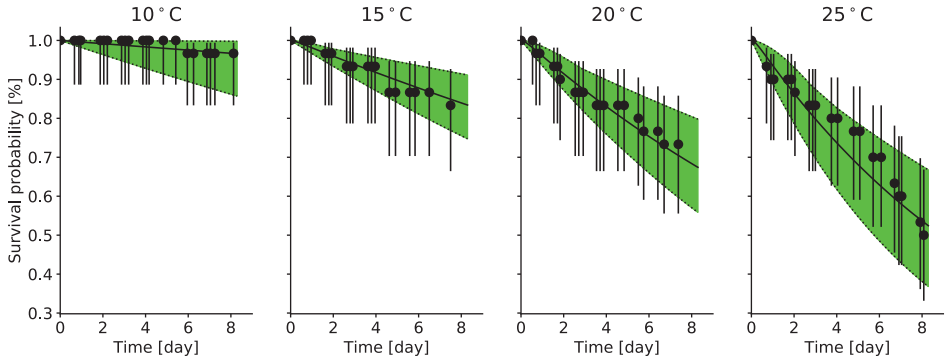

Figure 4.3: Model calibration of the survival probability for *Gammarus pulex* over time. Solid lines show the model for the respective exposure scenarios (i.e.,10, 15, 20, 25 °C), and dotted lines represent their lower and upper confidence intervals. The experiments' mean measured survival is plotted as dots with their Wilson score. For this calibration, T_c was set to 11 °C. Source for original experimental data: Henry et al., 2017

4.3.2 Model simulations for different temperature scenarios

Model simulations for the constant exposures to different temperatures (Figure 4.4, A) showed a steep increase of the damage to its maximum (Figure 4.4, B), where the highest temperature had the highest maximum damage. The damage and the survival probability (Figure 4.4, C) for the 10 °C scenario did not change as the applied temperature was below T_c. The survival probability for 15 and 20 °C decreased over time, with a steeper decrease for the higher temperature. For the daily temperature fluctuation scenario (Figure 4.4, D), the damage increased sharply during the periods where the temperature exceeded T_c, reached its maximum, and decreased as quickly again when the temperature dropped below T_c (Figure 4.4, E). The resulting survival probability decreased over time (Figure 4.4, F). When applying the daily temperature fluctuations and adding a heatwave of a period of 10 days and a temperature increase of 4°C at day 10 (Figure 4.4, G), the damage showed the same dynamics as for the daily temperature fluctuation scenario and increased to a higher maximum during the heatwave period (Figure 4.4, H). In the predicted survival probability, this is reflected in a sharp decrease during the heatwave period, after which the slope recovers to the same level as before (Figure 4.4, I).

When testing different combinations of heatwave intensity (i.e., from 3 to 6 °C) and durations (i.e., from 7 to 100 days), the respective survival probability at the end of the simulation period was plotted in a heatmap (Figure 4.5). The figure shows the non-linear effect of temperature, where a higher intensity has more effect than a longer duration. Clearly, high intensities combined with long durations result in the lowest survival probability.

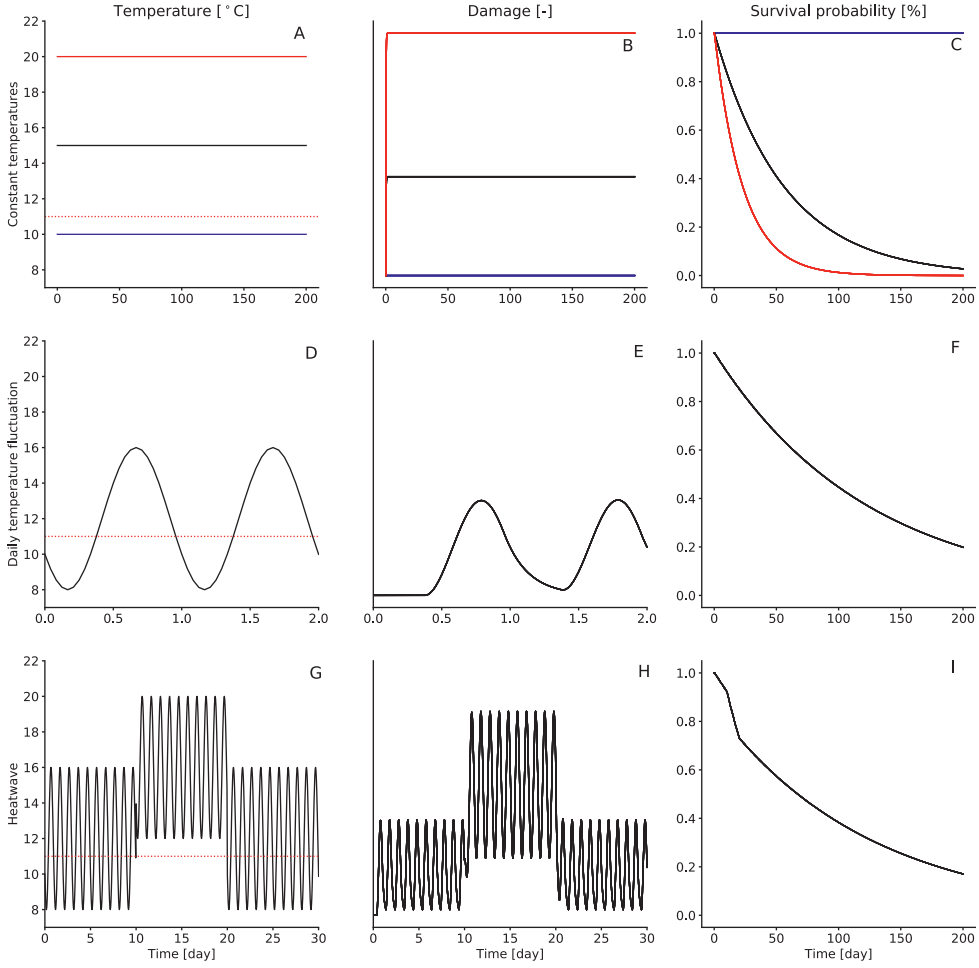

Figure 4.4: Model simulations of damage and survival probability for different temperature scenario types. The different temperature scenario types are constant temperature scenarios (top row), daily temperature fluctuation (middle row), and daily temperature fluctuations with heatwaves (bottom row). T_c with 11 °C is marked with a dotted horizontal line. NOTE: While the survival probability is plotted for the whole simulation time (i.e., 200 days), the temperature and damage are plotted only for a representative period of the simulation (i.e., 2 and 30 days) for the daily temperature fluctuation and heatwave scenarios. Simulations were done with $h_b = 0$.

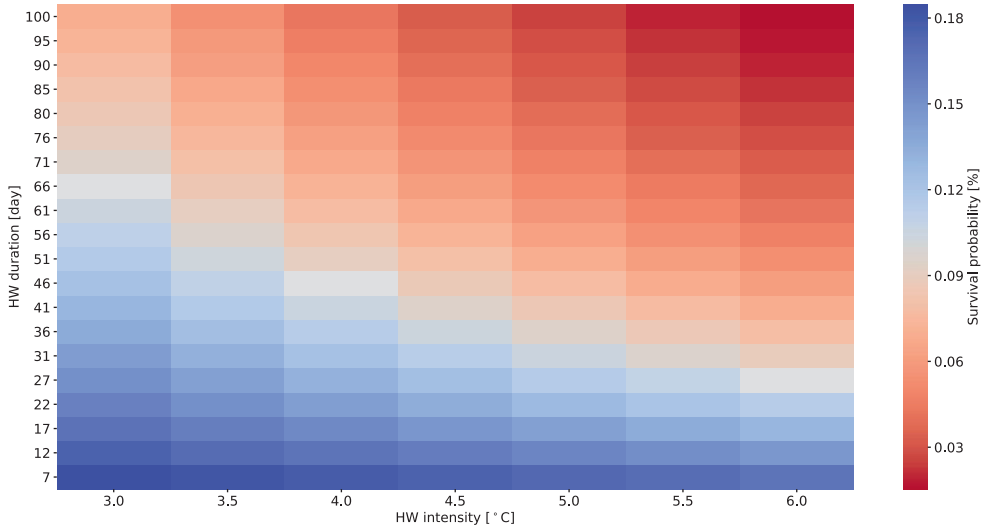

Figure 4.5: Heatmap for the survival probability at the end of the simulation period (t=200 days) depending on different heatwave intensities and durations. During the heatwave the base water temperature (daily temperature fluctuations of 4 °C around the average of 12 °C) was increased by the intensity. For each scenario, the heatwave start was at day 10. Simulations were done with $h_b = 0$.

4.4 Discussion

The temperature damage model presented in this study combines two models: the relatively new thermal injury model, as explained by Jørgensen et al. (Jørgensen et al., 2021), and the well-established GUTS (Jager and Ashauer, 2018a). The most important features we added to the concept of the thermal injury model are to allow for injury or damage recovery, which was not represented before, and to relate the equations to the GUTS framework by including the hazard function that allows fitting the model on survival data. Both features will be essential for future use in environmental risk assessment. To allow for damage recovery is necessary for the simulations of realistic temperature scenarios, where temperatures will vary from harmful to harmless conditions. Further, implementing the hazard function will facilitate coupling the temperature damage model in a multiple-stressor scenario with a chemical stressor modeled in GUTS.

Based on our visual judgment and the quantitative model efficiency measures ($R^2 = 0.9521$, NRMSE = 0.0287), the effect of temperature on *G. pulex* survival, as measured by Henry et al., 2017 was captured accurately in the model calibration of our new temperature damage model (Figure 4.3). Based on the goodness of fit parameter values, the calibration result also complies with the criteria laid down by the EFSA scientific opinion on TK-TD modeling (EFSA (PPR), 2018).

As frequently observed in model calibrations of the GUTS-RED parameters (Sardi et al., 2019), we found a high value for the dominant rate k_T, representing fast kinetics (Table 4.3). Due to the close relatedness of both model approaches (i.e., the GUTS framework and the temperature damage model), similar consequences of fast kinetics are observed, i.e., that other parameters (here: b_T) also run into the boundaries of the parameter space explorer (Supporting Information, Figure S1). This implies that the effect of temperature on mortality is fast. The model cannot distinguish between 'fast' and 'very fast'. Therefore, a wide range of b_T values gives an equally good fit to the data, where eventually, b_T can converge against the set boundary value (or infinity). As argued for GUTS-RED models elsewhere (Jager, 2014), one or two additional observations on mortality early in the experiment would have probably made a difference in pinpointing the value of b_T.

Looking at the model simulations for different scenarios (Figure 4.4), we observe fast damage dynamics, as it is driven by a high value for k_T (5.76 d^{-1}). This implies that when the temperature threshold is exceeded, effects on mortality can be seen within one day. On the other hand, when the temperature falls below the threshold, effects on mortality also disappear within one day (Figure 4.4, I). In the context of heatwave simulations, it appears that the intensity of the heatwave has more effect on the survival probability than its duration (Figure 4.5). However, as expected, the combination of high intensities and long durations resulted in the highest effect on survival. Overall, the model can be used to predict the effect of complex temperature scenarios, including the non-linear effect of heatwaves and daily temperature fluctuation.

4.2 Model assumptions and limitations

Like every model, the temperature damage model is based on assumptions, herewith simplifying the complex reality it represents. For this model, the most crucial assumption centers around the threshold for the temperature effect (T_c). In the chemical GUTS-RED-SD approach, the threshold is determined as the value of the external concentration that does not affect the survival probability. In the temperature damage model, however, we currently do not calibrate T_c, but we fix T_c based on biological knowledge (see arguments in methods section). Furthermore, in the chemical model, the background mortality is based on the control treatment, where no chemical stressor is assumed to be present. The difficulty with the temperature effect modeling is that it is unclear under which temperature conditions no effects on survival will occur since there is nothing like a non-exposed experiment. For effect modeling, observations in control experiments are of crucial importance for parameter estimates. Choosing the optimal temperature condition for the control is hence crucial for estimating the temperature effect on survival. If the control treatment already impacts survival, the overall effect of temperature will be underestimated.

Another central assumption of the presented model is the assumption of temperature damage as a latent state variable for the actual processes affected by temperature, causing damage in the organism. As potentially every physiological process is governed by temperature, it seems unlikely to quantify the actual damage done by a certain temperature for each process (i.e., damage to macromolecules, impact on functioning, or denaturation of enzymes). Consequently, we choose the approximation of an overall temperature damage as presented in this study, similar to the approach used in the chemical GUTS approach (Jager and Ashauer, 2018a). In contrast to the chemical GUTS, the damage calculated here is not scaled to a concentration but remains dimensionless (Table 4.3). This makes it even more difficult to interpret the damage state in a meaningful way. At the same time, it still enables an insight into the damage dynamics in relation to the applied temperature scenario. In our simulations, we observed that damage accumulation is driven by the external temperature dynamics above T_c and that it recovers in the periods where the temperature is below T_c (Figure 4.4, E).

Currently, no critical temperature is defined at the lower side of the temperature preferendum, while in reality, those conditions will also be stressful (Pörtner et al., 2017; Verheyen and Stoks, 2023). However, most species are adapted to low temperatures by overwintering strategies (Bale and Hayward, 2010), and some species can even resist freezing (Murphy, 1983). At low temperatures, all metabolic rates slow down according to the Arrhenius equation, making the effect of low temperature more gradual (Logan et al., 1976). Determining these effects would require experimental data that includes the full range of temperature scenarios to capture both ends of the temperature performance curve.

Another obstacle with defining species' thermal tolerances on both sides (i.e., lower and upper temperature limits) is that they are different between populations or even with the organism life-stage due to phenotypic plasticity (Bowler and Terblanche, 2008; Madeira et al., 2020; Schulte et al., 2011; Sinclair et al., 2016). The acclimatization of organisms has been shown to alter their thermal performance curves (Pörtner, 2010; Semsar-kazerouni and Verberk, 2018) and their sensitivity to chemical stressors (Silva et al., 2020). The dataset used here was based on *G. pulex*, originating from a relatively cold stream (9 °C), hence validating the current calibrated model with survival data of *G. pulex* from different locations will likely fail. When validating the temperature damage model, adjustments to the threshold parameter (T_c) are likely to be needed to account for differences in life stages and their life history regarding acclimatization temperatures. However, looking at this from another perspective, using data from different populations could facilitate investigating intra-species sensitivity differences. In any case, while these circumstances should be considered for model calibration, validation, and application, they do not undermine the potential of the temperature damage model to be a useful tool to study the effect of temperature in separation from chemical stressors.

4.3 Relevance for environmental risk assessment of chemicals

As previously shown in empirical studies, temperature itself can influence organisms' survival, depending on the actual experienced temperature and the duration of exposure (Kivivuori and Lahdes, 1996). In this case, we considered temperature as an additional stressor for the individual rather than a modulating factor of chemical stressors. Although studies have investigated the combined effects of temperature and chemicals, (Camp and Buchwalter, 2016; Goussen et al., 2020; Huang et al., 2023; Schäfer and Piggott, 2018) currently, temperature is not implemented as an additional stressor in chemical risk assessments. With extreme events projected to increase in their frequency and magnitude (IPCC, 2019; Johnson et al., 2018; Woolway et al., 2021), we saw the need to develop a novel temperature damage model with the goal of including temperature as an additional and modulating stressor into TK-TD models for chemicals. To achieve this multiple-stressor assessment through mechanistic modeling, the presented temperature damage model should be combined with the chemical GUTS-RED following the approach previously used for mixture toxicity (Bart et al., 2022, 2021). The first and simplest option is to assume independent action of temperature and chemical effects, hence adding hazards due to temperature and chemicals. However, beyond this most obvious option, identifying the interaction type (i.e., synergistic or antagonistic), testing which stressor is driving the interaction, and finally simulating and predicting the combined effect has already been successfully demonstrated in the GUTS mixture model (Bart et al., 2022).

Furthermore, a combination of the new temperature damage model and the GUTS-T approach, where temperature modulates the chemical parameters, should be explored (Mangold-Döring et al., 2022a). Considering the spectrum of temperature performance curves, it seems likely that temperature acts as both a modulating factor and a stressor when considering the whole temperature spectrum. Thus, combining the newly developed temperature damage model with GUTS mixture and GUTS-T seems a promising approach to get insights into the mechanistic interactions of temperature and chemical stress. This ultimately enables us to investigate the effects of chemicals in current and future climate scenarios and thus supports a realistic and protective risk assessment for chemicals in the environment.

Supporting Information for Chapter 4

S01 Derivation of the model equations

Here we describe the development of the temperature damage module presented in this study, starting from the state-of-the-art damage module for chemicals as part of the widely used General Unified Threshold model of Survival (GUTS). The previously described GUTS approach(Ashauer et al., 2011; Jager and Ashauer, 2018a) simulates the probability of death of individuals over time-based on measured survival data. As proposed by Jager and Ashauer, the mechanistic approach of GUTS, though developed and increasingly used for chemical risk assessment, can be applied to other stressors that cause effects on survival (Jager and Ashauer, 2018a).

For the damage module in GUTS, a one-compartment model is assumed with first-order kinetics (eq. S4). Here, the damage accrual is proportional to the external water concentration of the chemical (C_w), and the damage repair is proportional to the amount of damage (D^*). With those state variables and the damage accrual rate (k_a) and the damage repair rate (k_r), we can describe the damage dynamics for chemicals over time (t) with eq. S4.

$$\frac{dD^*(t)}{dt} = k_a \cdot C_w(t) - k_r \cdot D^*(t) \qquad \text{eq. S4}$$

In the temperature damage model, the damage accrual depends on the external temperature condition over time, expressed as some function g(T(t)). The first step is, thus, replacing the temperature with the chemical concentration as the stressor in eq. S4.

$$\frac{dD_T{}^*(t)}{dt} = k_a \cdot g\big(T(t)\big) - k_r \cdot D_T{}^*(t) \qquad \text{eq. S5}$$

As damage (D*) is a latent state variable that we cannot measure directly, the parameterization of both rates (k_a and k_r) will likely fail. To separate k_a from the other variable, we can rearrange eq. S5 by separating the damage accrual.

$$\frac{dD_T{}^*(t)}{dt} = k_a \cdot \left(g\big(T(t)\big) - \frac{k_r}{k_a} \cdot D_T{}^*(t)\right) \qquad \text{eq. S6}$$

Then, we define in eq. S7 a scaled temperature damage (D_T) by multiplying the real temperature damage (D_T*) by the repair and damage accrual quotient. Rearranging the equation then defines the real damage based on the scaled damage in eq. S8

$$D_T(t) = \frac{k_r}{k_a} \cdot D_T^*(t) \quad \text{eq. S7}$$

$$D_T^*(t) = \frac{k_a}{k_r} \cdot D_T(t) \quad \text{eq. S8}$$

As we cannot measure $D_T(t)$ directly, it's scale is arbitrary and we cannot determine the factor k_a/k_r. Therefore, we replace D* with scaled damage D and then simplify.

$$\frac{k_a}{k_r} \cdot \frac{dD_T(t)}{dt} = k_a \cdot \left(g\big(T(t)\big) - \frac{k_r}{k_a} \cdot \frac{k_a}{k_r} \cdot D_T(t) \right) \quad \text{eq. S9}$$

$$\frac{k_a}{k_r} \cdot \frac{dD_T(t)}{dt} = k_a \cdot \left(g\big(T(t)\big) - D_T(t) \right) \quad \text{eq. S10}$$

Dividing both sides by ka/kr eq. S11 and simplify leads to eq. S12.

$$\frac{k_a}{k_r} \cdot \frac{k_r}{k_a} \cdot \frac{dD_T(t)}{dt} = k_a \cdot \frac{k_r}{k_a} \cdot \left(g\big(T(t)\big) - D_T(t) \right) \quad \text{eq. S11}$$

$$\frac{dD_T(t)}{dt} = k_r \left(g\big(T(t)\big) - D_T(t) \right) \quad \text{eq. S12}$$

Describing accrual of temperature-related damage

The next step, starting from eq. S12 is to define the function that impacts the temperature-related damage accrual over time g(T(t)).

The most straightforward approach would be to use the external temperature over time T(t). We know, however, that within the temperature niche of the organism, there is no damage caused by temperature to be expected. Thus, we should define a threshold temperature T_c above which temperature causes damage. Below this threshold, the temperature probably still modulates, as discussed elsewhere (Huang et al., 2023; Mangold-Döring et al., 2022a; Schulte et al., 2011).

The limitations of this simple approach lie in the assumption that the damage caused by temperature increases linearly with temperature. Empirically, we know that temperatures' effect on survival is best described by an exponential relationship (references see introduction).

A model that accounts for this exponential relationship has already been developed by Jørgensen et al. with the temperature injury model (Jørgensen et al., 2021). With the aim to develop "a unifying model to estimate thermal tolerance limits in ectotherms across static, dynamic, and fluctuating exposures to thermal stress", their model enables the cross-study comparison of thermal tolerance measures.

Their model is constructed of similar parts to the GUTS model (Table S4). However, it comes with its own limitations. The model does not consider an injury or damage repair mechanism and assumes that it will stay above T_c once T surpasses T_c. This considerably limits the use of this model to be applied on realistic temperature scenarios, varying from temperatures in- and outside of the temperature niche of the organism.

Thus, we decided to use the exponential expression of Jørgensen et al. as the function to express the influence of temperature-related damage accrual (eq. S13). Combining this with our temperature damage model considering damage repair leads to the final temperature damage module (eq. S14).

$$g\big(T(t)\big) = e^{\alpha(T(t)-T_{c*})} \qquad \text{eq. S13}$$

$$\frac{dD_T(t)}{dt} = k_T \cdot (e^{\alpha(T(t)-T_{c*})} - D_T(\mathrm{t})) \qquad \text{eq. S14}$$

This new temperature-related damage model describes the effect on survival induced by stressful (in contrast to modulating) temperature conditions. To estimate the model parameter based on the measured survival, the rest of the model is defined as in the main script (eq. 4.1-4.3).

Table S4: Table to outline parallels in concepts (Jørgensen vs. GUTS). GUTS-RED parameter are used.

Symbol pairs (GUTS ~ Jørgensen)	Function	GUTS explanation and unit	Jorgensen explanation and unit
$D_w \sim d$	Damage/injury state variable	Damage level in an organism, scaled to external concentration	Accumulated injury/damage
$C_w \sim T$	Stressor state variables	Chemical exposure concentration, i.e., mol · L^{-1}	Temperature, i.e., K
$m_w \sim R_0$	Threshold for damage/injury accumulation	Median of the distribution of thresholds, concentration of chemical in the environment, i.e., mol · L^{-1}	Temperature-related injury accumulation rate that exactly matches the injury repair rate at T_c, unit of injury per time, i.e., t^{-1}
$k_d \sim R$	Damage/injury accumulation rate	k_d = dominant rate constant, per time (i.e., d^{-1})	Temperature-related injury accumulation rate, per time (i.e., h^{-1})

S02 Model calibration

Model calibration with T_c =11 °C

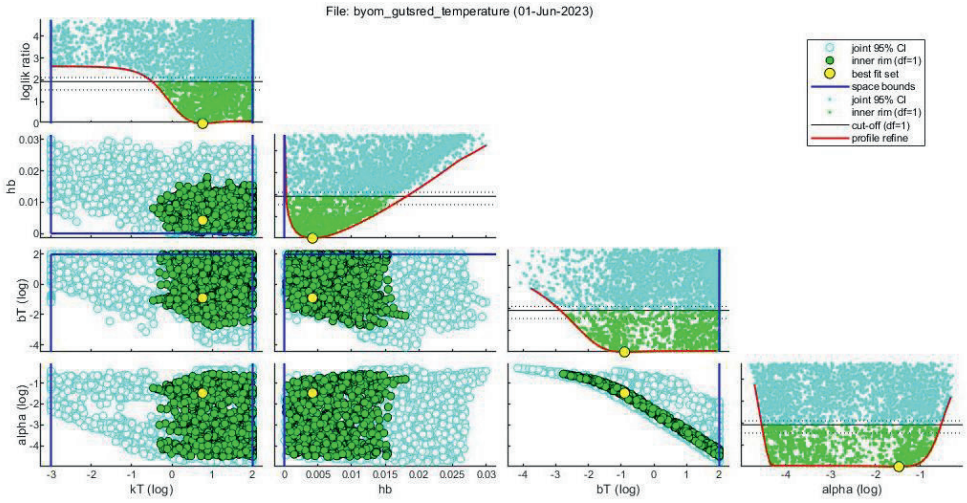

Figure S6: Parameter space plot, calibration (for T_c = 11 °C). The plots on the diagonal show the profile likelihoods for the individual parameters. The scatter plots underneath are the 95% joint confidence regions. The yellow dots mark the best-fit values for each parameter and green dots show the parameter sets within the critical value (i.e., under the horizontal black line). The parameter symbols and units can be obtained from Table 1 in the main script.

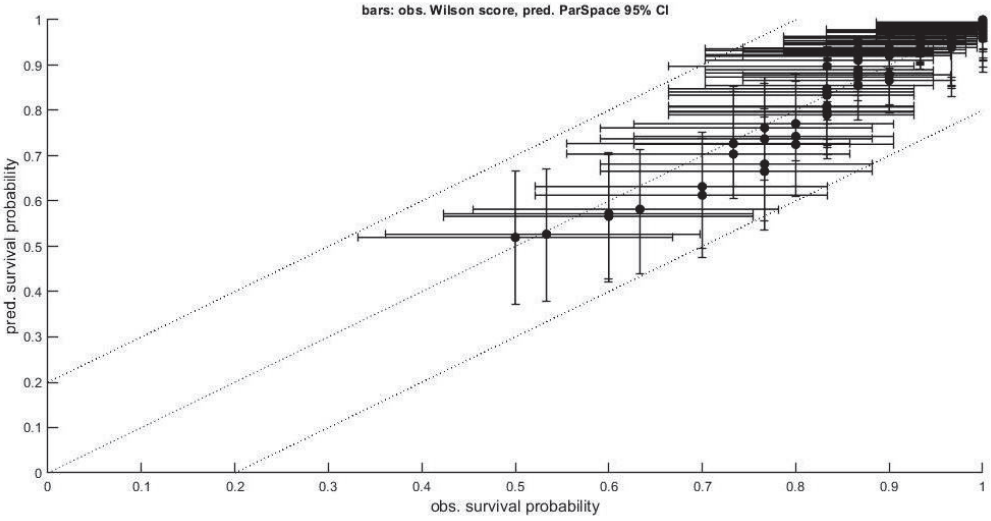

Figure S7: Predicted and observed survival probability for model calibration (for T_c = 11 °C). Vertical error bars represent the uncertainty of the model prediction (their 95% confidence intervals). Horizontal error bars are the Wilson scores intervals of the observed survival data.

Model calibration with T_c =14 °C

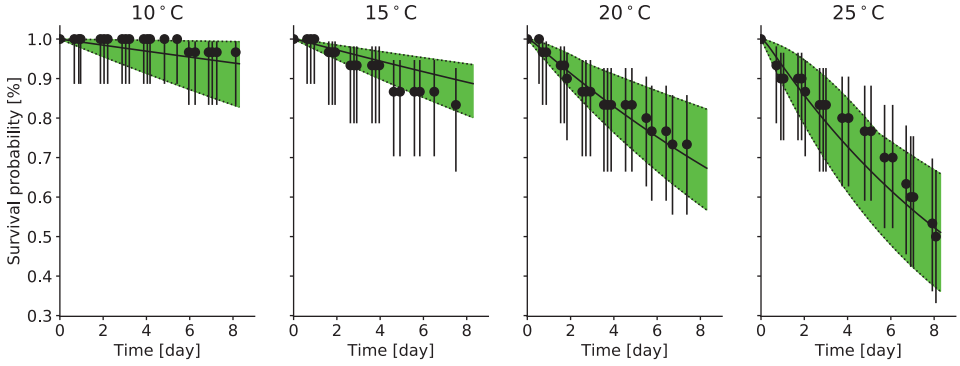

Figure S8: Model calibration of the survival probability for *Gammarus pulex* over time is plotted. Solid lines show the model for the respective exposure scenarios (i.e.,10, 15, 20, 25 °C), and dotted lines represent their lower and upper confidence intervals. The experiments' mean measured survival is plotted as dots with their Wilson score. For this calibration, T_c was set to 14 °C. Source for original experimental data: Henry et al., 2017

Table S5: Temperature damage model variable and parameter symbols and explanations. For model variables the respective model equation is provided, and for the parameters their best fit value along with their 95% confidence interval is provided. For this calibration, T_c was set to 14 °C.

Symbols	Explanation	Unit	Value	95 % CI
Variables				
D_T	Damage due to temperature	[-]	Eq. 4.1	
h_T	hazard for individual in temperature damage model	d^{-1}	Eq. 4.2	
S_T	Survival probability for individual in temperature damage model	[-]	Eq. 4.3	
T	Absolute temperature (here: water temperature)	K	Forcing variable (model input)	
Parameters (AIC = 284, R^2 = 0.9148 and NRMSE = 0.0383)				
k_T	dominant rate for temperature related damage accrual and/or temperature related damage repair	d^{-1}	6.56	0.009-100*
α	Scaling parameter for the temperature effect	K^{-1}	6.78^{-05}	3.46^{-05}-0.372
T_c	Critical temperature where damage accumulation starts	K	287.15	set value
h_b	background hazard rate	d^{-1}	0.008	0.001-0.022
b_T	killing rate temperature	d^{-1}	100*	0.001-100*

*Boundary of the parameter space explorer

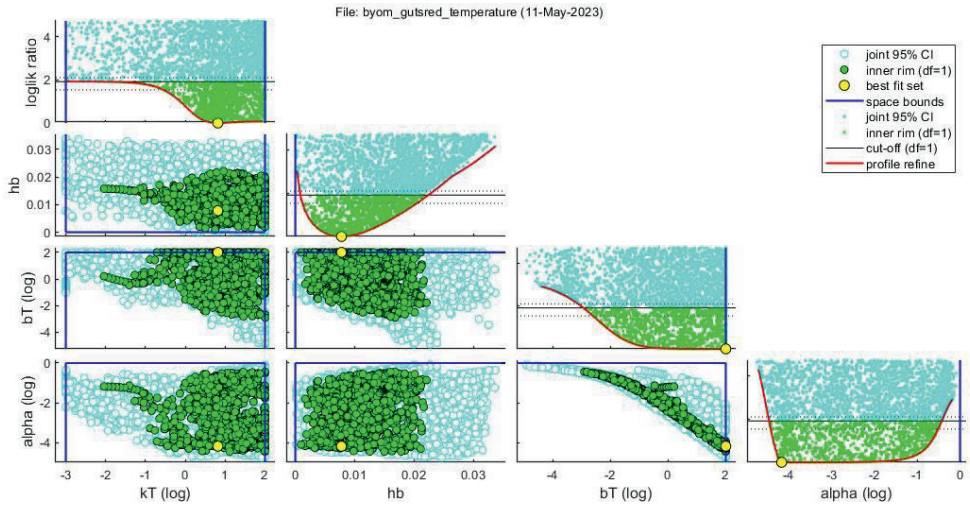

Figure S9: Parameter space plot, calibration (for T_c = 14 °C). The plots on the diagonal show the profile likelihoods for the individual parameters. The scatter plots underneath are the 95% joint confidence regions. The yellow dots mark the best-fit values for each parameter and green dots show the parameter sets within the critical value (i.e., under the horizontal black line). The parameter symbols and units can be obtained from Table 1 in the main script.

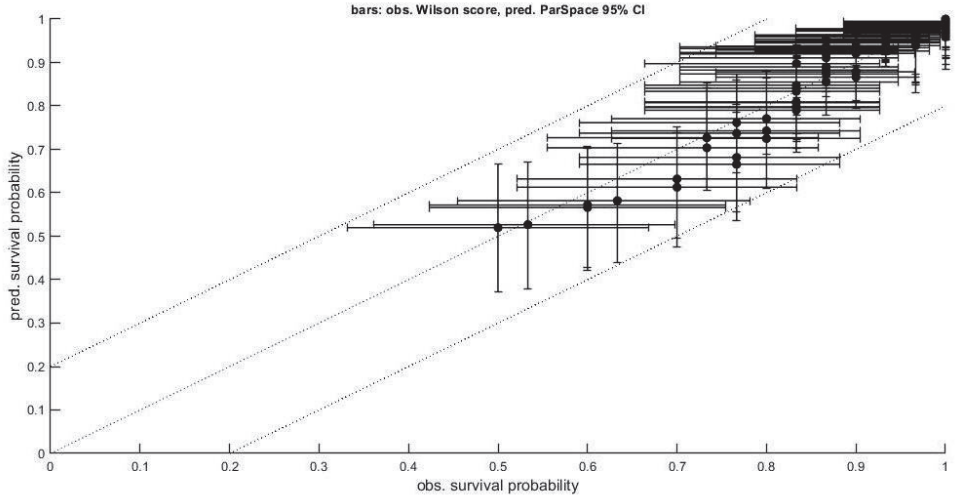

Figure S10: Predicted and observed survival probability for model calibration (for T_c = 14 °C). Vertical error bars represent the uncertainty of the model prediction (their 95% confidence intervals). Horizontal error bars are the Wilson scores intervals of the observed survival data.

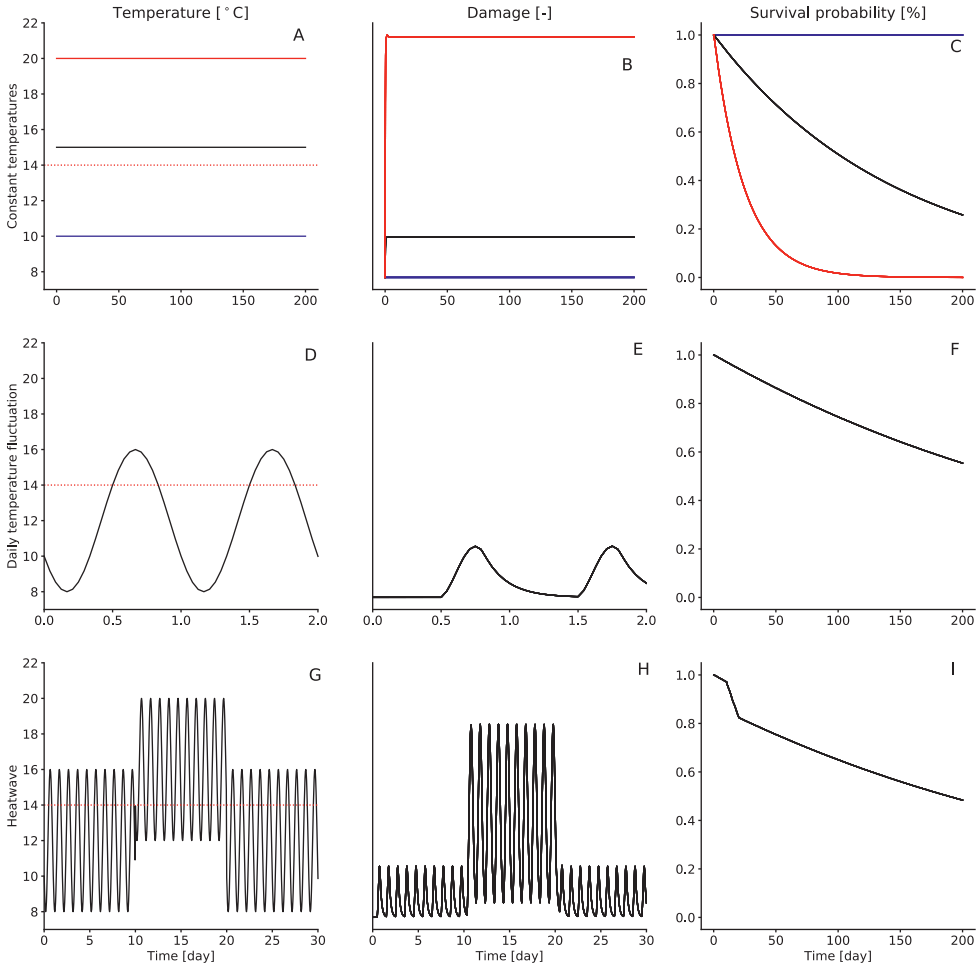

Figure S11: Model simulations of damage and survival probability for different temperature scenario types. The different temperature scenario types are constant temperature scenarios (top row), daily temperature fluctuation (middle row), and daily temperature fluctuations with heatwaves (bottom row). T_c with 14 °C is marked with a dotted horizontal line. NOTE: While the survival probability is plotted for the whole simulation time (i.e., 200 days), the temperature and damage are plotted only for a representative period of the simulation (i.e., 2 and 30 days) for the daily temperature fluctuation and heatwave scenarios. Simulations were done with $h_b = 0$.

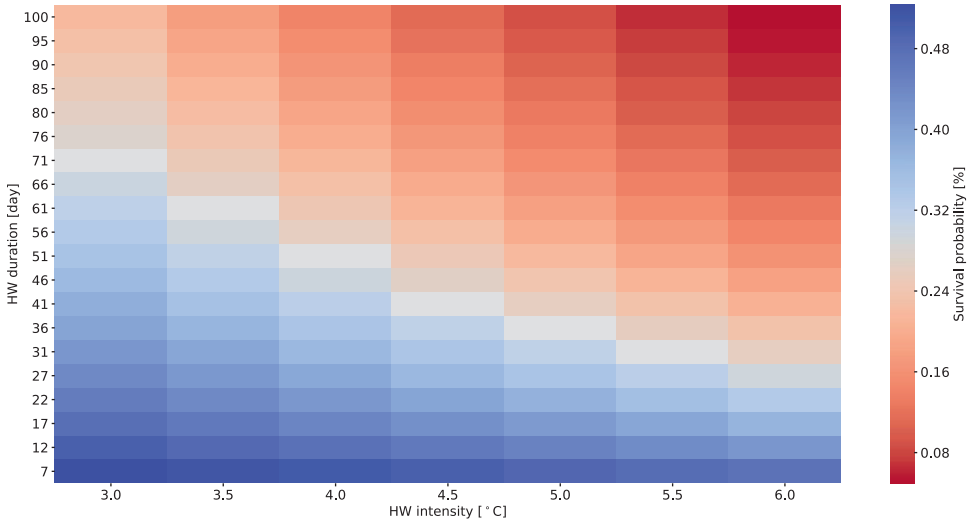

Figure S12: Heatmap for the survival probability at the end of the simulation period (t=200 days) depending on different heatwave intensities and durations. During the heatwave the base water temperature (daily temperature fluctuations of 4 °C around the average of 12 °C) was increased by the intensity. For each scenario, the heatwave start was at day 10. Simulations were done with $h_b = 0$ and $T_c = 14$°C.

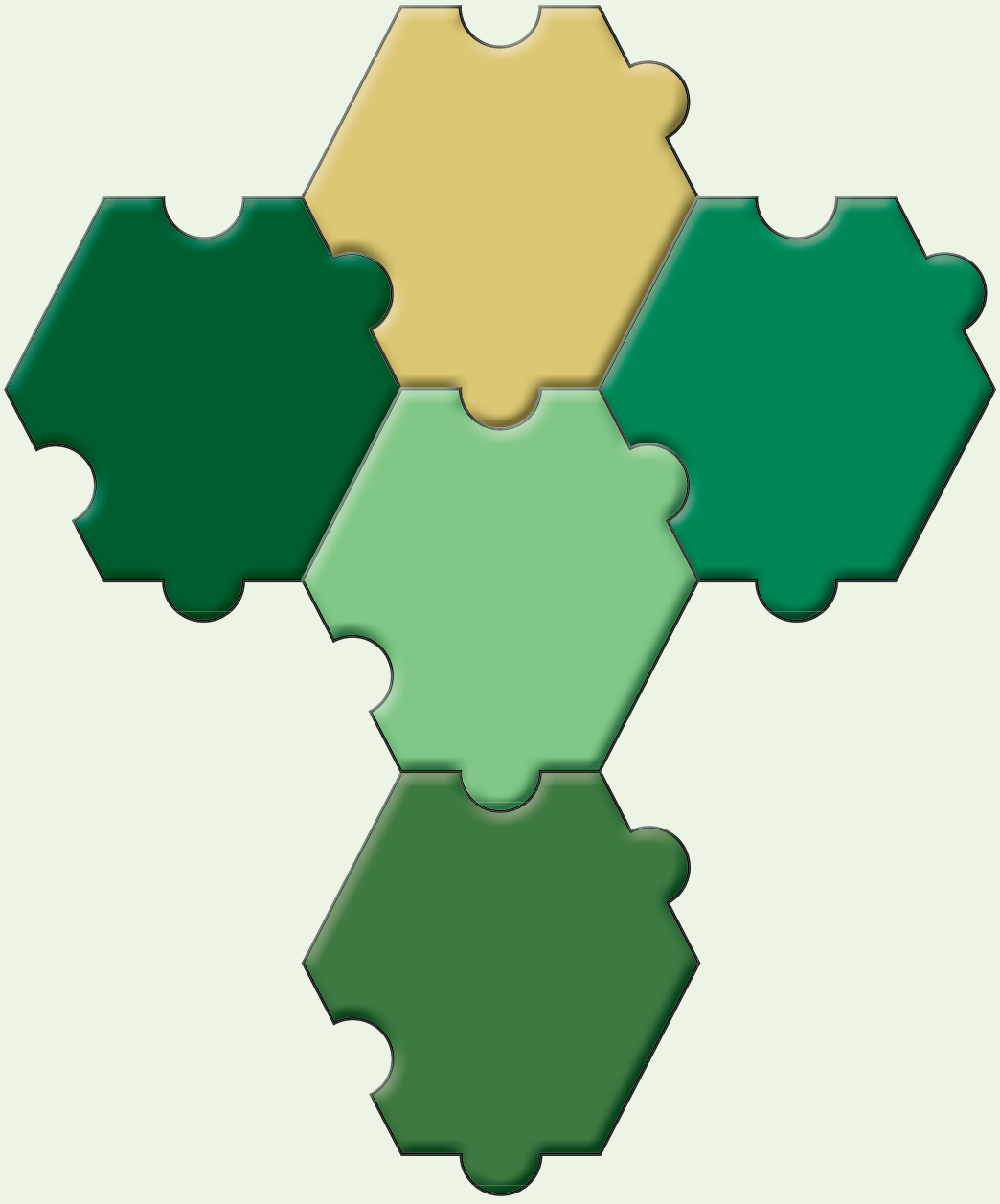

Chapter 5

Elimination resistant: Characterizing multi-compartment toxicokinetics of the neonicotinoid thiacloprid in the amphipod *Gammarus pulex* using bioconcentration and receptor binding assays

Figure 5.1: Graphical abstract of Chapter 5. Illustration of the chemical flows between the exposure medium (i.e., water on the left), the organism *Gammarus pulex* (middle) and the membrane proteins (right) modeled in the toxicokinetic-receptor model developed in this chapter.

This chapter is based on:
Johannes Raths, Linda Schinz, Annika Mangold-Döring, Juliane Hollender, 2023. Elimination resistant: Characterizing multi-compartment toxicokinetics of the neonicotinoid thiacloprid in the amphipod *Gammarus pulex* using bioconcentration and receptor binding assays.

Environ. Sci. Technol. 2023, 57, 24, 8890–8901
https://doi.org/10.1021/acs.est.3c01891

Abstract

Delayed toxicity is a phenomenon observed for aquatic invertebrates exposed to nicotinic acetylcholine receptor (nAChR) agonists, such as neonicotinoids. Furthermore, recent studies have described an incomplete elimination of neonicotinoids by exposed amphipods. However, a mechanistic link between receptor binding and toxicokinetic modeling has not been demonstrated yet. The elimination of the neonicotinoid thiacloprid in the freshwater amphipod *Gammarus pulex* was studied in several toxicokinetic exposure experiments, complemented with in vitro and in vivo receptor binding assays. Based on the results, a two-compartment model was developed to predict uptake and elimination kinetics of thiacloprid in *G. pulex.* An incomplete elimination of thiacloprid, independent of elimination phase duration, exposure concentrations, and pulses, was observed. Additionally, the receptor binding assays indicated irreversible binding of thiacloprid to the nAChRs. Accordingly, a toxicokinetic-receptor model consisting of a structural and a membrane protein (i.e., nAChR) compartment was developed. The model successfully predicted internal thiacloprid concentrations across various experiments. Our results help in understanding the delayed toxic and receptor-mediated effects towards arthropods caused by neonicotinoids. Furthermore, the results suggest that more awareness towards long-term toxic effects of irreversible receptor binding is needed in a regulatory context. The developed model supports future toxicokinetic assessment of receptor binding contaminants.

5.1 Introduction

Neonicotinoids are one of the most widely applied classes of insecticides globally (Casida, 2018; Jeschke et al., 2013) with seven of them being commercially available worldwide: imidacloprid, thiacloprid, thiamethoxam, clothianidin, acetamiprid, nitenpyram, and dinotefuran (molecular structures provided in SI5-A1) (Casida, 2018; Simon-Delso et al., 2015b). However, the widespread use and the toxicity of neonicotinoid insecticides towards numerous non-target insect species, particularly pollinators (Morrissey et al., 2015b; van der Sluijs et al., 2013), resulted in several bans of these insecticides in the last decade (i.e., imidacloprid, clothianidin, thiamethoxam and thiacloprid for outdoor usages in the EU (European Commission, 2022). Nevertheless, neonicotinoids are still extensively used in most other countries, such as the USA (US EPA, 2013) and China (Wang et al., 2020). Furthermore, the butenolide insecticide flupyradifurone, which potentially exerts less toxicity towards pollinators but has a similar mode of action, was introduced as a replacement candidate in 2015 (Jeschke et al., 2015b).

Several properties of neonicotinoids contributed to their worldwide adoption and versatility, replacing more problematic insecticides such as carbamates and organophosphates (Casida and Durkin, 2013). Neonicotinoids are persistent, water-soluble, systemic and highly selective insecticides with low toxicity and bioaccumulation potential in vertebrates (Jeschke et al., 2011; Simon-Delso et al., 2015b). Neonicotinoids interfere with neural transmission in the central nervous system of invertebrates. They act as a (partial) agonist of the nicotinic acetylcholine receptors (nAChRs, Figure 5.2) and compete with the endogenous neurotransmitter acetylcholine (ACh). In contrast to ACh, neonicotinoids are not hydrolyzed by acetylcholine esterase, leading to their prolonged action at the nAChRs (Thany, 2010). This interference causes a continuous activation of the nAChRs, ultimately resulting in symptoms of neurotoxicity, such as paralysis. Differences in the subunits of the receptors in vertebrates and arthropod species result in a much stronger affinity and subsequent toxicity of neonicotinoids towards arthropods, with insects being the most sensitive class (Thompson et al., 2020; van der Sluijs et al., 2013).

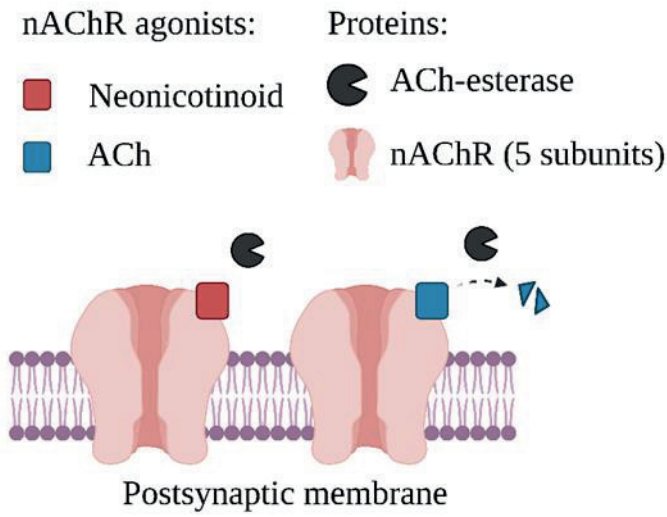

Figure 5.2: Illustration of the competition of neonicotinoids and ACh for nAChRs in the synaptic cleft. The hydrolysis of ACh by ACh-esterase is visualized with a dotted arrow. The nAChR is comprised of 5 subunits and corresponding potential agonist binding sites.

Besides pollinators, neonicotinoids also affect aquatic organisms as they can reach surface waters through spray drift or run-off events (Morrissey et al., 2015b). Since neonicotinoids are systemic insecticides designed for fast uptake and distribution in plants, contaminated plant material may be another route of neonicotinoid exposure (Englert et al., 2017a, 2017b). Recent studies have shown that the pollution levels of neonicotinoids in water bodies often exceed the environmental quality standards (EQS) (Morrissey et al., 2015b; Stehle et al., 2023), provoking mostly chronic adverse effects on aquatic, non-target arthropods. Both acute and delayed toxicity (Beketov and Liess, 2008), as well as long recovery times (i.e., 10 weeks up to more than 7 months; (Beketov et al., 2008; Focks et al., 2018; Li et al., 2021), have been observed in thiacloprid-exposed aquatic invertebrates, such as *Gammarus pulex* (Linnaeus, 1758), during laboratory and mesocosm experiments. Gammarids are frequently used in aquatic monitoring studies (Kunz et al., 2010a; Lauper et al., 2021) due to their ecological importance for detritus decomposition, trophic transfer of nutrients and contaminants (Baudin and Garnier-Laplace, 1994), and widespread occurrence (Chaumot et al., 2015; Kunz et al., 2010a). They are also typical non-target organisms and can take up contaminants through the gills (respiration) or their diet (i.e., contaminated leaves) (Kunz et al., 2010a).

The enrichment of a substance from the water phase into an organism is called bioconcentration. In the regulatory registration process of chemicals, bioconcentration factors (BCFs) and toxicokinetic rates are commonly determined in uptake and elimination experiments with fish according to OECD 305 (OECD, 2012b, p. 305). Due to ethical

considerations, analogously designed studies for invertebrates were proposed as an alternative (Kosfeld et al., 2020; Schlechtriem et al., 2019). Commonly, toxicokinetic parameters are derived using a simplified one-compartment approach (Ashauer et al., 2010). However, exploring the kinetics of certain compounds requires more complex (i.e., two-compartment) approaches to be sufficiently captured (Ashauer et al., 2010; Cedergreen et al., 2017; Jager et al., 2017). Such is the case for neonicotinoids, as recent studies indicate that these substances are not completely eliminated from amphipods in neither laboratory (Raths et al., 2023a; Švara et al., 2021) nor field (Lauper et al., 2021) environments.

We hypothesized that the irreversible binding to the nAChRs causes the elimination resistance. For testing this hypothesis, we characterized the non-eliminating fraction of thiacloprid in *G. pulex* by performing several uptake-elimination experiments with a prolonged elimination phase, and different exposure concentrations and exposure pattern (i.e., pulsed exposure). We selected thiacloprid because it was still permitted for use in Switzerland in 2019 and found in field experiments in gammarids even when no thiacloprid was detected in the surface water (Lauper et al., 2021). The relevance of binding to nAChRs for the elimination resistance of thiacloprid was evaluated by performing both *in vivo* and *in vitro* nAChR binding assays. Thereby, irreversible binding was defined as no measurable depletion on the experimental time scale of up to 8 days. Eventually, based on the combined results of the uptake-elimination experiments and receptor-binding assays, a toxicokinetic model was developed to account for compounds with specific receptor-binding properties and to help understanding long-term toxic effects caused by irreversible binding.

5 Material and methods

5.2.1 Test animals

Specimens of *G. pulex* were collected from an uncontaminated creek near Zurich (Mönchaltdorfer Aa, 47.2749 °N, 8.7892 °E), located in a landscape conservation area. The sampling and experimental timeline covered the months of October (kinetic experiment I and concentration dependence II and III), November (pulsed exposure IV) and January (*in vivo* and *in vitro* receptor binding assay V and VI), at water temperatures of 12, 7, and 1°C, respectively. Genetic specifications of the population are provided elsewhere (Raths et al., 2023a). Gammarids were kept in artificial pond water (APW; (Naylor et al., 1989) with a pH of 7.9 and at 15.5 °C. Details on the acclimation procedure are provided in SI5-A2. Lipid content was determined gravimetrically (SI5-A3, Raths et al., 2023). Data for lipid, protein, and thiacloprid contents are reported on a wet weight basis but can be converted to a dry weight basis using an experimentally determined factor of 5.4 (Raths et al., 2023a).

5.2.2 Toxicokinetic experiments

Toxicokinetic experiments consisted of an uptake phase, where gammarids were exposed to test medium containing thiacloprid, followed by an elimination phase, where gammarids were transferred to medium without thiacloprid. All experiments were conducted in aerated 6 L glass tanks filled with APW, if not specified otherwise. A water temperature of 15.5 ± 1 °C and a 12:12 h light-dark cycle were maintained during the experiments. Gammarids were only fed during the elimination phase to avoid sorption of thiacloprid to leaves and subsequent dietary uptake of sorbed thiacloprid. General experimental designs, as well as exposure times and concentrations are displayed in Table 5-1.

Table 5.1: Overview of the duration of the different toxicokinetic experiments and test concentrations.

No.	Experiment	Exposure [d]	Elimination [d]	Thiacloprid [µg L^{-1}]
I	Kinetic experiment	2	8	50 (200 nM)
II	Concentration dependence - low	20, 20, 4	5, 5, 4	0.05, 0.5, 5
III	Concentration dependence - high	2	2	5, 50, 500, 1500, 5000
IV	Pulsed exposure[a]	2	3	5, 50
V	*In vivo* receptor assay	2	2	50
VI	*In vitro* receptor assay	[b]	[b]	[b]

a = Three subsequent sequences of exposure and elimination were applied.

b = Test conditions are specified in the in vitro receptor binding section.

In order to confirm the previously observed incomplete elimination of thiacloprid from amphipods (Lauper et al., 2021; Raths et al., 2023a), a kinetic experiment with a prolonged elimination phase was performed (Table 1, I). Samples were taken in duplicates at regular time intervals.

To test a potential concentration dependence of thiacloprid bioconcentration (i.e., due to a maximal binding capacity), gammarids were exposed to seven different thiacloprid concentrations (Table 1, II and III). The exposure and elimination times were chosen to guarantee steady state conditions of both exposure and elimination. However, no steady state was reached during the uptake phase of the 0.05 µg L^{-1} exposure. Gammarids were sampled in triplicates at the end of the exposure and elimination phase. Additionally, samples for more time points (every 5 days) were taken during the exposure to 0.5 and 0.05 µg L^{-1} in order to obtain kinetic data for the toxicokinetic-receptor model.

To evaluate whether the residual thiacloprid body burden increases when gammarids are repeatedly exposed to thiacloprid, gammarids were exposed to three consecutive pulses of thiacloprid (Table 1, IV). During each of the three pulses, gammarids were sampled in triplicates on days 1, 2, 3, and 5 of each pulse.

Supplementing toxicokinetic experiments, including investigations on thiacloprid sorption to the exoskeleton and the contribution of physiological activity (i.e., respiration) to toxicokinetics using dead gammarids, are described in SI5-A4 and SI5-A10.

Gammarids that died during the experiments were removed from the test system and not sampled. Shortly before the start of each experiment, (< 1 h) control samples of medium and gammarids were taken. Gammarids for tissue analysis (4 per replicate) were collected, rinsed with nanopure water (NPW), dry blotted, weighed (wet weight), snap frozen in liquid nitrogen, and stored at -20 °C until extraction.

5.2.3 Sample preparation

Tissue extracts were prepared by liquid extraction as described elsewhere (Rösch et al., 2016). First, 300 mg of 1 mm zirconia/silica beads (BioSpec Products, Inc.), 100 µL of internal standard (ISTD, 250 µg L^{-1} thiacloprid-d4 in methanol) and 500 µL of methanol were added. Then, samples were homogenized using a tissue homogenizer (2 x 15 s at 6 m s^{-1}; FastPrep, MP Biomedicals) before centrifugation (10 000 x g, 6 min, 4 °C). The supernatant was collected using syringes and filtered through 0.45 µm regenerated cellulose filters (BGB Analytic AG). Filters were washed with 400 µL of pure methanol and the two collected filtrates were combined. Medium samples (500 µL) were collected from the tanks, spiked with 100 µL of ISTD and mixed with 400 µL of methanol.

5.2.4 Membrane protein isolation and *in vivo* receptor binding assay

Total protein and membrane protein content was determined based on isolation methods adapted from Maloney et al. (2021). The workflow is illustrated in SI5-A5. In brief, gammarid samples were taken shortly before (< 1 h) the corresponding toxicokinetic experiments started, dry blotted on paper tissue, weighed, and snap frozen in liquid nitrogen. Samples were homogenized using approximately 300 mg of 1 mm zirconia/silica beads (pre-cooled 4 °C, BioSpec Products, Inc.) with a pre-cooled tissue lyser (15 s, 6 s^{-1}, 4 °C; Bead Ruptor Elite, OMNI International). Next, dissociation medium (DM) was added (1 mL/per sample, 4 °C) to the tubes and samples were homogenized again. The DM consisted of a buffer of 20 mM sodium phosphate and 150 mM sodium chloride (pH 7.0) as well as 0.1 mM phenylmethylsulfonyl fluoride (PMSF), 1 mM ethylenediaminetetraacetic acid (EDTA), 0.33 mg L^{-1} pepstatin, 0.33 mg L^{-1} chymostatin and 0.33 mg L^{-1} leupeptin for protease inhibition. Samples were centrifuged (30 min, 1000 x g, 4 °C) and the supernatant (SN1) collected with a pipette. The pellet was resuspended in DM (1 mL/sample, 4 °C), centrifuged again (10 min, 1000 x g, 4 °C) and the supernatant (SN2) combined with SN1 in 8 mL ultracentrifuge vials. A subsample of the combined supernatants was used for determination

of the total protein content. Afterward, the volume was adjusted to 7 mL using cold DM and samples were ultracentrifuged (43,000 x g, 30 min, 4 °C, Ultracentrifuge CP100NX, Hitachi). Subsequently, the supernatant was carefully removed with a pipette and the pellet was resuspended (membrane protein extract) in 4 mL of DM. The concentrations of proteins in the supernatant and membrane protein extract were quantified using the Pierce BCA Protein Assay Kit (ThermoFisher Scientific) and calculated as described in SI5-A5.

For the *in vivo* receptor assay, exposed gammarids (Table 1, V) were sampled at the end of the exposure and at the end of the elimination phase (12 replicates each). Six replicates were extracted using the liquid extraction method for the determination of total thiacloprid content (recovery control). The other six replicates (fractionation) were treated as follows (Figure 5.3): Membrane protein extraction was performed as described above. Afterward, the membrane protein pellet was extracted for bound thiacloprid with 900 µL MeOH after the addition of 100 µL ISTD and filtered through 0.45 µm cellulose filters. Additionally, thiacloprid was extracted from the debris (particles at the bottom after centrifugation at 1000 g) and in the supernatant (after ultracentrifugation at 43,000 x g). The debris was extracted using methanol as described for gammarid tissue extractions. The supernatant was sampled like the medium samples (see sample preparation). The measured thiacloprid concentrations were normalized to the total body weight.

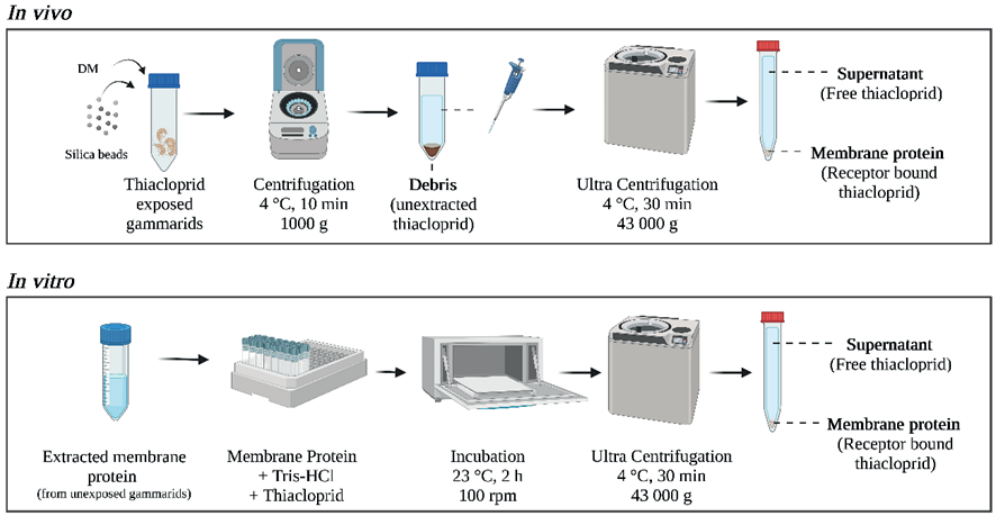

Figure 5.3: The two performed nAChR binding approaches (in vivo: top, in vitro: bottom). DM = dissociation medium. The fractions analyzed by online-SPE LC-HRMS/MS (debris, supernatant, membrane protein) are indicated by bold letters.

5.2.5 *In vitro* receptor binding assay

The *in vitro* nAChR binding assay was performed based on the methods described by Maloney et al. (2021). The methods were adapted to our facilities and to the use of non-radioactively labeled thiacloprid (Figure 5.3). The receptor binding assay was prepared by combining 0.27 mg of membrane protein (0.5 mL of membrane protein extract) and 6 mL of Tris-HCl buffer (10 mM, pH = 7.4) spiked with thiacloprid in 8 mL ultracentrifuge vials. Final concentrations of thiacloprid in the vials corresponded to 0, 2.5, 5, 10, 25 and 50 nM. Each concentration was tested in four technical replicates split over multiple runs of the assay (8 vials each). After incubation for 2 h at 23 °C and 100 rpm, samples were ultracentrifuged (43,000 x g, 30 min, 4 °C). The incubation medium was sampled by combining 500 µL of the supernatant with 400 µL of MeOH and 100 µL of ISTD. The rest of the supernatant was removed, the pellet resuspended in 6.5 mL of Tris-HCl and the suspension ultracentrifuged again. Subsequently, the supernatant was removed and the pellet was extracted for thiacloprid concentration as described for gammarid tissue extractions. Each assay included a protein recovery control in order to correct the measured receptor-bound amount of thiacloprid for the membrane protein lost during the extraction steps.

5.2.6 Chemical analysis

All collected samples were stored at -20 °C until chemical analysis. Chemical analysis was performed using an automated online solid phase extraction system coupled with reversed phase (C18 column, Atlantis T3, 5 µm, 3×150 mm) liquid chromatography and high-resolution tandem mass spectrometer (online-SPE-LC-HRMS/MS) using the Orbitrap technology (Thermo Fisher Scientific Inc.). Ionization was performed using an electrospray ionization interface. Specifications on the used mass spectrometers and the parameter settings are provided in SI5-A6.

Thiacloprid was quantified in positive mode with the internal standard using TraceFinder 5.1 (Thermo Fisher Scientific Inc.) for peak integration. Additionally, a suspect screening using commonly known transformation products of thiacloprid was performed. Detailed information on quality control and quantification is provided in SI5-A7.

5.2.6 Data analysis

Total tissue bioconcentration factors ($BCF_{SS,Total}$ in L kg^{-1}) under steady state conditions were calculated for the toxicokinetic experiments II and III as the ratio of measured total tissue

concentration at the end of the uptake phase ($C_{Tissue,\,u}$) and the average measured exposure concentration (C_{Water}):

$$BCF_{SS,Total} = \frac{C_{Tissue,u}}{C_{Water}} \quad \text{(Eq. 5.1)}$$

Additionally, corresponding BCFs of the structure (defined below, Figure 5.4) compartment ($BCF_{SS,Structure}$ in L kg^{-1}) for the concentration dependent toxicokinetic experiment were determined by subtracting the elimination resistant fraction at the end of the elimination phase ($C_{tissue,e}$) from the concentration at the end of the uptake phase:

$$BCF_{SS,Structure} = \frac{C_{Tissue,u} - C_{Tissue,e}}{C_{Water}} \quad \text{(Eq. 5.2)}$$

Receptor binding properties of thiacloprid were modeled from the *in vitro* assay by determining the maximal irreversible binding parameter B_{Max} (µmol kg^{-1} membrane protein) and the equilibrium dissociation constant K_d (nM). B_{Max} is indicative of the maximum number of nAChR binding sites. Correspondingly, it is also a measure of the nAChR density of an organism if each receptor contains one specific binding site for thiacloprid. The equilibrium dissociation constant K_d represents the binding affinity of thiacloprid to nAChRs and is defined as the ligand concentration to achieve a half-maximum binding at equilibrium (Hulme and Trevethick, 2010).

The specific binding ($C_{Specific}$, µmol kg^{-1} membrane protein) model accounted for one-site, specific binding under equilibrium conditions:

$$C_{Specific} = \frac{B_{Max} \cdot C_{Free}}{K_d + C_{Free}} \quad \text{(Eq. 5.3)}$$

where C_{Free} (nM) is the concentration in the *in vitro* receptor binding assay medium. The model was applied to the assay medium concentrations of 0 to 25 nM, because unspecific binding at these concentrations was negligible compared to specific binding. Receptor binding was modeled in GraphPad Prism 9.4 (GraphPad Software, Inc.). The modeled receptor binding parameters were additionally confirmed using an unspecific binding model with an extended set of medium concentrations (SI5-A8).

Statistical analysis and data visualization were performed using GraphPad Prism 9.4 (GraphPad Software, Inc.). Significant differences between categorical variables were tested by ANOVA if not stated otherwise. The level of significance was set to 0.05. Normal distribution and homoscedasticity of the residuals were assumed. The law of error propagation was applied to all calculations (Tellinghuisen, 2001).

5.2.7 Toxicokinetic modeling

A toxicokinetic model, including receptor binding (toxicokinetic-receptor model), was developed to describe the observed toxicokinetics of thiacloprid in *G. pulex*. Receptor models describing the kinetics of ligand-receptor complexes have been previously described for other organisms (Johnson and Goody, 2011; Yassen et al., 2005) and discussed in the context of toxicokinetic-toxicodynamic models (Jager and Kooijman, 2005). Irreversible binding of thiacloprid to the nAChR was the core assumption of our model. Specifically, we assumed a two-compartment model with a structure (S) and a membrane protein (MP) compartment incorporated into the structure compartment (Figure 5.4). While there is a bidirectional exchange between the structure compartment of the organism and the environment (i.e., water), the interaction of the structure compartment with the membrane protein compartment is unidirectional due to the irreversible receptor binding (k_{off} = 0). There is no direct interaction between water and the MP compartment. The model assumptions and reasoning are described in further detail in SI5-A9.

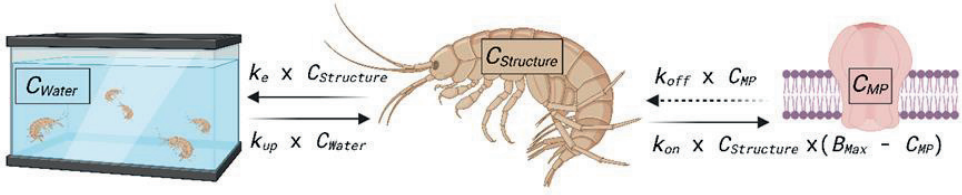

Figure 5.4: Illustration of the toxicokinetic-receptor model based on Equations 5 and 6. The volume of the water basin is assumed to be infinite compared to the volume of exposed gammarids. The weight ratio of the membrane protein (MP) and the structure compartment is defined as FMS (membrane protein content, here 1%). Elimination from the MP compartment was set to zero (k_{off} = 0), because no elimination could be determined during the toxicokinetic experiments and model development.

The formation of the ligand-receptor complex and its dissociation can be described through an ordinary differential equation. The change of the concentration of ligand-bound receptors, here approximated as the change of the thiacloprid concentration in the membrane protein compartment C_{MP} (µmol kg^{-1}) over time t (d), depends on the ligand (thiacloprid) concentration in the structure compartment $C_{Structure}$ (µmol kg^{-1}) and the concentration of free receptors N_R (µmol kg^{-1}), multiplied with the second-order rate k_{on} (kg µmol^{-1} d^{-1}). The first order rate k_{off} (d^{-1}) determines the dissociation of the complex, depending on the concentration of ligand-bound receptors.

$$\frac{dC_{MP}(t)}{dt} = k_{on} \cdot C_{Structure}(t) \cdot N_R(t) - k_{off} \cdot C_{MP}(t) \qquad \text{(Eq. 5.4)}$$

Our experimental results indicated an irreversible binding of thiacloprid at the temporal scale of the experiments. Furthermore, no parameter value for k_{off} significantly different from zero could be determined. Thus, the dissociation rate k_{off} was set to zero. With these observations, and the assumption that the total number of receptors N_{R0} (µmol kg^{-1}) is equal

to the sum of ligand-bound receptors (N_{RL}) and free receptors ($N_R = N_{R0} - N_{RL}$), and further approximating N_{R0} as the maximal binding capacity B_{max} (µmol kg^{-1}), Equation 4 can be rearranged as follows:

$$\frac{dC_{MP}(t)}{dt} = k_{on} \cdot C_{Structure}(t) \cdot \left(B_{max} - C_{MP}(t)\right) \quad \text{(Eq. 5.5)}$$

The concentration in the structure compartment $C_{Structure}$ can be determined using the following ordinary differential equation:

$$\frac{dC_{Structure}(t)}{dt} = k_u \cdot C_w(t) - k_e \cdot C_{Structure}(t) - \frac{dC_{MP}(t)}{dt} \cdot FMS \quad \text{(Eq. 5.6)}$$

Where k_u (L kg^{-1} d^{-1}) is the uptake rate, C_W (µM) the water concentration of the exposure medium, k_e (d^{-1}) the elimination rate, and FMS (0.01) the factor to correct the proportion of membrane protein compared to the structure compartment.

The total tissue concentration C_{Total} (µmol kg^{-1}) can be calculated by adding the two equations:

$$C_{Total}(t) = C_{Structure} + C_{MP} \cdot FMS \quad \text{(Eq. 5.7)}$$

The modeled kinetic bioconcentration factor ($BCF_{kin,Structure}$ in L kg^{-1}) in the structure compartment was determined as the ratio of k_u and k_e:

$$BCF_{kin,Structure} = \frac{k_u}{k_e} \quad \text{(Eq. 5.8)}$$

The internal concentrations derived from the toxicokinetic experiments were used to calibrate and validate the toxicokinetic-receptor model (Eq. 5.5 to 5.7). Model calibration was done with data of constant exposures (0.05, 0.5, 5, 50, and 1500 µg L^{-1}). The parameter space explorer (Jager, 2021b) was used for the optimization of the model parameter and to produce the confidence intervals of the model curves. The resulting best-fit model parameters were subsequently used to simulate model predictions. To validate this approach, the predictions were compared with both constant (5, 50, 500 and 5000 µg L^{-1}) and pulsed (5 and 50 µg L^{-1}) exposure scenarios. All calculations were performed in MATLAB 2021b using the Bring Your Own Model (BYOM) modeling platform (www.debtox.info/byom.html, version 6.2). Model scripts are provided on GitHub (https://github.com/NikaGoldring/TK-receptor).

5.3 Results and discussion

5.3.1 Lipid and protein content

The determined lipid contents (wet weight basis) were 0.7 ± 0.2% (toxicokinetic experiments) and 0.4 ± 0.2% (gammarids used for *in vivo* and *in vitro* receptor binding

assay, mean ± SD, n = 3). Lipid contents were in a similar range to that observed elsewhere (Dalhoff et al., 2018; Raths et al., 2023a). The observed decrease in lipid content from fall to winter may be due to the use of energy reserves, such as storage lipids (Dalhoff et al., 2018). No lipid normalization of accumulated thiacloprid was performed as lipid content was demonstrated to have no significant influence on bioconcentration of polar organic contaminants in amphipods (Raths et al., 2023a).

The total protein content (wet weight basis) across the experiments ranged from 4.4 to 5.0% and are within the range reported for other gammarid populations (Dalhoff et al., 2018). The average membrane protein content was 1.0 ± 0.1% and higher than reported for other aquatic invertebrates and methods (Maloney et al., 2021).

5.3.2 Exposure medium

The measured medium concentrations of all performed toxicokinetic experiments were within 20% of the nominal concentrations (SI B), which is in line with the OECD 305 requirements (OECD, 2012b). Concentrations of the elimination medium were below the limit of quantification (generally 0.01 µg L^{-1}, but 0.001 for the low exposure concentrations of 0.5 and 0.05 µg L^{-1}), confirming a low impact for reuptake from the medium, except for minor residues after exposure with concentrations ≥ 500 µg L^{-1}. Relative O_2 saturation (> 85%), pH (7.9 ± 0.1) and water temperatures were stable (15.5 ± 1 °C) during the experiments.

5.3.3 Exposure concentration-dependent toxicokinetics

The internal concentrations of gammarids exposed to different concentrations of thiacloprid (0.5 – 5000 µg L^{-1}) increased significantly along the concentration gradient from an average of 0.23 ± 0.03 to 39 ± 4 µmol kg^{-1} at the end of the uptake phase (Figure 5.5). However, the difference in internal concentration between the lowest and the highest concentration was only a factor of 150 despite a 10,000-fold difference in exposure concentration. The developed toxicokinetic model (Table 5.3) demonstrated that steady state conditions would be reached within the exposure time window for all applied exposure concentrations. At the end of the elimination phase, no significant difference between remaining tissue concentrations was observed (0.18 ± 0.04 to 0.39 ± 0.13 µmol kg^{-1}). Furthermore, no statistical difference between tissue concentrations at the end of the exposure and elimination phase was observed for concentrations equal to or lower than 5 µg L^{-1}. Thus, the present data indicate a concentration dependence of the whole-body bioconcentration of thiacloprid in *G. pulex* due to a saturation of the second, elimination-resistant, membrane protein compartment.

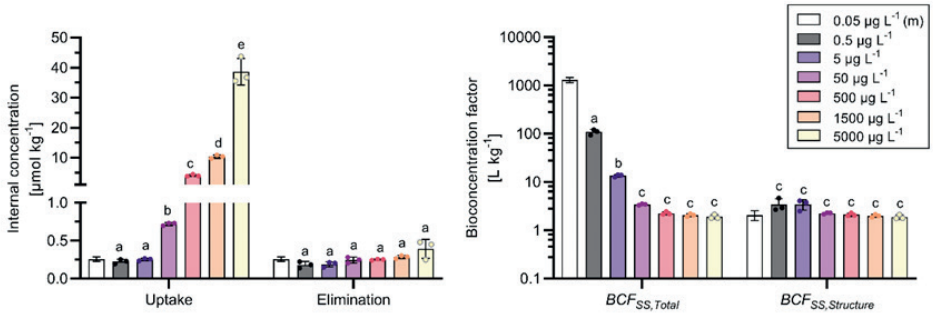

Figure 5.5: Internal concentrations (left) of thiacloprid at the end of the uptake and elimination phase at different exposure concentrations. Calculated uncorrected $BCF_{SS,Total}$ and the $BCF_{SS,Structure}$ (right). Data are presented as individual data points and mean ± SD (n = 3). Letters indicate significant differences between the groups (two-way ANOVA, $p < 0.05$, log transformation, Tukey's post-hoc test). For 0.05 µg L-1 (m) data were modeled using the toxicokinetic-receptor model, because no steady state was reached during this experiment (20 days).

In order to account for the two-compartment bioconcentration kinetics, two different bioconcentration factors were calculated (Figure 5.5). The $BCF_{SS,Total}$ was calculated from the tissue and medium concentration at the end of the uptake phase (Eq. 5.1), representing the whole body concentration. It showed a clear concentration dependence, ranging from 1.9 ± 0.2 L kg^{-1} at the highest exposure concentration towards a 60 times higher value (109 ± 14 L kg^{-1}) at the lowest exposure concentration that reached steady state (0.5 µg L^{-1}). The $BCF_{SS,Structure}$, calculated by subtracting the elimination resistant fraction from the total tissue concentration (Eq. 5.2), resulted in much more similar bioconcentration factors (2.5 ± 0.8 L kg^{-1}), which were also in range of the modeled $BCF_{kin,Structure}$ (2.0 L kg^{-1}, Eq. 5.8) of the structure compartment. The difference between the $BCF_{SS,Total}$ and $BCF_{SS,Structure}$ was not significantly different for the high exposure concentrations (500 to 5000 µg L^{-1}), due to the small relative contribution of the membrane protein compartment to the whole body concentration.

All calculated $BCF_{SS,Total}$ in the present study were below the B criterion (BCF ≥ 2000 L kg^{-1}; (OECD, 2012b) threshold and in range of those reported for neonicotinoids in *G. pulex* and other aquatic species (0.2 – 70; (Ashauer et al., 2010; Huang et al., 2021; Li et al., 2021; Yang et al., 2022). However, considering the increasing $BCF_{SS,Total}$ with decreasing exposure concentration - caused by the saturation of the membrane protein compartment - the BCF of thiacloprid would continue to increase at lower, field-relevant concentrations. For instance, at concentrations below 30 ng L^{-1} the $BCF_{SS,Total}$ could increase above the regulatory threshold (BCF ≥ 2000 L kg^{-1}) and at ≤ 12 ng L^{-1} above the very bioaccumulative criterion (BCF ≥ 5000 L kg^{-1}), given a long enough exposure time. Measured neonicotinoid concentrations in surface waters are typically in this ng L^{-1} range (Lauper et al., 2021; Morrissey et al., 2015b; Stehle et al., 2023). Thus, the concentration dependence of

neonicotinoid accumulation would also explain the much higher accumulation of neonicotinoids observed in the field compared to laboratory studies (Lauper et al., 2021).

Previous investigations that determined internal concentrations of neonicotinoids in crustaceans (Li et al., 2021) may not have observed such two-compartment kinetics because of very high (mg L^{-1} range) exposure concentrations masking the elimination resistant fraction (e.g. 5000 µg L^{-1}, Figure 5.5). These high exposure concentrations were applied due to the low acute toxicity of neonicotinoids towards crustaceans, but probably also to guarantee a proper quantification of the compound in tissue samples. The methods applied in the present study facilitated the determination of medium and tissue concentrations of exposure experiments down to the ng L^{-1} range and allowed detecting the elimination resistant thiacloprid amount. Thus, testing bioconcentration at lower exposure concentrations may improve the detection and understanding of discrepancies between laboratory and field experiments (Lauper et al., 2021).

5.3.4 Pulsed exposure

The measured tissue concentrations in gammarids exposed to three consecutive pulses of thiacloprid are shown in Figure 5.6. In the 50 µg L^{-1} exposure treatment, all internal concentrations were, on average, three times higher during the uptake phase after one and two days (0.76 ± 0.04 µmol kg^{-1}) than during the elimination phase (0.23 ± 0.03 µmol kg^{-1}). A similar pattern but lower internal concentrations at the end of the uptake phases were observed in the 5 µg L^{-1} treatment (SI5-A11). The measured internal concentrations, including the elimination resistant fraction after one and three days of elimination, were similar to the concentrations measured in the concentration dependent toxicokinetics experiments. Thus, the pulsed exposure experiment supported the observed elimination resistance of the membrane protein compartment. Furthermore, it was demonstrated that the non-eliminating residues reached the maximum binding capacity already after the first exposure pulse and remained unchanged afterward. These results may help interpreting toxic effects observed in pulsed exposure scenarios elsewhere (Focks et al., 2018; Nyman et al., 2013b).

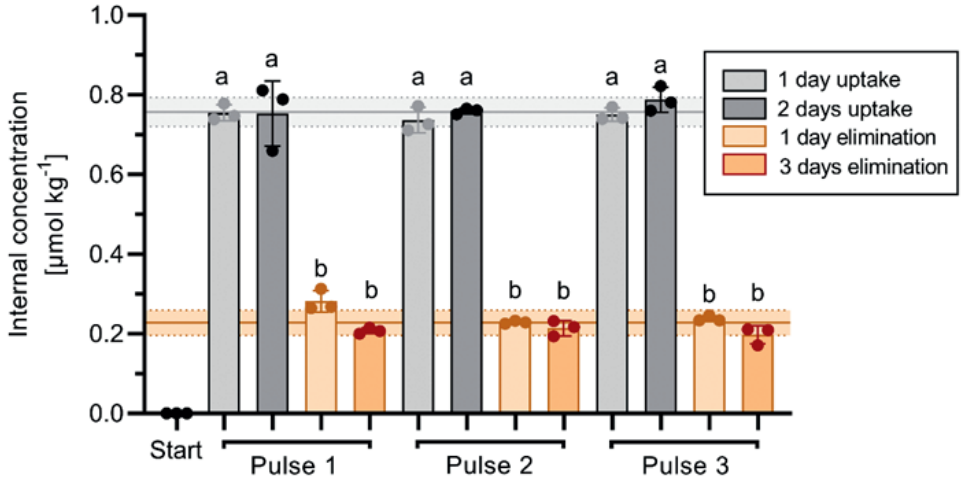

Figure 5.6: Internal thiacloprid concentrations in *G. pulex* sampled during the pulsed exposure experiment at 50 µg L^{-1}. Lines represent the average (± SD, n = 18) tissue concentration determined in gammarids sampled during the uptake phase (grey) and elimination phase (orange). Significant differences within each exposure pulse concentration are indicated by letters (two-way ANOVA, $p < 0.05$, Tukey's post-hoc test).

5.3.5 Receptor-binding assays

The amount of thiacloprid recovered in the *in vivo* receptor binding assay matched the concentrations of the conventionally extracted (whole body burden) samples of both the exposure and elimination phase (Figure 5.7). After the uptake phase, most thiacloprid was recovered in the supernatant (64%), followed by membrane proteins (19%) and debris (16%). Thiacloprid associated with the different fractions may be interpreted as follows: 1. supernatant = free thiacloprid (i.e., structure compartment) or thiacloprid detached from membrane proteins or associated with membrane proteins that were not separated during ultracentrifugation, 2. debris = thiacloprid that was not extracted by the dissociation medium (i.e., incomplete membrane protein extraction, association with the exoskeleton, incorporation into un-lysed tissue), and 3. membrane proteins = thiacloprid associated with membrane proteins such as the nAChRs. Binding or sorption to the exoskeleton (i.e., debris fraction, exuviae analysis SI5-A4) seemed to be of low importance for thiacloprid body burdens, other than suggested for other chemicals in crustaceans in earlier reports (Lauper et al., 2021; Li et al., 2021).

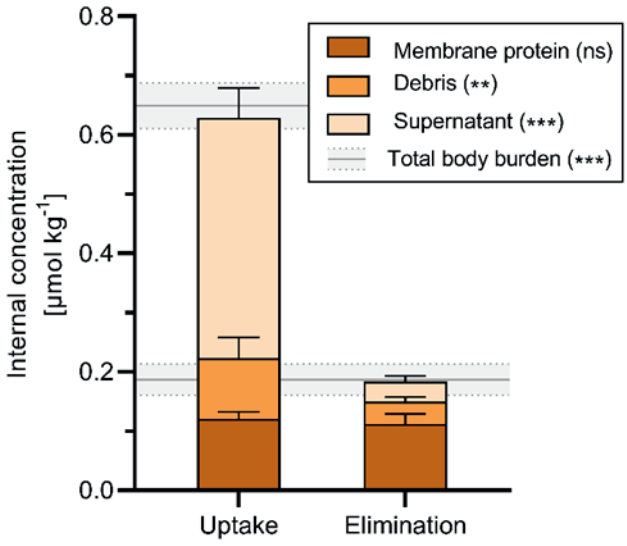

Figure 5.7: Thiacloprid concentrations recovered in the different fractions of the in vivo nAChR binding assay presented as stacked bar plots. The grey line indicates the concentration determined from the unfractionated extract (lower line = elimination, upper line = uptake). Data are presented as mean ± SD (n = 6). Significant decreases from the end of uptake to the end of elimination phase are indicated by asterisks (n.s. = $p \geq 0.05$, ** = $p < 0.01$, *** = $p < 0.001$; two-way ANOVA, Tukey's post-hoc test).

The amount of thiacloprid in the supernatant and the debris decreased significantly by more than 90 and 60%, respectively, during the elimination phase. In contrast, thiacloprid concentrations in membrane protein remained constant from the exposure to the elimination phase. At the end of the elimination phase, thiacloprid associated to membrane protein accounted for the largest amount (61%) of the total body burden. The *in vivo* receptor-binding assay indicated that the elimination-resistant fraction of thiacloprid in *G. pulex* may be caused by irreversible binding to parts of the membrane proteins, such as the nAChRs.

Parameters from the one-site, specific binding model (R^2 = 0.83, SI5-A8) of the *in vitro* ligand binding assay are presented in Table 5-2. Similar parameters were estimated with the unspecific binding model (B_{Max} = 5.5 and K_d = 0.41, SI5-A8). While the CI of B_{Max} was narrow (< 15%), K_d was estimated with considerable uncertainty due to the insufficient coverage of the binding isotherm in the proximate region of K_d (Scatchard plot). However, even in previous studies covering lower exposure concentrations and with a more sensitive radio-labelled method, similar confidence intervals were obtained (Maloney et al., 2021). An extrapolation of B_{Max} to the whole organism (C_{BMax}), correcting for membrane protein recovery after the *in vitro* assay (24%) and membrane protein content (1%), resulted in a whole-body concentration of 0.24 µmol kg^{-1}. Such concentration is in a similar range to the elimination resistant fraction determined in the toxicokinetic experiments and *in vivo* binding

assay. Thus, the utilization of *in vivo* and *in vitro* receptor binding assays seemed to be sufficient to upscale receptor-binding processes to the whole organism level, which provides potential for novel toxicokinetic research approaches.

Table 5.2: Thiacloprid binding parameters estimated with the one-site, specific binding model. Parameters are presented with the corresponding 95% CIs. R2 = 0.83. C_{BMax} = maximal nAChR bound thiacloprid amount extrapolated to the whole body of *G. pulex* using the membrane protein content FMS and the membrane protein recovery rate of 24% throughout the in vitro assay. C_{BMax} is equal to the receptor density in the whole organism, assuming one binding site per receptor.

Parameter	Best fit	95% CI	Unit	Explanation
B_{Max}	5.7	5.1 – 6.4	µmol kg^{-1}	Maximal binding capacity (membrane protein)
K_d	0.41	0.15 – 0.85	nM	Equilibrium dissociation constant
C_{BMax}	0.24	0.21 – 0.27	µmol kg^{-1}	B_{Max} scaled to organism level

The B_{Max} values obtained from the *in vivo* receptor binding assay may be compared to existing studies with imidacloprid, as both imidacloprid and thiacloprid were suggested to bind to the same nAChR binding site (one of five subunits) in cockroach neurons (Tan et al., 2007). Therefore, the B_{Max} values of the two neonicotinoids are also indicative of the receptor densities in different arthropod species. (Maloney et al., 2021) reported B_{Max} values for imidacloprid in 13 invertebrate species ranging from 51 × 10^{-6} to 6.5 µmol kg^{-1}. The B_{Max} for thiacloprid in *G. pulex* was closest to the values reported for imidacloprid in *Chironomus riparius* and *C. dilutus* larvae (Maloney et al., 2021). Since nAChRs are not only located in the peripheral and the central nervous system but also in muscular tissues (Hogg et al., 2003), the high binding capacity in both organism types may result from a high proportion of muscular tissue (SI5-A12). Furthermore, it should be noted that similar molar concentrations of imidacloprid at the end of the elimination phase from toxicokinetic experiments with two other *G. pulex* populations (Mangold-Döring et al., 2022b; Švara et al., 2021) were comparable to the observations for thiacloprid in the present study. These findings support the suggested similar nAChR binding capabilities of the two neonicotinoids in gammarids.

The methods from (Maloney et al., 2021) using radiolabeled imidacloprid could be sufficiently adapted to less specialized laboratory equipment and the measurement of unlabeled ligands. However, the adaptation resulted in several drawbacks, such as the need for larger sample volumes and time-consuming ultracentrifugation. Possible optimizations, such as the reduction of the assay to a microplate layout to reduce centrifugation steps and losses, are discussed in SI5-A13.

5.3.6 Toxicokinetic-receptor model

The thiacloprid concentrations in *G. pulex* tissue (Figure 5.8) showed a steady increase during the exposure phase of the kinetic experiments. The increase in tissue concentrations was slowing down considerably between days 1 and 2 at exposure concentrations ≥ 5 µg L^{-1}. During the first day of the elimination phase, thiacloprid was rapidly removed from the structure compartment, but no elimination occurred from the membrane protein compartment, which determines the remaining total tissue concentration. This behavior is consistent with the observations of the receptor binding assays.

The determined model parameters are provided in Table 5-3. The calibrated best-fit model parameter resulted in an overall R^2 of 0.99 in describing the measured total internal concentration of thiacloprid in *G. pulex*. The quality of the fit by visual examination was deemed satisfactory (Figure 5.8 and S5-6). The profile likelihoods (Figure S5-7, plots on the diagonal) of k_u, k_e, and B_{Max} were well-defined (i.e., u-shaped and crossing the critical value on both ends). k_{on} could not be identified as this process seemed to be much faster than k_u and the time resolution of the observations. Therefore, the optimization algorithm hit the arbitrarily set upper limit for this parameter. Thus, the association process might be seen as instantaneous, given the available dataset. The likelihood-based joint-confidence regions (Figure S5-7, scatter plots) showed a strong correlation of the model parameters k_u and k_e, expressed in their narrow-shaped ellipse. The calibrated model showed high accuracy in predicting the measured concentrations of the validation datasets for both constant (Figure S5-8) and pulsed exposure scenarios (Figure S5-9). Physiological inactivity of gammarids (SI5-A11) had a noticeable impact by reducing toxicokinetic rates, but only minor effects on B_{Max} and $BCF_{kin,Structure}$.

Table 5.3: Optimized model parameters of the toxicokinetic receptor model with their corresponding 95% CIs, R2 = 0.99. CBMax = maximal nAChR bound thiacloprid amount extrapolated to the whole body of G. pulex using the membrane protein content FMS.

Parameter	Best fit	95% CI	Unit	Explanation
k_u	10.6	8.5 – 13.6	L kg^{-1} d^{-1}	Uptake rate
k_e	5.2	4.2 – 6.7	d^{-1}	Elimination rate
k_{on}	200	37.6 – 200*	kg µmol^{-1} d^{-1}	Association rate for the ligand-receptor complex
k_{off}	0	fixed	d^{-1}	Dissociation for the ligand-receptor complex
B_{Max}	25.0	22.7 – 29.4	µmol kg^{-1}	Maximal binding capacity (membrane protein)
C_{BMax}	0.25	0.23 – 0.29	µmol kg^{-1}	B_{Max} scaled to organism level

*Boundary of the parameter space explorer.

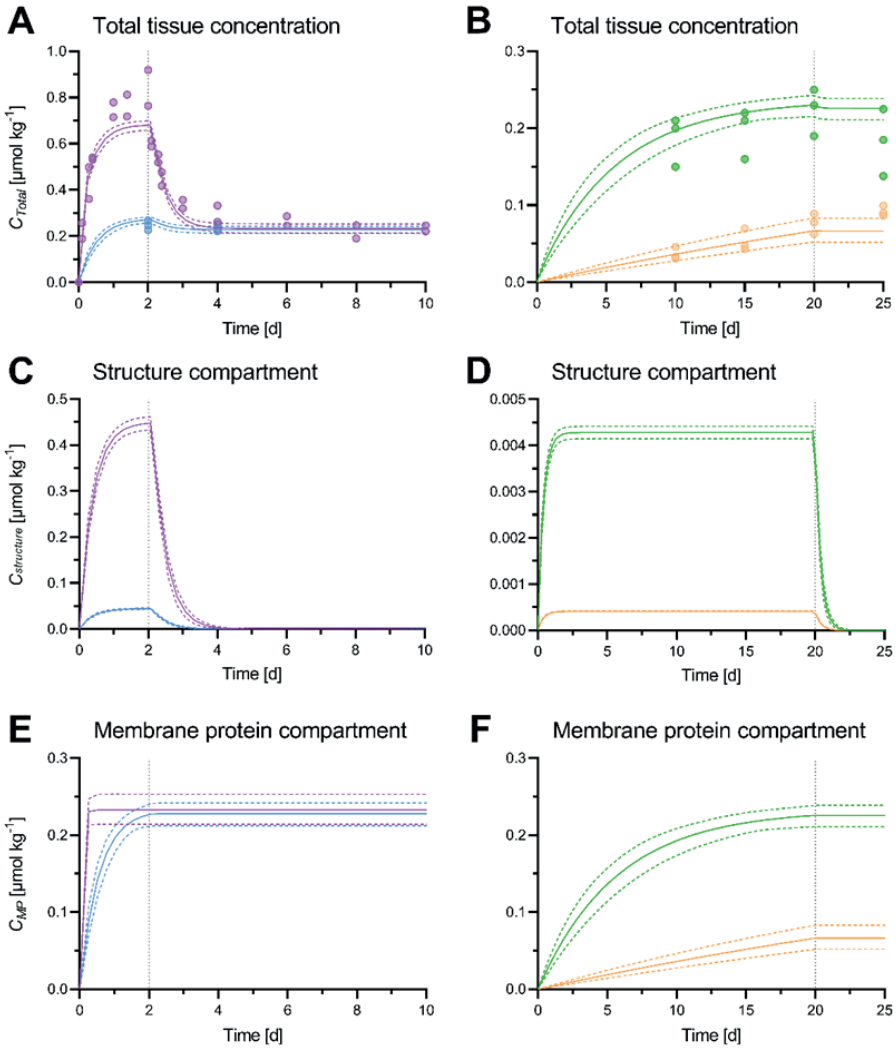

Figure 5.8: Total thiacloprid tissue concentrations (A, D), structure compartment (B, E), and membrane protein compartment (C, F) concentrations presented as measured values (dots) and toxicokinetic-receptor model fits (lines) from the model calibration. Colored dotted lines represent the 95% CIs. Grey dotted lines indicate the change from uptake to elimination phase. Please note the different y-axis scales. The presented membrane protein concentration is up-scaled to the total tissue concentration to allow a better comparison. Underlying model parameters are provided in Table 5-2. The complete dataset is plotted in Figure S5-6.

One assumption of the developed model was irreversible binding, which resulted in a fixed value of zero for k_{off}. No elimination of thiacloprid during the present experiments could be observed by statistical nor modeling means. However, this assumption may not hold true for much longer experimental times. For instance, a recovery time of 45 days was determined by toxicokinetic-toxicodynamic (TK-TD) modeling for imidacloprid exposed daphnids (Li et al., 2021), but no recovery was identified for gammarids in a different study (Mangold-Döring et al., 2022b). In competition binding assays, it was demonstrated that the binding affinity of neonicotinoids is much higher than acetylcholine, but neonicotinoids may still be removed if acetylcholine is available in large excess (Lind et al., 1998). This mechanism may eventually result in a slow recovery of affected nAChRs. Furthermore, organisms may recover by deconstructing affected receptors and generating new receptors dynamically. These mechanisms may also lead to lower B_{Max} values at very low exposure concentrations (<< 0.5 µg L^{-1}), which take a considerably longer time to reach the maximal C_{MP} concentration.

The developed model assumed well-mixed compartments as a simplification. However, this might not be appropriate for the representation of receptors in different organs. It is known that different nAChRs of various organ types (i.e., muscles and nervous system) are built from different subunits (Matsuda et al., 2001). The proportion of these receptor/subunit types may change across species, seasons, and developmental state, thus affecting the suitability of the applied membrane protein content normalization. Furthermore, this may limit the extrapolation of the total nAChR density based on receptor bound neonicotinoids.

The profile likelihood analysis revealed an identification problem with the parameter k_{on}, whose upper boundary could not be distinguished from infinity (Figure S5-7, plots on the diagonal). This problem can be associated with so-called 'fast kinetics' extensively discussed by experts before (Jager and Ashauer, 2018b). That is, when fast kinetics are observed, the steady-state is reached before the first measurement. In the present study, this was the case for the receptor-bound fraction, because no independent kinetic measurements of the receptor bound fraction were feasible. Thus, the data do not hold the exact information about how quickly a steady state between structure and membrane protein compartment is achieved, and it might thus be as likely as instantaneously. To minimize the effect of this parameter and avoid numerical problems on the joint-confidence regions, the fixed boundary of the parameter space explorer (i.e., 200) was used as upper boundary of k_{on}. Consequently, also the assumption of instantaneous binding could be another way of simplifying the present model. The described observation is in line with the high receptor affinity of thiacloprid to nAChRs, indicating that the speed of *in vivo* receptor binding kinetics is limited by the initial uptake of thiacloprid into the structure compartment.

Biotransformation of thiacloprid in amphipods neither was reported in the literature nor was it found in a screening (SI5-A7) for reported biotransformation products (e.g. thiacloprid amide) in bacteria (Zhao et al., 2019). Thus, in order to also display toxicokinetics of neonicotinoids or other receptor bound compounds that are biotransformed in amphipods (e.g. imidacloprid; (Huang et al., 2023, 2021), the presented model may be extended by considering biotransformation. However, further research would be needed in order to understand and implement the exact mechanisms of biotransformation, such as compartment dependent biotransformation and binding of biotransformation products to the nAChRs.

5.3.7 Considerations for risk assessment

In the present study, we demonstrated that irreversible binding to membrane proteins such as the nAChRs explains the observed elimination resistance (Lauper et al., 2021; Raths et al., 2023a; Švara et al., 2021) of neonicotinoids from amphipod tissue. Consequently, this elimination resistant fraction may explain the delayed toxic effects and irreversible damages towards aquatic arthropods that were previously reported (Beketov et al., 2008; Beketov and Liess, 2008; Huang et al., 2023; Nyman et al., 2014). In fact, the membrane protein associated fraction may be interpreted as either irreversible damage to the nAChR, or continuous exposure due to elimination resistance, depending on the point of view. The here provided mechanistic insights may help to improve the understanding of toxicokinetics, toxicodynamics, and adverse outcome pathways (AOPs) of neonicotinoids in arthropods. Such considerations may be important for the risk assessment of neonicotinoids, as well as their replacement candidates (i.e., flupyradifurone; Jeschke et al., 2015) and other contaminants with (irreversible) receptor binding properties. Furthermore, existing TK-TD modeling approaches (Focks et al., 2018; Gergs et al., 2021; Huang et al., 2023; Mangold-Döring et al., 2022a) may be updated based on the present findings.

The standard bioaccumulation assessment, according to OECD 305 (OECD, 2012b) using fish, generally assumes one-compartment kinetics, an independence of bioaccumulation parameters from exposure concentrations and a relevance of bioaccumulation only for compounds with high log K_{OW} values. However, our toxicokinetic investigations on neonicotinoids in aquatic invertebrates demonstrated a strong exposure concentration dependence due to a maximum binding capacity and no elimination from the membrane protein compartment. These mechanisms may result in bioconcentration factors above the threshold value for the B criterion (2000) at concentrations typically observed in the environment (ng L^{-1} range; (Morrissey et al., 2015b; Stehle et al., 2023). In contrast to multi-compartment kinetics caused by sorption to exoskeleton/cuticula of aquatic invertebrates (Dalhoff et al., 2020), the here reported second compartment consists of a

bioactive, and thus toxicological relevant, fraction. Similar mechanisms for elimination-resistant bioactive fractions may exist for other compound classes with observed multi-compartment kinetics, such as strobilurins in amphipods (Kosfeld et al., 2020; Raths et al., 2023a). However, further research is needed to understand the underlying mechanisms and toxicological relevance. In order to account for concentration-dependent bioaccumulation, a category such as “elimination resistant” or “receptor bound” may be important for establishing new testing guidelines; i.e. for the proposed bioaccumulation studies using arthropods (Schlechtriem et al., 2022, 2019). With our developed toxicokinetic-receptor model, we provide the required modeling platform for such implementations.

Furthermore, the usefulness of environmental threshold concentrations for elimination-resistant compounds such as neonicotinoids may be reconsidered (Stehle et al., 2023). Exposed organisms may accumulate neonicotinoids over their lifetime and eventually reach saturation of the nAChRs regardless of the exposure concentration. Furthermore, environmental parameters may have an impact on toxicokinetics of neonicotinoids. For instance, temperature was demonstrated to exert an exponential relationship with uptake and elimination rates in amphipods (Raths et al., 2023a). This may result in much faster saturation of the nAChRs, especially if high water concentrations co-occur with higher temperatures, such as during a run-off event in the summer, and consequently enhance the exposure risks towards aquatic arthropods. However, further investigations of the interaction of temperature and neonicotinoid exposure are needed to evaluate this risk.

Supporting Information Available

The Supporting Information is available free of charge at
https://pubs.acs.org/doi/10.1021/acs.est.3c01891

1) Data on the measured concentrations of kinetic experiments, concentration-dependent toxicokinetic experiments, pulsed exposure experiments, in vivo receptor-binding experiments, and in vitro receptor-binding experiments (XLSX)

2) Neonicotinoid insecticides, test animal acclimation, lipid content, investigations on exoskeleton sorption, protein content, online SPE LC-HRMS/MS settings and quality control, in vitro receptor-binding assay, details on the toxicokinetic-receptor model, impact of physiological activity on toxicokinetics, pulsed exposure, gammarid cross-section, and possible receptor-binding assay optimizations (PDF)

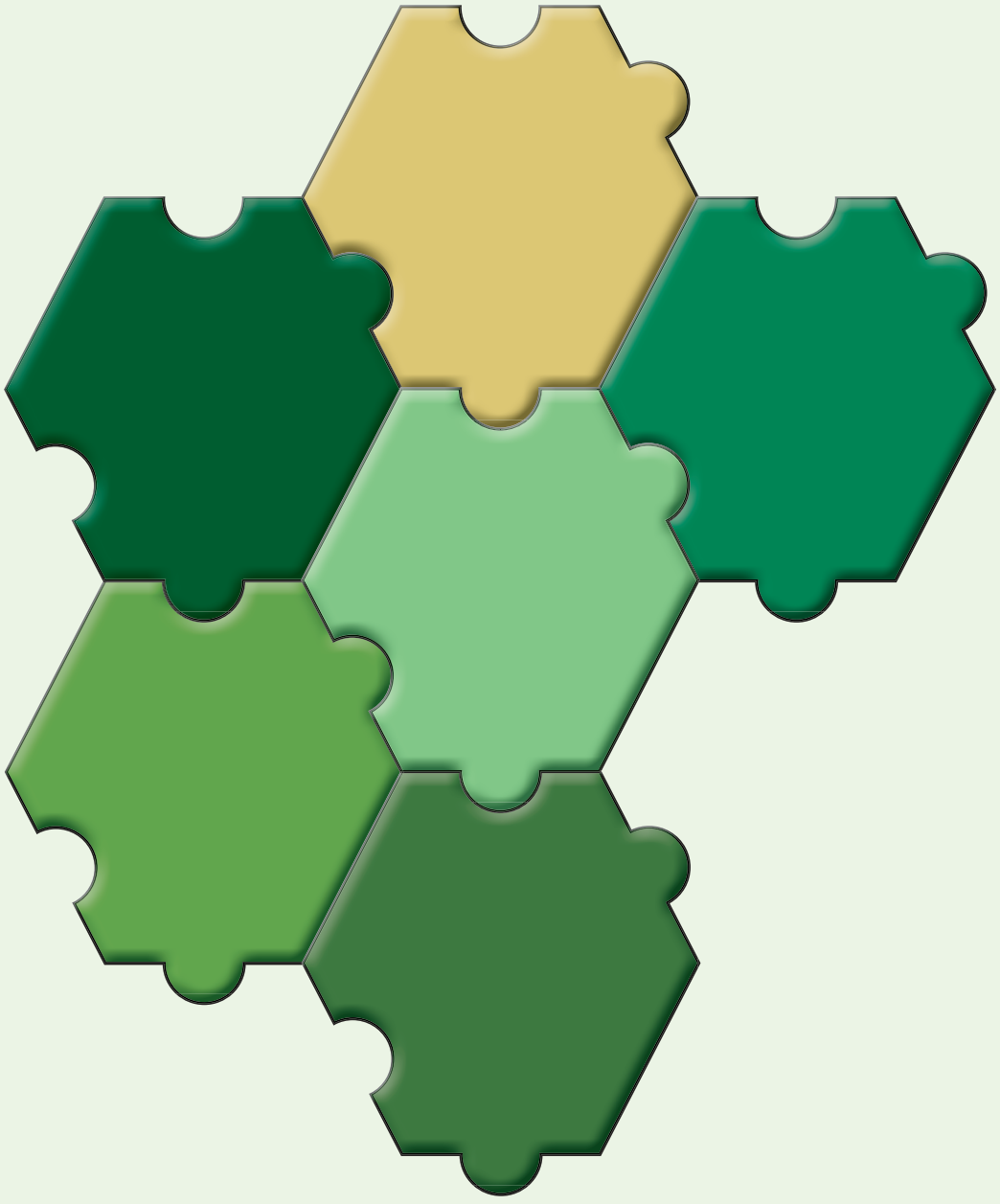

Chapter 6

How relevant are temperature corrections of toxicity parameters in population models for environmental risk assessment of chemicals?

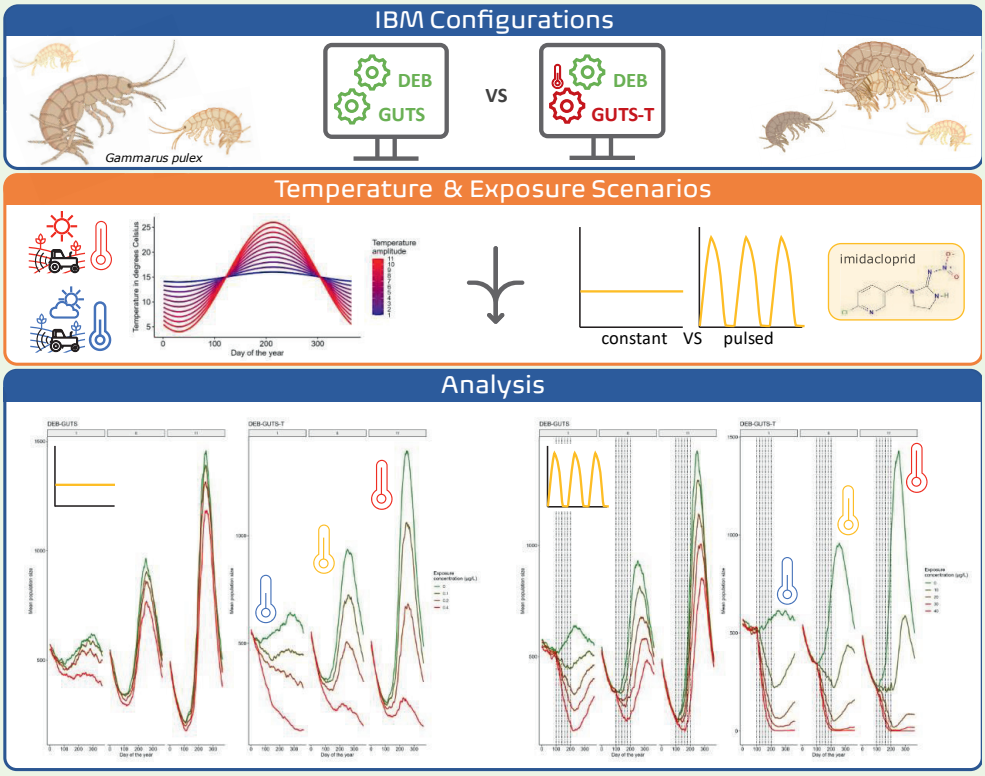

Figure 6.1: Graphical abstract of Chapter 6. Overview presenting the workflow of this chapter from the used model configurations over the scenarios to the analysis.

Annika Mangold-Döring, Willem B. Buddendorf, Paul J. van den Brink, Johannes M. Baveco

Abstract

Population models provide insights into population dynamics under diverse exposure scenarios, enhancing environmental risk assessment (ERA) of chemicals. In this study, we investigate the interplay of temperature and imidacloprid exposure on population dynamics using an Individual-Based Model (IBM) incorporating a dynamic energy budget (DEB) model for population dynamics and toxicokinetic-toxicodynamic models of the General Unified Threshold model for Survival (GUTS) framework to predict toxicity effects. For this, we tested different model configurations, where i) only the DEB parameters are corrected for temperature, as is common practice, and ii) where also the TKTD parameters of the GUTS model are corrected for temperature. In doing so, we aim to evaluate the importance of temperature corrections in the GUTS model within an IBM framework. Our findings reveal that increased temperature amplitudes widen observed population size ranges during simulations, but exposure scenarios counteract this effect by reducing maximum population sizes. The combined effect yields an overall negative trend at lower temperature extremes, reducing population size. These results highlight the necessity of temperature-sensitive parameterization in population models for a protective risk assessment under the projected future climate conditions with increased variability. Future considerations include incorporating local adaptations and acclimatization, particularly in different climate zones, to accurately interpret population model outcomes in the context of evolving environmental conditions. Such insights contribute to the refinement of ecological realism in ERA, enhancing the robustness of chemical risk management strategies.

6.1 Introduction

Ecological models can help us to study, formulate and understand the fundamental processes of the real-life system they represent by integrating the basic building blocks of the system of interest. In environmental risk assessment (ERA) of chemicals, population models are powerful tools (Forbes et al., 2009; Schmolke et al., 2017), especially as the protection goals are often defined on the population level (EFSA (PPR), 2010). Population models provide robust and traceable insights into population dynamics under a wide range of exposure scenarios that would otherwise be associated with too high costs and time demand to be evaluated in (semi-)field experiments. With their demographic endpoints (i.e., intrinsic population growth rates, equilibrium densities), they are primarily used in the "higher tier" ERA (EFSA (PPR), 2018; Larras et al., 2022a). Briefly, the "tiered approach" in ERA separates different levels of complexity regarding the experimental system used for the assessment. While always starting at Tier 1, it can thus be possible to refine the biotic and abiotic factors in pursuit of a more realistic assessment scenario in higher tiers.

Frequently used types of population models are individual-based models (IBMs) making up half of the population models used in the ERA of plant protection products (Larras et al., 2022a). In IBMs, the population is constructed from many individual organisms that can have specific attributes. The life histories of individuals are tracked and they interact with each other and with their local environment. From these interactions population dynamics emerge, that might be influenced by environmental changes or stressors. As the variety of processes that can be implemented in IBMs is manifold, experts see a high potential to use them in ERA (Accolla et al., 2021; EFSA (PPR), 2014; Forbes et al., 2016).

Temperature is an important abiotic factor, especially in seasonal environments, influencing basic organismal processes like aging, growth, and reproduction (S. A. L. M. Kooijman, 2010) and also the toxicokinetics and toxicodynamics (TKTD) of chemicals in individuals (Huang et al., 2023; Mangold-Döring et al., 2022a; Raths et al., 2023b). These influences are generally considered through the Arrhenius equation (Arrhenius, 1889), correcting all rate parameters. Considering the future prediction of increasing temperature extremes due to climate change, there is a rising concern about temperature effects on organisms' health, especially regarding temperature induced increased sensitivity to chemical stressors (Hermann et al., 2023; Polazzo et al., 2022). Recent investigations have highlighted the importance of temperature's influence on TKTD processes on the individual level (Mangold-Döring et al., 2022; Raths et al., 2023). In IBM's, the individual growth and development is often based on the dynamic energy budget (DEB) model (S. A. L. M. Kooijman, 2010) frequently coupled with a TKTD model for chemical effects, like the General Unified Threshold model for Survival (GUTS) (Jager and Ashauer, 2018a). There are thus, at least two modules within an IBM where temperature should be considered (i.e., the GUTS and the DEB module)

when assessing the effects of chemicals on population dynamics in different exposure scenarios. Therefore, the research objectives of this study aimed at examining the relevance of including temperature corrections in the GUTS models within the IBM framework. For this, we are assessing the impacts of chemical exposure on *Gammarus pulex*, a frequently studied freshwater crustacean, contributing to organic matter decomposition (Maltby et al., 2002) and representing a good model organism for ecotoxicological studies (Kunz et al., 2010b). Specifically, we will focus on the insecticide imidacloprid and its effects under different temperature and exposure scenarios. As a proof of concept approach, we seek to compare and evaluate the performance of two different model configurations: i) the standard DEB-GUTS where only the DEB parameters are corrected for temperature, as is common practice, and ii) the DEB-GUTS-T, where also the TKTD parameters of the GUTS model are corrected for temperature.

By testing these different model configurations, we aim to evaluate the importance of temperature corrections in the GUTS model within an IBM framework. The study will provide insights into the effects of accounting for temperature in the GUTS model for population responses to imidacloprid exposure under constant and pulsed exposure conditions and varying temperature scenarios. Ultimately, this research has the potential to contribute to the advancement of the use of IBM models in ERA, through increased realism in population models and process based understanding of effect mechanisms, herewith aiding in developing more robust chemical risk assessment and risk management strategies.

6.2 Methods

In the individual-based population model (IBM), each individual contains a dynamic-energy-budget (DEB) model and a reduced version of the General Unified Threshold model of Survival (GUTS-RED). As a toxicokinetic-toxicodynamic (TKTD) model, GUTS-RED describes the internal damage depending on the external exposure concentration over time (i.e., TK part) and quantifies the daily survival probability (i.e., TD part) (Jager and Ashauer, 2018a). No feedbacks between the DEB and the GUTS model were implemented due to the proof-of-concept character of this study, but they should be considered for future use (Jager, 2020a; Jager et al., 2023).

Including temperature in a population model for a seasonal environmental risk assessment implies the presence of temperature-dependent processes. Indeed, for the DEB module these temperature dependent processes are growth and development, where development determines when reproduction starts. For the pesticide impact on survival (i.e., simulated by the GUTS-RED module), we compare the standard GUTS to the temperature corrected GUTS-T (Mangold-Döring et al., 2022a). To explore the net impact of these temperature

modulated processes on population dynamics in a seasonal environment, we implemented different IBM configurations, i.e., with DEB-GUTS modules or DEB-GUTS-T modules (Figure 6.2). Note that we will refer to the DEB-GUTS, and DEB-GUTS-T to keep it short, while in fact using the GUTS-RED versions in both configurations.

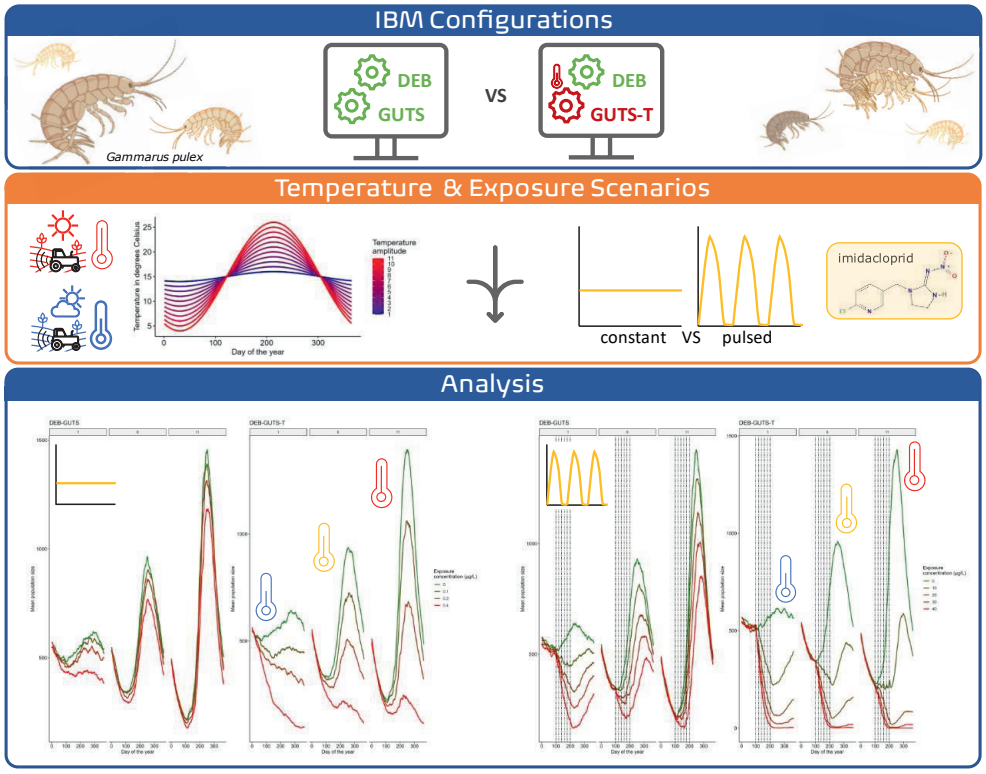

Figure 6.2: Conceptual figure of the study workflow. Two model configurations of the individual based (IBM) population model for *Gammarus pulex* were compared: the DEB-GUTS and the DEB-GUTS-T configuration. These model configurations were used to simulate population dynamics in different temperature and imidacloprid exposure scenarios (i.e., constant and pulsed exposure). The simulation results were compared between the model configuration and scenarios in the final analysis step.

Starting from the NetLogo implementation described in Martin et al. 2012 (Martin et al., 2012), the scaled standard DEB model (Kooijman et al., 2008) was implemented and verified in the software Smalltalk (Squeak 5.3) using the open-source Squeak integrated programming environment (www.squeak.org). The standard DEB model was parameterized on the entry in the Add-my-Pet (AmP) species collection (https://www.bio.vu.nl/thb/deb/deblab/add_my_pet/species_list.html) for *G. pulex* (Zimmer et al., ("Add-my-Pet," 2021) parameter estimated based on version 20210703). Model equations and parameters can be found in the supporting information S03.

The GUTS-T model was developed by Mangold-Döring et al. (2022) and calibrated for *G. pulex* exposed to imidacloprid at three different temperatures, using data previously published (Huang et al., 2023, 2022c). Briefly, we extended standard GUTS model scripts available within the Bring Your Own Model (BYOM) modeling platform (https://debtox.info/byom.html, version 6.2), with the Arrhenius temperature correction based on previously applied approaches (Gergs et al., 2019; Mangold-Döring et al., 2022a). Based on the reasoning discussed in Mangold-Döring et al. parameters with time in their unit were corrected with the Arrhenius equation, i.e., the dominant rate k_d and the killing rate b_w (Mangold-Döring et al., 2022a). For the standard GUTS, the parameters at reference temperature (20 °C) were applied and not corrected for the actual temperature scenario. GUTS-T model equations and parameters can be found in the supporting information S02.

The experimental data used for the calibration comprised survival recordings of field-caught *G. pulex* from the Heelsumse brook (coordinates: 51.973400, 5.748697). During the 28 days exposure to a full factorial exposure to different imidacloprid concentrations (i.e., 0, 0.3, 1, 3, 10, and 30 $\mu g \cdot L^{-1}$) and temperatures (i.e., 7, 11, and 15 °C), the effects on mortality were assessed. The organisms (size: 5.23 mm, sd:1.09 mm) were fed with *Populus* leaves (Huang et al., 2023). We calibrated both the stochastic death (SD) and individual tolerance (IT) model versions in both configurations. GUTS model parameters were estimated based on the Nelder-Mead simplex algorithm provided in the BYOM platform. Their 95 % confidence intervals were estimated through the likelihood region method. The best fitting value for the parameter estimates were subsequently used in the IBM.

The different IBM configurations (i.e., DEB-GUTS and DEB-GUTS-T) were used to simulate different environmental scenarios, i.e., various temperatures and static or pulsed exposure conditions. The different scenarios were simulated over 18 years. Each simulation started with an initialization period of three years without exposure, followed by a period of 10 years with either a constant exposure to imidacloprid (i.e., 0.0 to 1.0 $\mu g\ L^{-1}$ with an interval of 0.1 $\mu g\ L^{-1}$) or pulsed exposure scenarios. Pulsed exposure scenarios consisted of six consecutive concentration peaks, starting at day number 100, with a 20-day interval between each peak (i.e., at day-in-year numbers 100, 120, 140, 160, 180 and 200). The duration of these peaks was 24 hours, with a constant peak concentration ranging from 10 to 100 $\mu g\ L^{-1}$ with an interval of 10 $\mu g\ L^{-1}$.

The seasonal water temperature was simulated using a forcing function with time, with a maximum at the end of July. The temperature was simulated to be fluctuating around the average temperature T_{av} (15 °C), in a cos curve (eq.6.1). The different temperature scenarios were added as a range of temperature amplitudes T_{amp} of 1 to 11 °C with an interval of 1 °C (Figure *6.3*).

$$T(t) = T_{av} - T_{amp} \cdot \cos\left(\frac{t - shift}{365} \cdot 2\pi\right) \quad \text{eq 6.1}$$

The value of the parameter *shift* sets the timing of the day with annual minimum temperature after January 1st and the day with maximum temperature after July 1st. Here, we chose a value of 31 to shift the day with minimum temperature from January 1st to 31st and with the maximum temperature from July 1st to 31st.

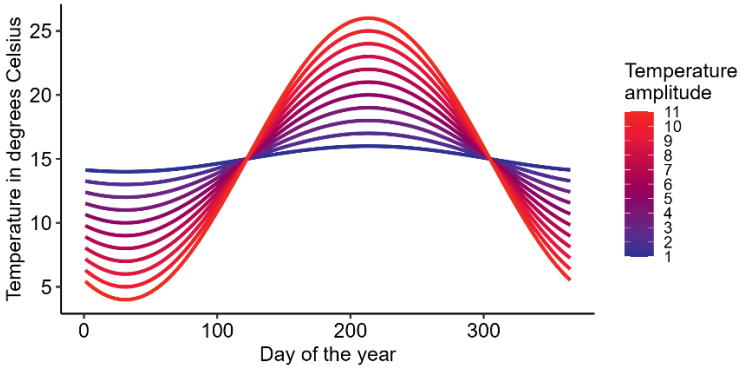

Figure 6.3: Applied temperature scenarios. The temperature over one year of simulation is plotted for different temperature amplitudes.

Model simulations results were further processed in R studio (version 4.3.0) to analyze the mean population size of simulation replicates (n=5) with the described scenario settings. A time series analysis of the first year of imidacloprid application was performed, followed by a cumulative frequency distribution analysis to cover the whole exposure period, i.e., mean daily population sizes during the 10 years of exposure. The two model configurations were then also compared directly through a 1:1 equality line plotting different quantiles of the mean population size.

6.3 Results and discussion

During the evaluation of the model simulations for the different exposure and temperature scenarios, we observed that some scenarios led to the extinction of the population. Those scenarios (i.e., for constant exposures higher than 0.4 µg · L^{-1}, for pulsed higher than 40 µg · L^{-1}, and the temperature amplitude 11 °C or higher) were thus excluded for further analysis. Further, we will primarily show the SD model results here, while the IT model results are provided in the supporting information S01.

What is more, although both SD and IT calibrations resulted in a good visual fit (Supporting Information, S02, Figure S6.9 and Figure S6.11), when looking at the likelihood-based joint-

confidence regions for the model parameter (Supporting Information 02, Figure S6.10 and Figure S6.12), we see identifiability problems as previously described for this dataset (Mangold-Döring et al., 2022a). Briefly, as the experimental data does not hold enough information (i.e., too little differences in effect measured between concentrations), the model parameter and/or its lower and upper boundary may not be defined conclusively. Hence, we do not have enough information to know the exact value for the parameter of $k_{d,}$ for instance. Due to the lack of a better-suited dataset (i.e., including both chemical and temperature scenarios) and the proof of concept character of this study, we decided to use the calibrated best-fitting values as presented (Supporting Information, S02, Table S6.5 and Table S6.6). Alternatively, one or more model parameters could have been fixed in the estimation process, e.g., based on literature knowledge, to allow a better parameter estimation with defined parameter boundaries for the remaining parameters. Nevertheless, we must provide an exact value as input for the IMB model, and here, we chose the best-fitting estimates based on experimental data as described. Further implications of this will be outlined in the following.

6.3.1 Comparing model simulation over the first year of application.

When evaluating the model simulations of the first year of imidacloprid application, we observed considerable differences between the used model configurations in the constant exposure scenarios for the SD model (Figure 6.4). For the standard DEB-GUTS, where no temperature correction is done on the TKTD parameters, the range of the mean population size at control conditions over the first year increased with increasing temperature amplitudes from a maximum population size of roughly 600 at 1 °C to 1300 at 10 °C amplitude (Figure 6.4, A1-A3, green lines). The same trend was observed in the model simulations with the DEB-GUTS-T configuration (Figure 6.4, B1-B3, green lines). Thus, as expected, temperature amplitude drives the population dynamics, with mean population sizes following the same pattern as the applied temperature amplitude scenario (Figure *6.3*), with a minor phase-shift in timing, i.e., the model curves follow the shape of the yearly temperature scenario, simply shifted on the time-axis (Figure *6.4*). This pattern can also be explained by the seasonal dynamics observed for *G. pulex* (Hynes, 1955; Welton, 1979).

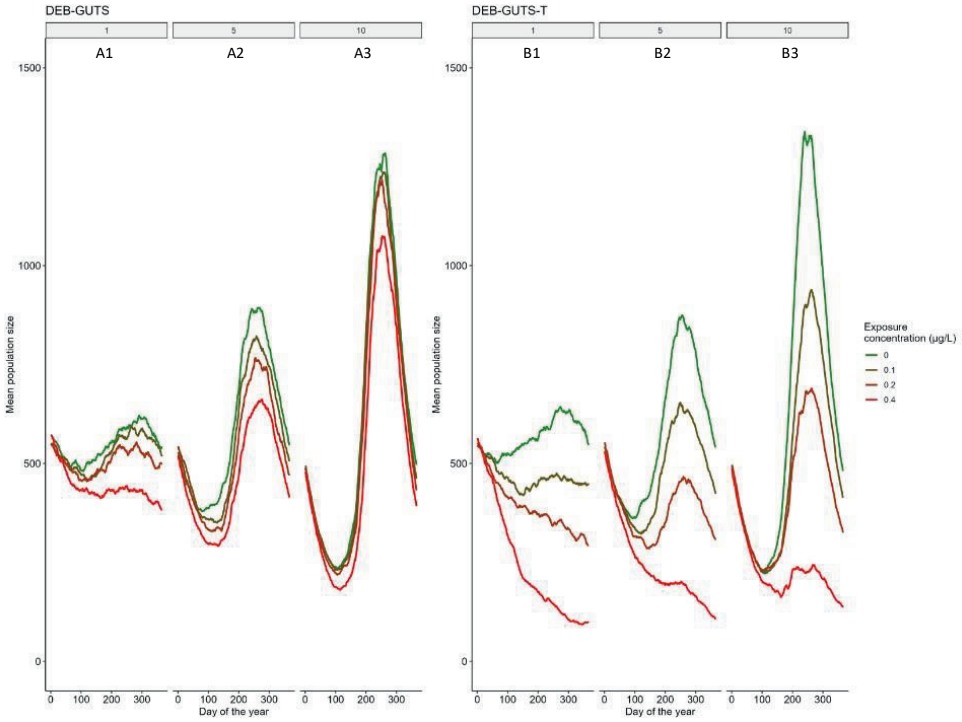

Figure 6.4: Simulation results of the mean population size of *Gammarus pulex* in the first year of constant imidacloprid application at different exposure concentrations and temperature scenarios for both model configurations (SD). The mean of the population size of n = 5 model simulations for each configuration and scenario is plotted over the year of the first application, in days of the year, starting on January 1st. The plots on the left side of the figure (A1-A3) show the results of the simulation with the DEB-GUTS configuration, and the right side (B1-B3) displays the DEB-GUTS-T configuration results. The different environmental scenarios encompass different exposure concentrations, displayed in different colors ranging from 0 to 0.4 µg · L^{-1}, and the different temperature amplitudes are shown in the different panels for each configuration, i.e., A1 and B1 show the temperature scenario with the amplitude of 1 °C, A2 and B2 for 5 °C and A3 and B3 for 10 °C.

Imidacloprid affects the population size maxima and minima in a dose-dependent manner, i.e., increasing adverse effects with increasing exposure concentration (Figure 6.4, A1). This effect is amplified in the DEB-GUTS-T model configuration (Figure 6.4, B1). However, we did not observe the same difference in population sizes between the model configurations using the IT version of the GUTS model (results displayed in the supporting information, S01, Figure S6.1 and Figure S6.2). To explain this, in the following, we want to discuss two different aspects of the model.

Firstly, we postulated that the chemical effect on population dynamics depends on the chosen death mechanism. Conceptually, the GUTS-IT model version relates to the idea that individuals differ in their sensitivity, while in GUTS-SD, the death of the organisms is a stochastic process (Jager and Ashauer, 2018a). Thus, in the SD version, all organisms have the same sensitivity towards the chemical, and the chance of dying increases with increasing concentration. Contrastingly, in the IT version, the organisms differ in their sensitivity, and

the chance to die is 100 % once their individual threshold concentration is reached. Consequently, these different model approaches result in different outcomes in long-term settings, especially in constant exposure conditions (Jager and Ashauer, 2018, Chapter 1.4). Specifically, the SD mechanisms will lead to an ongoing decline of the population over time with continuous exposure, while for the IT mechanism, the sensitive individuals will be dead once the concentration reaches its equilibrium, while the less-sensitive ones will survive no matter how long the exposure lasts.

Secondly, we also looked at the calibrated values for the GUTS-RED models (Supporting Information 02, Table S6.5 and Table S6.6). As discussed in Mangold-Döring et al. 2022, the most straightforward approach to consider temperature effects on the TKTD model parameter is assuming that the parameters with time in their unit need to be scaled with the Arrhenius temperature (Mangold-Döring et al., 2022a). For the GUTS-RED version used in this study, this includes the dominant rate k_d for both IT and SD versions and the killing rate b_w for SD only. Note that the background hazard rate is accounted for in the DEB model. Thus, to avoid accounting for this twice, it is not considered in the GUTS models of either configuration. The calibrated values were significantly different, with k_d = 0.02982 d^{-1} for the SD version and k_d = $1e^{-6}$ d^{-1} for the IT version; both values correspond to the reference temperature of 20 °C. Therefore, we wanted to explore the importance of k_d for the observed differences in mean population sizes. By artificially setting the k_d of the SD model version to $1e^{-6}$ d^{-1} and repeating the simulations, we could show that the value of k_d was responsible for the observed differences in the modeled exposure scenarios, as they were absent in these additional simulations (Supporting Information S01, Figure S6.7 and Figure S6.8). Therefore, we concluded that the observed differences in chemical sensitivity of the population between SD and IT model versions are more likely to be associated with the parameter estimation than actual differences between the death mechanisms. The value around 0.03 d^{-1} for the SD model simply results in more uptake as a k_d = $1e^{-6}$. Furthermore, the additional temperature modulation of the killing rate in the SD model version in the DEB-GUTS-T approach might add to the discussed differences between the IT and SD versions.

Particularly noteworthy is the significant influence of the temperature correction in the low, 1 °C temperature amplitude scenario of the SD model (Figure 6.4, B1). While the DEB-GUTS configuration uses the reference value for k_d at 20 °C, this value is corrected to lower temperatures in the DEB-GUTS-T model, i.e., to temperatures below the reference temperature ranging from 14-16 °C (Figure 6.3). This results in the parameter being lower than in the uncorrected DEB-GUTS configuration throughout the simulation period (Supporting Information S02, Figure S6.13). A small value for k_d represents so-called “slow kinetics” and leads to a linear accumulation of internal concentration at constant exposure, and practically no elimination (discussed in Jager, 2020b, section 4.4 Slow kinetics). Even though the value is bigger than the reference value in the summer period of the simulation

for the 10 °C temperature amplitude scenario (Supporting Information S02, Figure S6.13), the driving factor for the observed population decline is the period where k_d is corrected below the reference value resulting in slow kinetics.

Looking at the results for the pulsed exposure scenarios for the SD model (Figure 6.5), we observed similar trends as described for the constant exposure settings. However, the concentration effect on the population size is greater in the pulsed scenarios for the DEB-GUTS (Figure 6.5, A1) as in the constant exposure scenario (Figure 6.4, A1), due to the higher exposure levels. For the DEB-GUTS-T model simulations, we observed a significant decrease in population size for concentration pulses above and including 20 $\mu g \cdot L^{-1}$ (Figure 6.5, B1-B3). Furthermore, in the 40 $\mu g \cdot L^{-1}$ exposure treatment, the population got extinct in all temperature amplitude scenarios in the temperature corrected simulations (Figure 6.5, B1-B3, light red lines), while this is not the case when the toxicity is not corrected for temperature (Figure 4, A1-A3, light red lines). Thus, in the pulsed exposure scenarios, the temperature correction of the DEB-GUTS-T impacts the chemical effect quite substantially at all levels of exposure. This is again associated to the calibrated value for k_d in the SD model and the discussed implications of its temperature correction towards slow kinetics in low temperature scenarios.

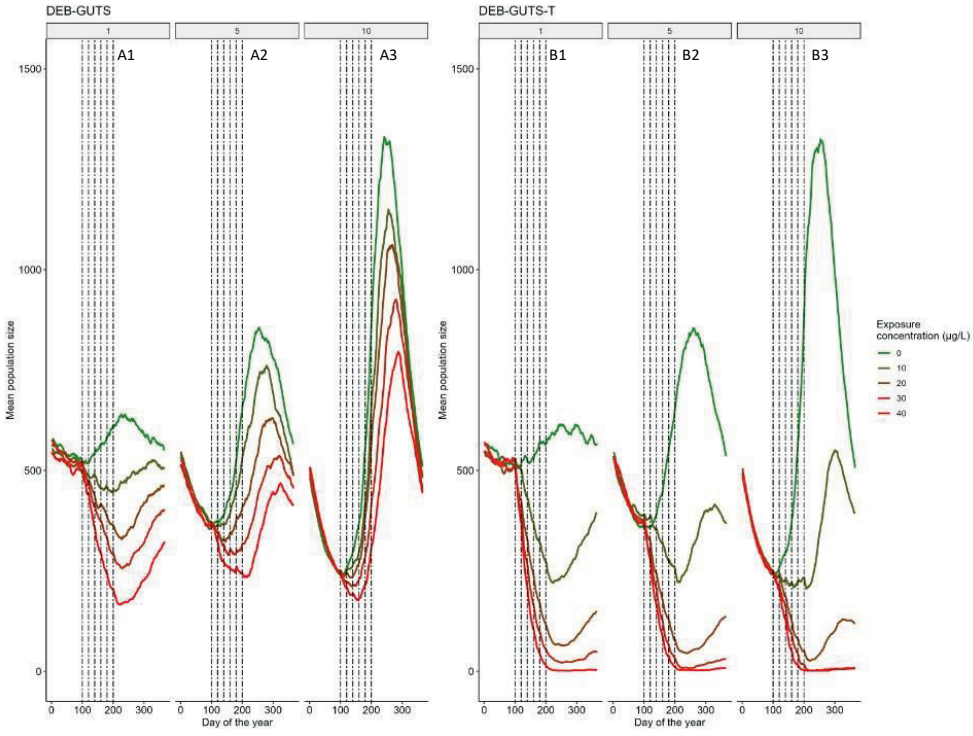

Figure 6.5: Simulation results of the mean population size of *Gammarus pulex* in the first year of pulsed imidacloprid application at different exposure concentrations and temperature scenarios for both model configurations (SD). The mean of the population size of n = 5 model simulations for each configuration and scenario is plotted over the year of the first application, in days of the year, starting on January 1st. The plots on the left side of the figure (A1-A3) show the results of the simulation with the DEB-GUTS configuration, and the right side (B1-B3) displays the DEB-GUTS-T configuration results. The vertical dotted lines indicate the exposure pulses of imidacloprid concentrations ranging from 0 to 40 µg · L^{-1} (i.e., displayed in different colors) were applied for 1 day at days 100, 120, 140, 160, 180, and 200. The different temperature amplitudes are shown in the different panels for each configuration, i.e., A1 and B1 show the temperature scenario with the amplitude of 1 °C, A2 and B2 for 5 °C, and A3 and B3 for 10 °C, respectively.

Furthermore, all the pulses occur in the period with rising temperature (9 April up till 18 July). While in the constant scenarios, the populations are still showing a reproduction peak in the summer month, just at a lower level compared to the control (Figure 6.4, B1-B3), the three highest concentrations in the pulsed exposure, either die out or increase in size after the summer period (i.e., when temperature declines and exposure has stopped), and thus at a much slower rate (Figure 6.5, B2 and B3). In reality, a population disturbed in this way will be impacted in their recovery potential as this is mainly driven by the reproductive period (Galic et al., 2012).

Interestingly, in Figure S6.1 and Figure S6.2, B1-B3 we observed, that when correcting the TKTD parameter for temperature, the IT model exhibits even smaller changes than the SD

model across the applied imidacloprid concentrations, particularly in the 1 °C amplitude group. This result is in contrast with the observed increased concentration effect in the SD version of DEB-GUTS-T as previously discussed. However, as discussed earlier, for the IT version the only temperature corrected parameter was k_d, the dominant rate constant, which was calibrated to $1e^{-6}$ d^{-1} at reference temperature. Thus, this value got even smaller when corrected for the applied temperatures in this scenario and we correct only from slow kinetics to slower kinetics, making stochastic artefacts the most likely explanation for the observed differences.

6.3.2 Comparing model simulation over the whole simulation period.

When plotting the mean population sizes of each day for the five model replicates and over the 10 year exposure period in a cumulative frequency distribution, the different temperature scenarios show different shapes, i.e., from almost straight vertical for the lowest temperature amplitude (Figure 6.6, A1 blue line) to a nearly convex line for the highest temperature amplitude (Figure 6.6, A1 red line). A vertical line indicates a relatively constant mean population size throughout the whole simulation period, as the mean population size does not differ in its frequency between the days. In general, the steeper the slope of the curve in the beginning, the more observations were made in the lower ranges of population sizes. For the different temperature scenarios, the trend is that the observed population size range increases with increasing temperature amplitude. For example, under control conditions, the range of population sizes is the biggest in the 10 °C temperature amplitude scenario, with the lowest value around 150 and the highest value at 1500 (Figure 6.6, A1 red line). For the other temperature scenarios the mean population size range is smaller, with a general trend of Q10 values decreasing and Q90 values increasing with increasing temperature amplitude. The Q50 values are marking the intersection of all temperature scenarios, which is observed across chemical exposure scenarios. With increasing exposure concentration, the range of population sizes decreased.

In these cumulative frequency figures, the steeper the slope, the less variation there is in population size over time. Thus it is easy to see, that there are less profound seasonal density fluctuations in the low temperature amplitudes than in the high ones, which is also reflected in the quantiles plots (Figure 6.7, green dots) and the results of a single year as shown previously (Figure 6.4). The same trend is observed in the DEB-GUTS-T configuration (Figure 6.6, B1-B3), however, more pronounced, with the 0.4 $\mu g \cdot L^{-1}$ treatment showing the same cumulative frequency with mostly low population sizes observed throughout all temperature scenarios (Figure 6.6, B4), due to extinction.

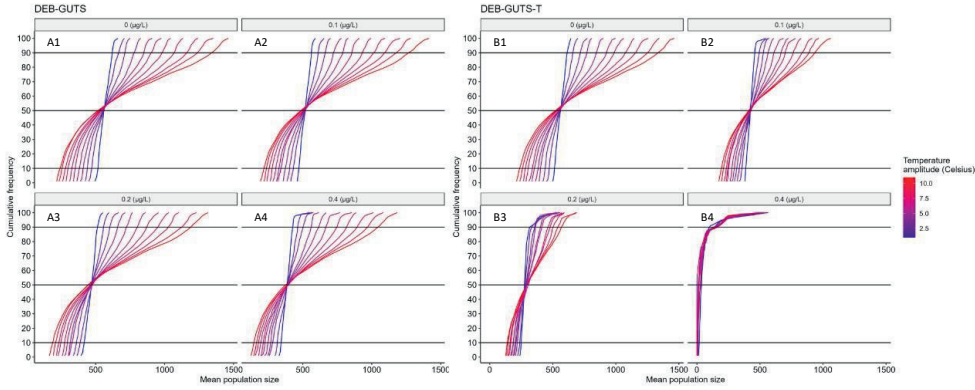

Figure 6.6: Cumulative frequency distribution of mean *Gammarus pulex* population sizes exposed to constant concentrations of imidacloprid at different temperature scenarios (SD). The cumulative frequencies of mean daily population sizes (n = 5) over the 10 year exposure period are plotted for each temperature amplitude (1-10 °C) represented in the color scale from blue to red at different constant exposure concentrations, i.e., 0, 0.1, 0.2, and 0.4 µg · L^{-1}. The top panel (A1-A4) shows the results of the DEB-GUTS model, and the same scenario combinations for the DEB-GUTS-T model are displayed in the lower panel (B1-4), both for the SD model version. Horizontal lines mark the cumulative frequency distribution's 10^{th}, 50^{th}, and 90^{th} quantiles.

Firstly, we can see that an increased temperature amplitude widens the range of observed population sizes during the simulated period (Figure 6.6, A1-A4). This effect is, however, countered by the exposure scenarios, decreasing the observed maximum and minimum population sizes with increasing imidacloprid concentrations (Figure 6.6, A1-A4). Effectively, on one end of the temperature spectrum, the trend of the combined effect is offsetting, i.e., increased temperature amplitudes increases the population size gradient while increased concentration decreases the population size gradient. At lower temperature extremes, the combined effect results in an overall negative trend, reducing the population size gradient. The same trend is observed for the DEB-GUTS-T configuration, although the combined effect is predominantly negative (Figure 6.6, B1-B4). This can be explained by the increasing population dynamic under increasing temperature amplitudes (i.e., the mean population size gradient increases), while the changing temperature causes TKTD parameter changes resulting in the discussed slow kinetics effect leading to a lower population size over time (section 6.3.1).

Bringing these results into perspective of future climate scenarios, where more frequent extreme temperatures are predicted (IPCC, 2019; Johnson et al., 2018; Woolway et al., 2021), we can expect higher population density fluctuations in the future. However, locally adapted populations in different climate zones, i.e., Scandinavia, central Europe and the Mediterranean (Foucreau et al., 2014) already experience different magnitudes of temperature fluctuations at present. Thus, it will be important to interpret population model results considering the local populations and potential acclimatization (Pörtner and Farrell,

2008) or evolutionary adaptions of their thermal window (Stoks et al., 2017; Verheyen and Stoks, 2019b).

Looking at the same data displayed as quantiles (i.e., the horizontal lines in Figure 6.6), we can compare the results of the DEB-GUTS and DEB-GUTS-T versions based on the 1:1 equality line, representing the agreement of the two model configurations (Figure 6.7). Thus, we observe the control exposure scenarios (i.e., green dots) align with this 1:1 line for all quantiles across temperature amplitudes in SD (Figure 6.7, A-C) and IT (Figure 6.7, D-F) model versions. However, for the SD models in the Q10 plot, the highest temperature amplitude results in the lowest population size (Figure 6.7, A), while for the Q90 plot, we see the opposite orientation of those scenarios (Figure 6.7, C). For the Q50, there was no clear trend observed (Figure 6.7, B). Furthermore, with higher exposure concentration, the DEB-GUTS-T model shows lower population sizes throughout the simulation period, i.e., in all quantiles (Figure 6.7, A-C), as shown by the increasingly vertical dots indicating that the influence of temperature amplitude on population dynamics decreases with increasing concentrations. This is in contrast to the DEB-GUTS model, where temperature amplitude remains an important factor driving populations dynamics, regardless of concentration level, which would be indicated by the presence of horizontal dots. An exception to this is seen for the medians (Figure 6.7, B and E), where there is very little variation between temperature amplitudes in both models and dots appear clumped. This is because the median is similar across temperature amplitudes, after all the average temperature is the same for all temperature scenarios which on average evens out differences between scenarios. For the IT model versions, the results of both model configurations are similar (i.e., in line with the equality line) across the different temperature and concentration settings (Figure *6.7*, D-F). Similar results were observed in the pulsed exposure scenarios (Figure S6.6).

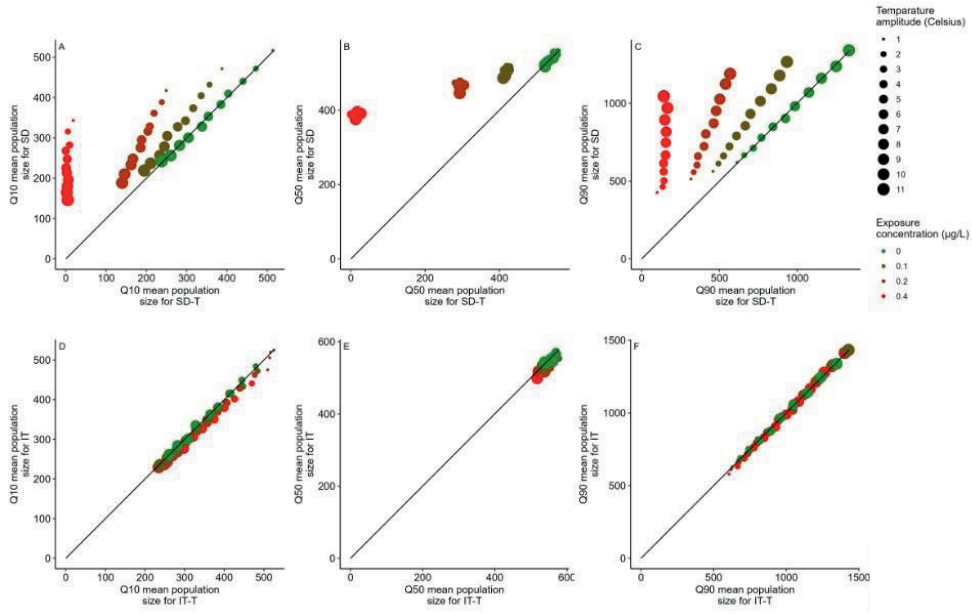

Figure 6.7: Mean *Gammarus pulex* population size quantiles and line of equality comparing the different model configurations for constant exposure to imidacloprid. The top panel (A-C) shows the results for the SD model versions and the lower panel (D-F) display the results for the IT models. The black diagonal line represents the 1:1 line, or line of equality, indicating when both model configurations produced the same results. The 10th, 50th, and 90th quantiles of the mean population size for the different environmental scenarios were plotted for DEB-GUTS against those of the DEB-GUTS-T model configuration. While the size of the dots indicates the temperature amplitude (1-11 °C), the colors refer to the exposure concentration of imidacloprid in µg · L^{-1}.

These results highlight the importance of considering temperature influences on TKTD parameters in IBMs. For example, the Q90 mean population size for the DEB-GUTS-T decreases significantly with increasing imidacloprid concentration, i.e., Q90 values shift to the left of the x-axis with an almost vertical line for 0.4 µg · L^{-1}. At the same time, the DEB-GUTS models still show a wide range of population sizes over the y-axis (Figure 6.7, C).

6.3.3 Implications for scenario development in environmental risk assessment.

While these result are explainable by the nature of the model and how temperature is implemented (i.e., increasing the temperature speeds up all biological processes implemented in the IBM, i.e., growth and reproduction) (S. A. L. M. Kooijman, 2010), our simulated results remain theoretic. For instance, temperature can also act as an additional stressor (Chapter 4), which was not implemented here. Furthermore, the current IBM model does not account for different temperature sensitivity at different life stages (Madeira et al., 2020), that might be integrated in the field observations. To investigate how this aspect influences population dynamics, it would need to be modeled explicitly in the standard DEB

model. Therefore, we cannot compare them directly to data observed in laboratory or field (semi-)studies.

Nevertheless, individual-based population models are powerful tools for evaluating the effect of chemicals on freshwater species. The simulation results presented in this study showed that considering temperature influences on the TKTD model parameter of a DEB-GUTS model combination is essential when evaluating different temperature scenarios. Due to the effect of temperature on the speed of toxicokinetic and physiological processes, both field or lab experiments and model simulations need to be performed through longer periods when performed at lower environmental temperatures. Alternatively, if the relationship between the pesticide effect with temperature is known, experiments might be performed at higher temperatures to reduce the experimental period and thus, associated costs.

It should be highlighted, that simulations with FOCUS scenarios (temperature and concentration) or real time concentration time series are possible as performed previously in higher tier risk assessments (EFSA, 2020). To explore the seasonal effect of pesticide application, model simulations with exposures during different times of the year, i.e., late autumn or early spring, should be considered. Furthermore, other climate change scenarios, like increased mean temperatures (instead of the raised amplitude applied in this study) or heatwave scenarios could be tested. Finally, local population's adaptation to different climate zones with different temperature extremes should be considered, facilitating zone specific registration of pesticides.

6 Supporting Information

S01 – Additional results

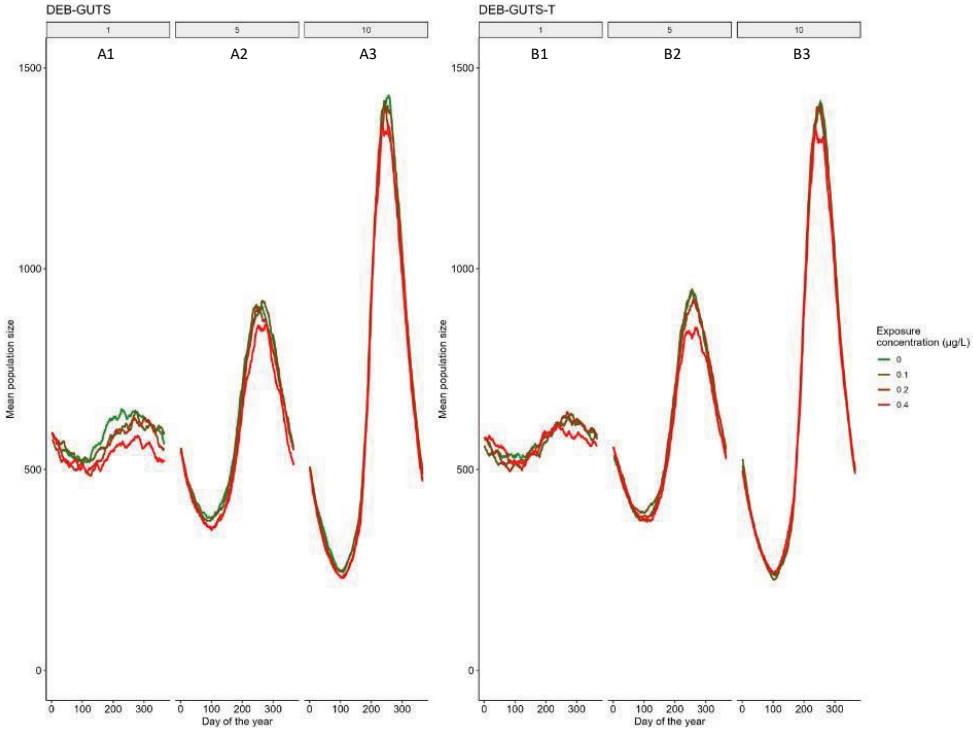

Figure S6.1: Simulation results of the mean population size of *Gammarus pulex* in the first year of constant imidacloprid application at different exposure concentrations and temperature scenarios for both model configurations (IT). The mean of the population size of n = 5 model simulations for each configuration and scenario is plotted over the year of the first application, in days of the year, starting on January 1st. The plots on the left side of the figure (A1-A3) show the results of the simulation with the DEB-GUTS configuration, and the right side (B1-B3) displays the DEB-GUTS-T configuration results. The different environmental scenarios encompass different exposure concentrations, displayed in different colors ranging from 0 to 0.4 µg · L^{-1}, and the different temperature amplitudes are shown in the different panels for each configuration, i.e., A1 and B1 show the temperature scenario with the amplitude of 1 °C, A2 and B2 for 5 °C and A3 and B3 for 10 °C, respectively.

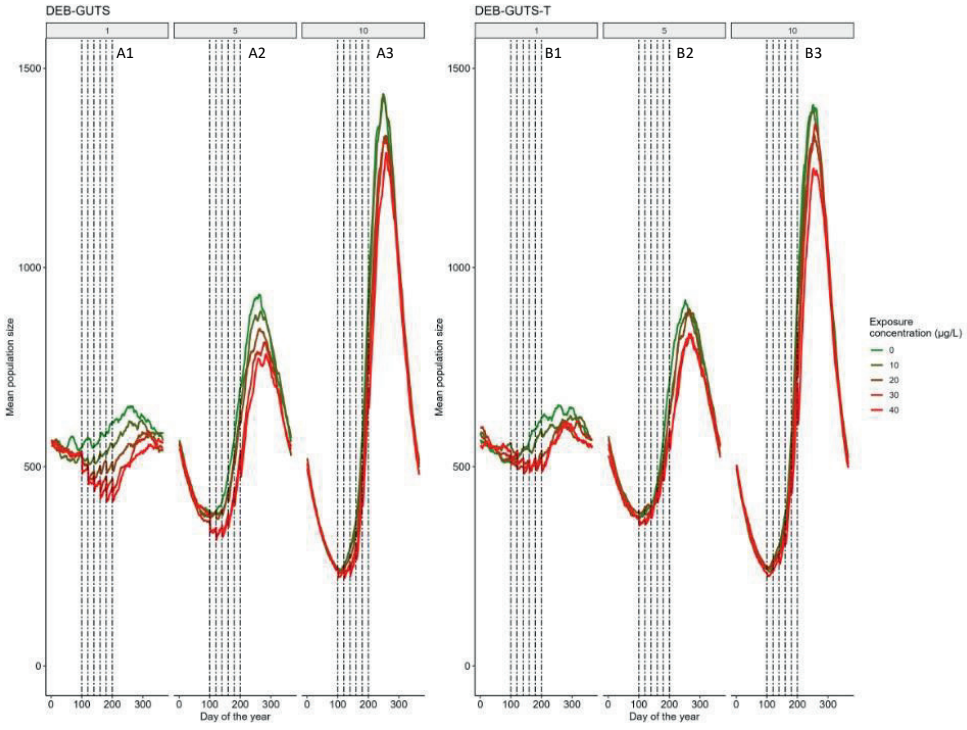

Figure S6.2: Simulation results of the mean population size of *Gammarus pulex* in the first year of pulsed imidacloprid application at different exposure concentrations and temperature scenarios for both model configurations (IT). The mean of the population size of n = 5 model simulations for each configuration and scenario is plotted over the year of the first application, in days of the year, starting on January 1st. The plots on the left side of the figure (A1-A3) show the results of the simulation with the DEB-GUTS configuration, and the right side (B1-B3) displays the DEB-GUTS-T configuration results. The vertical dotted lines indicate the exposure pulses of imidacloprid concentrations ranging from 0 to 40 µg · L^{-1} (i.e., displayed in different colors) were applied for 1 day at days 100, 120, 140, 160, 180, and 200. The different temperature amplitudes are shown in the different panels for each configuration, i.e., A1 and B1 show the temperature scenario with the amplitude of 1 °C, A2 and B2 for 5 °C, and A3 and B3 for 10 °C, respectively.

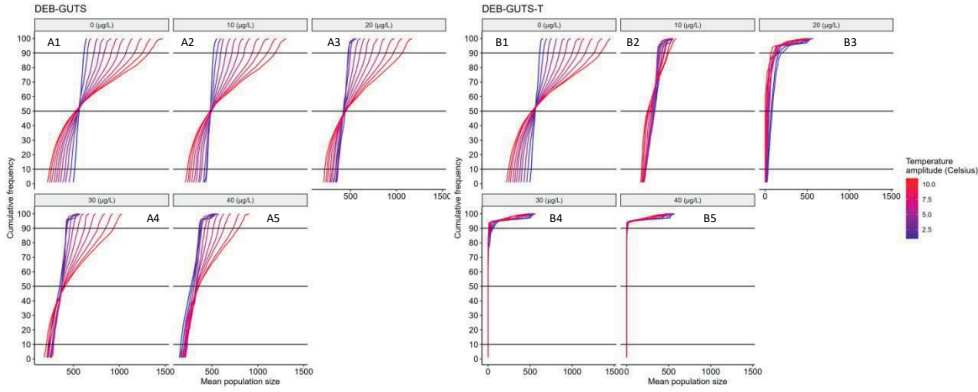

Figure S6.3: Cumulative frequency distribution of mean *Gammarus pulex* population sizes exposed to pulsed concentrations of imidacloprid at different temperature scenarios (SD). The cumulative frequencies of mean population sizes are plotted for each temperature amplitude (1-10 °C) represented in the color scale from blue to red at different pulsed exposure concentrations of imidacloprid ranging from 0 to 40 µg · L^{-1} (i.e., displayed in different colors) applied for 1 day at days 100, 120, 140, 160, 180, and 200. The top panel (A1-A5) shows the results of the DEB-GUTS model, and the same scenario combinations for the DEB-GUTS-T model are displayed in the lower panel (B1-5), both for the SD model version. Horizontal lines mark the cumulative frequency distribution's 10th, 50th, and 90th quantiles.

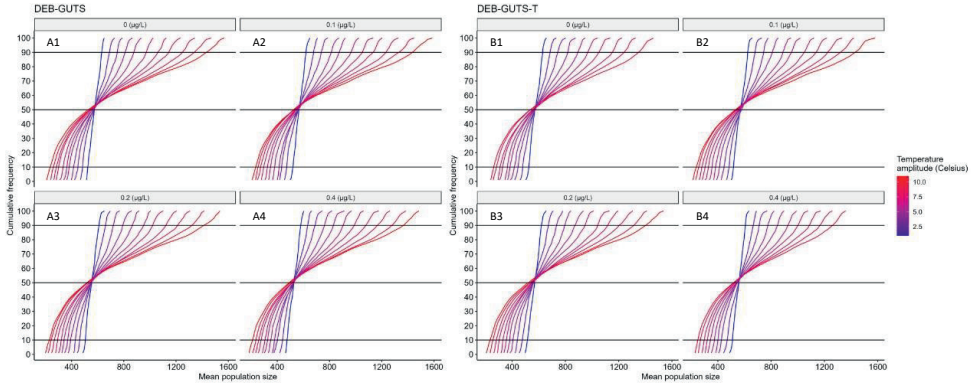

Figure S6.4 : Cumulative frequency distribution of mean *Gammarus pulex* population sizes exposed to constant concentrations of imidacloprid at different temperature scenarios (IT). The cumulative frequencies of mean population sizes are plotted for each temperature amplitude (1-11 °C) represented in the color scale from blue to red at different constant exposure concentrations, i.e., 0, 0.1, 0.2, and 0.4 µg · L^{-1}. The top panel (A1-A4) shows the results of the DEB-GUTS model, and the same scenario combinations for the DEB-GUTS-T model are displayed in the lower panel (B1-4), both for the IT model version. Horizontal lines mark the cumulative frequency distribution's 10th, 50th, and 90th quantiles.

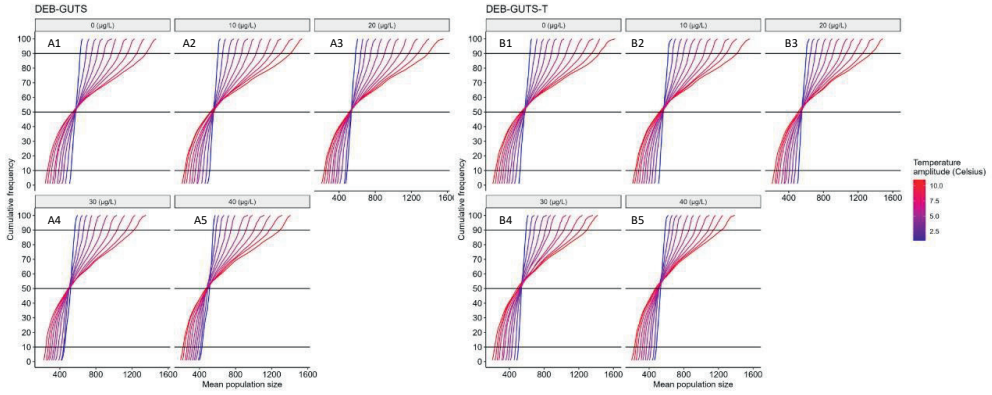

Figure S6.5: Cumulative frequency distribution of mean *Gammarus pulex* population sizes exposed to pulsed concentrations of imidacloprid at different temperature scenarios (IT). The cumulative frequencies of mean population sizes are plotted for each temperature amplitude (1-11 °C) represented in the color scale from blue to red at different pulsed exposure concentrations of imidacloprid ranging from 0 to 40 µg · L^{-1} (i.e., displayed in different colors) applied for 1 day at days 100, 120, 140, 160, 180, and 200. The top panel (A1-A5) shows the results of the DEB-GUTS model, and the same scenario combinations for the DEB-GUTS-T model are displayed in the lower panel (B1-5), both for the SD model version. Horizontal lines mark the cumulative frequency distribution's 10th, 50th, and 90th quantiles.

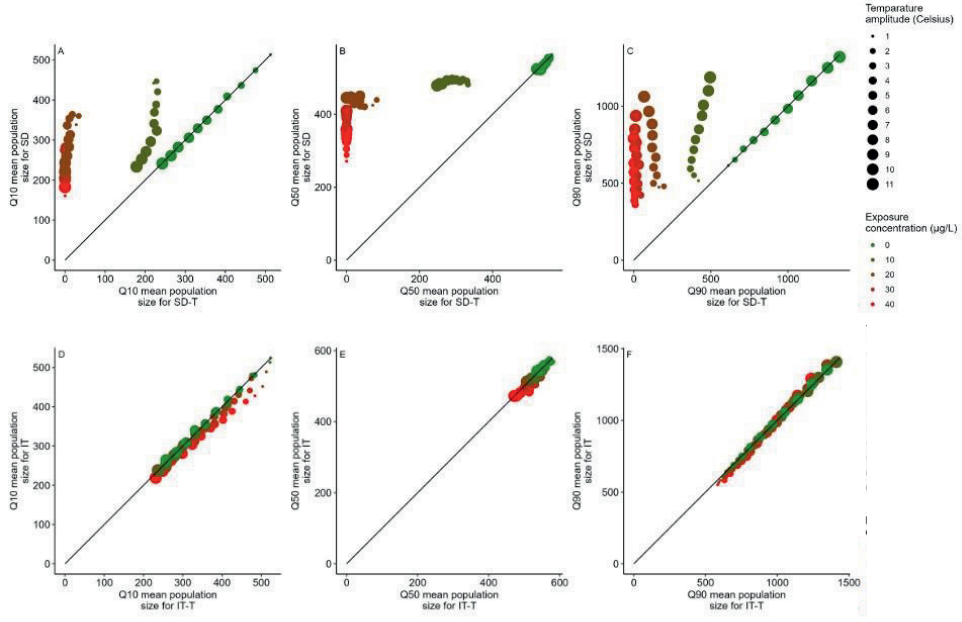

Figure S6.6: Mean *Gammarus pulex* population size quantiles and line of equality comparing the different model configurations for pulsed exposure to imidacloprid. The top panel (A-C) shows the results for the SD model versions and the lower panel (D-F) display the results for the IT models. The black diagonal line represents the 1:1 line, or line of equality, indicating when both model configurations produced the same results. The 10th, 50th, and 90th quantiles of the mean population size for the different environmental scenarios were plotted for DEB-GUTS against those of the DEB-GUTS-T model configuration. While the size of the dots indicates the temperature amplitude (1-11 °C), the colors refer to the exposure concentration of imidacloprid in µg · L^{-1}.

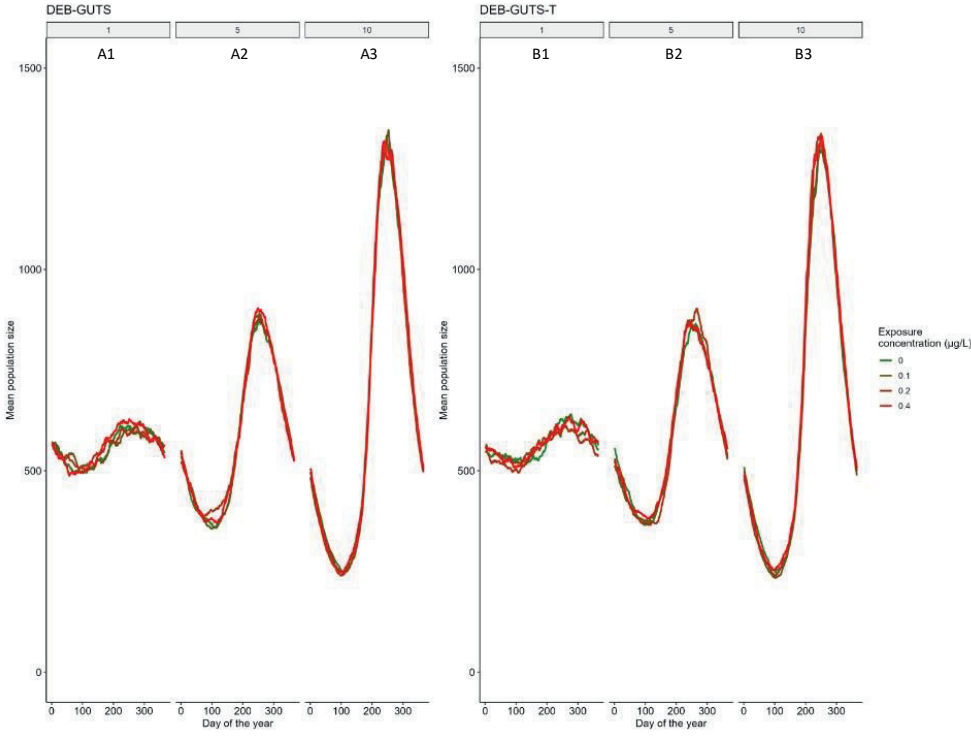

Figure S6.7: Modified k_d - Simulation results of the mean population size of *Gammarus pulex* in the first year of constant imidacloprid application at different exposure concentrations and temperature scenarios for both model configurations (SD. The mean of the population size of n = 5 model simulations for each configuration and scenario is plotted over the year of the first application, in days of the year, starting on January 1st. The plots on the left side of the figure (A1-A3) show the results of the simulation with the DEB-GUTS configuration, and the right side (B1-B3) displays the DEB-GUTS-T configuration results. The different environmental scenarios encompass different exposure concentrations, displayed in different colors ranging from 0 to 0.4 µg · L-1, and the different temperature amplitudes are shown in the different panels for each configuration, i.e., A1 and B1 show the temperature scenario with the amplitude of 1 °C, A2 and B2 for 5 °C and A3 and B3 for 10 °C, respectively.

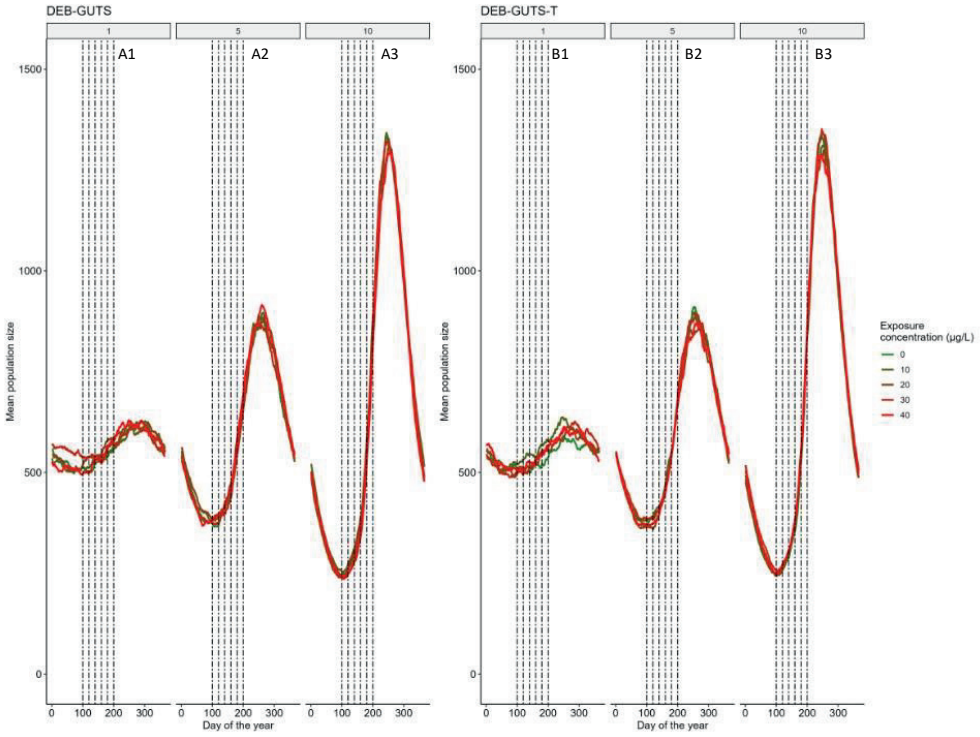

Figure S6.8: Modified k_d - Simulation results of the mean population size of *Gammarus pulex* in the first year of pulsed imidacloprid application at different exposure concentrations and temperature scenarios for both model configurations (SD). The mean of the population size of n = 5 model simulations for each configuration and scenario is plotted over the year of the first application, in days of the year, starting on January 1st. The plots on the left side of the figure (A1-A3) show the results of the simulation with the DEB-GUTS configuration, and the right side (B1-B3) displays the DEB-GUTS-T configuration results. The vertical dotted lines indicate the exposure pulses of imidacloprid concentrations ranging from 0 to 40 µg · L^{-1} (i.e., displayed in different colors) were applied for 1 day at days 100, 120, 140, 160, 180, and 200. The different temperature amplitudes are shown in the different panels for each configuration, i.e., A1 and B1 show the temperature scenario with the amplitude of 1 °C, A2 and B2 for 5 °C, and A3 and B3 for 10 °C, respectively.

S02 - GUTS-RED-T model equations and calibration results

Link to repository: https://git.wur.nl/AMD21/temperature_explicit_guts_red.git

Table S6.4: Model equations and symbols for the parameters and variables used. Symbols used are given with their explanation and unit of the parameter and variables they represent. SD = stochastic death; IT = individual tolerance

Model	Equation	
Arrhenius	$k_x(T) = k_{x,T_{ref}} \cdot e^{\left(\frac{T_A}{T_{ref}} - \frac{T_A}{T}\right)}$ k_x is a rate parameter: k_d , h_b and, b_w $k_{x,ref}$ is the respective rate parameter at the reference temperature	eq. (1)
Damage dynamics	$\frac{dD_w(t)}{dt} = k_d \cdot \left(C_w(t) - D_w(t)\right)$	eq. (2)
SD model	$h_z = b_w \cdot \max(0,\ D_w(t) - m_w) + h_b$	eq. (3)
	$\frac{S_{SD}(t)}{dt} = -h_z \cdot S$	eq. (4)
IT model	$F(t) = \frac{1}{1+\left(\frac{D_{w,max}}{m_w}\right)^{\beta}}$	eq. (5)
	$D_{w,max} = \max_{0<\tau<t} D_w(\tau)$	eq. (6)
	$\beta = \frac{\log 39}{\log F_s}$	eq. (7)
	$S_{IT}(t) = \left(1 - F\left(D_{w,max}\right)\right) \cdot e^{-h_b \cdot t}$	eq. (8)

Symbol	Explanation	Unit
Temperature parameters		
T	Temperature	K
T_{ref}	Reference temperature (20 °C = 293.15 K)	K
T_A	Arrhenius temperature used to correct parameters	K
GUTS-RED model parameter and variables		
C_w	Concentration of the chemical in the exposure medium	µg · L^{-1}
D_w	Scaled damage, referenced to internal concentration	µg · kg^{-1}
h_z	Hazard rate for an individual with threshold z	[d^{-1}]
S	Survival probability in a population of individuals	[-]

$F(m_w, \beta)$	Cumulative log-logistic distribution function of the thresholds	[-]
β	Shape parameter for the distribution of thresholds (F)	[-]
t	Time	day
k_d or $k_d(T)$	Dominant rate of damage dynamics for chemical inside the organims (corrected for temperature, at 20 °C)	d^{-1}
h_b or $h_b(T)$	Background hazard rate (corrected for temperature, at 20 °C)	d^{-1}
m_w	Median of the distribution of thresholds (F), referenced to water concentration	$\mu g \cdot kg^{-1}$
b_w or $b_w(T)$	Killing rate, referenced to water concentration(corrected for temperature, at 20 °C) – For SD model only	$kg \cdot \mu g^{-1} \cdot d^{-1}$
F_s	Fraction spread in the distribution of thresholds (F) – For IT model only	[-]

SD model

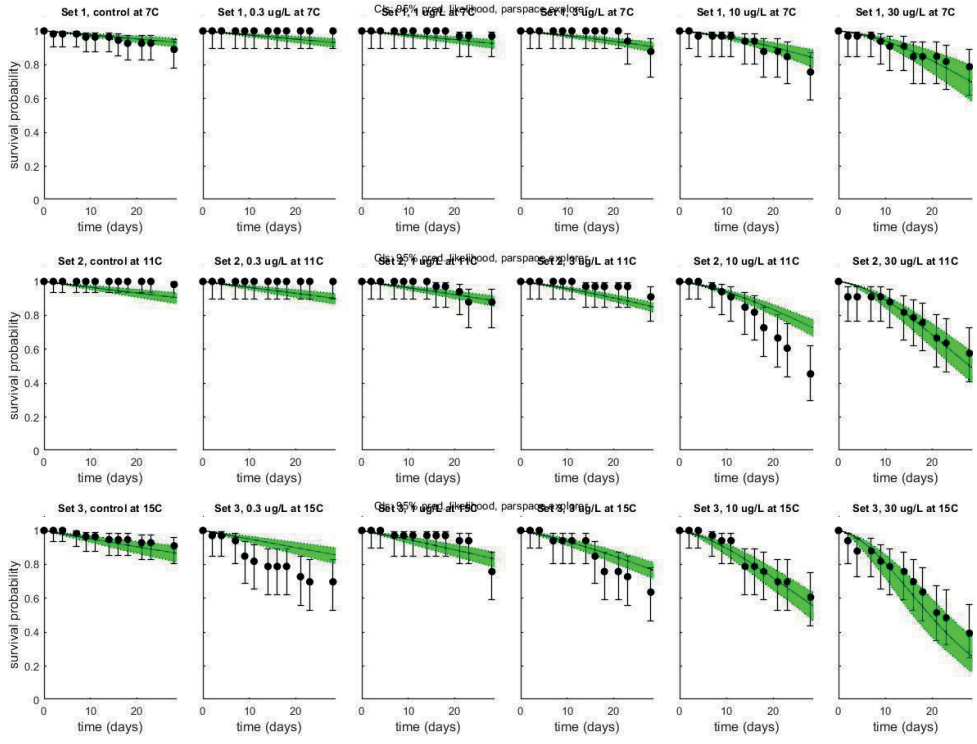

Figure S6.9: GUTS-RED-SD model fits for the survival of *Gammarus pulex* exposed to imidacloprid at different temperatures. Black dots represent the measured survival (replicates pooled) at the different exposure levels in µg per L and the different temperatures in degrees Celsius (column headings). The black line shows the GUTS-RED-SD model prediction for survival, and the dotted black lines show the boundaries of its 95 % confidence interval (green area).

Table S6.5: SD parameters. AIC = 749.59

Parameter	unit	value	lower 95 % CI	upper 95 % CI
k_d	d^{-1}	0.02982	1.517e-4	0.3707
m_w	$\mu g \cdot L^{-1}$	1e-6*	1e-6*	0.4183
h_b	d^{-1}	0.007848	0.004780	0.01302
b_w	$\mu g \cdot L^{-1} \cdot d^{-1}$	0.01123	0.002586	1*
T_A	K	7450	4335	1.142e+04

* edge of 95% parameter CI has run into a boundary

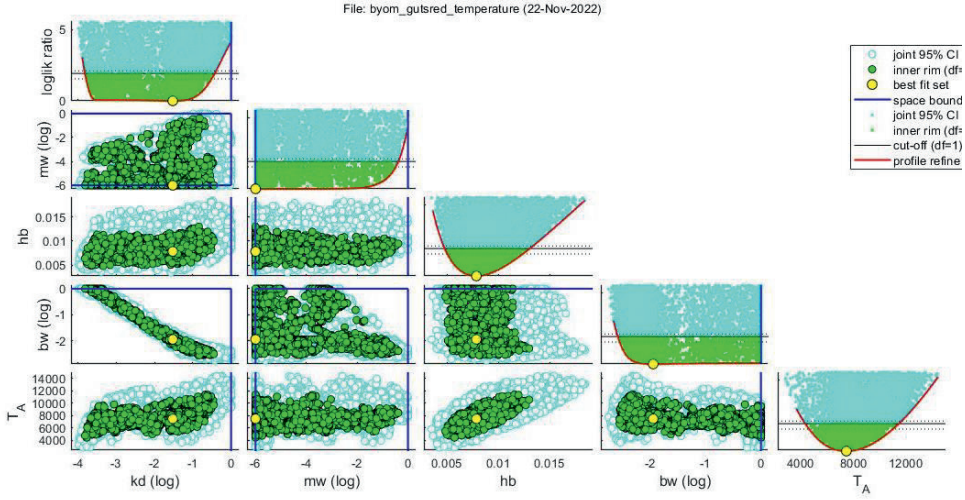

Figure S6.10: Parameter-space plot for the fit of **GUTS-RED-SD**. The plots on the diagonal show the profile likelihoods for the individual parameters and the other plots are the 95% joint confidence regions. Yellow dots mark the best-fit values, green dots show parameter sets within the critical value (horizontal black line). The parameter sets between the dotted horizontal lines are used for the confidence intervals on model curves.

IT model

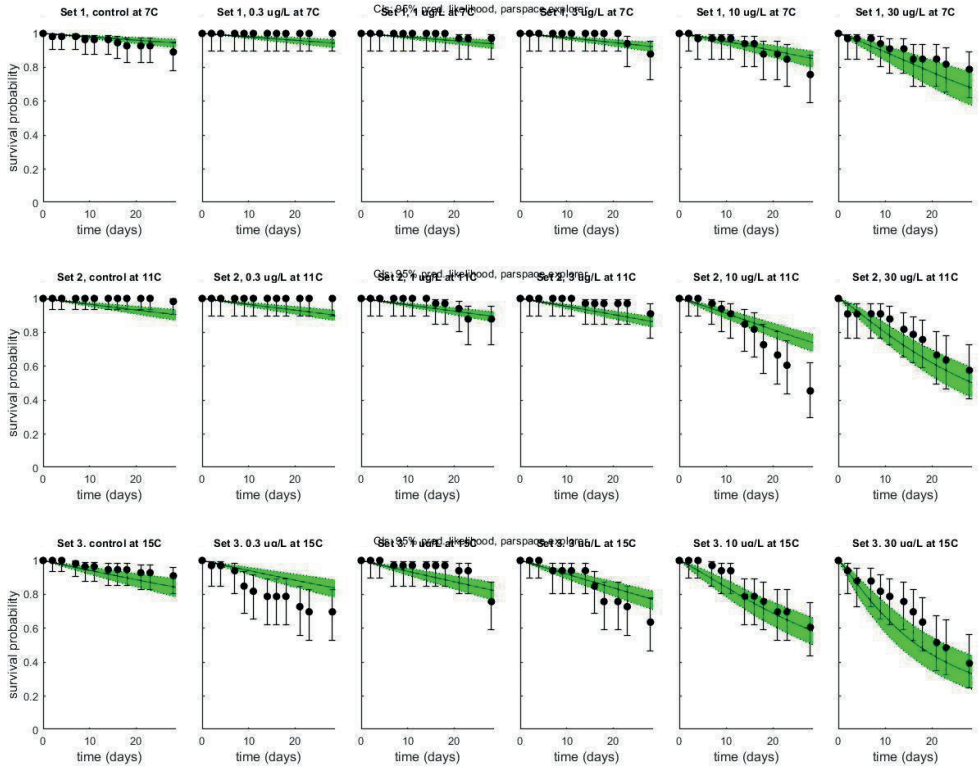

Figure S6.11: GUTS-RED-IT model fits for the survival of *Gammarus pulex* exposed to imidacloprid at different temperatures. Black dots represent the measured survival (replicates pooled) at the different exposure levels in µg per L and the different temperatures in degrees Celsius (column headings). The black line shows the GUTS-RED-IT model prediction for survival, and the dotted black lines show the boundaries of its 95 % confidence interval (green area).

Table S6.6: IT parameters. AIC = 758.93

Parameter	unit	value	lower 95 % CI	upper 95 % CI
k_d	d^{-1}	1e-6*	1e-6*	0.02809
m_w	$\mu g \cdot L^{-1}$	2.68e-4	1.579e-4	6.516
h_b	d^{-1}	0.01157	0.006846	0.01932
Fs	-	19.12	10.55	39.40
T_A	K	1.102e+04	6648	1.574e+04

* edge of 95% parameter CI has run into a boundary

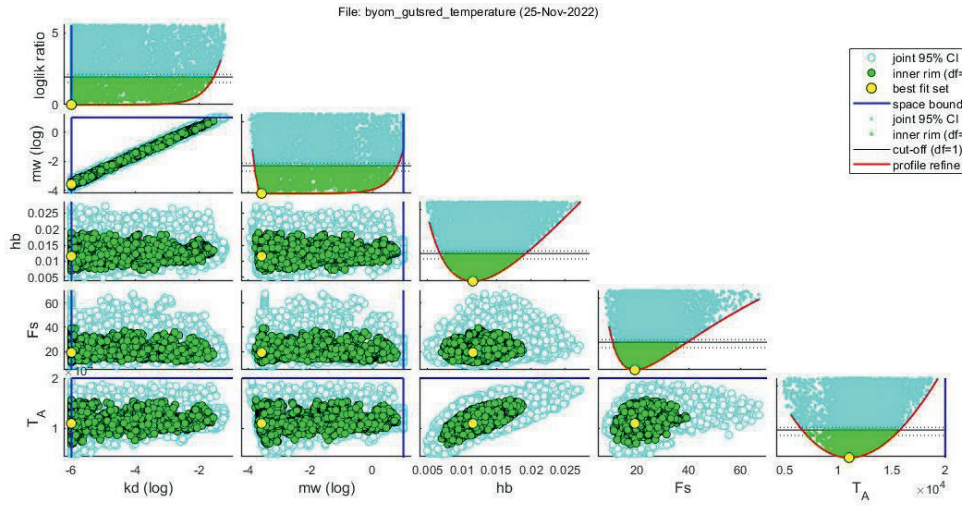

Figure S6.12: Parameter-space plot for the fit of **GUTS-RED-IT**. The plots on the diagonal show the profile likelihoods for the individual parameters and the other plots are the 95% joint confidence regions. Yellow dots mark the best-fit values, green dots show parameter sets within the critical value (horizontal black line). The parameter sets between the dotted horizontal lines are used for the confidence intervals on model curves.

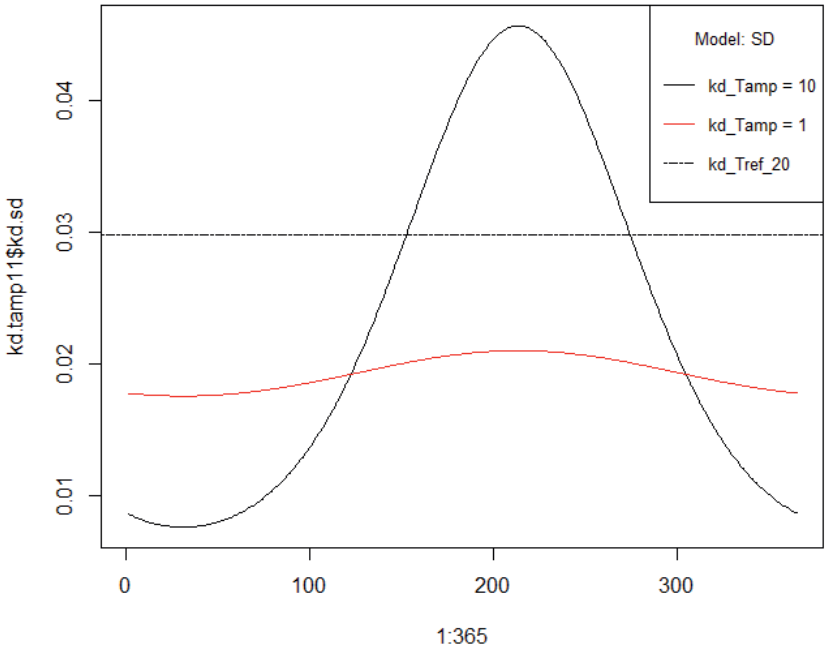

Figure S6.13: Value for the (temperature corrected) dominant rate kd over one simulation period (one year).

S03: An individual-based DEB/GUTS model for *Gammarus pulex*

Contents

1 Model description

1.1 Purpose

The purpose of the model is to simulate freshwater shrimp *Gammarus pulex* population dynamics under varying environmental conditions, with a special focus on interactions with water temperature and pesticides, applying DEB theory to simulate metabolic processes of individuals and GUTS to simulate toxico-kinetic toxico-dynamic processes associated with pesticide exposure.

1.2 Entities, state variables and scales

Entities in the model are freshwater shrimp individual females and square cells representing the habitat. For individuals we distinguish between life stages embryo, juvenile and adult. The model landscape consists of two-dimensional 1 m^2 cells (patches) in a user-defined configuration making up the landscape.

Individuals are characterized by the spatial unit they reside in (discrete coordinates) and by their age (in days).

To control implementation complexity, sub-entities of individuals are defined, representing an individual's dynamic energy budget (DEB) and toxicodynamic-toxicokinetic (TKTD) sub-models. For the latter the GUTS implementation (Jager et al. 2011) is used.

A DEB sub-entity is characterized by structure (L, unit: cm), determining actual size, feeding rates and maintenance costs; scaled reserves (U_E, unit: d cm), serving as intermediate storage of energy between feeding and mobilization processes; scaled maturity (U_H, unit: d cm), the continuous state variable that regulates transitions between embryo, juvenile and adult stages; scaled reproduction buffer (U_R, unit: d cm) where energy is stored that will be converted into eggs at reproductive events. As in (Martin et al. 2012) the scaled version of the standard DEB model (Kooijman 2010) is used here, where the dimension of energy or mass is scaled out.

Optionally a DEB sub-entity has an ageing submodel based on DEB theory with state variables damage inducing compounds ($\ddot{q}$) and damage ($\dot{h}$).

A GUTS sub-entity is characterized by state variables (scaled) damage (D_w) and hazard (H).

The spatial entities are characterized by their coordinates (within the landscape), water temperature, food conditions, and pesticide concentration. Temperature is considered a landscape property and identical for all cells.

The model proceeds in discrete daily time steps. A subset of the processes is simulated with a smaller (hourly) time step: toxico-kinetic and toxico-dynamic processes for the GUTS model.

1.3 Process overview and scheduling

Every time step the following processes, or submodels, are scheduled. Within each submodel processes are strictly synchronized, at least conceptually. Where needed, update of state is postponed until all individuals have been processed, eliminating the need to randomize each iteration the order in which individuals are processed. Submodels are discussed in detail in section 1.7.

The dynamics of the DEB model, formulated as a set of differential equations, are simulated with a discrete daily time step. The following pseudo-code gives an overview about the model's main loop:

```
setDailyEnvironmentalConditions

        update temperature, etc

setLocalExposureConcentration

        update local concentration of pesticide

move

        simulate movement of individuals

        individuals do: [:each | each calcMovement]

calcGUTSDynamics

        toxico-kinetics & toxico-dynamics with hourly time step

        individuals do: [:each | each guts calcDynamics]

calcLocalFeedingAndFoodDynamics

        simulate feeding and food dynamics with hourly time step, to estimate average
        feeding rate per individual (scaled f)

calcDEBDynamics

        calculate the changes in reserves, length and aging

        individuals do: [:each | each deb calcChangeDEB]

        individuals do: [:each | each deb calcAging]

        update DEB state variables

        individuals do: [:each | each deb updateStateVariables]

calcMortality

        effectuate background and/or aging mortality

        individuals do: [:each | each effectuateNaturalMortality]

calcDensDepMortality

        effectuate direct or indirect (starvation) density-dependent mortality

calcPesticideMortality

        effectuate mortality from pesticide exposure

        individuals do: [:each | each guts effectuateHazard]

calcReproduction

        when buffer allows creation of a new clutch of offspring do so

        individuals do: [:each | each deb calcReproduction]

incrementTime

        set time to time + time step

        increment the age of each individual by the time step
```

1.4 Design concepts

Basic principles. The model is based on the DEB theory (Kooijman 1993, 2000, 2010). An overview of the concepts can be found in Kooijman (2001) or Nisbet et al. (2000). The theory is based on the general principle that metabolic processes are proportional to surface area or body volume and a full balance for mass and energy.

Emergence. Traits of the individual and structure and dynamics of the population emerge from the properties of metabolic organization and indirect interactions of individuals via competition for food.

Stochasticity. Movement of juveniles and adults is random, with a specified probability density function. All mortality rates are treated as probabilistic. In the DEB model additional stochasticity is included by allowing individuals to vary in some of the DEB parameters. As in (Martin et al. 2012) we apply the method of (Kooijman et al. 1989) where the surface-area-specific maximum assimilation rate of individual is set from multiplying the species-specific value with an individual-specific "scatter multiplier" (a log-normally distributed random number with a user-defined standard deviation).

Adaptation. The model does not include adaptive behavior; in particular, DEB parameters vary among individuals but remain constant over an individual's lifespan. Consequently, the design concepts "objectives", "learning" and "prediction" do not apply to this model. Individuals sense ambient temperatures, and rate constants are adapted accordingly.

Interaction. With density-dependent mortality, individuals interact indirectly, as their presence increases the mortality rate experienced by all individuals in the same patch.

Observation. Size and structure of the population as well as spatial distribution of the individuals for different concentrations of toxicant, food resource amounts and distributions can be compared. Currently analyzed scenarios are non-spatial, and focus on impact of chemical exposure under different patterns of seasonal temperature.

1.5 Initialization

The DEB coefficients for *Gammarus pulex* are obtained from the add-my-pet (AmP) database, based on the *abj* type (with growth acceleration) (Kooijman 2014).

Simulations start with a user-defined number of individuals in each spatial unit (cell, patch). To avoid complications (embryos of this species develop in the mother's brood pouch) these individuals are juveniles with scaled maturity U_H between scaled maturity at birth U_H^b and scaled maturity at puberty U_H^p, with structural length of around 0.025 cm and assuming a scaled reserve density of 0.7. The corresponding scaled reserve level U_E is then calculated

as $U_E = eL^3/\dot{v}$. To avoid defining a completely identical initial population cohort, the initial value of L is randomized between individuals, according to a Normal distribution with mean 0.025 and standard deviation of 0.001. Initialization with a less synchronized population, consisting of both juveniles and adults should be possible as well, but has not been tested.

1.6 Input data

The main environmental driver of the modeled system is the ambient water temperature. The forcing function for water temperature is optionally replaced by daily input data, without further spatial differentiation.

Chemical exposure is modeled by using hourly data for pesticide concentration in water per spatial unit. When input data are specified for a period of a single year, data will be wrapped around when running multiyear simulations.

1.7 Submodels

DYNAMIC ENERGY BUDGET MODEL

The implementation of the model for individual growth and development started from the scaled version of the standard DEB model (Kooijman et al. 2008) and its NetLogo implementation described in (Martin et al. 2012). The scaled standard DEB model was extended with formulations accounting for temperatures other than the reference temperature. An alternative algorithm to define energy content of new-born individuals was applied, avoiding the complications of the 'maternal effects rule'. Species-specific elements of life-history were added (embryos developing in brood pouch). Energy intake can be linked to species-specific, dynamic, food availability.

A version of the scaled standard DEB model was implemented accounting for metabolic acceleration - the *abj* version of standard DEB - using the latest coefficients from the AmP database.

A short description of the standard elements of DEB model and theory is given below, providing only the main equations and coefficients. For more background the reader is referred to (Kooijman et al. 2008) for the scaled version of DEB, to (Martin et al. 2012) for a reference implementation, and in general to the DEB book (Kooijman 2010) and the very extensive literature on the use of DEB theory. A more extensive description is provided for the extensions and modifications to the standard model.

The AmP database provides the coefficients for the energy-based notation of the standard DEB model. (Kooijman et al. 2008) describes how the scaled DEB model is derived from the standard model, using compound parameters that combine several of the (12) primary coefficients of the standard DEB model. For ease of comparison with AmP, all primary parameters of the standard DEB model are listed in Table 1.1, using the energy dimension.

Using the terminology of DEB-IBM (Martin et al. 2012) the two compound parameters (combinations of primary parameters) g and $\dot{k}_M$ are defined as follows. The energy investment ratio, g (dimensionless), is:

$$g = \frac{[E_G]\dot{v}}{\kappa\{\dot{p}_{Am}\}}$$

While the specific somatic maintenance rate, $\dot{k}_M$ (rate, t^{-1}) is defined as:

$$\dot{k}_M = \frac{[\dot{p}_M]}{[E_G]}$$

Table 1.1: The 12 primary DEB parameters as they appear in the AmP database. Note that for length the unit cm is used. The last 3 columns give the names under which the variables appear in the AmP database, the NetLogo implementation (Martin et al. 2012) and the current Smalltalk implementation.

Symbol	Unit	Description	AmP	NetLogo	Small-talk
$\{\dot{F}_m\}$	$ld^{-1}cm^{-2}$	{F_m}, max spec searching rate	F_m	F_m	fMRate
$\{\dot{p}_{Am}\}$	$Jd^{-1}cm^{-2}$	{p_Am}, spec assimilation flux	p_Am	p_am	pAm
K_X	-	digestion efficiency of food to reserve	kap_X		kapX
$\dot{v}$	cm d^{-1}	energy conductance	v	v_rate	vRate
κ	-	Allocation fraction to soma	kap	kap	kap
$[E_G]$	J cm^{-3}	[E_G], spec cost for structure	E_G	E_G	eG
$\{\dot{p}_T\}$	$J\ d^{-1}cm^{-2}$	{p_T}, surf-spec somatic maint	p_T		pT
$[\dot{p}_M]$	$J\ d^{-1}cm^{-3}$	[p_M], vol-spec somatic maint	p_M	p_m	pM
E_H^b	J	Maturity at birth	E_Hb	E_H^b	eHExpB
E_H^p	J	Maturity at puberty	E_Hp	E_H^p	eHExpP
$\dot{k}_J$	d^{-1}	maturity maint rate coefficient	k_J	k_J_rate	kJRate
K_R	-	Reproduction efficiency	kap_R	kap_R	kapR

Scaled DEB

A further simplification of the equations is obtained by scaling the state variables reserves, maturity and reproduction buffer size, by dividing them by the maximum surface-area-specific assimilation rate $\{\dot{p}_{Am}\}$. Also, the life-stage transition parameters have to be divided by $\{\dot{p}_{Am}\}$

$U_H^p = \frac{E_H^p}{\{\dot{p}_{Am}\}}$ and $U_H^b = \frac{E_H^b}{\{\dot{p}_{Am}\}}$

The resulting equations specifying the scaled DEB model are given below, from the DEB-IBM user manual.

The dynamics of the scaled reserve U_E:

$$\frac{d}{dt}U_E = S_A - S_C$$

with $S_A = fL^2$ representing the scaled assimilation flux

and $S_C = L^2 \frac{ge}{g+e}\left(1 + \frac{L\dot{k}_M}{\dot{v}}\right)$ representing the scaled energy mobilization flux

and $e = \dot{v}\frac{U_E}{L^3}$

Table 1.2: Scaled and compound parameters used in DEB-IBM.

Symbol	Unit	Description	NetLogo	Smalltalk
U_H^b	d cm^2	Scaled maturity at birth	U_H^b	uHExpB
U_H^p	d cm^2	Scaled maturity at puberty	U_H^p	uHExpP
g	-	energy investment ratio	g	g
$\dot{k}_M$	d^{-1}	somatic maintenance rate coefficient	k_M_rate	kMRate

The coefficient f refers to the (scaled) functional response. For ad-libidum feeding conditions it is set to 1.

The dynamics of scaled maturity U_H (immature individuals):

$\frac{d}{dt}U_H = (1-\mathrm{K})S_C - \dot{k}_J U_H$ for $U_H < U_H^p$ else $\frac{d}{dt}U_H = 0$

The dynamics of the scaled reproduction buffer U_R (mature individuals):

$\frac{d}{dt}U_R = (1-\mathrm{K})S_C - \dot{k}_J U_H^p$ for $U_H > U_H^p$ else $\frac{d}{dt}U_R = 0$

The dynamics of structural length under non-starvation conditions are given by:

$$\frac{d}{dt}L = \frac{1}{3}\left(\frac{\dot{v}}{gL^2}S_C - \dot{k}_M L\right)$$

Ageing

Mortality from ageing can be accounted for in an 'ageing' submodel based on the idea that damage-inducing compounds accumulate at a rate proportional to energy mobilization. Damage production is defined as scaled ageing acceleration q with dynamics:

$$\frac{d}{dt}\ddot{q} = \left(\ddot{q}\frac{L^3}{\left(\frac{\dot{v}}{gk_M}\right)^3}S_G + \ddot{h}_a\right)e\left(\frac{\dot{v}}{L} - \dot{r}\right) - \dot{r}q \text{ with } \dot{r} = \frac{3}{L}\frac{d}{dt}L$$

and with the resulting scaled hazard rate due to ageing amounting to:

$$\frac{d}{dt}\dot{h} = \ddot{q} - \dot{r}\dot{h}\ .$$

In the ageing submodel S_G represents the Gompertz stress coefficient and $\ddot{h}_a$ the Weibull aging acceleration parameter. Both coefficients are available from the AmP website.

Temperature

Impact of temperature on growth and development is incorporated in the model, following (Kooijman 2010), chapter 1.3. The adjustment of metabolic reaction rate to a temperature different from a chosen reference temperature is given by:

$$\dot{k}(T) = \dot{k}_1 e^{\left(\frac{T_A}{T_1} - \frac{T_A}{T}\right)}$$

with T representing the absolute temperature (°K), T_1 a reference temperature (°K), T_A the Arrhenius temperature, $\dot{k}$ the metabolic rate with $\dot{k}_1$ its value at reference temperature.

The Arrhenius temperature T_A is defined as E_a/R, with E_a representing the activation energy (J mol^{-1}) and R the gas constant (8.31441 J K^{-1} mol^{-1}). T_A values listed in (Kooijman 2010), table 1.2, range from approximately 5000 to 15000 K. Underlying activation energy values thus range from 41 to 125 kJ mol^{-1}. T_A values are species-specific and an estimate of its value is available from the AmP website. For *Gammarus pulex* the species-specific AmP estimate is 10000 °K. From a refit of the DEB model on the AmP data, a value of 10560 °K resulted; this value is used in the analyses. The reference temperature is 20 °C.

All the DEB rates (symbols with dots) are corrected for temperature, by multiplying the rate at reference temperature with this factor $e^{\left(\frac{T_A}{T_1} - \frac{T_A}{T}\right)}$. The Weibull aging parameter $\ddot{h}_a$ needs to be multiplied twice. Maturity levels U_H^p and U_H^b will not be affected by temperature.

The AmP data do not provide an estimate of a lower temperature boundary, as discussed in (Kooijman 2010) chapter 1.3.7. A lower boundary was therefore not used.

Starvation

Starvation can be accounted for in standard DEB by assuming different starvation rules to apply. Most rules assume a rechanneling of energy fluxes allowing at least the maintenance requirements to be met. The example case worked out in (Martin et al. 2012) is reproduced below.

In case the reserve density becomes smaller than the scaled length, growth is set to zero and energy flux into the maturity or reproduction buffer is diverted to somatic maintenance. If all energy that can be diverted is not sufficient to cover maintenance costs, the individual is assumed to die. In equations:

When reserve density falls below scaled length

$e < L/L_M$ with $L_M = \frac{\dot{v}}{k_M g}$ (maximum length an individual can grow to)

growth will be set to zero and enough energy will be diverted from the energy heading to the maturity buffer (in case of juveniles) or to reproduction buffer (adults) to cover maintenance costs. When growth is zero, the mobilization of reserves is simply:

$$eL^2$$

The amount of energy needed to cover maintenance costs is found by setting dL/dt=0 in the equation for scaled length dynamics resulting in:

$$\frac{\dot{k}_M g}{\dot{v}} L^3$$

Thus, the required energy that should go into the κ branch is:

$$S_C = \frac{\kappa \dot{k}_M g}{\dot{v}} L^3$$

Of which only the amount $\kappa e L^2$ can be covered by the original flux and the rest is obtained from diverting from energy headed to maturity or reproduction buffer. The maturity or reproduction buffer receives the remaining energy (after subtracting the somatic maintenance costs):

$$\frac{d}{dt} U_H = (1-\kappa) S_C - \dot{k}_J U_H - \kappa L^2 (\frac{L}{L_M} - e) \quad \text{when } U_H < U_H^p$$

$$\frac{d}{dt} U_R = (1-\kappa) S_C - \dot{k}_J U_H^p - \kappa L^2 (\frac{L}{L_M} - e) \quad \text{when } U_H > U_H^p$$

When applying the following conditions as leading to death of the individual,

$$\frac{d}{dt} U_H < 0$$

$$U_R < 0$$

it is effectively assumed that the whole reproduction buffer can be emptied while the maturation buffer may stop growing but can never decrease.

Typified model abj

The description of the scaled DEB above relates to the standard DEB model (type *std*). For *Gammarus pulex* the *abj* type is appropriate; it is the current one on the AmP site. This type includes a phase of growth acceleration, between birth and metamorphosis (http://www.debtheory.org/wiki/index.php?title=Typified_models). Before and after acceleration isomorphy applies. Metamorphosis occurs before puberty at maturity E_H^j. The *abj* model is a one-parameter extension of model *std*. An *abj* version of the scaled standard DEB is developed, based on the description in (Zimmer et al. 2014) and using the coefficients from the current AmP database. The *Gammarus* DEB coefficients from AmP are listed in Appendix AmP coefficients.

As in (Zimmer et al. 2014) a shape correction function *M(L)* is defined as:

$$\begin{cases} M(L) = \dfrac{L_b}{L_b} = 1 \; if \; U_H < U_H^b \\ M(L) = \dfrac{L}{L_b} \; if \; U_H^b < U_H < U_H^j \\ M(L) = \dfrac{L_j}{L_b} \; if \; U_H > U_H^j \end{cases}$$

where L_j refers to the length at metamorphosis and L_b to length at birth. In the model we now need to store the value of L_b and L_j for each individual. The surface-area specific assimilation rate $\{\dot{p}_{Am}\}$ is multiplied by the shape correction function to make it increase with length during the acceleration phase, but constant before birth and after metamorphosis. The energy conductance $\dot{v}$ is defined as $\{\dot{p}_{Am}\}/E_m$; therefore also $\dot{v}$ has to be multiplied with *M(L)*. In the scaled model, rate $\{\dot{p}_{Am}\}$ does not occur anymore. However, for the model version with dynamic food we use $fL^2\{\dot{p}_{Am}\}M(L)$ to calculate the real assimilation flux, that is needed to obtain the change in food concentration.

In the implementation of the *abj* model under dynamic temperature and food conditions thus no further adaptations were made, apart from applying the correction function on $\{\dot{p}_{Am}\}$ and $\dot{v}$.

Brood pouch

The life history of *Gammarus pulex*, with embryos developing in the mother's brood pouch, requires a reproduction buffer handling rule added to the model, as in the standard DEB model eggs turn immediately into independent individuals. For eggs developing in a brood pouch a connection between egg and mother has to been maintained until day of hatching. One way to achieve this is described in the DEB-IBM User Manual (section 4.2.2) (Martin et al. 2012). An alternative approach is followed by (Gergs et al. 2014) , who let the mother individual at embryo creation time create an additional internal DEB model representing the embryo, to keep track of development in the brood pouch, identical for all embryos. When leaving the brood pouch, new individuals are created, each with an internal DEB module that is a copy of this embryonal DEB. We combine the two approaches by treating embryos as individuals immediately after conception but keeping them inside the mother's brood pouch until the clutch is released at hatching time. When the mother dies, all embryos it contains die as well; when the mother moves, all its embryos move with her. When density-dependent mechanisms play a role, embryos are not included in local density estimates.

Embryo energy investment

In standard DEB, at the moment of hatching or birth an embryo is assumed to have the energy density of the mother at the time of embryo creation ('maternal effects rule'). To be able to set energy density at the time of embryo creation (Martin et al. 2012) used a bisection method. They iteratively simulated embryo development for a range of energy densities, thus performing a simulation within a simulation, to determine the energy density at embryo creation time that would lead to the right energy density at hatching.

Here the simpler approach is followed of (Gergs et al. 2014), SI pages 7 and 8, reproduced below. Alternative approaches were presented in (Kooijman 2009).

At certain time steps, when the accumulated energy in the reproductive buffer of the mother is sufficient to produce a clutch of embryos of at least the minimum clutch size, the accumulated energy is converted into a number of embryos *R*:

$$R = \frac{k_r U_R}{U_E^0}$$

With k_r the reproduction efficiency and U_E^0 the cost of a single embryo. At embryo creation time a fixed scaled reserve density is assumed (set to the maternal *e*). When embryos surpass the scaled maturity at birth threshold ($U_H > U_H^b$) they are released from the pouch and a new clutch is formed. At birth (hatching), the embryonic energy reserve level is recalculated as

$$U_E = \frac{eL^3}{v}$$

Thus, the reserve level dynamics during embryonic development are ignored and U_E^0 is only used to determine the clutch size.

Individual variation

Inter-individual variation in DEB coefficients is incorporated in the same way as in (Martin et al. 2012) by applying scatter on a primary DEB coefficient, the surface-area-specific maximum assimilation rate $\{\dot{p}_{Am}\}$. A 'scatter-multiplier' (*sm*) is defined per individual as EXP(Gaussian(0,*cv*)), with *cv* being the standard deviation of the Gaussian probability density function. Here *cv* is set to 0.1 as a default. Coefficient $\{\dot{p}_{Am}\}$ is multiplied by the individual *sm*. In our scaled model this implies that U_H^b, U_H^b and g have to be divided by *sm*. Also (Koch and De Schamphelaere 2020) found, when testing on which of the 12 standard-DEB coefficients inter-individual imposed variability lead to the best fit, that the surface-area-specific maximum assimilation rate performed best. For the investigated

species, the copepod *Nitocra spinipes*, this implied drawing the parameter from a log-normal distribution with standard deviation of 0.15.

MOVEMENT

Juvenile and adult individuals may move from one spatial cell to another. Movement is thus grid-based, in an environment consisting of discrete spatial units. Embryos will move with their mother. Only crawling & swimming is accounted for, as a faithful representation of dispersal (transport) by drift in streams will require a specification of the hydrology of the system.

Movement is simulated as a number of steps of a grid-based random walk. The number of steps to take per day is probabilistic, drawing from a Poisson probability density function with the mean set to 1/residence time. Average residence time within a square 1 m^2 cell can be obtained from empirical data on movement, or derived from e.g., correlated random walk simulations on a continuous coordinate system, using a detailed movement model. For an example of the latter, for the related species *Asellus aquaticus*, see (Van den Brink et al. 2007). In the simulations in (Van den Brink et al. 2007) average residence time for *Asellus* was set to 51 minutes, resulting in on average 28 cell to cell moves per day. For *Gammarus pulex*, a roughly four times higher mobility was assumed in (Baveco et al. 2014), leading to an estimated 100 cell to cell moves per day. (Galic et al. 2014) used a value of 6 m for the standard deviation of the (Gaussian) distribution of daily covered distances in a linear waterbody.

Note that the scenarios studied here are non-spatial. Thus, the process of movement between neighboring cells can be ignored.

DENSITY DEPENDENCE

A simple density-dependent feedback mechanism is included, as density-dependent mortality (DDM), assuming a linear relationship between local density and the resulting density-dependent mortality rate μ_d:

$$\mu_d = \mu_{dd} \times N$$

Here μ_{dd} represents the density-dependent mortality (DDM) coefficient (m2 ind-1 d-1) and N the relevant local density (ind m-2), defined as the density of juveniles and adults together.

MORTALITY

Different sources of mortality are accounted for. Ageing mortality is part of the DEB submodel. Density-dependent mortality is included as the mechanism for density dependent regulation of population size. Mortality from chemical exposure is accounted for in the GUTS submodel.

An additional constant background mortality, with rate μ_b, may be assumed, representing a constant mortality factor caused by environmental conditions, e.g., predation.

GUTS

The GUTS models as described below can be used as independent modules for the evaluation of toxicity effects resulting from 'internal damage'. No links (feedback) between GUTS and DEB are incorporated yet (e.g., no dilution of internal concentration by growth; no scaling of rate constants with changing surface to volume ratio), but these links would be straightforward to implement.

Toxicokinetic model and damage dynamics

The simplest GUTS version assumes a one-compartment model and links external concentrations directly to the scaled damage. The choice of the so-called 'reduced GUTS' (GUTS-RED) implies that the dominant rate constant k_D ($time^{-1}$) is determined directly from the raw observed survival data without internal concentration measurements. The dynamics of the scaled damage, denoted D_w (t) in this case, is described by the following differential equation

$$\frac{\mathrm{d}D_w(\mathrm{t})}{\mathrm{dt}} = \mathrm{k_D} \times (\mathrm{C_{ext}}(\mathrm{t}) - D_w(\mathrm{t}))$$

Toxicodynamics and death mechanisms

The scaled damage is linked to the stochastic death (SD) or individual tolerance (IT) models to describe the respective survival over time. Combinations of the choice of the scaled damage and the death mechanism give clearly defined acronyms for the different variants of GUTS, e.g., GUTS-RED-SD for the combination of the scaled damage without consideration of internal concentrations and the SD mechanism, or GUTS-IT for the full GUTS model accounting for internal concentrations in combination with the IT mechanism.

In the SD model, a hazard rate is calculated following the differential equation

$$\frac{dH(t)}{dt} = b \times \max(0, D(t) - z)$$

which describes hazard increasing in proportion to killing rate constant b, when the scaled damage exceeds the internal threshold concentration z. For the parametrization of the SD model, the killing rate constant b ([D]$^{-1}$ time^{-1}) and internal threshold concentration z ([D]) must be estimated from the survival data; [D] stands here for the unit of the scaled damage. The parameter values are kept constant during the simulated time, the processes of toxicokinetics and -dynamics are captured by the ordinary differential equations.

In the SD model, the probability of an individual to survive until time t is calculated as

$$S_{SD}(t) = e^{-H(t)} \times e^{-h_b \times t}$$

where h_b (time^{-1}) is the background mortality rate constant.

In the IT model, the survival probability of an individual to survive until time t is calculated following the cumulative log-logistic distribution of the thresholds z in a group of individuals, given by the function

$$F(t) = \frac{1}{1+\left(\frac{\max_{0 \le \tau \le t} D(\tau)}{m}\right)^{-\beta}}$$

where m is the median of the distribution of z ([D]) and β (-) is the shape parameter of the distribution.

In the IT model, the survival is related to the maximum scaled damage rather than to the actual scaled damage because death is irreversible, meaning that also under decreasing concentrations, the level of mortality in a simulated group of individuals could not become lower again. In the IT model, the survival probability of an individual to survive until time t is then calculated by

$$S_{IT}(t) = (1 - F(t)) \times e^{-h_b \times t}$$

Note that in the IBM, background mortality with rate h_b is dealt with separately from toxicant-induced mortality. Thus, the exponential term $e^{-h_b \times t}$ can be removed from the equations for survival, presented above.

In the individual-based population model each individual contains a DEB and a GUTS-RED model. The GUTS-RED model keeps track of internal damage (the toxico-kinetics part) and quantifies daily survival probability (the toxico-dynamics part). GUTS dynamics are simulated with a timestep smaller than one hour, to avoid possible numerical instability. For the SD model, the individual probability of surviving a day of exposure is obtained from

values of survival over time S at the start and at the end of the day. The resulting mortality risk over day t is then given by (Charles et al. 2009):

$$\mu_{x(t)} = 1 - \frac{S_{(t)}}{S_{(t-1)}}$$

For the IT model, the internal damage level at the end of the day is compared to the individual threshold. This requires of course that at birth, each individual is assigned such a threshold, drawn from the log-logistic distribution assumed in the GUTS IT model, and defined by parameters α (m_w in the IT model) and β (also β in the IT model). At the end of a daily timestep, it is checked whether the maximum damage exceeds the individual tolerance threshold, for each individual. If so, the individual dies.

FEEDING & FOOD DYNAMICS

Feeding & DEB

The assimilation flux is in the scaled model represented by fL^2, where f represents the functional response (between 0 and 1). For f it is usually assumed that it depends on food density X according to a Monod equation:

$$f = \frac{X}{K_X + X}$$

in which K_X is the half-saturation constant.

In the studied scenarios no food limitation is assumed; thus f is set to 1.

Temperature

For temperature, observed values can be used, or a simple forcing function, e.g., with a maximum end of July and fluctuating between T_{av}-T_{amp} and T_{av}+T_{amp} (with T_{av} representing the average temperature and T_{amp} the temperature amplitude:

$$T(t) = T_{av} - T_{amp} \cdot \cos\left(\frac{t - shift}{365} \cdot 2\pi\right)$$

The value of parameter *shift* sets the timing of the day with annual minimum temperature after January 1 and the day with maximum temperature after July 1. E.g., a value of 31 shifts this day with minimum temperature from January 1 to January 31. Default parameter values matching West-European conditions may be T_{av} = 13 °C, T_{amp} = 10 °C and shift = 31 days (Olitrault et al. 2019).

2 Conceptual model evaluation

The implementation of the *Gammarus* population model as described in this document is entirely based on conceptual (sub)models for which a considerable and solid body of theory is readily available. With respect to these sub-models, no new theory is developed here. These constituent parts are:

DEB theory: we based the implementation on the scaled standard DEB with temperature-dependent rates. Non-standard additions to the model implementation include an approach avoiding the complexity of the 'maternal effects rule'. A species-specific 'extension' was added to deal with embryos developing in the brood pouch of the mother. An *abj* version of DEB model was used, accounting for a phase of growth acceleration between birth and metamorphosis. This version is for *Gammarus pulex* the current one on the AmP site.

GUTS modeling: reduced GUTS models requiring 3 parameters (excluding the background hazard rate) are implemented following the guidelines in the EFSA scientific opinion (EFSA 2018).

Other aspects related to life-history and ecology of *Gammarus pulex*, e.g. its **movement**, are obtained from previous model implementations and modeling studies (Baveco et al. 2014, Galic et al. 2014). The analysis of model behavior focusses however exclusively on non-spatial scenarios.

Incorporation of temperature-dependent DEB rates allows us to deal with **seasonal environments**. We combined seasonality with a standard mechanism for regulation of population density, by density dependent mortality (based on the local density of juveniles and adults).

3 Calibration

Two life-history coefficients, related to reproduction, were set by simple calibration procedures.

Brood size

For *Gammarus pulex*, the brood size has been found to depend on the length of the reproducing female (Hynes 1955), following the regression equation:

$$broodsize(L) = 4.72 \cdot L - 23.653$$

with *L* representing the real length of the mother in mm. For the largest females (11.5 mm), observed brood size was 29. Real length relates to volumetric *length* as used in the DEB

model (in cm) as *L* = 10 * *length* / shape-factor. For *Gammarus*, the shape coefficient amounts to 0.23453. When applying the equation as is, the brood size will be overestimated by approximately a factor 4. Therefore, we divide the value from the original equation by 4:

$$broodsize(L) = (4.72 \cdot L - 23.653)/4$$

The resulting distribution of realized brood sizes in a 10-year simulation of population dynamics, at constant temperature of 15 °C, is shown in Figure 14.

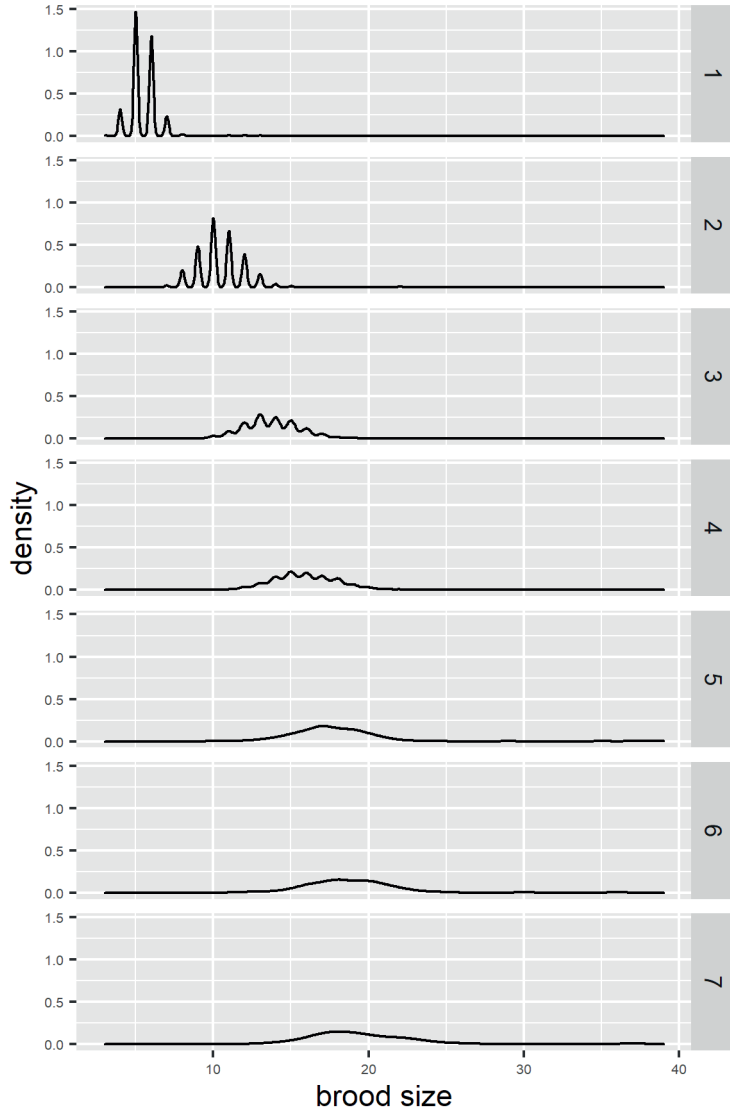

Figure 14. Density plots showing the brood size distributions, for the different broods (levels in the plot), in a simulation of population dynamics. Note that brood numbers above 7 occur only rarely, and are excluded from the plot.

uEgg

A second coefficient that was determined by calibration is *uEgg*, providing the energy required to produce a single offspring (cm^2 d), after being multiplied by DEB coefficient *kap_R*, the reproduction efficiency. The value used in the *Asellus* version of the model (0.029357688), leads to brood development times that are far longer than observed for *Gammarus*. Temperature-dependent brood development data, see references in (Galic et al. 2014), predict brood development times of 22 to 23 days at 15 °C. Testing different multiplication factors applied on the *Asellus* value, indicate that for a multiplication factor ¼ the resulting development time – at least for the first brood! – is around 22 days (Figure 15).

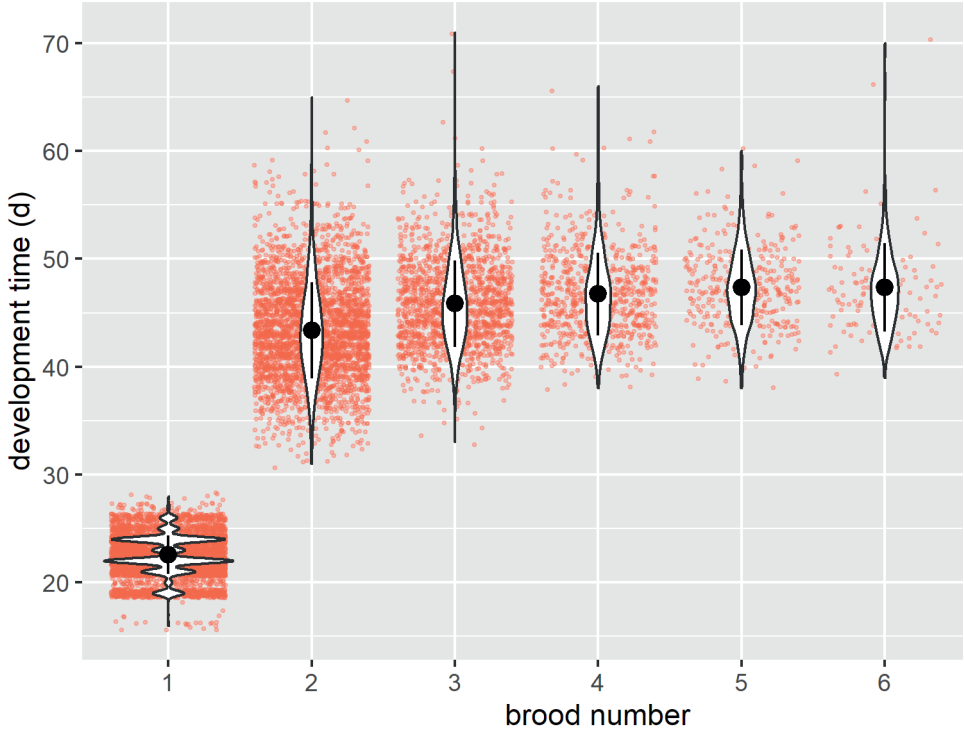

Figure 15. Violin plots of the development times of the different broods, as realized in a 10-year simulation of population dynamics at 15 °C. Brood numbers higher than 7 occur rarely and are excluded from the plot.

4 References

Baveco, J. M., S. Norman, I. Roessink, N. Galic, and P. J. V. d. Brink. 2014. Comparing population recovery after insecticide exposure for four aquatic invertebrate species using models of different complexity. Environmental Toxicology and Chemistry **33**:1517-1528.
EFSA. 2018. Scientific Opinion on the state of the art of Toxicokinetic/Toxicodynamic (TKTD) effect models for regulatory risk assessment of pesticides for aquatic organisms. EFSA Journal **16**:e05377.
Galic, N., R. Ashauer, H. Baveco, A.-M. Nyman, A. Barsi, P. Thorbek, E. Bruns, and P. J. Van den Brink. 2014. Modeling the contribution of toxicokinetic and toxicodynamic processes to the recovery of Gammarus pulex populations after exposure to pesticides. Environmental Toxicology and Chemistry **33**:1476-1488.
Gergs, A., T. G. Preuss, and A. Palmqvist. 2014. Double Trouble at High Density: Cross-Level Test of Resource-Related Adaptive Plasticity and Crowding-Related Fitness. PloS one **9**.
Jager, T., C. Albert, T. G. Preuss, and R. Ashauer. 2011. General Unified Threshold Model of Survival - a Toxicokinetic-Toxicodynamic Framework for Ecotoxicology. Environmental Science & Technology **45**:2529-2540.
Koch, J., and K. A. C. De Schamphelaere. 2020. Estimating inter-individual variability of dynamic energy budget model parameters for the copepod Nitocra spinipes from existing life-history data. Ecological Modelling **431**:109091.
Kooijman, S., T. Sousa, L. Pecquerie, J. van der Meer, and T. Jager. 2008. From food-dependent statistics to metabolic parameters, a practical guide to the use of dynamic energy budget theory. Biological Reviews **83**:533-552.
Kooijman, S., N. Vanderhoeven, and D. C. Vanderwerf. 1989. POPULATION CONSEQUENCES OF A PHYSIOLOGICAL MODEL FOR INDIVIDUALS. Functional Ecology **3**:325-336.
Kooijman, S. A. L. M. 2009. What the egg can tell about its hen: Embryonic development on the basis of dynamic energy budgets. Journal of Mathematical Biology **58**:377-394.
Kooijman, S. A. L. M. 2010. Dynamic Energy Budget Theory for Metabolic Organisation. Third edition. Cambridge University Press, Cambridge.
Kooijman, S. A. L. M. 2014. Metabolic acceleration in animal ontogeny: An evolutionary perspective. Journal of Sea Research **94**:128-137.
Martin, B. T., E. I. Zimmer, V. Grimm, and T. Jager. 2012. Dynamic Energy Budget theory meets individual-based modelling: a generic and accessible implementation. Methods in Ecology and Evolution **3**:445-449.
Olitrault, M., D. Azam, A. Gallard, and A. Quemeneur. 2019. Données physicochimiques issues du Projet EMERITAT : Utilisation de modèles d'exposition aux pesticides pour la reconstitution et la mise en oeuvre de scénarios réalistes de contamination de mésocosmes permettant d'étudier les impacts d'itinéraires techniques sur les organismes aquatiques. Portail Data Inra.
Van den Brink, P. J., J. M. Baveco, J. Verboom, and F. Heimbach. 2007. An individual-based approach to model spatial population dynamics of invertebrates in aquatic ecosystems after pesticide contamination. Environmental Toxicology and Chemistry **26**:2226-2236.
Zimmer, E. I., V. Ducrot, T. Jager, J. Koene, L. Lagadic, and S. Kooijman. 2014. Metabolic acceleration in the pond snail Lymnaea stagnalis? Journal of Sea Research **94**:84-91.

Appendix AmP coefficients

AmP parameters estimated for the *Abj* DEB model for *Gammarus pulex* (refit of the AmP data)


```
{
	"Primary parameters at reference temperature (20 deg. C)" : {
		"symbol" : [
			"value",
			"units",
			"description"
		],
		"T_A" : [
			"10560",
			"K",
			"Arrhenius temperature"
		],
		"p_Am" : [
			"44.462",
			"J/d.cm^2",
			"{p_Am}, spec assimilation flux"
		],
		"F_m" : [
			"6.5",
			"l/d.cm^2",
			"{F_m}, max spec searching rate"
		],
		"kap_X" : [
			"0.8",
			"-",
			"digestion efficiency of food to reserve"
		],
		"kap_P" : [
			"0.1",
			"-",
			"faecation efficiency of food to faeces"
		],
		"v" : [
			"0.02037",
			"cm/d",
			"energy conductance"
		],
		"kap" : [
			"0.8833",
			"-",
			"allocation fraction to soma"
		],
		"kap_R" : [
			"0.95",
			"-",
```

```
                "reproduction efficiency"
            ],
            "p_M" : [
                "337.4",
                "J/d.cm^3",
                "[p_M], vol-spec somatic maint"
            ],
            "p_T" : [
                "0",
                "J/d.cm^2",
                "{p_T}, surf-spec somatic maint"
            ],
            "k_J" : [
                "0.002",
                "1/d",
                "maturity maint rate coefficient"
            ],
            "E_G" : [
                "4446.0",
                "J/cm^3",
                "[E_G], spec cost for structure"
            ],
            "E_Hb" : [
                "0.06737",
                "J",
                "maturity at birth"
            ],
            "E_Hj" : [
                "2.105",
                "J",
                "maturity at metam"
            ],
            "E_Hp" : [
                "2.108",
                "J",
                "maturity at puberty"
            ],
            "h_a" : [
                "3.278e-06",
                "1/d^2",
                "Weibull aging acceleration"
            ],
            "s_G" : [
                "0.0001",
                "-",
                "Gompertz stress coefficient"
            ]
    },
    "Parameters specific for this entry at reference temperature (20 deg. C)" : {
            "symbol" : [
                "value",
                "units",
```

```
            "description"
],
"Lw2_0" : [
            "0.5408",
            "cm",
            "initial  length for tL2 data"
],
"Lw3_0" : [
            "0.5473",
            "cm",
            "initial  length for tL3 data"
],
"Lw4_0" : [
            "0.5509",
            "cm",
            "initial  length for tL4 data"
],
"Lw5_0" : [
            "0.3756",
            "cm",
            "initial  length for tL5 data"
],
"Lw6_0" : [
            "0.3967",
            "cm",
            "initial  length for tL6 data"
],
"Lw7_0" : [
            "0.409",
            "cm",
            "initial  length for tL7 data"
],
"del_M" : [
            "0.2353",
            "-",
            "shape coefficient"
],
"f" : [
            "1",
            "-",
            "scaled functional response for 0-var data"
],
"t_0" : [
            "0",
            "d",
            "time at start development"
],
"z_m" : [
            "0.1343",
            "-",
            "zoom factor for male"
]
```

```
	},
	"Temperature parameters" : {
		"symbol" : [
			"value",
			"units",
			"description"
		],
		"T_A" : [
			"10560",
			"K",
			"Arrhenius temperature"
		],
		"T_ref" : [
			"293.15",
			"K",
			"Reference temperature"
		]
	},
	"Chemical parameters" : {
		"" : [
			"Food",
			"Structure",
			"Reserve",
			"Faeces"
		],
		"Chemical potentials (J/C-mol)" : [
			"525000",
			"500000",
			"550000",
			"480000"
		],
		"Specific density for dry weight (g/cm^3)" : [
			"0.17",
			"0.17",
			"0.17",
			"0.17"
		]
	}
}
```

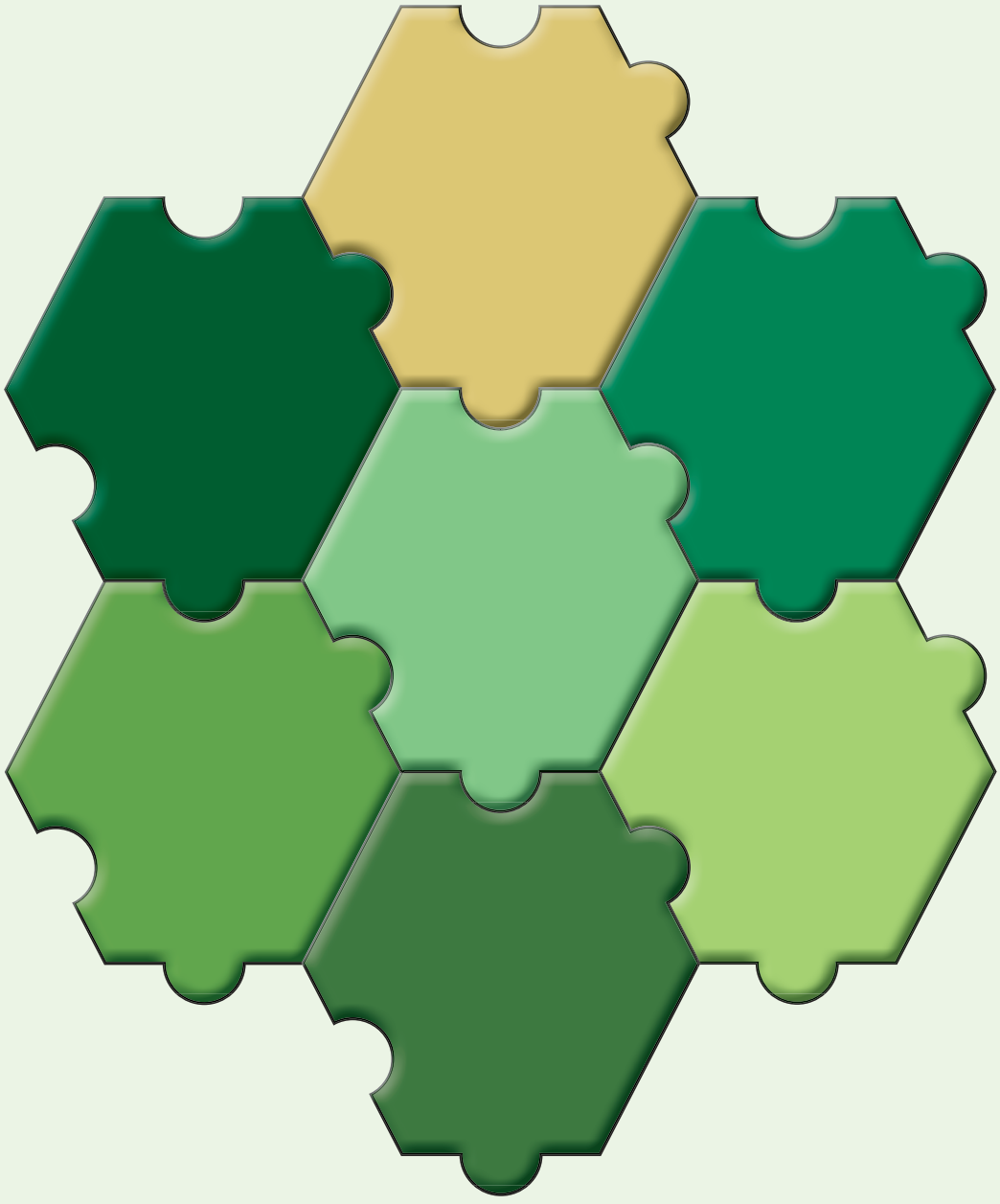

Chapter 7

General discussion

7.1 Introduction

Modeling the effect of temperature and chemicals at different levels of biological organization is undoubtedly a topic relevant for current and future environmental risk assessment. It joins two major environmental threats or stressors: temperature and chemicals[1], whose relevance will only increase in the future (Bernhardt et al., 2017; Noyes et al., 2009a; Woolway et al., 2021). Since 1955, the production and diversity of chemicals increased at rates that are as concerning as other drivers for global change (Bernhardt et al., 2017). Similarly, temperature as a consequence of global climate change will increase in general, i.e., global warming (IPCC, 2019), but is also projected to become more extreme, i.e., colder and warmer extreme weather events occurring more frequently in the future (IPCC, 2012).

By using modeling approaches, this research topic supports the ethical considerations of the three R principles, aiming to bring the number of animal experiments down (Russell and Burch, 1959). Modeling tools contribute to the principles of this framework by means of informing the design of animal experiments (i.e., refinement), obtaining mechanistic information from fewer animal testing (i.e., reduction) and finally by providing alternatives through simulations and predictions (i.e., replacement). Herewith, modeling approaches facilitate resource efficiency, i.e., cost and time effective analysis.

Lastly, this research aligns with one of the priority research questions to guarantee a sustainable environmental quality (Van den Brink et al. 2018); with the question being rank 4: *How can we develop mechanistic modeling to extrapolate adverse effects across levels of biological organization?* The modeling approaches used in this thesis, e.g., mechanistic effect models and population models, enable to extrapolate effects measured at one biological level to another (Gergs et al., 2019; Jager and Klok, 2010; Martin et al., 2013).

Thus, the overall aim of this thesis was to develop and improve mechanistic effect models to assess the effect of temperature and chemicals at different levels of biological organization. In this last chapter, I discuss the findings of this thesis, connect them to each other, and discuss them within a broader perspective. This final chapter also provides recommendations for future research and a personal reflection on the role of science communication in fostering the application of models in environmental risk assessment.

[1] If not explicitly stated otherwise, when referring to “chemicals” in this chapter, I use this term thinking of substances of anthropogenic origin. This includes synthetic chemicals that we either purposefully disperse in the environment, like pesticides, but also substances that enter the environment as a consequence of their use in our society, i.e., pharmaceuticals and industrially or commercially used compounds.

7.2 Why should we care about temperature?

The various social impacts associated with global temperature changes include adverse effects on agriculture (Raza et al., 2019) and water resources, posing a threat to global food security and human health (L. Chen et al., 2021; M. Chen et al., 2021; IPCC, 2019). Environmental impacts at the ecological level include habitat shits (Menéndez et al., 2008; Van der Putten et al., 2010), and the disruptions of natural communities (Polazzo et al., 2023). Altogether these impacts pose a threat to the delicate balance of ecosystems as a whole (Cardinale et al., 2012).

While chemicals have been the central element of research in ecotoxicology from the start, temperature has not always been seen or prioritized as a stressor or a modulating factor in environmental systems. Although temperature is always present during laboratory or field studies, it was mainly reported as a background environmental variable rather than actively considered as an experimental variable of interest. Similar as the field of global change research failed to consider the rising risk of chemicals in the future (Bernhardt et al., 2017), it seems as if the field of ecotoxicology overlooked temperature as a considerable driver of chemical risk. However, temperature has gained relevance in recent decades within environmental research and ecotoxicology, as indicated in the rise of the fraction of environmental publications with “temperature” in their title (*Figure 7.1*).

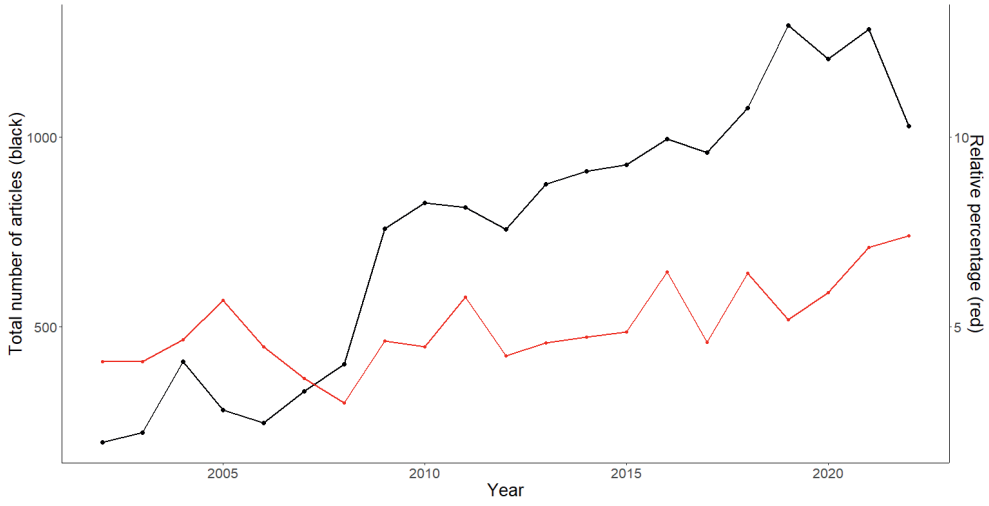

Figure 7.1: Number of journal articles in environmental science from 2002 to 2022. Displayed on the left y-axis in black are the number of journal articles in the field of environmental research as categorized by Scopus with the search string: TITLE-ABS-KEY (ecotoxicology) AND (LIMIT-TO (SUBJAREA, "ENVI")) AND (LIMIT-TO (DOCTYPE,"ar")). The relative increase of papers including temperature (right y-axis in red) was calculated based on the total number of articles in ecotoxicology including temperature as searched with the string: TITLE-ABS-KEY (ecotoxicology AND temperature) AND (LIMIT-TO (SUBJAREA,"ENVI")) AND (LIMIT-TO(DOCTYPE,"ar")).

So, temperature moved from a somewhat stable background variable to a concerningly unstable factor of primary research interest. But why is it important to consider temperature in the context of environmental risk assessment of chemicals? The simple answer is that temperature affects all biological, physical and chemical rates in nature, so it likely also affects the risk of chemicals. Hence, if we know that temperature conditions will change in the future, we must consider its potential effect on the risks of chemicals to the environment (Noyes et al., 2009a). More specifically, there are different ways in which temperature may influence chemicals' relevance in the environment. Firstly, temperature affects the substances themselves, i.e., it impacts chemicals' fate and transport (Kong et al., 2014; Roth et al., 2023), affecting the exposure aspect of environmental risk assessment. Secondly, temperature influences biological processes, herewith altering the effects chemicals have on organisms. This is reflected through changes in species sensitivity either due to climate-induced toxicant sensitivity (CITS) or toxicant-induced climate sensitivity (TICS) (Hooper et al., 2013), leading to a change in the outcome of an environmental risk assessment. As both of these temperature-chemical interactions have been recognized empirically (Hermann et al., 2023; Janssens et al., 2018; Patra et al., 2007; Theys et al., 2020; Verheyen et al., 2019), the environmental risk assessment of chemicals could be insufficient when possible interactions with temperature are not taken into account.

Therefore, the main objectives of this thesis aim to support environmental risk assessment of chemicals by

1. investigating the effects of temperature on toxicokinetic-toxicodynamic processes,
2. deriving an individual level model to describe the effects of temperature as a stressor, and
3. implementing the effects of temperature on the toxicity of insecticides in effect models at different levels of biological organization.

In the following, I highlight the main conclusions and implications of my research in relation to these objectives.

7.3 The effects of temperature on toxicokinetic and toxicodynamic processes

In **Chapter 2** of this thesis, we generated experimental data providing mechanistic background how temperature influences an organism’s sensitivity toward chemicals. For this, we used two different insecticides, imidacloprid, and flupyradifurone, which both caused increased mortality and food consumption inhibition in *Gammarus pulex* with increasing temperature. However, we identified differences in the effect sizes between the tested

compounds with smaller effects caused by flupyradifurone. Compound-specific differences in how temperature alters the effects of chemicals have been reported previously (Harwood et al., 2009; Heugens et al., 2001; Holmstrup et al., 2010; Noyes et al., 2009a). Our results add to the existing knowledge that even between insecticides with the same molecular target (i.e., the nicotinic acetylcholine receptor nAChR), the extent of temperature's influence can be compound-specific.

The next step was to investigate how temperature can be implemented as an explicit factor in effect models. Effect models like toxicokinetic-toxicodynamic (TK-TD) models enable us to understand toxicity beyond the standard dose-response relationship by introducing a time dimension (Jager et al., 2006; T. Jager et al., 2011). The widely used General Unified Threshold model of Survival (GUTS) is a TK-TD model framework deemed ready for use in environmental risk assessment by an expert panel of the European Food Safety Authority (EFSA (PPR), 2018). While there have been previous attempts to include temperature in GUTS models (Gergs et al., 2019), they did not allow investigation of the influence of temperature on the separate model processes (i.e., toxicokinetic and toxicodynamic processes). As we generated the necessary dataset to evaluate the effect of temperature on those processes separately (**Chapter 2**), we could investigate the influence of temperature on TK-TD model parameters by using GUTS in **Chapter 3**. We discovered that including the temperature scaling explicitly by means of the Arrhenius equation improved model performance.

Although our updated model enables to predict the effect of insecticides at various temperatures, expanding the understanding of toxicity in time with an additional temperature dimension still requires an extensive experimental dataset to parameterize the model (**Chapter 3**). Thus, for chemical-species combinations with no or a limited amount of experimental data, the application of this model is cumbersome. By including temperature we add an additional factor to the key challenge of ecotoxicology: assessing chemical's risks to a wide range of species based on data derived from a narrow number of species. However, frameworks proposing the use of species-traits in predicting cross-species sensitivity (Rubach et al., 2011; Van den Berg et al., 2019), can be expanded by temperature tolerance as an additional trait. Likewise, chemical characteristics can be used to predict the potential temperature influence on TK-TD parameters, i.e., by applying quantitative structure-activity relationships (QSARs) (Jager and Kooijman, 2008).

In **Chapter 3**, we found a difference in how toxicokinetic and toxicodynamic model parameters scaled with temperature. Our results hint against the simple assumption that all processes scale with temperature to the same extent. This assumption has been voiced in literature (Jager and Ashauer, 2018a) and was successfully applied in a related modeling approach, the dynamic energy budget (DEB) modeling (S. A. L. M. Kooijman, 2010). It is

based on the universal scaling of chemical reactions as described by the Arrhenius equation (Arrhenius, 1889), which results in acceptable accuracy in the range of relevant temperatures when applied to metabolic rates (S. A. L. M. Kooijman, 2010). With our results (**Chapter 3**), we provide evidence for a more complex scaling of toxicokinetic and toxicodynamic model parameters, potentially justified in the different nature of the underlying processes, e.g., uptake through passive diffusion for TK and more complex enzyme mediated processes for TD, as outlined in the supporting information of **Chapter 3**.

7.4 Temperature as a stressor

While the GUTS-T models from **Chapter 3** introduced temperature as a modulating factor in effect models, another approach was explored in **Chapter 4**, where we considered temperature as a stressor on its own. By introducing a novel temperature damage model, we built a tool to assess temperature effects on individuals, enhancing our understanding of temperature effects. With this model, we demonstrated that the damage concept is applicable to other stressors than chemicals and exhibited the model's ability to predict temperature effects in simulations for various temperature scenarios. This model is envisioned to be applied in a mixture approach to incorporate temperature as an additional stressor in effect models (Figure 7.2).

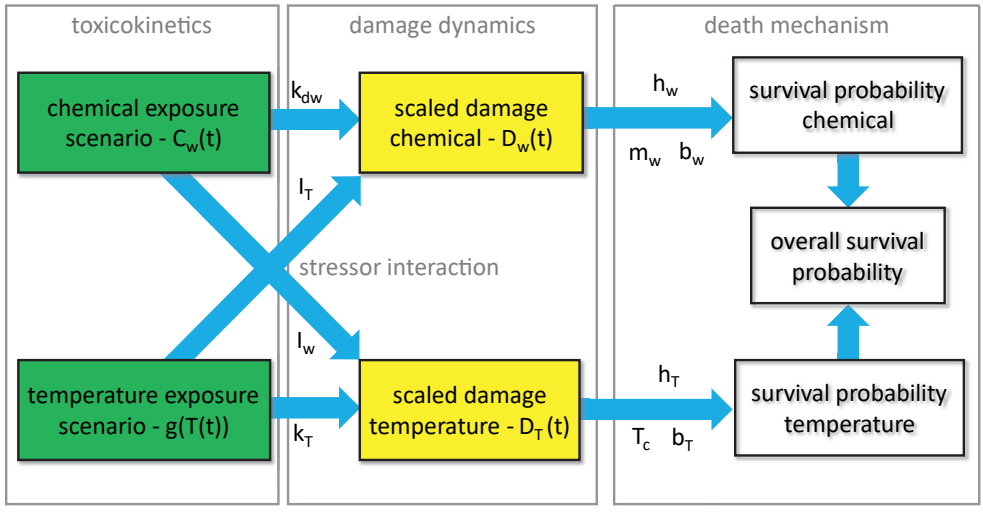

Figure 7.2. Conceptual figure to combine the temperature damage model of Chapter 4, with the framework presented in Bart et al. 2021; 2022. Green boxes represent the exposure scenarios, yellow boxes represent damage state variables and white boxes the survival. Cw(t) = external water concentration for the chemical over time, Dw(t) = scaled damage of the chemical over time, k_{dw} = dominant rate constant for chemical damage; I_w = interaction factor of chemical on temperature, h_w = hazard rate for individual in chemical damage model, m_w = median of the threshold distribution, b_w = killing rate chemical, g(T(t)) = external (water) temperature over time, $D_T(t)$ = scaled damage of temperature over time, k_T = dominant rate constant for temperature damage, I_T = interaction factor of temperature on chemical , h_T = hazard rate for

individual in temperature damage model, T_c = critical temperature where damage accumulation starts, b_T = killing rate temperature. Modified from Bart et al. 2021.

Such a GUTS extension resemble the ones made for chemical mixtures, which enable the evaluation of the damage caused by two different stressors, while the stressors may lead to the same or a dissimilar form of damage (Bart et al., 2022, 2021). For chemical mixtures the reasoning behind a shared form of damage (i.e., damage addition model) are the same mode of action (i.e., same molecular target, acting on same or similar physiological processes). To model the combined effect of the exposure to a chemical and temperature stress, starting by adding the hazard rates, thus assuming that temperature acts independently, appears reasonable. Eventually, applying the approach by Bart et al. to investigate the interaction between both stressors, would allow to classify them as additive, synergistic or antagonistic (Bart et al., 2022), providing valuable insights in the mechanistic understanding of this stressor combination.

To construct such a multi-stressor TKTD model, both approaches presented here, i.e., temperature as a modulating factor (**Chapter 3**) and temperature as an additional stressor (**Chapter 4**) could be combined. The mean temperature ranges observed and projected for global climate change (Calvin et al., 2023), are within the range where temperature will likely act as a modulating factor. However, the 4 °C temperature increase as the worst case scenario in the global mean temperature evolves from temperature changes that include higher and lower absolute temperature differences. Furthermore, the projection for increased heatwave amplitude and frequency (Woolway et al., 2021) imply the need to also consider temperature as an additional stressor for future environmental risk assessment of chemicals.

7.5 Modeling effects of temperature on the toxicity of insecticides at different levels of biological organization

The ambition to extrapolate adverse effects of chemicals across levels of biological organization has been voiced frequently due to the fact that effects are mostly assessed at the individual level, while the protection goals for the environmental risk assessment of chemicals are often set at the population level. Not only can it help to reduce the amount of experiments needed significantly, but it also provides a systematic understanding of the ecosystem as a whole.

Considering new approaches that can help to reduce the amount of experiments needed, **Chapter 5** shows that interdisciplinary research, combining methods from molecular biology and in silico modeling, provides insights into the underlying molecular mechanisms on a remarkable level of detail. Briefly, we successfully calibrated and validated a new

toxicokinetic-receptor model by combining data from in vivo and in vitro receptor-binding assays and laboratory exposure studies. With this, we provide evidence for an irreversible receptor binding of the neonicotinoid thiacloprid in *Gammarus pulex*, suggesting that the toxicokinetics of thiacloprid are best represented by a two-compartment model, where the second compartment represents the membrane proteins, including the target receptor (i.e., nAChR) of this insecticide.

As a step towards obtaining an improved systematic understanding of the ecosystem as a whole, **Chapter 6** describes how we incorporated temperature-corrected GUTS models into individual based population models (IBMs), and we discuss the relevance of the additional temperature correction of the GUTS parameter in such IBMs, as well as its influence on the predicted population dynamics.

Implementing a detailed toxicokinetic receptor model as presented in **Chapter 5** into the individual level based GUTS framework would be relatively straightforward (although this has not been explored in this thesis), and thus enables to link the receptor level, to the individual, and finally, to the population level by means of an IBM. For the future of cross-level extrapolations, the linking of the sub-organismal level (i.e., molecular initiating events like receptor binding) with individual level approaches like GUTS and population level models like GUTS based IBMs, appears like a great way forward (Murphy, C.A. et al. 2018). To enable this, experimental and modeling approaches should be applied jointly (as in **Chapter 2** and **5**), building a new, stronger basis for environmental risk assessment.

7.6 Everything, everywhere, all at once – Embracing (enough) complexity

Complexity is an attribute that is inherent to biological systems. While this complexity is what fascinates researchers and powers their drive to understand the matter in front of them, it is, at the same time, a rather frustrating burden for environmental policymakers and risk assessors. The level of understanding required to build a representable effect model may not align with the level of understanding required to make practical decisions to protect the environment. And even more importantly, the time needed for such understanding may be disconnected from the time we have to make decisions in environmental policy. Therefore, when addressing complexity in environmental risk assessment we need to do so in an “efficient, robust and understandable” way, “that makes biological sense”(Forbes and Calow 2013). This can be achieved through a common understanding of modeling tools and their features (i.e., what they can and cannot do, their uncertainties or variability in detail) in combination with an agreement of a shared protection goal.

In pursuit of an agreement of a shared protection goal, we should ask ourselves, do we want to protect everything, everywhere, all at once? Solely understanding an organism's sensitivity towards chemicals is already a complex problem, as Sanne van den Berg outlined in impressively clear and pressing terms in her thesis entitled: "Improving cross-species extrapolation of chemical sensitivity" (van den Berg 2020). Next to species traits like their life cycle duration and respiration mode (Van den Berg et al. 2019), species sensitivity to chemicals is also influenced by factors like exposure duration and the endpoint under consideration (van den Berg 2020; van den Berg et al. 2021). The findings of this thesis and the additional aspects discussed in this chapter mostly add to the complexity of understanding the effect of chemicals on organisms, now adding temperature as an additional factor that should be taken into account. So how do we deal with this complexity? One approach could be to try to understand everything, everywhere, all at once, and build very complex models. However, the payoff in time and costs of adding complexity, will decrease for too complex models (Grimm et al., 2005). Another approach could be to focus on the main drivers of the emergent phenomena under study, which may vary according to the protection goal under consideration. Considering the importance of temperature as a stressor to aquatic ecosystems, for instance, further studies have to be done to rank temperature among commonly found stressors like urban land use, eutrophication, and mean annual water flow (Lemm et al., 2021).

Science, in general, constantly questions itself. A theory is valid for as long as it can repeatedly stand true, considering new empirical evidence. This evidence is usually obtained from practical experiments. Also, in ecotoxicology, standardized laboratory exposure experiments still built the basis for environmental risk assessment of chemicals. Although it is frequently indicated in the literature that species sensitivity should not be described as a single variable, survival (or the equivalent endpoint of mortality) is the most common descriptor of species sensitivity in ecotoxicological studies. For the future, striving to connect different levels of biological organization, I think we should question the current approach in ecotoxicology and acknowledge that effect models significantly increase the value of the data generated in those standard laboratory experiments for environmental risk assessment. By introducing time and temperature dimensions as presented in this thesis, effect models significantly increase the value of the data generated in standard laboratory experiments and increase the possibilities to propagate effects between the different levels of biological organization.

Considering the common understanding of modeling tools and their features, a lot of progress has been made in the last couple of decades considering the acceptability of models in regulatory science (Grimm et al., 2014; Schmolke et al., 2010). To mention a broadly relatable and striking example we can look at how model-based projections of Covid-19 spread influenced travel restrictions and border closures (McBryde et al., 2020). These

models managed to decompose a biological phenomenon into its most important factors. Obviously, they did not promise to end the pandemic or cure a Covid-19 infection. Still, they managed to shed light on how one person can infect another, or maybe multiple others, depending on an individual's behavior. The applicability domain of Covid-19 models was clear, and their uncertainties and variabilities were directly experienced in the day-to-day lives of citizens worldwide. Crucial for the regulatory acceptance of Covid-19 models was that the models themselves facilitated communication between academic researchers, risk assessors, policymakers, and even the general public. Ideally, effect models of the future can manage to achieve the same.

The main challenge for future environmental risk assessments is to improve the conversation between academic researchers, risk assessors, and policymakers. In my understanding, in the field of ecotoxicology, effect models are the way to do that.

7.7 Communication is key

In this last part of my general discussion, I want to highlight the role of science communication in promoting the application of effect models for environmental risk assessment of chemicals. Specifically, I want to touch upon two aspects, referring to different kinds of science communication. Firstly, *scientific science communication* as performed by scientists for scientists through peer-reviewed publications, conference presentations, and the occasional debate next to the coffee machine at the office. Secondly, the communication of scientific results or practices by either scientists or other science communicators (i.e., communication officers or journalists) directed to an audience without or with a limited scientific background, often broadly referred to as “the general public”. This second kind of science communication I call *citizen science communication*.

Ecotoxicology is already a mix of two disciplines: ecology and toxicology. There are, however, even more disciplines involved in the environmental risk assessment of chemicals, such as biochemistry, cellular biology, physiology, statistics, and mathematical modeling (Astuto et al., 2022). In general, interdisciplinary collaboration is massively impacted by the respective jargon of each field and the lack of awareness of such. We as scientists forget to reconnect with our past selves, who had to learn all those words, and often take their understanding by others for granted. This problem is accompanied by the issue that we might even use the same scientific term while meaning different things. A personal example for this phenomenon I made with the word “mechanistic,” which has subtle differences in emphasis and application between biologists and ecologists. With my bachelor studies of biology in mind, this term refers to understanding the precise molecular processes that underlie the biological phenomena observed (i.e., genetical, biochemical or physiological

processes). Whereas in ecology, I learned later, a mechanistic approach entails cause-and-effect relationships between organisms, their environment, and other ecological factors to identify biological processes that govern population dynamics, species interactions, and ecosystem functioning. Thus, when talking about "mechanistic modeling" among biologists, they will likely refer to a model for gene expression dynamics at the individual or sub-individual level. In contrast, the same term will refer to population or ecosystem-level models when used by ecologists. And in-between those two perspectives, I now find myself as an ecotoxicologist, working with toxicokinetic-toxicodynamic effect models within individual-based models extrapolating between those levels, wondering what words to use.

Next to minor or mayor challenges in scientific science communication implied by the use of language, the respective norms and values underlying the different actors engaged in a conversation can cause potential obstacles. Thus, all stakeholders within the environmental risk assessment process (i.e., university researchers, industry, government, and other decision-makers) need to invest time and effort to understand each other's language, values and norms to collaborate effectively. So how is this going so far? Despite the progress of the so-called *new approach methodologies* like *in vitro* or *in silico* methods, their full potential to inform regulatory decisions is not yet applied in chemical hazard and risk assessment (Di Nicola et al., 2023; Westmoreland et al., 2022). The reason often seems to be a mismatch in the confidence level towards these approaches between researchers who develop and apply them in the academic or industrial research context and assessors at the regulatory agencies that could be using them in the decision-making process (but see EFSA (PPR) 2018; Larras et al. 2022).

Thus, it is my impression is that we vastly underestimate the importance of effective science communication as a key to advancing environmental risk assessment. Therefore, I propose looking at citizen science communication for inspiration. With the introduction of this thesis (**Chapter 1**), I took on the challenge to write my first citizen science communication piece about my research. Despite my personal interest in science communication, I call it a challenge as this writing style is not at all within my comfort zone. I did it partly to prove to myself that I can do it, but mostly because I think we learn valuable skills for scientific science communication if we engage more in citizen science communication.

The most important aspect we should learn from citizen science communication, is to learn to find common ground by identifying "the smallest shared reality". The science communicator Mai Thi Nguyen-Kim writes about this in her book *Die kleinste Gemeinsame Wirklichkeit* (Nguyen-Kim, 2021). She rightfully declares that finding this common ground, this smallest shared reality, is the basis for every meaningful debate.

So, for the future of ecotoxicology, let's find our smallest shared reality, and start talking from there.

References

Accolla, C., Vaugeois, M., Grimm, V., Moore, A.P., Rueda-Cediel, P., Schmolke, A., Forbes, V.E., 2021. A Review of Key Features and Their Implementation in Unstructured, Structured, and Agent-Based Population Models for Ecological Risk Assessment. Integrated Environmental Assessment and Management 17, 521–540. https://doi.org/10.1002/ieam.4362

Add-my-Pet [WWW Document], 2021. . Gammarus pulex, version 2021/07/30. URL https://www.bio.vu.nl/thb/deb/deblab/add_my_pet/entries_web/Gammarus_pulex/Gammarus_pulex_res.html

Agatz, A., Ashauer, R., Brown, C.D., 2014. Imidacloprid perturbs feeding of Gammarus pulex at environmentally relevant concentrations. Environmental Toxicology and Chemistry 33, 648–653. https://doi.org/10.1002/etc.2480

Agatz, A., Brown, C.D., 2014. Variability in feeding of Gammarus pulex: moving towards a more standardised feeding assay. Environmental Sciences Europe 26, 15. https://doi.org/10.1186/s12302-014-0015-4

Arenas-Sánchez, A., López-Heras, I., Nozal, L., Vighi, M., Rico, A., 2019. Effects of increased temperature, drought, and an insecticide on freshwater zooplankton communities. Environmental Toxicology and Chemistry 38, 396–411. https://doi.org/10.1002/etc.4304

Arnot, J.A., Gobas, F.A.P.C., 2006. A review of bioconcentration factor (BCF) and bioaccumulation factor (BAF) assessments for organic chemicals in aquatic organisms. Environmental Reviews 14, 257–297.

Arrhenius, S., 1889. Über die Reaktionsgeschwindigkeit bei der Inversion von Rohrzucker durch Säuren. Zeitschrift für Physikalische Chemie 4U, 226–248. https://doi.org/10.1515/zpch-1889-0416

Arroyo, J.I., Díez, B., Kempes, C.P., West, G.B., Marquet, P.A., 2022. A general theory for temperature dependence in biology. Proceedings of the National Academy of Sciences 119, e2119872119. https://doi.org/10.1073/pnas.2119872119

Ashauer, R., Agatz, A., Albert, C., Ducrot, V., Galic, N., Hendriks, J., Jager, T., Kretschmann, A., O'Connor, I., Rubach, M.N., Nyman, A.-M., Schmitt, W., Stadnicka, J., Brink, P.J. van den, Preuss, T.G., 2011. Toxicokinetic-toxicodynamic modeling of quantal and graded sublethal endpoints: A brief discussion of concepts. Environmental Toxicology and Chemistry 30, 2519–2524. https://doi.org/10.1002/etc.639

Ashauer, R., Caravatti, I., Hintermeister, A., Escher, B.I., 2010. Bioaccumulation kinetics of organic xenobiotic pollutants in the freshwater invertebrate Gammarus pulex modeled with prediction intervals. Environ Toxicol Chem 29, 1625–36. https://doi.org/10.1002/etc.175

Ashauer, R., Escher, B.I., 2010. Advantages of toxicokinetic and toxicodynamic modelling in aquatic ecotoxicology and risk assessment. Journal of Environmental Monitoring 12, 2056–2061. https://doi.org/10.1039/C0EM00234H

Astuto, M.C., Di Nicola, M.R., Tarazona, J.V., Rortais, A., Devos, Y., Liem, A.K.D., Kass, G.E.N., Bastaki, M., Schoonjans, R., Maggiore, A., Charles, S., Ratier, A., Lopes, C., Gestin, O., Robinson, T., Williams, A., Kramer, N., Carnesecchi, E., Dorne, J.-L.C.M., 2022. In Silico Methods for Environmental Risk Assessment: Principles, Tiered Approaches, Applications, and Future Perspectives, in: Benfenati, E. (Ed.), In Silico Methods for Predicting Drug Toxicity, Methods in Molecular Biology. Springer US, New York, NY, pp. 589–636. https://doi.org/10.1007/978-1-0716-1960-5_23

Authority (EFSA), E.F.S., Adriaanse, P., Boivin, A., Klein, M., Jarvis, N., Stemmer, M., Fait, G., Egsmose, M., 2020. Scientific report of EFSA on the 'repair action' of the FOCUS surface water scenarios. EFSA Journal 18, e06119. https://doi.org/10.2903/j.efsa.2020.6119

Bale, J.S., Hayward, S.A.L., 2010. Insect overwintering in a changing climate. Journal of Experimental Biology 213, 980–994. https://doi.org/10.1242/jeb.037911

Bart, S., Jager, T., Robinson, A., Lahive, E., Spurgeon, D.J., Ashauer, R., 2021. Predicting Mixture Effects over Time with Toxicokinetic–Toxicodynamic Models (GUTS): Assumptions, Experimental Testing, and Predictive Power. Environ. Sci. Technol. https://doi.org/10.1021/acs.est.0c05282

Bart, S., Short, S., Jager, T., Eagles, E.J., Robinson, A., Badder, C., Lahive, E., Spurgeon, D.J., Ashauer, R., 2022. How to analyse and account for interactions in mixture toxicity with toxicokinetic-toxicodynamic models. Science of The Total Environment 843, 157048. https://doi.org/10.1016/j.scitotenv.2022.157048

Bartlett, A.J., Hedges, A.M., Intini, K.D., Brown, L.R., Maisonneuve, F.J., Robinson, S.A., Gillis, P.L., de Solla, S.R., 2018. Lethal and sublethal toxicity of neonicotinoid and butenolide insecticides to the mayfly, Hexagenia spp. Environmental Pollution 238, 63–75. https://doi.org/10.1016/j.envpol.2018.03.004

Baudin, J.P., Garnier-Laplace, J., 1994. Accumulation, release, and tissue distribution of 110mAg from natural food (Gammarus pulex) by the common carp, Cyprinus carpio L. Arch. Environ. Contam. Toxicol. 27. https://doi.org/10.1007/BF00214836

Bednarska, A.J., Choczyński, M., Laskowski, R., Walczak, M., 2017. Combined effects of chlorpyriphos, copper and temperature on acetylcholinesterase activity and toxicokinetics of the chemicals in the earthworm Eisenia fetida. Environmental Pollution 220, 567–576. https://doi.org/10.1016/j.envpol.2016.10.004

Bednarska, A.J., Jevtić, D.M., Laskowski, R., 2013. More ecological ERA: incorporating natural environmental factors and animal behavior. Integr Environ Assess Manag 9, e39-46. https://doi.org/10.1002/ieam.1444

Beketov, M.A., Liess, M., 2008. Acute and delayed effects of the neonicotinoid insecticide thiacloprid on seven freshwater arthropods. Environmental Toxicology and Chemistry 27, 461–470. https://doi.org/10.1897/07-322R.1

Beketov, M.A., Schäfer, R.B., Marwitz, A., Paschke, A., Liess, M., 2008. Long-term stream invertebrate community alterations induced by the insecticide thiacloprid: Effect concentrations and recovery dynamics. Science of The Total Environment 405, 96–108. https://doi.org/10.1016/j.scitotenv.2008.07.001

Bennett, J.M., Calosi, P., Clusella-Trullas, S., Martínez, B., Sunday, J., Algar, A.C., Araújo, M.B., Hawkins, B.A., Keith, S., Kühn, I., Rahbek, C., Rodríguez, L., Singer, A., Villalobos, F., Ángel Olalla-Tárraga, M., Morales-Castilla, I., 2018. GlobTherm, a global database on thermal tolerances for aquatic and terrestrial organisms. Sci Data 5, 180022. https://doi.org/10.1038/sdata.2018.22

Bernhardt, E.S., Rosi, E.J., Gessner, M.O., 2017. Synthetic chemicals as agents of global change. Frontiers in Ecology and the Environment 15, 84–90. https://doi.org/10.1002/fee.1450

Bowler, K., Terblanche, J.S., 2008. Insect thermal tolerance: what is the role of ontogeny, ageing and senescence? Biological Reviews 83, 339–355. https://doi.org/10.1111/j.1469-185X.2008.00046.x

Brown, C.T., Yahn, J.M., Karasov, W.H., 2021. Warmer temperature increases toxicokinetic elimination of PCBs and PBDEs in Northern leopard frog larvae (Lithobates pipiens). Aquat. Toxicol. 234, 105806. https://doi.org/10.1016/j.aquatox.2021.105806

Buchwalter, D.B., Jenkins, J.J., Curtis, L.R., 2003. Temperature influences on water permeability and chlorpyrifos uptake in aquatic insects with differing respiratory strategies. Environmental Toxicology and Chemistry 22, 2806–2812. https://doi.org/10.1897/02-350

Burnham, K.P., Anderson, D.R. (Eds.), 2002. Information and Likelihood Theory: A Basis for Model Selection and Inference, in: Model Selection and Multimodel Inference: A Practical Information-Theoretic Approach. Springer, New York, NY, pp. 49–97. https://doi.org/10.1007/978-0-387-22456-5_2

Calvin, K., Dasgupta, D., Krinner, G., Mukherji, A., Thorne, P.W., Trisos, C., Romero, J., Aldunce, P., Barrett, K., Blanco, G., Cheung, W.W.L., Connors, S., Denton, F., Diongue-Niang, A., Dodman, D., Garschagen, M., Geden, O., Hayward, B., Jones, C., Jotzo, F., Krug, T., Lasco, R., Lee, Y.-Y., Masson-Delmotte, V., Meinshausen, M., Mintenbeck, K., Mokssit, A., Otto, F.E.L., Pathak, M., Pirani, A., Poloczanska, E., Pörtner, H.-O., Revi, A., Roberts, D.C., Roy, J., Ruane, A.C., Skea, J., Shukla, P.R., Slade, R., Slangen, A., Sokona, Y., Sörensson, A.A., Tignor, M., Van Vuuren, D., Wei, Y.-M., Winkler, H., Zhai, P., Zommers, Z., Hourcade, J.-C., Johnson, F.X., Pachauri, S., Simpson, N.P., Singh, C., Thomas, A., Totin, E., Arias, P., Bustamante, M., Elgizouli, I., Flato, G., Howden, M., Méndez-Vallejo, C., Pereira, J.J., Pichs-Madruga, R., Rose, S.K., Saheb, Y., Sánchez Rodríguez, R., Ürge-Vorsatz, D., Xiao, C., Yassaa, N., Alegría, A., Armour, K., Bednar-Friedl, B., Blok, K., Cissé, G., Dentener, F., Eriksen, S., Fischer, E., Garner, G., Guivarch, C., Haasnoot, M., Hansen, G., Hauser, M., Hawkins, E., Hermans, T., Kopp, R., Leprince-Ringuet, N., Lewis, J., Ley, D., Ludden, C., Niamir, L., Nicholls, Z., Some, S., Szopa, S., Trewin, B., Van Der Wijst, K.-I., Winter, G., Witting, M., Birt, A., Ha, M., Romero, J., Kim, J., Haites, E.F., Jung, Y., Stavins, R., Birt, A., Ha, M., Orendain, D.J.A., Ignon, L., Park, S., Park, Y., Reisinger, A., Cammaramo, D., Fischlin, A., Fuglestvedt, J.S., Hansen, G., Ludden, C., Masson-Delmotte, V., Matthews, J.B.R., Mintenbeck, K., Pirani, A., Poloczanska, E., Leprince-Ringuet, N., Péan, C., 2023. IPCC, 2023: Climate Change 2023: Synthesis Report. Contribution of Working Groups I, II and III to the Sixth Assessment Report of the Intergovernmental Panel on Climate Change [Core Writing Team, H. Lee and J. Romero (eds.)]. IPCC, Geneva, Switzerland. Intergovernmental Panel on Climate Change (IPCC). https://doi.org/10.59327/IPCC/AR6-9789291691647

Camp, A.A., Buchwalter, D.B., 2016. Can't take the heat: Temperature-enhanced toxicity in the mayfly Isonychia bicolor exposed to the neonicotinoid insecticide imidacloprid. Aquatic Toxicology 178, 49–57. https://doi.org/10.1016/j.aquatox.2016.07.011

Cardinale, B.J., Duffy, J.E., Gonzalez, A., Hooper, D.U., Perrings, C., Venail, P., Narwani, A., Mace, G.M., Tilman, D., Wardle, D.A., Kinzig, A.P., Daily, G.C., Loreau, M., Grace, J.B., Larigauderie, A., Srivastava, D.S., Naeem, S., 2012. Biodiversity loss and its impact on humanity. Nature 486, 59–67. https://doi.org/10.1038/nature11148

Casida, J.E., 2018. Neonicotinoids and Other Insect Nicotinic Receptor Competitive Modulators: Progress and Prospects. Annu. Rev. Entomol. 63, 125–144. https://doi.org/10.1146/annurev-ento-020117-043042

Casida, J.E., 2011. Neonicotinoid Metabolism: Compounds, Substituents, Pathways, Enzymes, Organisms, and Relevance. J. Agric. Food Chem. 59, 2923–2931. https://doi.org/10.1021/jf102438c

Casida, J.E., Durkin, K.A., 2013. Neuroactive Insecticides: Targets, Selectivity, Resistance, and Secondary Effects. Annu. Rev. Entomol. 58, 99–117. https://doi.org/10.1146/annurev-ento-120811-153645

Cedergreen, N., Dalhoff, K., Li, D., Gottardi, M., Kretschmann, A.C., 2017. Can Toxicokinetic and Toxicodynamic Modeling Be Used to Understand and Predict Synergistic Interactions between Chemicals? Environ. Sci. Technol. 51, 14379–14389. https://doi.org/10.1021/acs.est.7b02723

Cereja, R., 2020. Critical thermal maxima in aquatic ectotherms. Ecological Indicators 119, 106856. https://doi.org/10.1016/j.ecolind.2020.106856

Cerveny, D., Fick, J., Klaminder, J., McCallum, E.S., Bertram, M.G., Castillo, N.A., Brodin, T., 2021. Water temperature affects the biotransformation and accumulation of a psychoactive pharmaceutical and its metabolite in aquatic organisms. Environment International 155, 106705. https://doi.org/10.1016/j.envint.2021.106705

Chaumot, A., Geffard, O., Armengaud, J., Maltby, L., 2015. Gammarids as reference species for freshwater monitoring, in: Aquatic Ecotoxicology. Elsevier, pp. 253–280.

Chen, L., Chang, J., Wang, Y., Guo, A., Liu, Y., Wang, Q., Zhu, Y., Zhang, Y., Xie, Z., 2021. Disclosing the future food security risk of China based on crop production and water scarcity under diverse socioeconomic and climate scenarios. Science of The Total Environment 790, 148110. https://doi.org/10.1016/j.scitotenv.2021.148110

Chen, M., Haq, S.M.A., Ahmed, K.J., Hussain, A.H.M.B., Ahmed, M.N.Q., 2021. The link between climate change, food security and fertility: The case of Bangladesh. PLOS ONE 16, e0258196. https://doi.org/10.1371/journal.pone.0258196

Cold, A., Forbes, V.E., 2004. Consequences of a short pulse of pesticide exposure for survival and reproduction of Gammarus pulex. Aquatic Toxicology 67, 287–299. https://doi.org/10.1016/j.aquatox.2004.01.015

Dalhoff, K., Gottardi, M., Rinnan, Å., Rasmussen, J.J., Cedergreen, N., 2018. Seasonal sensitivity of Gammarus pulex towards the pyrethroid cypermethrin. Chemosphere 200, 632–640. https://doi.org/10.1016/j.chemosphere.2018.02.153

Dalhoff, K., Hansen, A.M.B., Rasmussen, J.J., Focks, A., Strobel, B.W., Cedergreen, N., 2020. Linking Morphology, Toxicokinetic, and Toxicodynamic Traits of Aquatic Invertebrates to Pyrethroid Sensitivity. Environ. Sci. Technol. 54, 5687–5699. https://doi.org/10.1021/acs.est.0c00189

Dangles, O., Gessner, M.O., Guerold, F., Chauvet, E., 2004. Impacts of stream acidification on litter breakdown: Implications for assessing ecosystem functioning. Journal of Applied Ecology 41, 365–378. https://doi.org/10.1111/j.0021-8901.2004.00888.x

de Souza, C.M., Massi, K.G., Rodgher, S., 2023. Meta-analysis reveals negative responses of freshwater organisms to the interactive effects of pesticides and warming. Biologia. https://doi.org/10.1007/s11756-023-01334-5

Di Nicola, M.R., Cattaneo, I., Nathanail, A.V., Carnesecchi, E., Astuto, M.C., Steinbach, M., Williams, A.J., Charles, S., Gestin, O., Lopes, C., Lamonica, D., Tarazona, J.V., Dorne, J.L.C.M., 2023. The use of new approach methodologies for the environmental risk assessment of food and feed chemicals. Current Opinion in Environmental Science & Health 31, 100416. https://doi.org/10.1016/j.coesh.2022.100416

EFSA Panel on Plant Protection Products and their Residues (PPR), 2014. Scientific Opinion on good modelling practice in the context of mechanistic effect models for risk assessment of plant protection products. EFSA Journal 12, 3589. https://doi.org/10.2903/j.efsa.2014.3589

EFSA Panel on Plant Protection Products and their Residues (PPR), 2010. Scientific Opinion on the development of specific protection goal options for environmental risk assessment of pesticides, in particular in relation to the revision of the Guidance Documents on Aquatic and Terrestrial Ecotoxicology (SANCO/3268/2001 and SANCO/10329/2002). EFSA Journal 8, 1821. https://doi.org/10.2903/j.efsa.2010.1821

EFSA Panel on Plant Protection Products and their Residues (PPR), Ockleford, C., Adriaanse, P., Berny, P., Brock, T., Duquesne, S., Grilli, S., Hernandez-Jerez, A.F., Bennekou, S.H., Klein, M., Kuhl, T., Laskowski, R., Machera, K., Pelkonen, O., Pieper, S., Smith, R.H., Stemmer, M., Sundh, I., Tiktak, A., Topping, C.J., Wolterink, G.,

Cedergreen, N., Charles, S., Focks, A., Reed, M., Arena, M., Ippolito, A., Byers, H., Teodorovic, I., 2018. Scientific Opinion on the state of the art of Toxicokinetic/Toxicodynamic (TKTD) effect models for regulatory risk assessment of pesticides for aquatic organisms. EFSA Journal 16, e05377. https://doi.org/10.2903/j.efsa.2018.5377

Englert, D., Bakanov, N., Zubrod, J.P., Schulz, R., Bundschuh, M., 2017a. Modeling Remobilization of Neonicotinoid Residues from Tree Foliage in Streams—A Relevant Exposure Pathway in Risk Assessment? Environ. Sci. Technol. 51, 1785–1794. https://doi.org/10.1021/acs.est.6b05213

Englert, D., Zubrod, J.P., Pietz, S., Stefani, S., Krauss, M., Schulz, R., Bundschuh, M., 2017b. Relative importance of dietary uptake and waterborne exposure for a leaf-shredding amphipod exposed to thiacloprid-contaminated leaves. Scientific Reports 7, 16182. https://doi.org/10.1038/s41598-017-16452-9

European Commission, 2022. Neonicotinoids [WWW Document]. URL https://food.ec.europa.eu/plants/pesticides/approval-active-substances/renewal-approval/neonicotinoids_en (accessed 7.31.22).

Fent, K., 2013. Ökotoxikologie: Umweltchemie - Toxikologie - Ökologie. Georg Thieme Verlag.

Focks, A., Belgers, D., Boerwinkel, M.C., Buijse, L., Roessink, I., Van den Brink, P.J., 2018. Calibration and validation of toxicokinetic-toxicodynamic models for three neonicotinoids and some aquatic macroinvertebrates. Ecotoxicology 27, 992–1007. https://doi.org/10.1007/s10646-018-1940-6

Forbes, V.E., Galic, N., Schmolke, A., Vavra, J., Pastorok, R., Thorbek, P., 2016. Assessing the risks of pesticides to threatened and endangered species using population modeling: A critical review and recommendations for future work. Environmental Toxicology and Chemistry 35, 1904–1913. https://doi.org/10.1002/etc.3440

Forbes, V.E., Hommen, U., Thorbek, P., Heimbach, F., Brink, P.J.V. den, Wogram, J., Thulke, H.-H., Grimm, V., 2009. Ecological models in support of regulatory risk assessments of pesticides: developing a strategy for the future. Integrated Environmental Assessment and Management 5, 167–172. https://doi.org/10.1897/IEAM_2008-029.1

Foucreau, N., Cottin, D., Piscart, C., Hervant, F., 2014. Physiological and metabolic responses to rising temperature in Gammarus pulex (Crustacea) populations living under continental or Mediterranean climates. Comparative Biochemistry and Physiology Part A: Molecular & Integrative Physiology 168, 69–75. https://doi.org/10.1016/j.cbpa.2013.11.006

Fox, J., Weisberg, S., 2018. An R Companion to Applied Regression. SAGE Publications.

Freitas, R., Coppola, F., Costa, S., Pretti, C., Intorre, L., Meucci, V., Soares, A.M.V.M., Solé, M., 2019. The influence of temperature on the effects induced by Triclosan and Diclofenac in mussels. Science of The Total Environment 663, 992–999. https://doi.org/10.1016/j.scitotenv.2019.01.189

Fusetto, R., Denecke, S., Perry, T., O'Hair, R.A.J., Batterham, P., 2017. Partitioning the roles of CYP6G1 and gut microbes in the metabolism of the insecticide imidacloprid in Drosophila melanogaster. Scientific Reports 7. https://doi.org/10.1038/s41598-017-09800-2

Galic, N., Baveco, H., Hengeveld, G.M., Thorbek, P., Bruns, E., van den Brink, P.J., 2012. Simulating population recovery of an aquatic isopod: Effects of timing of stress and landscape structure. Environmental Pollution 163, 91–99. https://doi.org/10.1016/j.envpol.2011.12.024

Gergs, A., Hager, J., Bruns, E., Preuss, T.G., 2021. Disentangling Mechanisms Behind Chronic Lethality through Toxicokinetic–Toxicodynamic Modeling. Environmental Toxicology and Chemistry 40, 1706–1712. https://doi.org/10.1002/etc.5027

Gergs, A., Rakel, K.J., Liesy, D., Zenker, A., Classen, S., 2019. Mechanistic Effect Modeling Approach for the Extrapolation of Species Sensitivity. Environ. Sci. Technol. 53, 9818–9825. https://doi.org/10.1021/acs.est.9b01690

Giorio, C., Safer, A., Sánchez-Bayo, F., Tapparo, A., Lentola, A., Girolami, V., van Lexmond, M.B., Bonmatin, J.-M., 2021. An update of the Worldwide Integrated Assessment (WIA) on systemic insecticides. Part 1: new molecules, metabolism, fate, and transport. Environ Sci Pollut Res 28, 11716–11748. https://doi.org/10.1007/s11356-017-0394-3

Glaberman, S., White, K., 2014. Environmental Fate and Ecological Risk Assessment for Foliar, Soil Drench, and Seed Treatment Uses of the New Insecticide Flupyradifurone (BYI 02960) (No. D415164).

Goss, L.B., Bunting, D.L., 1983. Daphnia development and reproduction: Responses to temperature. Journal of Thermal Biology 8, 375–380. https://doi.org/10.1016/0306-4565(83)90025-6

Goussen, B., Rendal, C., Sheffield, D., Butler, E., Price, O.R., Ashauer, R., 2020. Bioenergetics modelling to analyse and predict the joint effects of multiple stressors: Meta-analysis and model corroboration. Science of The Total Environment 749, 141509. https://doi.org/10.1016/j.scitotenv.2020.141509

Grimm, V., Augusiak, J., Focks, A., Frank, B.M., Gabsi, F., Johnston, A.S.A., Liu, C., Martin, B.T., Meli, M., Radchuk, V., Thorbek, P., Railsback, S.F., 2014. Towards better modelling and decision support: Documenting model development, testing, and analysis using TRACE. Ecological Modelling, Population Models for Ecological Risk Assessment of Chemicals 280, 129–139. https://doi.org/10.1016/j.ecolmodel.2014.01.018

Grimm, V., Martin, B.T., 2013. Mechanistic effect modeling for ecological risk assessment: Where to go from here? Integrated Environmental Assessment and Management 9, e58–e63. https://doi.org/10.1002/ieam.1423

Grimm, V., Revilla, E., Berger, U., Jeltsch, F., Mooij, W.M., Railsback, S.F., Thulke, H.-H., Weiner, J., Wiegand, T., DeAngelis, D.L., 2005. Pattern-Oriented Modeling of Agent-Based Complex Systems: Lessons from Ecology. Science 310, 987–991. https://doi.org/10.1126/science.1116681

Haque, Md.N., Nam, S.-E., Kim, B.-M., Kim, K., Rhee, J.-S., 2020. Temperature elevation stage-specifically increases metal toxicity through bioconcentration and impairment of antioxidant defense systems in juvenile and adult marine mysids. Comparative Biochemistry and Physiology Part C: Toxicology & Pharmacology 237, 108831. https://doi.org/10.1016/j.cbpc.2020.108831

Harwood, A.D., You, J., Lydy, M.J., 2009. Temperature as a Toxicity Identification Evaluation Tool for Pyrethroid Insecticides: Toxicokinetic Confirmation. Environmental Toxicology and Chemistry; Oxford 28, 1051–8.

Henry, Y., Piscart, C., Charles, S., Colinet, H., 2017. Combined effect of temperature and ammonia on molecular response and survival of the freshwater crustacean Gammarus pulex. Ecotoxicology and Environmental Safety 137, 42–48. https://doi.org/10.1016/j.ecoenv.2016.11.011

Hermann, M., Peeters, E.T.H.M., Van den Brink, P.J., 2023. Heatwaves, elevated temperatures, and a pesticide cause interactive effects on multi-trophic levels of a freshwater ecosystem. Environmental Pollution 327, 121498. https://doi.org/10.1016/j.envpol.2023.121498

Heugens, E.H.W., Hendriks, A.J., Dekker, T., Straalen, N.M. van, Admiraal, W., 2001. A Review of the Effects of Multiple Stressors on Aquatic Organisms and Analysis of Uncertainty Factors for Use in Risk Assessment. Critical Reviews in Toxicology 31, 247–284. https://doi.org/10.1080/20014091111695

Heugens, E.H.W., Jager, T., Creyghton, R., Kraak, M.H.S., Hendriks, A.J., Van Straalen, N.M., Admiraal, W., 2003. Temperature-Dependent Effects of Cadmium on Daphnia magna: Accumulation versus Sensitivity. Environ. Sci. Technol. 37, 2145–2151. https://doi.org/10.1021/es0264347

Heye, K., Lotz, T., Wick, A., Oehlmann, J., 2019. Interactive effects of biotic and abiotic environmental stressors on carbamazepine toxicity in the non-biting midge Chironomus riparius. Water Research 156, 92–101. https://doi.org/10.1016/j.watres.2019.03.007

Hogg, R.C., Raggenbass, M., Bertrand, D., 2003. Nicotinic acetylcholine receptors: from structure to brain function, in: Reviews of Physiology, Biochemistry and Pharmacology, Reviews of Physiology, Biochemistry and Pharmacology. Springer, Berlin, Heidelberg, pp. 1–46. https://doi.org/10.1007/s10254-003-0005-1

Holmstrup, M., Bindesbøl, A.-M., Oostingh, G.J., Duschl, A., Scheil, V., Köhler, H.-R., Loureiro, S., Soares, A.M.V.M., Ferreira, A.L.G., Kienle, C., Gerhardt, A., Laskowski, R., Kramarz, P.E., Bayley, M., Svendsen, C., Spurgeon, D.J., 2010. Interactions between effects of environmental chemicals and natural stressors: A review. Science of The Total Environment, Cumulative Stressors - Risk assessment of mixtures of chemicals and combinations of chemicals and natural stressors 408, 3746–3762. https://doi.org/10.1016/j.scitotenv.2009.10.067

Honda, H., Tomizawa, M., Casida, J.E., 2006. Neonicotinoid metabolic activation and inactivation established with coupled nicotinic receptor-CYP3A4 and -aldehyde oxidase systems. Toxicology Letters 161, 108–114. https://doi.org/10.1016/j.toxlet.2005.08.004

Hooper, M.J., Ankley, G.T., Cristol, D.A., Maryoung, L.A., Noyes, P.D., Pinkerton, K.E., 2013. Interactions between chemical and climate stressors: A role for mechanistic toxicology in assessing climate change risks. Environmental Toxicology and Chemistry 32, 32–48. https://doi.org/10.1002/etc.2043

Huang, A., Mangold-Döring, A., Focks, A., Zhang, C., Van den Brink, P.J., 2022a. Comparing the acute and chronic toxicity of flupyradifurone and imidacloprid to non-target aquatic arthropod species. Ecotoxicology and Environmental Safety 243, 113977. https://doi.org/10.1016/j.ecoenv.2022.113977

Huang, A., Mangold-Döring, A., Guan, H., Boerwinkel, M.-C., Belgers, D., Focks, A., Brink, P.J.V. den, 2022b. The effect of temperature on toxicokinetics and the chronic toxicity of insecticides towards Gammarus pulex. accepted manuscript at Science of the Total Environment.

Huang, A., Mangold-Döring, A., Guan, H., Boerwinkel, M.-C., Belgers, D., Focks, A., van den Brink, P., 2022c. Data for: The effect of temperature on toxicokinetics and the chronic toxicity of insecticides towards Gammarus pulex 2. https://doi.org/10.17632/6dbgkhzxvx.2

Huang, A., Mangold-Döring, A., Guan, H., Boerwinkel, M.-C., Belgers, D., Focks, A., Van den Brink, P.J., 2023. The effect of temperature on toxicokinetics and the chronic toxicity of insecticides towards Gammarus pulex. Science of The Total Environment 856, 158886. https://doi.org/10.1016/j.scitotenv.2022.158886

Huang, A., Roessink, I., van den Brink, N.W., van den Brink, P.J., 2022d. Size- and sex-related sensitivity differences of aquatic crustaceans to imidacloprid. Ecotoxicology and Environmental Safety 242, 113917. https://doi.org/10.1016/j.ecoenv.2022.113917

Huang, A., van den Brink, N.W., Buijse, L., Roessink, I., van den Brink, P.J., 2021. The toxicity and toxicokinetics of imidacloprid and a bioactive metabolite to two aquatic arthropod species. Aquatic Toxicology 235, 105837. https://doi.org/10.1016/j.aquatox.2021.105837

Hulme, E.C., Trevethick, M.A., 2010. Ligand binding assays at equilibrium: validation and interpretation. British Journal of Pharmacology 161, 1219–1237. https://doi.org/10.1111/j.1476-5381.2009.00604.x

Hynes, H.B.N., 1955. The Reproductive Cycle of Some British Freshwater Gammaridae. Journal of Animal Ecology 24, 352–387. https://doi.org/10.2307/1718

IPCC, 2019. IPCC Special Report on Climate Change, Desertification, Land Degradation, Sustainable Land Management, Food Security, and Greenhouse gas fluxes in Terrestrial Ecosystems.

IPCC, I.P. on C.C., 2012. Managing the Risks of Extreme Events and Disasters to Advance Climate Change Adaptation: Special Report of the Intergovernmental Panel on Climate Change. Cambridge University Press.

Jager, T., 2021a. Robust Likelihood-Based Approach for Automated Optimization and Uncertainty Analysis of Toxicokinetic-Toxicodynamic Models. Integrated Environmental Assessment and Management 17, 388–397. https://doi.org/10.1002/ieam.4333

Jager, T., 2021b. Robust Likelihood-Based Approach for Automated Optimization and Uncertainty Analysis of Toxicokinetic-Toxicodynamic Models. Integrated Environmental Assessment and Management 17, 388–397. https://doi.org/10.1002/ieam.4333

Jager, T., 2020a. Revisiting simplified DEBtox models for analysing ecotoxicity data. Ecological Modelling 416, 108904. https://doi.org/10.1016/j.ecolmodel.2019.108904

Jager, T., 2020b. Interpretation of output of the openGUTS software.

Jager, T., 2014. Reconsidering sufficient and optimal test design in acute toxicity testing. Ecotoxicology 23, 38–44. https://doi.org/10.1007/s10646-013-1149-7

Jager, T., Albert, C., Preuss, T., Ashauer, R., 2011. General unified threshold model of survival - a toxicokinetic-toxicodynamic framework for ecotoxicology. Environ. Sci. Technol. 45, 2529–2540.

Jager, Tjalling, Albert, C., Preuss, T.G., Ashauer, R., 2011. General Unified Threshold Model of Survival - a Toxicokinetic-Toxicodynamic Framework for Ecotoxicology. Environ. Sci. Technol. 45, 2529–2540. https://doi.org/10.1021/es103092a

Jager, T., Ashauer, R., 2018a. Modelling survival under chemical stress A comprehensive guide to the GUTS framework.

Jager, T., Ashauer, R., 2018b. Modelling survival under chemical stress: A comprehensive guide to the GUTS framework. Toxicodynamics Ltd, York, UK.

Jager, T., Goussen, B., Gergs, A., 2023. Using the standard DEB animal model for toxicokinetic-toxicodynamic analysis. Ecological Modelling 475, 110187. https://doi.org/10.1016/j.ecolmodel.2022.110187

Jager, T., Heugens, E.H.W., Kooijman, S.A.L.M., 2006. Making sense of ecotoxicological test results: towards process-based models. Ecotoxicol. 15, 305–314.

Jager, T., Klok, C., 2010. Extrapolating toxic effects on individuals to the population level; the role of Dynamic Energy Budgets. Phil. Trans. R. Soc. B 365, 3531–3540.

Jager, T., Kooijman, S.A.L.M., 2008. A biology-based approach for quantitative structure-activity relationships (QSARs) in ecotoxicity. Ecotoxicology 18, 187. https://doi.org/10.1007/s10646-008-0271-4

Jager, T., Kooijman, S.A.L.M., 2005. Modeling Receptor Kinetics in the Analysis of Survival Data for Organophosphorus Pesticides [WWW Document]. ACS Publications. https://doi.org/10.1021/es050817y
Jager, T., Øverjordet, I.B., Nepstad, R., Hansen, B.H., 2017. Dynamic Links between Lipid Storage, Toxicokinetics and Mortality in a Marine Copepod Exposed to Dimethylnaphthalene. Environ. Sci. Technol. 51, 7707–7713. https://doi.org/10.1021/acs.est.7b02212
Janssens, L., Verberk, W., Stoks, R., 2018. A widespread morphological antipredator mechanism reduces the sensitivity to pesticides and increases the susceptibility to warming. Science of The Total Environment 626, 1230–1235. https://doi.org/10.1016/j.scitotenv.2018.01.179
Janzén, D.L.I., Bergenholm, L., Jirstrand, M., Parkinson, J., Yates, J., Evans, N.D., Chappell, M.J., 2016. Parameter Identifiability of Fundamental Pharmacodynamic Models. Frontiers in Physiology 7, 590. https://doi.org/10.3389/fphys.2016.00590
Jeschke, P., Nauen, R., Beck, M.E., 2013. Nicotinic Acetylcholine Receptor Agonists: A Milestone for Modern Crop Protection. Angewandte Chemie International Edition 52, 9464–9485. https://doi.org/10.1002/anie.201302550
Jeschke, P., Nauen, R., Gutbrod, O., Beck, M.E., Matthiesen, S., Haas, M., Velten, R., 2015a. Flupyradifurone (Sivanto™) and its novel butenolide pharmacophore: Structural considerations☆. Pesticide Biochemistry and Physiology, Insecticide and Acaricide Modes of Action and their Role in Resistance and its Management 121, 31–38. https://doi.org/10.1016/j.pestbp.2014.10.011
Jeschke, P., Nauen, R., Gutbrod, O., Beck, M.E., Matthiesen, S., Haas, M., Velten, R., 2015b. Flupyradifurone (Sivanto™) and its novel butenolide pharmacophore: Structural considerations☆. Pesticide Biochemistry and Physiology, Insecticide and Acaricide Modes of Action and their Role in Resistance and its Management 121, 31–38. https://doi.org/10.1016/j.pestbp.2014.10.011
Jeschke, P., Nauen, R., Schindler, M., Elbert, A., 2011. Overview of the Status and Global Strategy for Neonicotinoids. J. Agric. Food Chem. 59, 2897–2908. https://doi.org/10.1021/jf101303g
Johnson, K.A., Goody, R.S., 2011. The Original Michaelis Constant: Translation of the 1913 Michaelis–Menten Paper. Biochemistry 50, 8264–8269. https://doi.org/10.1021/bi201284u
Johnson, N.C., Xie, S.-P., Kosaka, Y., Li, X., 2018. Increasing occurrence of cold and warm extremes during the recent global warming slowdown. Nat Commun 9, 1724. https://doi.org/10.1038/s41467-018-04040-y
Jones, P.D., Mann, M.E., 2004. Climate over past millennia. Reviews of Geophysics 42. https://doi.org/10.1029/2003RG000143
Jørgensen, L.B., Malte, H., Ørsted, M., Klahn, N.A., Overgaard, J., 2021. A unifying model to estimate thermal tolerance limits in ectotherms across static, dynamic and fluctuating exposures to thermal stress. Scientific Reports 11, 1–14. https://doi.org/10.1038/s41598-021-92004-6
Jusup, M., Sousa, T., Domingos, T., Labinac, V., Marn, N., Wang, Z., Klanjšček, T., 2017. Physics of metabolic organization. Physics of Life Reviews 20, 1–39. https://doi.org/10.1016/j.plrev.2016.09.001
Kassahn, K.S., Crozier, R.H., Pörtner, H.O., Caley, M.J., 2009. Animal performance and stress: responses and tolerance limits at different levels of biological organisation. Biological Reviews 84, 277–292. https://doi.org/10.1111/j.1469-185X.2008.00073.x
Kivivuori, L.A., Lahdes, E.O., 1996. How to measure the thermal death of Daphnia? A comparison of different heat tests and effects of heat injury. Journal of Thermal Biology 21, 305–311. https://doi.org/10.1016/S0306-4565(96)00014-9
Kong, D., MacLeod, M., Cousins, I.T., 2014. Modelling the influence of climate change on the chemical concentrations in the Baltic Sea region with the POPCYCLING-Baltic model. Chemosphere 110, 31–40. https://doi.org/10.1016/j.chemosphere.2014.02.044
Kooijman, S. a. L.M., Sousa, T., Pecquerie, L., Van Der Meer, J., Jager, T., 2008. From food-dependent statistics to metabolic parameters, a practical guide to the use of dynamic energy budget theory. Biological Reviews 83, 533–552. https://doi.org/10.1111/j.1469-185X.2008.00053.x
Kooijman, S.A.L.M., 2010. Dynamic Energy Budget theory for metabolic organisation. Cambridge Univ. Press, Cambridge.
Kooijman, S. A. L. M., 2010. Dynamic Energy Budget Theory for Metabolic Organisation. Cambridge University Press.
Kosfeld, V., Fu, Q., Ebersbach, I., Esser, D., Schauerte, A., Bischof, I., Hollender, J., Schlechtriem, C., 2020. Comparison of Alternative Methods for Bioaccumulation Assessment: Scope and Limitations of In Vitro Depletion Assays with Rainbow Trout and Bioconcentration Tests in the Freshwater Amphipod Hyalella azteca. Environmental Toxicology and Chemistry 39, 1813–1825. https://doi.org/10.1002/etc.4791
Kunz, P.Y., Kienle, C., Gerhardt, A., 2010a. Gammarus spp. in Aquatic Ecotoxicology and Water Quality Assessment: Toward Integrated Multilevel Tests, in: Whitacre, D.M. (Ed.), Reviews of Environmental Contamination and Toxicology Volume 205, Reviews of Environmental Contamination and Toxicology. Springer, New York, NY, pp. 1–76. https://doi.org/10.1007/978-1-4419-5623-1_1
Kunz, P.Y., Kienle, C., Gerhardt, A., 2010b. Gammarus spp. in Aquatic Ecotoxicology and Water Quality Assessment: Toward Integrated Multilevel Tests, in: Whitacre, D.M. (Ed.), Reviews of Environmental Contamination and Toxicology Volume 205, Reviews of Environmental Contamination and Toxicology. Springer, New York, NY, pp. 1–76. https://doi.org/10.1007/978-1-4419-5623-1_1
LaLone, C.A., Villeneuve, D.L., Wu-Smart, J., Milsk, R.Y., Sappington, K., Garber, K.V., Housenger, J., Ankley, G.T., 2017. Weight of evidence evaluation of a network of adverse outcome pathways linking activation of the nicotinic acetylcholine receptor in honey bees to colony death. Sci Total Environ 584–585, 751–775. https://doi.org/10.1016/j.scitotenv.2017.01.113
Larras, F., Beaudouin, R., Berny, P., Charles, S., Chaumot, A., Corio-Costet, M.-F., Doussan, I., Pelosi, C., Leenhardt, S., Mamy, L., 2022a. A meta-analysis of ecotoxicological models used for plant protection product risk assessment before their placing on the market. Science of The Total Environment 844, 157003. https://doi.org/10.1016/j.scitotenv.2022.157003
Larras, F., Charles, S., Chaumot, A., Pelosi, C., Le Gall, M., Mamy, L., Beaudouin, R., 2022b. A critical review of effect modeling for ecological risk assessment of plant protection products. Environ Sci Pollut Res. https://doi.org/10.1007/s11356-022-19111-3
Lauper, B.B., Anthamatten, E., Raths, J., Arlos, M., Hollender, J., 2021. Systematic Underestimation of Pesticide Burden for Invertebrates under Field Conditions: Comparing the Influence of Dietary Uptake and Aquatic Exposure Dynamics. ACS Environ. Au 2(2). https://doi.org/10.1021/acsenvironau.1c00023
Lemm, J.U., Venohr, M., Globevnik, L., Stefanidis, K., Panagopoulos, Y., van Gils, J., Posthuma, L., Kristensen, P., Feld, C.K., Mahnkopf, J., Hering, D., Birk, S., 2021. Multiple stressors determine river ecological status at the

European scale: Towards an integrated understanding of river status deterioration. Global Change Biology 27, 1962–1975. https://doi.org/10.1111/gcb.15504
Li, H., Zhang, Q., Su, H., You, J., Wang, W.-X., 2021. High Tolerance and Delayed Responses of Daphnia magna to Neonicotinoid Insecticide Imidacloprid: Toxicokinetic and Toxicodynamic Modeling. Environ. Sci. Technol. 55, 458–467. https://doi.org/10.1021/acs.est.0c05664
Lind, R.J., Clough, M.S., Reynolds, S.E., Earley, F.G.P., 1998. [3H]Imidacloprid Labels High- and Low-Affinity Nicotinic Acetylcholine Receptor-like Binding Sites in the AphidMyzus persicae(Hemiptera: Aphididae). Pesticide Biochemistry and Physiology 62, 3–14. https://doi.org/10.1006/pest.1998.2364
Litchman, E., Thomas, M.K., 2023. Are we underestimating the ecological and evolutionary effects of warming? Interactions with other environmental drivers may increase species vulnerability to high temperatures. Oikos 2023, e09155. https://doi.org/10.1111/oik.09155
Logan, J.A., Wollkind, D.J., Hoyt, S.C., Tanigoshi, L.K., 1976. An Analytic Model for Description of Temperature Dependent Rate Phenomena in Arthropods 1. Environmental Entomology 5, 1133–1140. https://doi.org/10.1093/ee/5.6.1133
Lohner, T.W., Warwick Fisher, S., 1990. Effects of pH and temperature on the acute toxicity and uptake of carbaryl in the midge, Chironomus riparius. Aquatic Toxicology 16, 335–353. https://doi.org/10.1016/0166-445X(90)90045-Q
Lydy, M.J., Belden, J.B., Ternes, M.A., 1999. Effects of Temperature on the Toxicity of M-Parathion, Chlorpyrifos, and Pentachlorobenzene to Chironomus tentans. Arch. Environ. Contam. Toxicol. 37, 542–547. https://doi.org/10.1007/s002449900550
Maazouzi, C., Piscart, C., Legier, F., Hervant, F., 2011. Ecophysiological responses to temperature of the “killer shrimp” Dikerogammarus villosus: Is the invader really stronger than the native Gammarus pulex? Comparative Biochemistry and Physiology Part A: Molecular & Integrative Physiology 159, 268–274. https://doi.org/10.1016/j.cbpa.2011.03.019
Macaulay, S.J., Buchwalter, D.B., Matthaei, C.D., 2020. Water temperature interacts with the insecticide imidacloprid to alter acute lethal and sublethal toxicity to mayfly larvae. New Zealand Journal of Marine and Freshwater Research 54, 115–130. https://doi.org/10.1080/00288330.2019.1614961
Macaulay, S.J., Hageman, K.J., Piggott, J.J., Matthaei, C.D., 2021. Time-cumulative effects of neonicotinoid exposure, heatwaves and food limitation on stream mayfly nymphs: A multiple-stressor experiment. Science of The Total Environment 754, 141941. https://doi.org/10.1016/j.scitotenv.2020.141941
Madeira, D., Madeira, C., Costa, P.M., Vinagre, C., Pörtner, H.-O., Diniz, M.S., 2020. Different sensitivity to heatwaves across the life cycle of fish reflects phenotypic adaptation to environmental niche. Marine Environmental Research 105192. https://doi.org/10.1016/j.marenvres.2020.105192
Mallet, J.P., Charles, S., Persat, H., Auger, P., 1999. Growth modelling in accordance with daily water temperature in European grayling (Thymallus thymallus L.). Can. J. Fish. Aquat. Sci. 56, 994–1000. https://doi.org/10.1139/f99-031
Maloney, E.M., 2020. Cumulative Toxicities of Neonicotinoid Insecticides and Their Mixtures to Sensitive Freshwater Insects (Ph.D. Dissertation). University of Saskatchewan, Saskatoon, SK, Canada.
Maloney, E.M., Sykes, H., Morrissey, C., Peru, K.M., Headley, J.V., Liber, K., 2020. Comparing the Acute Toxicity of Imidacloprid with Alternative Systemic Insecticides in the Aquatic Insect Chironomus dilutus. Environmental Toxicology and Chemistry 39, 587–594. https://doi.org/10.1002/etc.4639
Maloney, E.M., Taillebois, E., Gilles, N., Morrissey, C.A., Liber, K., Servent, D., Thany, S.H., 2021. Binding properties to nicotinic acetylcholine receptors can explain differential toxicity of neonicotinoid insecticides in Chironomidae. Aquatic Toxicology 230, 105701. https://doi.org/10.1016/j.aquatox.2020.105701
Maltby, L., Blake, N., Brock, T.C.M., Van den Brink, P.J., 2005. Insecticide species sensitivity distributions: Importance of test species selection and relevance to aquatic ecosystems. Environmental Toxicology and Chemistry 24, 379–388. https://doi.org/10.1897/04-025R.1
Maltby, L., Clayton, S.A., Wood, R.M., McLoughlin, N., 2002. Evaluation of the Gammarus pulex in situ feeding assay as a biomonitor of water quality: Robustness, responsiveness, and relevance. Environmental Toxicology and Chemistry 21, 361–368. https://doi.org/10.1002/etc.5620210219
Mangold-Döring, A., Huang, A., van Nes, E.H., Focks, A., van den Brink, P.J., 2022a. Explicit Consideration of Temperature Improves Predictions of Toxicokinetic–Toxicodynamic Models for Flupyradifurone and Imidacloprid in Gammarus pulex. Environ. Sci. Technol. https://doi.org/10.1021/acs.est.2c04085
Mangold-Döring, A., Huang, A., van Nes, E.H., Focks, A., van den Brink, P.J., 2022b. Explicit Consideration of Temperature Improves Predictions of Toxicokinetic–Toxicodynamic Models for Flupyradifurone and Imidacloprid in Gammarus pulex. Environ. Sci. Technol. https://doi.org/10.1021/acs.est.2c04085
Martin, B.T., Jager, T., Nisbet, R.M., Preuss, T.G., Hammers-Wirtz, M., Grimm, V., 2013. Extrapolating ecotoxicological effects from individuals to populations: a generic approach based on Dynamic Energy Budget theory and individual-based modeling. Ecotoxicology 22, 574–583. https://doi.org/10.1007/s10646-013-1049-x
Martin, B.T., Zimmer, E.I., Grimm, V., Jager, T., 2012. Dynamic Energy Budget theory meets individual-based modelling: a generic and accessible implementation. Methods in Ecology and Evolution 3, 445–449. https://doi.org/10.1111/j.2041-210X.2011.00168.x
Matsuda, K., Buckingham, S.D., Kleier, D., Rauh, J.J., Grauso, M., Sattelle, D.B., 2001. Neonicotinoids: insecticides acting on insect nicotinic acetylcholine receptors. Trends in Pharmacological Sciences 22, 573–580. https://doi.org/10.1016/S0165-6147(00)01820-4
McBryde, E.S., Meehan, M.T., Adegboye, O.A., Adekunle, A.I., Caldwell, J.M., Pak, A., Rojas, D.P., Williams, B.M., Trauer, J.M., 2020. Role of modelling in COVID-19 policy development. Paediatric Respiratory Reviews 35, 57–60. https://doi.org/10.1016/j.prrv.2020.06.013
McGrath, K.E., Peeters, E.T.H.M., Beijer, J.A.J., Scheffer, M., 2007. Habitat-mediated cannibalism and microhabitat restriction in the stream invertebrate Gammarus pulex. Hydrobiologia 589, 155–164. https://doi.org/10.1007/s10750-007-0731-5
Menéndez, R., González-Megías, A., Lewis, O.T., Shaw, M.R., Thomas, C.D., 2008. Escape from natural enemies during climate-driven range expansion: a case study. Ecological Entomology 33, 413–421. https://doi.org/10.1111/j.1365-2311.2008.00985.x
Metcalfe, C.D., Helm, P., Paterson, G., Kaltenecker, G., Murray, C., Nowierski, M., Sultana, T., 2019. Pesticides related to land use in watersheds of the Great Lakes basin. Science of The Total Environment 648, 681–692. https://doi.org/10.1016/j.scitotenv.2018.08.169

Meynet, P., Davenport, R.J., Fenner, K., 2020. Understanding the Dependence of Micropollutant Biotransformation Rates on Short-Term Temperature Shifts. Environmental Science & Technology. https://doi.org/10.1021/acs.est.0c04017
Moe, S.J., Schamphelaere, K.D., Clements, W.H., Sorensen, M.T., Brink, P.J.V. den, Liess, M., 2013. Combined and interactive effects of global climate change and toxicants on populations and communities. Environmental Toxicology and Chemistry 32, 49–61. https://doi.org/10.1002/etc.2045
Moenickes, S., Schneider, A.-K., Mühle, L., Rohe, L., Richter, O., Suhling, F., 2011. From population-level effects to individual response: modelling temperature dependence in Gammarus pulex. Journal of Experimental Biology 214, 3678–3687. https://doi.org/10.1242/jeb.061945
Morrissey, C.A., Mineau, P., Devries, J.H., Sanchez-Bayo, F., Liess, M., Cavallaro, M.C., Liber, K., 2015a. Neonicotinoid contamination of global surface waters and associated risk to aquatic invertebrates: A review. Environment International 74, 291–303. https://doi.org/10.1016/j.envint.2014.10.024
Morrissey, C.A., Mineau, P., Devries, J.H., Sanchez-Bayo, F., Liess, M., Cavallaro, M.C., Liber, K., 2015b. Neonicotinoid contamination of global surface waters and associated risk to aquatic invertebrates: A review. Environment International 74, 291–303. https://doi.org/10.1016/j.envint.2014.10.024
Motomura, H., Narahashi, T., 2000. Temperature Dependence of Pyrethroid Modification of Single Sodium Channels in Rat Hippocampal Neurons. J. Membrane Biol. 177, 23–39. https://doi.org/10.1007/s002320001097
Mundim, K.C., Baraldi, S., Machado, H.G., Vieira, F.M.C., 2020. Temperature coefficient (Q10) and its applications in biological systems: Beyond the Arrhenius theory. Ecological Modelling 431, 109127. https://doi.org/10.1016/j.ecolmodel.2020.109127
Murphy, C.A., Nisbet, R.M., Antczak, P., Garcia-Reyero, N., Gergs, A., Lika, K., Mathews, T., Muller, E.B., Nacci, D., Peace, A., Remien, C.H., Schultz, I.R., Stevenson, L.M., Watanabe, K.H., 2018. Incorporating Suborganismal Processes into Dynamic Energy Budget Models for Ecological Risk Assessment: Linking AOP to DEB. Integr Environ Assess Manag 14, 615–624. https://doi.org/10.1002/ieam.4063
Murphy, D.J., 1983. Freezing Resistance in Intertidal Invertebrates. Annual Review of Physiology 45, 289–299. https://doi.org/10.1146/annurev.ph.45.030183.001445
Naylor, C., Maltby, L., Calow, P., 1989. Scope for growth in Gammarus pulex, a freshwater benthic detritivore. Hydrobiologia 188, 517–523. https://doi.org/10.1007/BF00027819
Nguyen-Kim, M.T., 2021. Die kleinste gemeinsame Wirklichkeit: Wahr, falsch, plausibel - die größten Streitfragen wissenschaftlich geprüft.
Nilsson, L.M., 1974. Energy Budget of a Laboratory Population of Gammarus pulex (Amphipoda). Oikos 25, 35–42. https://doi.org/10.2307/3543543
Noyes, P.D., Lema, S.C., 2015. Forecasting the impacts of chemical pollution and climate change interactions on the health of wildlife. Curr Zool 61, 669–689. https://doi.org/10.1093/czoolo/61.4.669
Noyes, P.D., McElwee, M.K., Miller, H.D., Clark, B.W., Van Tiem, L.A., Walcott, K.C., Erwin, K.N., Levin, E.D., 2009a. The toxicology of climate change: Environmental contaminants in a warming world. Environment International 35, 971–986. https://doi.org/10.1016/j.envint.2009.02.006
Noyes, P.D., McElwee, M.K., Miller, H.D., Clark, B.W., Van Tiem, L.A., Walcott, K.C., Erwin, K.N., Levin, E.D., 2009b. The toxicology of climate change: Environmental contaminants in a warming world. Environment International 35, 971–986. https://doi.org/10.1016/j.envint.2009.02.006
Nyman, A.-M., Hintermeister, A., Schirmer, K., Ashauer, R., 2013a. The Insecticide Imidacloprid Causes Mortality of the Freshwater Amphipod Gammarus pulex by Interfering with Feeding Behavior. PLOS ONE 8, e62472. https://doi.org/10.1371/journal.pone.0062472
Nyman, A.-M., Hintermeister, A., Schirmer, K., Ashauer, R., 2013b. The Insecticide Imidacloprid Causes Mortality of the Freshwater Amphipod Gammarus pulex by Interfering with Feeding Behavior. PLOS ONE 8, e62472. https://doi.org/10.1371/journal.pone.0062472
Nyman, A.-M., Schirmer, K., Ashauer, R., 2014. Importance of Toxicokinetics for Interspecies Variation in Sensitivity to Chemicals. Environ. Sci. Technol. 48, 5946–5954. https://doi.org/10.1021/es5005126
Odin, M., Ribeyre, F., Boudou, A., 1997. Depuration processes after exposure of burrowing mayfly nymphs (Hexagenia rigida) to methylmercury and cadmium from water column or sediment: effects of temperature and pH. Aquatic Toxicology 37, 125–137. https://doi.org/10.1016/S0166-445X(96)00818-1
OECD, 2012a. Test No. 211: Daphnia magna Reproduction Test. OECD Guidelines for the Testing of Chemicals, Section 2. https://doi.org/10.1787/9789264185203-en
OECD, 2012b. Test No. 305: Bioaccumulation in Fish: Aqueous and Dietary Exposure. OECD Publishing, Paris.
OECD, 2006. Current Approaches in the Statistical Analysis of Ecotoxicity Data: A guidance to application (annexes to this publication exist as a separate document). Organisation for Economic Co-operation and Development, Paris.
OECD, 2004. Test No. 202: Daphnia sp. Acute Immobilisation Test. Organisation for Economic Co-operation and Development, Paris.
Orr, S.E., Buchwalter, D.B., 2020. It's all about the fluxes: Temperature influences ion transport and toxicity in aquatic insects. Aquatic Toxicology 221, 105405. https://doi.org/10.1016/j.aquatox.2020.105405
Patra, R.W., Chapman, J.C., Lim, R.P., Gehrke, P.C., 2007. The effects of three organic chemicals on the upper thermal tolerances of four freshwater fishes. Environmental Toxicology and Chemistry 26, 1454–1459. https://doi.org/10.1897/06-156R1.1
Polazzo, F., Hermann, M., Crettaz-Minaglia, M., Rico, A., 2023. Impacts of extreme climatic events on trophic network complexity and multidimensional stability. Ecology 104, e3951. https://doi.org/10.1002/ecy.3951
Polazzo, F., Roth, S.K., Hermann, M., Mangold-Döring, A., Rico, A., Sobek, A., Van den Brink, P.J., Jackson, M.C., 2022. Combined effects of heatwaves and micropollutants on freshwater ecosystems: Towards an integrated assessment of extreme events in multiple stressors research. Global Change Biology 28, 1248–1267. https://doi.org/10.1111/gcb.15971
Pörtner, H.-O., 2010. Oxygen- and capacity-limitation of thermal tolerance: a matrix for integrating climate-related stressor effects in marine ecosystems. Journal of Experimental Biology 213, 881–893. https://doi.org/10.1242/jeb.037523
Pörtner, H.O., Bennett, A.F., Bozinovic, F., Clarke, A., Lardies, M.A., Lucassen, M., Pelster, B., Schiemer, F., Stillman, J.H., 2006. Trade-Offs in Thermal Adaptation: The Need for a Molecular to Ecological Integration. Physiological and Biochemical Zoology: Ecological and Evolutionary Approaches 79, 295–313. https://doi.org/10.1086/499986
Pörtner, H.-O., Bock, C., Mark, F.C., 2017. Oxygen- and capacity-limited thermal tolerance: bridging ecology and physiology. Journal of Experimental Biology 220, 2685–2696. https://doi.org/10.1242/jeb.134585

Pörtner, H.O., Farrell, A.P., 2008. Physiology and Climate Change. Science 322, 690–692. https://doi.org/10.1126/science.1163156
Raths, J., Švara, V., Lauper, B., Fu, Q., Hollender, J., 2023a. Speed it up: How temperature drives toxicokinetics of organic contaminants in freshwater amphipods. Global Change Biology 29, 1390–1406. https://doi.org/10.1111/gcb.16542
Raths, J., Švara, V., Lauper, B., Fu, Q., Hollender, J., 2023b. Speed it up: How temperature drives toxicokinetics of organic contaminants in freshwater amphipods. Global Change Biology 29, 1390–1406. https://doi.org/10.1111/gcb.16542
Raths, J.O., Švara, V., Lauper, B., Fu, Q., Hollender, J., 2022. Speed it up: How temperature drives toxicokinetics of organic contaminants in freshwater amphipods. in review at Global Change Biology.
Raza, A., Razzaq, A., Mehmood, S.S., Zou, X., Zhang, X., Lv, Y., Xu, J., 2019. Impact of Climate Change on Crops Adaptation and Strategies to Tackle Its Outcome: A Review. Plants 8, 34. https://doi.org/10.3390/plants8020034
Ritz, C., Baty, F., Streibig, J.C., Gerhard, D., 2015. Dose-Response Analysis Using R. PLOS ONE 10, e0146021. https://doi.org/10.1371/journal.pone.0146021
Roessink, I., Merga, L.B., Zweers, H.J., Brink, P.J.V. den, 2013. The Neonicotinoid Imidacloprid Shows High Chronic Toxicity to Mayfly Nymphs. Environmental Toxicology and Chemistry 32, 1096–1100. https://doi.org/10.1002/etc.2201
Rösch, A., Anliker, S., Hollender, J., 2016. How Biotransformation Influences Toxicokinetics of Azole Fungicides in the Aquatic Invertebrate Gammarus pulex. Environ. Sci. Technol. 50, 7175–7188. https://doi.org/10.1021/acs.est.6b01301
Roth, S.K., Hader, J.D., Domercq, P., Sobek, A., MacLeod, M., 2023. Scenario-based modelling of changes in chemical intake fraction in Sweden and the Baltic Sea under global change. Science of The Total Environment 888, 164247. https://doi.org/10.1016/j.scitotenv.2023.164247
Rubach, M.N., Ashauer, R., Buchwalter, D.B., De Lange, H., Hamer, M., Preuss, T.G., Töpke, K., Maund, S.J., 2011. Framework for traits-based assessment in ecotoxicology. Integrated Environmental Assessment and Management 7, 172–186. https://doi.org/10.1002/ieam.105
Russell, W.M.S., Burch, R.L., 1959. The principles of humane experimental technique. Methuen.
Sánchez-Bayo, F., Goka, K., Hayasaka, D., 2016. Contamination of the Aquatic Environment with Neonicotinoids and its Implication for Ecosystems. Frontiers in Environmental Science 4.
Sanford, M., Prosser, R. s., 2020. High-Frequency Sampling of Small Streams in the Agroecosystems of Southwestern Ontario, Canada, to Characterize Pesticide Exposure and Associated Risk to Aquatic Life. Environmental Toxicology and Chemistry 39, 2570–2587. https://doi.org/10.1002/etc.4884
Sardi, A.E., Augustine, S., Olsen, G.H., Camus, L., 2019. Exploring inter-species sensitivity to a model hydrocarbon, 2-Methylnaphtalene, using a process-based model. Environ Sci Pollut Res 26, 11355–11370. https://doi.org/10.1007/s11356-019-04423-8
Schäfer, R.B., Piggott, J.J., 2018. Advancing understanding and prediction in multiple stressor research through a mechanistic basis for null models. Global Change Biology 24, 1817–1826. https://doi.org/10.1111/gcb.14073
Schlechtriem, C., Kampe, S., Bruckert, H.-J., Bischof, I., Ebersbach, I., Kosfeld, V., Kotthoff, M., Schäfers, C., L'Haridon, J., 2019. Bioconcentration studies with the freshwater amphipod Hyalella azteca: are the results predictive of bioconcentration in fish? Environmental Science and Pollution Research 26, 1628–1641.
Schlechtriem, C., Kuehr, S., Moertl, C., 2022. Development of a bioaccumulation test using Hyalella azteca Final report.
Schmolke, A., Kapo, K.E., Rueda-Cediel, P., Thorbek, P., Brain, R., Forbes, V., 2017. Developing population models: A systematic approach for pesticide risk assessment using herbaceous plants as an example. Science of The Total Environment 599–600, 1929–1938. https://doi.org/10.1016/j.scitotenv.2017.05.116
Schmolke, A., Thorbek, P., DeAngelis, D.L., Grimm, V., 2010. Ecological models supporting environmental decision making: a strategy for the future. Trends in Ecology & Evolution 25, 479–486. https://doi.org/10.1016/j.tree.2010.05.001
Schuijt, L.M., Peng, F.-J., Berg, S.J.P. van den, Dingemans, M.M.L., Brink, P.J. van den, 2021. (Eco)toxicological tests for assessing impacts of chemical stress to aquatic ecosystems: Facts, challenges, and future. Science of the Total Environment. https://doi.org/10.1016/j.scitotenv.2021.148776
Schulte, P.M., Healy, T.M., Fangue, N.A., 2011. Thermal Performance Curves, Phenotypic Plasticity, and the Time Scales of Temperature Exposure. Integrative and Comparative Biology 51, 691–702. https://doi.org/10.1093/icb/icr097
Semsar-kazerouni, M., Verberk, W.C.E.P., 2018. It's about time: Linkages between heat tolerance, thermal acclimation and metabolic rate at different temporal scales in the freshwater amphipod Gammarus fossarum Koch, 1836. Journal of Thermal Biology 75, 31–37. https://doi.org/10.1016/j.jtherbio.2018.04.016
Sharpe, P.J.H., DeMichele, D.W., 1977. Reaction kinetics of poikilotherm development. Journal of Theoretical Biology 64, 649–670. https://doi.org/10.1016/0022-5193(77)90265-X
Silva, L.C.M., Daam, M.A., Gusmao, F., 2020. Acclimation alters glyphosate temperature-dependent toxicity: Implications for risk assessment under climate change. Journal of Hazardous Materials 385, 121512. https://doi.org/10.1016/j.jhazmat.2019.121512
Simon-Delso, N., Amaral-Rogers, V., Belzunces, L.P., Bonmatin, J.M., Chagnon, M., Downs, C., Furlan, L., Gibbons, D.W., Giorio, C., Girolami, V., Goulson, D., Kreutzweiser, D.P., Krupke, C.H., Liess, M., Long, E., McField, M., Mineau, P., Mitchell, E.A.D., Morrissey, C.A., Noome, D.A., Pisa, L., Settele, J., Stark, J.D., Tapparo, A., Van Dyck, H., Van Praagh, J., Van der Sluijs, J.P., Whitehorn, P.R., Wiemers, M., 2015a. Systemic insecticides (neonicotinoids and fipronil): trends, uses, mode of action and metabolites. Environ Sci Pollut Res 22, 5–34. https://doi.org/10.1007/s11356-014-3470-y
Simon-Delso, N., Amaral-Rogers, V., Belzunces, L.P., Bonmatin, J.M., Chagnon, M., Downs, C., Furlan, L., Gibbons, D.W., Giorio, C., Girolami, V., Goulson, D., Kreutzweiser, D.P., Krupke, C.H., Liess, M., Long, E., McField, M., Mineau, P., Mitchell, E.A.D., Morrissey, C.A., Noome, D.A., Pisa, L., Settele, J., Stark, J.D., Tapparo, A., Van Dyck, H., Van Praagh, J., Van der Sluijs, J.P., Whitehorn, P.R., Wiemers, M., 2015b. Systemic insecticides (neonicotinoids and fipronil): trends, uses, mode of action and metabolites. Environ Sci Pollut Res 22, 5–34. https://doi.org/10.1007/s11356-014-3470-y
Sinclair, B.J., Marshall, K.E., Sewell, M.A., Levesque, D.L., Willett, C.S., Slotsbo, S., Dong, Y., Harley, C.D.G., Marshall, D.J., Helmuth, B.S., Huey, R.B., 2016. Can we predict ectotherm responses to climate change using thermal performance curves and body temperatures? Ecology Letters 19, 1372–1385. https://doi.org/10.1111/ele.12686

Sokolova, I.M., Lannig, G., 2008. Interactive effects of metal pollution and temperature on metabolism in aquatic ectotherms: implications of global climate change. Climate Research 37, 181–201. https://doi.org/10.3354/cr00764

Sparks, T.C., Nauen, R., 2015. IRAC: Mode of action classification and insecticide resistance management. Pesticide Biochemistry and Physiology, Insecticide and Acaricide Modes of Action and their Role in Resistance and its Management 121, 122–128. https://doi.org/10.1016/j.pestbp.2014.11.014

Stehle, S., Ovcharova, V., Wolfram, J., Bub, S., Herrmann, L.Z., Petschick, L.L., Schulz, R., 2023. Neonicotinoid insecticides in global agricultural surface waters – Exposure, risks and regulatory challenges. Science of The Total Environment 867, 161383. https://doi.org/10.1016/j.scitotenv.2022.161383

Stoks, R., Verheyen, J., Van Dievel, M., Tüzün, N., 2017. Daily temperature variation and extreme high temperatures drive performance and biotic interactions in a warming world. Current Opinion in Insect Science, Global change biology * Molecular physiology 23, 35–42. https://doi.org/10.1016/j.cois.2017.06.008

Suchail, S., Guez, D., Belzunces, L.P., 2001. Discrepancy between acute and chronic toxicity induced by imidacloprid and its metabolites in Apis mellifera. Environmental Toxicology and Chemistry 20, 2482–2486. https://doi.org/10.1002/etc.5620201113

Sulukan, E., Baran, A., Şenol, O., Yildirim, S., Mavi, A., Ceyhun, H.A., Toraman, E., Ceyhun, S.B., 2022. The synergic toxicity of temperature increases and nanopolystrene on zebrafish brain implies that global warming may worsen the current risk based on plastic debris. Science of The Total Environment 808, 152092. https://doi.org/10.1016/j.scitotenv.2021.152092

Sumon, K.A., Ritika, A.K., Peeters, E.T.H.M., Rashid, H., Bosma, R.H., Rahman, Md.S., Fatema, Mst.K., Van den Brink, P.J., 2018. Effects of imidacloprid on the ecology of sub-tropical freshwater microcosms. Environmental Pollution 236, 432–441. https://doi.org/10.1016/j.envpol.2018.01.102

Sunday, J.M., Bates, A.E., Dulvy, N.K., 2012. Thermal tolerance and the global redistribution of animals. Nature Clim Change 2, 686–690. https://doi.org/10.1038/nclimate1539

Sutcliffe, D.W., Carrick, T.R., Willoughby, L.G., 1981. Effects of diet, body size, age and temperature on growth rates in the amphipod Gammarus pulex. Freshwater Biology 11, 183–214. https://doi.org/10.1111/j.1365-2427.1981.tb01252.x

Švara, V., Krauss, M., Michalski, S.G., Altenburger, R., Brack, W., Luckenbach, T., 2021. Chemical Pollution Levels in a River Explain Site-Specific Sensitivities to Micropollutants within a Genetically Homogeneous Population of Freshwater Amphipods. Environ. Sci. Technol. https://doi.org/10.1021/acs.est.0c07839

Tan, J., Galligan, J.J., Hollingworth, R.M., 2007. Agonist actions of neonicotinoids on nicotinic acetylcholine receptors expressed by cockroach neurons. NeuroToxicology 28, 829–842. https://doi.org/10.1016/j.neuro.2007.04.002

Tellinghuisen, J., 2001. Statistical Error Propagation. J. Phys. Chem. A 105, 3917–3921. https://doi.org/10.1021/jp003484u

Thany, S.H. (Ed.), 2010. Insect nicotinic acetylcholine receptors, Advances in experimental medicine and biology. Springer Science+Business Media ; Landes Bioscience, New York : Austin, Tex.

Theys, C., Verheyen, J., Tüzün, N., Stoks, R., 2020. Higher mean and fluctuating temperatures jointly determine the impact of the pesticide chlorpyrifos on the growth rate and leaf consumption of a freshwater isopod. Chemosphere 128528. https://doi.org/10.1016/j.chemosphere.2020.128528

Thompson, D.A., Lehmler, H.-J., Kolpin, D.W., Hladik, M.L., Vargo, J.D., Schilling, K.E., LeFevre, G.H., Peeples, T.L., Poch, M.C., LaDuca, L.E., Cwiertny, D.M., Field, R.W., 2020. A critical review on the potential impacts of neonicotinoid insecticide use: current knowledge of environmental fate, toxicity, and implications for human health. Environ. Sci.: Processes Impacts 22, 1315–1346. https://doi.org/10.1039/C9EM00586B

Tomizawa, M., Casida, J.E., 2004. NEONICOTINOID INSECTICIDE TOXICOLOGY: Mechanisms of Selective Action. Annu. Rev. Pharmacol. Toxicol. 45, 247–268. https://doi.org/10.1146/annurev.pharmtox.45.120403.095930

Tran, T.T., Dinh Van, K., Janssens, L., Stoks, R., 2020. The effect of warming on pesticide toxicity is reversed between developmental stages in the mosquito Culex pipiens. Science of The Total Environment 717, 134811. https://doi.org/10.1016/j.scitotenv.2019.134811

United Nations Environment Programme, 2019. Global chemicals outlook II: From legacies to innovative solutions (No. DTI/2230/GE).

US EPA, O., 2013. Schedule for Review of Neonicotinoid Pesticides [WWW Document]. URL https://www.epa.gov/pollinator-protection/schedule-review-neonicotinoid-pesticides (accessed 7.31.22).

Van den Berg, S.J.P., Baveco, H., Butler, E., De Laender, F., Focks, A., Franco, A., Rendal, C., Van den Brink, P.J., 2019. Modeling the Sensitivity of Aquatic Macroinvertebrates to Chemicals Using Traits. Environ. Sci. Technol. 53, 6025–6034. https://doi.org/10.1021/acs.est.9b00893

Van den Brink, P.J., Boxall, A.B.A., Maltby, L., Brooks, B.W., Rudd, M.A., Backhaus, T., Spurgeon, D., Verougstraete, V., Ajao, C., Ankley, G.T., Apitz, S.E., Arnold, K., Brodin, T., Cañedo-Argüelles, M., Chapman, J., Corrales, J., Coutellec, M.-A., Fernandes, T.F., Fick, J., Ford, A.T., Papiol, G.G., Groh, K.J., Hutchinson, T.H., Kruger, H., Kukkonen, J.V.K., Loutseti, S., Marshall, S., Muir, D., Ortiz-Santaliestra, M.E., Paul, K.B., Rico, A., Rodea-Palomares, I., Römbke, J., Rydberg, T., Segner, H., Smit, M., Gestel, C.A.M. van, Vighi, M., Werner, I., Zimmer, E.I., Wensem, J. van, 2018. Toward sustainable environmental quality: Priority research questions for Europe. Environmental Toxicology and Chemistry 37, 2281–2295. https://doi.org/10.1002/etc.4205

Van der Putten, W.H., Macel, M., Visser, M.E., 2010. Predicting species distribution and abundance responses to climate change: why it is essential to include biotic interactions across trophic levels. Phil. Trans. R. Soc. B 365, 2025–2034. https://doi.org/10.1098/rstb.2010.0037

van der Sluijs, J.P., Simon-Delso, N., Goulson, D., Maxim, L., Bonmatin, J.-M., Belzunces, L.P., 2013. Neonicotinoids, bee disorders and the sustainability of pollinator services. Current Opinion in Environmental Sustainability, Open issue 5, 293–305. https://doi.org/10.1016/j.cosust.2013.05.007

Vellinger, C., Felten, V., Sornom, P., Rousselle, P., Beisel, J.-N., Usseglio-Polatera, P., 2012. Behavioural and Physiological Responses of Gammarus pulex Exposed to Cadmium and Arsenate at Three Temperatures: Individual and Combined Effects. PLOS ONE 7, e39153. https://doi.org/10.1371/journal.pone.0039153

Verheyen, J., Delnat, V., Stoks, R., 2019. Increased Daily Temperature Fluctuations Overrule the Ability of Gradual Thermal Evolution to Offset the Increased Pesticide Toxicity under Global Warming. Environ. Sci. Technol. 53, 4600–4608. https://doi.org/10.1021/acs.est.8b07166

Verheyen, J., Stoks, R., 2023. Thermal Performance Curves in a Polluted World: Too Cold and Too Hot Temperatures Synergistically Increase Pesticide Toxicity. Environ. Sci. Technol. https://doi.org/10.1021/acs.est.2c07567

Verheyen, J., Stoks, R., 2019a. Current and future daily temperature fluctuations make a pesticide more toxic: Contrasting effects on life history and physiology. Environmental Pollution 248, 209–218. https://doi.org/10.1016/j.envpol.2019.02.022

Verheyen, J., Stoks, R., 2019b. Shrinking Body Size and Physiology Contribute to Geographic Variation and the Higher Toxicity of Pesticides in a Warming World. Environ. Sci. Technol. 53, 11515–11523. https://doi.org/10.1021/acs.est.9b03806

Wang, X., Goulson, D., Chen, L., Zhang, J., Zhao, W., Jin, Y., Yang, S., Li, Y., Zhou, J., 2020. Occurrence of Neonicotinoids in Chinese Apiculture and a Corresponding Risk Exposure Assessment. Environ. Sci. Technol. 54, 5021–5030. https://doi.org/10.1021/acs.est.9b07162

Welton, J.S., 1979. Life-history and production of the amphipod Gammarus pulex in a Dorset chalk stream. Freshwater Biology 9, 263–275. https://doi.org/10.1111/j.1365-2427.1979.tb01508.x

Westmoreland, C., Bender, H.J., Doe, J.E., Jacobs, M.N., Kass, G.E.N., Madia, F., Mahony, C., Manou, I., Maxwell, G., Prieto, P., Roggeband, R., Sobanski, T., Schütte, K., Worth, A.P., Zvonar, Z., Cronin, M.T.D., 2022. Use of New Approach Methodologies (NAMs) in regulatory decisions for chemical safety: Report from an EPAA Deep Dive Workshop. Regulatory Toxicology and Pharmacology 135, 105261. https://doi.org/10.1016/j.yrtph.2022.105261

Woolway, R.I., Jennings, E., Shatwell, T., Golub, M., Pierson, D.C., Maberly, S.C., 2021. Lake heatwaves under climate change. Nature 589, 402–407. https://doi.org/10.1038/s41586-020-03119-1

Yang, Y., Su, L., Huang, Y., Zhang, X., Li, C., Wang, J., Fan, L., Wang, S., Zhao, Y.H., 2022. Bio-uptake, tissue distribution and metabolism of a neonicotinoid insecticide clothianidin in zebrafish. Environmental Pollution 292, 118317. https://doi.org/10.1016/j.envpol.2021.118317

Yassen, A., Olofsen, E., Dahan, A., Danhof, M., 2005. Pharmacokinetic-Pharmacodynamic Modeling of the Antinociceptive Effect of Buprenorphine and Fentanyl in Rats: Role of Receptor Equilibration Kinetics. J Pharmacol Exp Ther 313, 1136–1149. https://doi.org/10.1124/jpet.104.082560

Zhao, Y.-X., Jiang, H.-Y., Cheng, X., Zhu, Y.-X., Fan, Z.-X., Dai, Z.-L., Guo, L., Liu, Z.-H., Dai, Y.-J., 2019. Neonicotinoid thiacloprid transformation by the N2-fixing bacterium Microvirga flocculans CGMCC 1.16731 and toxicity of the amide metabolite. International Biodeterioration & Biodegradation 145, 104806. https://doi.org/10.1016/j.ibiod.2019.104806

"I don't think I'm really listening unless I'm willing to be changed by you, and that doesn't mean that I'm going to agree with what you're saying, but I might be changed by something about you, some deeply held belief you have, about just living, about your dedication to your children, or something like that, and I might be touched by that. That's more important than hitting you over the head with my argument, I think, because it leads to more interaction."

Alan Alda

November 1st 2019, interview for the WNYC Studios radio show Science Friday

Netherlands Research School for the
Socio-Economic and Natural Sciences of the Environment

D I P L O M A

for specialised PhD training

The Netherlands research school for the
Socio-Economic and Natural Sciences of the Environment
(SENSE) declares that

Annika Mangold-Döring

born on 12 August 1993 in Birkesdorf, Germany

has successfully fulfilled all requirements of the
educational PhD programme of SENSE.

Wageningen, 13 November 2023

Chair of the SENSE board

Prof. dr. Martin Wassen

The SENSE Director

Prof. Philipp Pattberg

The SENSE Research School has been accredited by the Royal Netherlands Academy of Arts and Sciences (KNAW)

KONINKLIJKE NEDERLANDSE
AKADEMIE VAN WETENSCHAPPEN

The SENSE Research School declares that **Annika Mangold-Döring** has successfully fulfilled all requirements of the educational PhD programme of SENSE with a work load of 59.1 EC, including the following activities:

SENSE PhD Courses

- Environmental research in context (2019)
- Research in context activity: 'Initiator and organiser of the Science Communication Interest Group (2021-2023)'

Other PhD and Advanced MSc Courses

- Environmental Risk of Chemicals Now and in the Future, ITN training course (2019)
- Project and Time Management, Wageningen Graduate School (2019)
- Reviewing a scientific manuscript, Wageningen University (2019)
- Agent-based modelling with NetLogo, Georg-August-Universität Göttingen (2019)
- Meta Analysis, PE&RC graduate School (2020)
- Structural equation modelling, PE&RC graduate School (2020)
- Policy and regulation of chemicals, ITN training course (2020)
- Chemical Risk in the Future, ITN training course (2020)
- Impact, engagement and influence in the chemical risk area, ITN training course (2021)
- Thematic School on DEB theory for metabolic organization, DEB2021, online (2021)
- Dynamic Modelling of Toxic Effects, University of Copenhagen, DEBtox, online (2021)

External training at a foreign research institute

- Secondment at Norwegian Institute for Water Research (NIVA), online (2021)
- Secondment at Ibacon, Germany (2021)

Management and Didactic Skills Training

- Co-organisation of ECORISK2050 workshop - Chemical Risk in the Future (2020)
- Co-organisation of session at SETAC Europe 33rd Annual Meeting (2023)
- Supervising MSc student with thesis (2021)
- Teaching in the MSc course 'Chemical Stress Ecology and Ecotoxicology' (2020-2022)

Oral Presentations

- *A novel multi-species physiologically-based toxicokinetic modelling approach in support of chemicals risk assessment*, SETAC Europe 30st Annual Meeting, 3-7 May 2020, online
- *Temperature influence on the toxicokinetics of insecticides*. SETAC Europe 31st Annual Meeting, 3-6 May 2021, online
- *Does temperature influence pesticides' toxicokinetics and toxicodynamics alike? an investigation with the full-GUTS Model for Gammarus pulex*. SETAC Europe 32nd Annual Meeting, 15-19 May 2022, Copenhagen, Denmark

SENSE coordinator PhD education

Dr. ir. Peter Vermeulen

The research described in this thesis was part of the Innovative Training Network ECORISK2050 financially supported by the European Union's Horizon 2020 research and innovation program under the Marie Skłodowska-Curie grant agreement No 813124.

Financial support from the Aquatic Ecology and Water Quality Management Group of Wageningen University for printing this thesis is gratefully acknowledged.

Cover design and artwork by Bregje Jaspers | ProefschriftMaken & BioRender.com
Layout by Annika Mangold-Döring & ProefschriftMaken
Printed by ProefschriftMaken